**Distribution Agreement**

In presenting this thesis or dissertation as a partial fulfillment of the requirements for an advanced degree from Emory University, I hereby grant to Emory University and its agents the non-exclusive license to archive, make accessible, and display my thesis or dissertation in whole or in part in all forms of media, now or hereafter known, including display on the world wide web. I understand that I may select some access restrictions as part of the online submission of this thesis or dissertation. I retain all ownership rights to the copyright of the thesis or dissertation. I also retain the right to use in future works (such as articles or books) all or part of this thesis or dissertation.

Signature:

_____ _____

James Raymond Bowen Date

**Mechanisms of Flavivirus Antagonism of Innate Immune Signaling in Human Dendritic Cells**

By

James Raymond Bowen
Doctor of Philosophy
Graduate Division of Biological and Biomedical Science
Immunology and Molecular Pathogenesis

_____
Mehul S. Suthar, Ph.D.
Advisor

_____
Arash Grakoui, Ph.D.
Committee Member

_____
Jacob E. Kohlmeier, Ph.D.
Committee Member

_____
Anice C. Lowen, Ph.D.
Committee Member

_____
Edward S. Mocarski, Ph.D.
Committee Member

Accepted:

_____
Lisa A. Tedesco, Ph.D.
Dean of the James T. Laney School of Graduate Studies

_____
Date

**Mechanisms of Flavivirus Antagonism of Innate Immune Signaling in Human Dendritic Cells**

By

James Raymond Bowen
B.S. Biotechnology, Upstate Medical University, 2011

Advisor: Mehul S. Suthar, Ph.D.

An abstract of
A dissertation submitted to the Faculty of the
James T. Laney School of Graduate Studies of Emory University
in partial fulfillment of the requirements for the degree of
Doctor of Philosophy
in Graduate Division of Biological and Biomedical Science
Immunology and Molecular Pathogenesis
2017

## Abstract

Mechanisms of Flavivirus Antagonism of Innate Immune Signaling in Human Dendritic Cells

By James Raymond Bowen

West Nile virus (WNV) is a neurotropic flavivirus that remains a leading cause of mosquito-borne encephalitis in the United States. Zika virus (ZIKV), which is closely related to WNV, is an emerging mosquito-borne flavivirus that has sparked a global public health crisis due to a causal linkage to severe neonatal birth defects. Previous work has suggested that dendritic cells (DCs) are important cellular targets during infection with related flaviviruses, including dengue, yellow fever, and Japanese encephalitis viruses. However, the contributions of human DCs during WNV or ZIKV infection remains poorly understood. Here, we utilized primary human cells to demonstrate that monocyte-derived DCs (moDCs) support productive viral replication following infection with WNV and ZIKV. Using a systems biology approach, STAT5 was identified as a regulator of DC activation that was not activated during WNV or ZIKV infection. Consequently, molecules involved in antigen presentation and T cell activation were minimally induced during WNV and ZIKV infection, and functionally, WNV-infected moDCs dampened allogeneic T cell proliferation. Mechanistically, WNV and ZIKV blocked tyrosine phosphorylation of STAT5, and to a lesser extent STAT1 and STAT2, through impairment of Tyk2 and JAK1 activation. ZIKV, but not WNV, also selectively blocked type I IFN protein translation, without affecting the up-regulation of other antiviral proteins. Combined, our studies use primary human cells to reveal novel mechanisms used by WNV and ZIKV to subvert DC activation during productive infection within human moDCs.

The mechanisms and cell types involved in transplacental transmission of ZIKV are poorly understood. Here, we utilized primary human cells isolated from villous tissue of full-term placentae to demonstrate that ZIKV productively replicates within primary human placental macrophages, known as Hofbauer cells (HCs). ZIKV also infected cytotrophoblasts, although viral replication was delayed and more limited. ZIKV infection of HCs promoted up-regulation of T cell co-stimulatory molecules, production of pro-inflammatory cytokines, type I IFN secretion, and strong antiviral gene expression. Combined, our findings support a mechanism of transplacental transmission where ZIKV gains access to the developing fetus by directly infecting placental cells and disrupting the placental barrier.

# Mechanisms of Flavivirus Antagonism of Innate Immune Signaling in Human Dendritic Cells

By

James Raymond Bowen
B.S. Biotechnology, Upstate Medical University, 2011

Advisor: Mehul S. Suthar, Ph.D.

A dissertation submitted to the Faculty of the
James T. Laney School of Graduate Studies of Emory University
in partial fulfillment of the requirements for the degree of
Doctor of Philosophy
in Graduate Division of Biological and Biomedical Science
Immunology and Molecular Pathogenesis
2017

**ACKNOWLEDGEMENTS**

I could not be more thankful for all the support Mehul has given me throughout my PhD. He has always given me the freedom to excel, and struggle, through my scientific endeavors, while providing unending support at every step. I would not be the scientist that I am today without his guidance, enthusiasm, supportive words, and above all else, his willingness to go the extra mile to ensure my success. I have always enjoyed our scientific discussions and look forward to continued discussions in the future.

A special thank you to all members, past and present, of the Suthar laboratory family. Science is full of experimental and personal struggles, and having a supportive laboratory environment makes all the difference. In particular, much of the work presented in this dissertation on Zika virus would not have been completed as quickly as it was without help from Kendra Quicke, who contributed equally to much of this work. In addition, Justin O'Neal, Circe McDonald, and Matthew Zimmerman have all provided assistance with experiments at times when I needed help the most.

I must also extend a thank all members of my thesis committee, including Dr. Arash Grakoui, Dr. Edward Mocarski, Dr. Anice Lowen, and Dr. Jacob Kohlmeier. In addition to providing helpful input on my research, you have been a source of encouraging words and valuable career advice. You have truly been a mentorship team, and have made me a more rigorous scientist.

The most important acknowledgement is saved for last, and that is to my friends and family. I could not have asked for greater support during the last 27 years of my life, but particularly during the last 4 years of graduate school. The greatest support has come from my life partner, Sarah Hayward, whose unending love and understanding has made even the worst of times bearable. I could not ask for a more supportive significant other, especially through what has been some of the happiest but also most stressful moments of my life.

## TABLE OF CONTENTS

## LIST OF FIGURES AND TABLES

## ABBREVIATIONS

| Abbreviation | Term |
|---|---|
| ADE | Antibody dependent enhancement |
| BBB | Blood brain barrier |
| BMDC | Bone marrow derived dendritic cell |
| C | nucleocapsid |
| CARDs | Caspase activation and recruitment domains |
| CC | Collaborative cross |
| cDNA | Complementary deoxyribonucleic acid |
| ChIP-Seq | Chromatin immunoprecipitation sequencing |
| CMV | Cytomegalovirus |
| CNS | Central nervouse system |
| CTBs | Cytotrophoblasts |
| DC | Dendritic cell |
| DEGs | Differentially expressed genes |
| DENV | Dengue virus |
| DMEM | Dulbecco's modified eagle medium |
| DNA | Deoxyribonucleic acid |
| E | Envelope |
| EBOV | Ebola virus |
| EMCV | Encephalomyocarditis virus |
| eQTL | Expression quantitative trait locus |
| ER | Endoplasmic reticulum |
| FcRn | Neonatal Fc receptor |
| FFA | Focus forming assay |
| FFU | Focus forming unit |
| GAPDH | Glyceraldehyde 3-phosphate dehydrogenase |
| GEO | Gene expression omnibus |
| GM-CSF | Granulocyte macrophage colony stimulating factor |
| HCs | Hofbauer cells |
| hNPCs | Human neural progenitor cells |
| hpi | Hours post infection |
| HSV | Herpes simplex virus |
| IAV | Influenza A virus |
| IFIT | Interferon induced proteins with tetratricopeptide repeats |
| IFITM | Interferon induced transmembrane protein |
| IFN | Interferon |
| IFNAR | Type I interferon receptor |
| IFNLR | Interferon lambda receptor |
| IFNα | Interferon alpha |
| IFNβ | Interferon beta |
| IFNλ | Interferon lambda |

| | |
|---|---|
| IKKε | inhibitor of kappa-B kinase epsilon |
| IL | Interleukin |
| IL-10Rβ | Interleukin-10 receptor β |
| IL-1R | Interleukin-1 receptor |
| IRF | interferon regulatory factor |
| IκB | inhibitor of kappa-B |
| JAK | Janus associated kinase |
| JEV | Japanese encephalitits virus |
| LGP2 | Laboratory of genetics and physiology 2 |
| LGTV | Langat virus |
| MAMs | Mitochondrial associated membranes |
| MAVS | Mitochondrial antiviral signaling |
| MDA5 | Melanoma differentiation-associated gene 5 |
| mDC | Myeloid dendritic cell |
| MFI | Median fluorescence intensity |
| MHC | Major histocompatibility |
| moDC | Monocyte derived dendritic cell |
| MOI | Multiplicity of infection |
| mRNASeq | Messenger RNA sequencing |
| MyD88 | Myeloid differentiation primary response 88 |
| NEMO | NF-kappa-B essential modulator |
| NES | Normalized enrichment score |
| NFκB | Nuclear factor kappa-B |
| NHP | Non-human primate |
| NK cell | Natural killer cell |
| NPCs | Neural progenitor cells |
| NS | Non-structural |
| NS | Non-structural |
| NSCs | Neural stem cells |
| OAS1 | 2'-5'-oligoadenylate synthetase 1 |
| PBMCs | Peripheral blood mononuclear cells |
| PCR | Polymerase chain reaction |
| pDC | Plasmacytoid dendritic cell |
| PFU | Plaque forming unit |
| PKR | Protein kinase R |
| PPRs | Pattern recognition receptors |
| prM | Pre-membrane |
| qRT-PCR | Quantitative reverse transcriptase polymerase chain reaction |
| QTL | Quantitative trait locus |
| RIG-I | Retinoic acid-inducible gene I |
| RIPA | Radioimmunoprecipitation assay buffer |
| RLR | Retinoic acid-inducible gene I-like receptors |
| RNA | Ribonucleic acid |

| | |
|---|---|
| RPMI | Roswell park memorial institute medium |
| RV | Rotavirus |
| SD | Standard deviation |
| SEM | Standard error of the mean |
| SNPs | Single nucleotide polymorphisms |
| SOCS | Suppressor of cytokine signaling |
| ssRNA | Single stranded RNA |
| STAT | Signal transducer and activator of transcription |
| STBs | Syncytiotrophoblasts |
| TBK1 | TANK-binding kinase 1 |
| TLRs | Toll-like receptors |
| TORCH | Toxoplasma gondii, other, rubella virus, CMV, and HSV |
| TRAF | TNF receptor-associated factor |
| Tregs | Regulatory T cell |
| TRIF | TIR domain–containing adaptor-inducing IFN-β |
| US | United states |
| UV | Ultraviolet |
| WGCNA | Weighted gene coexpression network analysis |
| WNV | West Nile virus |
| YFV | Yellow Fever virus |
| ZIKV | Zika virus |

# CHAPTER 1. INTRODUCTION

## Part 1: Neurotropic flaviviruses

### A. West Nile Virus

West Nile virus (WNV) is a member of the Flaviviridae family, genus *flavivirus* and is closely related to dengue, yellow fever, Japanese encephalitis, and Zika viruses. The envelope (E) protein of mature WNV virions binds to target cells through an unknown host receptor and initiates receptor-mediated endocytosis (1, 2). Endosomal acidification triggers membrane fusion, viral particle disassembly, and delivery of the 10.8kb positive sense, single stranded RNA (ssRNA) genome into the host cytoplasm. The viral genome is translated at the rough endoplasmic reticulum (ER) into a single viral polypeptide that is cleaved by viral and host proteases to generate 3 structural proteins (E, pre-membrane/prM, and nucleocapsid/C) that encapsidate the viral particle and genome, as well as 7 non-structural (NS) proteins (NS1, NS2A, NS2B, NS3, NS4A, NS4B, and NS5) that serve critical functions in genome replication, polypeptide processing, and immune evasion. WNV initiates genome replication and particle assembly within invaginations of the ER membrane, where non-infectious, immature virions bud into the ER lumen and traffic through the host endocytic pathway. Viral particle maturation occurs within the trans-Golgi network, where glycosylation of the E protein and cleavage of prM to M by furin proteases generate infectious virions that exit the cell by exocytosis.

Host antiviral effector molecules that target each step of the viral life cycle have been identified, including inhibitors of cell entry (IFITM family) (3, 4), viral replication (OAS/RNase L system) (5, 6), protein translation (PKR and the IFIT family) (6, 7), and viral egress (viperin) (8). To maintain its pathogenicity, WNV has evolved multiple mechanisms to overcome the pressures imposed by these antiviral effector molecules, which has been recently reviewed in detail by multiple groups (9, 10). A better understanding of how the host restricts WNV replication, as well as the mechanisms used by the virus to antagonize these responses will inform the rational design of flavivirus-specific antiviral treatments.

***WNV disease in humans***

Human WNV infection was first described in 1937 in Uganda, causing sporadic outbreaks throughout Africa and Europe over the next 60 years (11). WNV was introduced into the United States (US) in 1999, where it caused a small outbreak of meningitis and encephalitis in New York City. WNV rapidly spread throughout the US, where it remains endemic and causes annual outbreaks of neuroinvasive disease. Globally, seropositivity for WNV is widespread and WNV remains a leading cause of mosquito-borne viral encephalitis worldwide. In the environment, WNV cycles between its mosquito vector, predominately of the *Culex* species, and birds, which serve as the primary reservoir and amplification host of WNV. Humans and other mammals serve as dead end hosts following the bite of an infected mosquito, failing to generate the prolonged and high titer viremia required to sustain a mosquito transmission

cycle. Following human infection, 1 in 5 individuals develop symptoms that range from a mild febrile illness to severe neuroinvasive disease. Neuroinvasion is a serious complication with long term sequelae that includes ocular involvement, cognitive impairment, muscle weakness, and flaccid paralysis (12). The current lack of vaccines or specific therapeutics approved for use in humans underpins the need to better understand the mechanisms of protective immunity during human WNV infection.

***WNV pathogenesis***

Using a murine model, three phases of WNV pathogenesis have been defined: early post-inoculation, visceral organ dissemination, and neuroinvasive phases (13). Following feeding and probing by a WNV-infected mosquito, high doses of virus are inoculated into the skin, while lower doses can also be deposited directly into the bloodstream (14). During the early post-inoculation phase, WNV infects keratinocytes and skin resident DCs, including epidermal Langerhans cells and dermal DCs, as initial targets of viral replication (13, 15). Viral spread to the skin draining lymph nodes leads to infection of LN resident DCs, resulting in viral amplification and viremia.

Once WNV reaches the circulation, the visceral organ dissemination phase begins with WNV spread to permissive peripheral tissues, including the spleen, where DCs are primary targets of viral replication and amplification (16). WNV initiates the neuroinvasive phase of pathogenesis after crossing the blood brain barrier (BBB) and directly infecting neurons within the central nervous

system (CNS) (17, 18). While the primary route used by WNV to cross the BBB remains unclear, increased blood brain barrier (BBB) permeability, direct infection of endothelial cells, retrograde axonal transport, and migration of infected leukocytes are all potential mechanisms (13).

While the mouse model has been of significant utility in parsing out critical events during WNV infection, our understanding of human WNV pathogenesis remains poorly understood. New small animal models that better reflect human disease, including use of the collaborative cross mouse model of genetic diversity, may help narrow this gap in our understanding (19). Given that the severity of WNV infection is primarily associated with the neuroinvasive phase, a better understanding of the mechanisms that restrict viral entry and replication within the CNS during human infection is of paramount importance.

***WNV immunity***

Using the mouse pathogenesis model, critical features of immune control have been defined during WVN infection. Early control of viremia is mediated by B cells through production of virus neutralizing IgM and IgG antibodies, both of which are critical for promoting viral clearance from the circulation and limiting viral dissemination (20, 21). Monoclonal antibodies with potent neutralization have also show therapeutic efficacy in post-exposure therapeutic trials in mice (22, 23). During human infection, IgM and IgG responses are rapidly induced and correspond with viral clearance from the serum (24). CD8+ T cell immunity, in part through secretion of perforin, is critical for viral clearance from the peripheral

tissues and CNS, where their absence leads to viral persistence (25, 26). CD4+ T cells are also critical for controlling viral replication within the CNS, where they help program B cell mediated antibody production and promote sustained CD8+ T cell responses (27). CD4+ regulatory T cells (Tregs) play an important role in dampening excessive immune responses and preventing immunopathology during WNV infection (28). During human infection, dysfunctional T cell immunity is associated with severe disease outcome (28-30). In addition to adaptive immunity, innate immune signaling is critical for early WNV detection and programming multiple aspects of the antiviral response. A more detailed discussion of the specific roles of innate immune signaling pathways can be found in Part II of this introduction.

**B. Zika virus**

Zika virus (ZIKV) is a neurotropic flavivirus with a 10.8kb positive sense, ssRNA genome that encodes 10 mature viral proteins, undergoing a similar viral cycle to that of WNV. While all known strains of ZIKV fall into a single serotype, genetic evidence suggests three distinct lineages: the East African, West African, and Asian lineages (31-33). ZIKV was first isolated in 1947 in the Ziika forest of Uganda from an infected sentinel rhesus macaque, monkey number 766, and subsequently from an infected *Aedes africanus* mosquito (34). After decades of silent and mostly undocumented circulation throughout Africa and Asia, a widespread outbreak occurred in 2007 on the Yap Island in Micronesia, where over 73% of the islands' population is predicted to have been infected with an

Asian lineage ZIKV (35). ZIKV continued to spread outside of Africa and Asia, resulting in widespread outbreaks in the pacific islands between 2013 and 2014, beginning in French Polynesia and spreading to Easter Island, the Cook Islands, Tahiti, and New Caledonia (36-38). By 2015, ZIKV had spread to Brazil, triggering a widespread and ongoing outbreak in the Americas (38).

In December of 2015, ZIKV was first detected within the United States (US) territories, including Puerto Rico where 34,963 cases were confirmed in 2016 (39). This was followed by autochthonous transmission in Florida (218 presumed cases) and Texas (6 presumed cases) in 2016, raising concerns of a ZIKV epidemic in the US (40-42). Although no locally acquired cases have occurred in the US in 2017, the ongoing outbreak in the US territories (502 confirmed cases as of June 7$^{th}$, 2017), along with continued importation of ZIKV through travel associated cases suggest a widespread outbreak remains a significant threat. The primary mosquito vectors of ZIKV, *Aedes aegypti* and *Aedes albopictus*, are also prevalent within the southern US, suggesting sustained autochthonous transmission could be supported (43, 44). The ability of ZIKV to be sexually transmitted is also of concern, providing a transmission route that could be maintained independently of a mosquito vector (45-48). However, the efficiency with which ZIKV can be transmitted through sexual contact during human infection remains unclear and will be important to determine. Continued surveillance, mosquito control measures, and antiviral and vaccine development efforts are necessary to prepare for, and possibly prevent what would be an unprecedented ZIKV outbreak in the US.

***ZIKV is causally linked to birth defects during congenital infection***

While ZIKV infection in immune competent adults generally results in a mild, self-limiting febrile illness, more severe complications have been described, including an association with Guillain-Barré syndrome and severe thrombocytopenia (49-51). ZIKV sparked a public health emergency because of increased incidence of microcephaly in Brazil in 2015, coincident with the emergence of ZIKV. Early studies in presumptively infected pregnant mothers revealed evidence of perinatal transmission and the presence of ZIKV in the amniotic fluid and fetal brain (52, 53). In many cases, *In utero* ZIKV infection corresponded with profound fetal defects, including ocular abnormalities, brain calcifications, cerebral atrophy, microcephaly, and fetal loss (52, 54-56). Non-human primate and murine animal models later confirmed a causal link between congenital ZIKV infection and the development of fetal abnormalities (57-59). Similar to humans, maternal ZIKV infection within murine models results in intrauterine growth restriction, placental insufficiency, *in utero* viral transmission, increased cell death within the fetal brain, and fetal demise (58, 59). The mechanisms leading to transplacental transmission of ZIKV are not fully understood, although recent work has provided valuable insight into potential transmission routes. Whether fetal abnormalities are caused primarily from placental damage, direct effects of viral replication within the fetal brain, or a combination of both is also currently unclear.

***Transplacental transmission of ZIKV***

The ability to cross the placental barrier is a unique feature of ZIKV that is not shared with other known human pathogenic flaviviruses. The frequency in which ZIKV reaches the fetus during human *in utero* infection is not known, but studies in non-human primates suggest it may be fairly common (57, 60). While the primary route of transplacental ZIKV transmission remains unclear, recent work, guided by previous studies with other vertically transmitted viruses, has provided valuable insight into potential mechanisms underlying transplacental ZIKV transmission.

Human chorionic villi, the fetal derived component of the placenta, are composed of a single layer of differentiated and fused trophoblasts, known as syncytiotrophoblasts (STBs). STBs are directly bathed in maternal blood and form an important placental barrier (61, 62). STBs are continually supplied throughout pregnancy by the differentiation of progenitor trophoblasts, known as cytotrophoblasts (CTBs), which underlie the STB layer and also invade into uterine wall and maternal decidua to support placental vascular remodeling (62). Fetal derived placental macrophages, known as Hofbauer cells (HCs), are also found within the chorionic villi underlying the STB layer.

While STBs are relatively resistant to ZIKV infection, HCs support productive viral replication during *ex vivo* infection (61, 63). ZIKV replication within HCs, but not STBs, has been confirmed within placental tissue obtained during *in vivo* human ZIKV infection (64). The less differentiated trophoblasts, CTBs, may also support viral replication (61, 65). Indeed, trophoblasts show

evidence of ZIKV infection within a mouse model of placental transmission, with STBs being less susceptible as compared to less differentiated trophoblastic cell types (58). Amniotic epithelial cells, which are the major cell type of the amniotic membrane that directly encases the fetus, have also been found to support ZIKV replication, suggesting possible spread from infected mother to fetus directly across the amniochorionic membrane (65).

While multiple cell types within the placenta have been shown to support ZIKV replication, the primary route of transplacental transmission still remains incompletely understood. Current work suggests a model whereby ZIKV bypasses the outer trophoblast layer without viral replication within STBs, possible by antibody-mediated transcytosis, transmigration of infected maternal immune cells, or through breaks within the STB layer caused by immune mediated placental damage. Cross-reactive immunity generated after a prior flavivirus infection, such as DENV, may also promote antibody-mediated transcytosis of ZIKV (66). Infection of the invasive CTBs that protrude into the maternal decidua may also be involved. Once through the STB layer, ZIKV then replicates within more permissive cell types, such as CTBs and HCs, and promotes spread to the fetal compartment, potentially through direct infection of amniotic epithelial cells. To fully elucidate the mechanisms of ZIKV transplacental transmission, future work within the murine model will be of use, but must be complemented by studies during human *in utero* infection, and within models that better reflect human pregnancy, such as non-human primates.

***ZIKV targets neuroprogenitor cells in the fetal brain***

Once ZIKV reaches the developing fetus, animal models and studies during human infection suggest that ZIKV primarily replicates within the fetal brain (64). Forebrain-specific human neural progenitor cells (hNPCs) differentiated from induced pluripotent stem cells and maintained as monolayers preferentially support viral replication as compared with undifferentiated pluripotent stem cells and terminally differentiated neurons (67). Pluripotent stem cells differentiated into neural organoids or neurospheres, 3D cultures that are thought to better reflect normal nervous system development, also show evidence of ZIKV infection (59, 68, 69). Most compelling, primary hNPCs acquired from 16-19 weeks of gestation, rather than differentiated *in vitro*, are susceptible to a persistent ZIKV infection (70). Notably, persistence of ZIKV RNA has also been found within human fetal brains during *in vivo* infection, suggesting ZIKV may persist within the fetal NPCs (64).

An intriguing and consistent finding among these different systems is that viral replication within hNPCs promotes apoptotic cell death and growth attenuation, a finding corroborated within murine models (71). Dysregulation of proliferation and cell cycle progression has also been noted during ZIKV infection in hNPCs, human neural organoid culture systems, and within murine infection models (67, 71, 72). ZIKV infection can also promote pre-mature differentiation of hNPCs into neurons, which combined with diminished proliferation and cell death, may further deplete the progenitor cell pool and may promote developmental abnormalities within the fetal brain (73). In contrast to the fetal

brain, neural stem cells (NSCs) are only found in limited quantities within specific regions of the adult brain. However, ZIKV is able to replicate, inhibit proliferation, and induce cell death within adult NSCs following infection within a murine model (74). This raises the possibility that the neurologic sequelae associated with adult ZIKV infection, including Guillain-Barré syndrome, may result from infection of adult NSCs. Nevertheless, the extent to which ZIKV targets NPCs during *in vivo* human fetal or adult infection remains unknown. Future studies will also need to clarify the mechanisms by which ZIKV reaches the developing fetal nervous system following transplacental transmission.

***ZIKV immunity***

Since the emergence of ZIKV in the Americas, significant insight has been made into the critical features of immune control. During the acute phase of human infection, ZIKV induces systemic pro-inflammatory cytokine responses (75). In a STAT2-deficient murine model, notably inflammatory cytokine responses were also found within the brain (76). Despite these findings, the cellular sources of pro-inflammatory responses during ZIKV infection are poorly understood. Human DCs do not secrete pro-inflammatory cytokines or type I IFN following ZIKV infection, suggesting that infected DCs may not be important source of inflammatory cues during *in vivo* infection (77). ZIKV infection in a lung carcinoma epithelial cell line induces IFNβ secretion, while primary human skin fibroblasts up-regulate pro-inflammatory cytokine gene expression during ZIKV infection (78, 79). Embryonic NPCs do not secrete pro-inflammatory cytokines,

despite the presence of persistent virus (70). Similarly, HCs are also poorly immunogenic during ZIKV infection, potentially reflecting imprinting from the tolerogenic environment they normally reside within (61). In contrast, cranial neural crest cells secrete multiple cytokines involved in inflammation and neurogenesis at levels that promote apoptosis and pre-mature neuronal differentiation during ZIKV infection (80). Combined, ZIKV infection can induce pro-inflammatory responses, but does so in a cell type specific manner. A better understanding of how inflammation is regulated within the placenta and developing fetus during ZIKV infection will be critical to understanding viral pathogenesis.

Multiple components of the adaptive immune response have also been implicated in control of ZIKV infection. Infection with ZIKV can induce broadly neutralizing and protective humoral immunity against both African and Asian lineage viruses (33). This suggests the presence of a single ZIKV serotype, which should simplify vaccine design. Antibodies generated against DENV, and to a lesser extent WNV, can cross-react with ZIKV. Despite cross-reactivity, anti-DENV or -WNV antibodies exhibit limited neutralization activity and might promote increased infection through antibody dependent enhancement (ADE) (66, 81). Passive transfer of DENV or WNV convalescent human serum at low treatment doses enhanced ZIKV pathogenesis within a murine model, while higher treatment doses were protective (81). Whether prior infection with DENV and WNV can similarly promote enhanced disease following secondary ZIKV challenge within the same host remains to be determined. It is also unclear

whether anti-DENV or anti-WNV antibodies are present at appropriate physiologic concentrations to mediate ADE during human *in vivo* ZIKV infection. Finally, the effect of ADE on ZIKV pathogenesis within a physiologic setting remains unknown. A better understanding of the *in vivo* relevance of ADE during ZIKV infection of an individual with prior flavivirus exposure, either through natural infection or vaccination, is of significant importance to current DENV and ZIKV vaccination efforts.

CD8+ T cell immunity is critical for protection during ZIKV infection. During the acute phase of infection, ZIKV-specific CD8+ T cells expand and are polyfunctional, exhibiting *in vivo* cytotoxicity (82). Depletion of CD8+ T cells within a murine model where T cells retain functional type I IFN signaling compromises viral clearance from the peripheral and CNS tissue compartments during ZIKV infection. Mice that genetically lack CD8+ T cells also become highly susceptible to lethal ZIKV infection in an anti-IFNAR blocking antibody model of infection. Notably, CD8+ T cells isolated from ZIKV-experienced mice enhance viral clearance when adoptively transferred into naïve animals prior to ZIKV infection. Using a neonatal C57Bl/6 model, CD8+ T cells have also been found to infiltrate into the CNS and may promote neurodegeneration (83). Altogether, this work suggests that a balanced CD8+ T cell responses is required to promote viral clearance without inducing overt immunopathology. Interestingly, recent work suggests that DENV-specific CD8+ T cells can cross-react with ZIKV and promote viral clearance during ZIKV infection of a DENV-immune mouse (84). The presence of protective, cross-reactive CD8+ T cell immunity has important

implications for the development of T cell vaccines that may provide protection against multiple flaviviruses.

**Part 2: Innate immune signaling during WNV and ZIKV infection**

Upon cellular entry and replication of flaviviruses, viral nucleic acids are primarily detected through the concerted efforts of two families of pattern recognition receptors (PRRs): the RIG-I like receptors (RLRs) and the Toll like receptors (TLRs). During viral infection, RLR and TLR signaling promotes antiviral immunity through the induction of pro-inflammatory cytokines (e.g. IL-1β, IL-6, TNF, CXCL8), antiviral effector molecules (e.g. viperin, IFITs, OAS), and type I and III IFN. Much of our understanding of how innate immune signaling programs antiviral immunity during flavivirus infection has relied on studies with WNV, aided through genetic ablation studies within the immune competent C57Bl/6 murine pathogenesis model (20). Similar studies with ZIKV have been hindered by its restricted species tropism and limited viral replication in immune competent mice (85). Consequently, the role of innate immune signaling during ZIKV infection has been mostly inferred from studies with WNV, with notable insights from *in vitro* infection systems. In the following sections, the tissue and cell type specific roles that RLR, TLR, and IFN signaling play in promoting viral clearance and resolution of WNV and ZIKV infection will be discussed in detail.

**A. RIG-I like receptor signaling**

The RLR family consists of the eponymous member RIG-I, as well as MDA5 and LGP2. The RLRs are located within the cytoplasm of nearly every cell of the body and distinguish host from pathogen by recognizing unique structures found within viral RNA (86). RIG-I and MDA5 contain N-terminal caspase activation and recruitment domains (CARDs) that interact with CARDs located within the N-terminus of the central adaptor protein, mitochondrial antiviral signaling (MAVS) (87). LGP2 lacks CARDs and does not signal through MAVS, but instead functions as a regulator of RLR signaling (88). RIG-I preferentially recognizes short dsRNA molecules, while MDA5 has a preference for longer dsRNA molecules (89). Upon ligand binding, RIG-I and MDA5 undergo conformation changes and post-translational modifications, including dephosphorylation and ubiquitination, which fully activate their ability to interact with MAVS (90, 91).

MAVS is localized to the outer membranes of mitochondria, peroxisomes, and mitochondrial associated membranes (MAMs), a subdomain of the endoplasmic reticulum (92, 93). MAVS localization to MAMs is required for signaling for poorly understood reasons, where cleavage and dislocation of MAVS from the MAMs by the NS3/4A protease of Hepatitis C virus abrogates signaling (92). Upon interaction with RIG-I or MDA5, MAVS is thought to undergo CARD-dependent oligomerization, forming large MAVS aggregates that can, *in vitro*, potently activate downstream signaling (94). MAVS recruits members of the TNF receptor-associated factor (TRAF) family, E3 ubiquitin ligase that

polyubiquitinate MAVS and promote the recruitment of NF-kappa-B essential modulator (NEMO), which itself recruits the serine/threonine protein kinases inhibitor of kappa-B kinase epsilon (IKKε) and TANK-binding kinase 1 (TBK1). IKKε and TBK1 phosphorylate and activate the latent transcription factors interferon regulatory factor-3 (IRF-3) and IRF-7, as well as nuclear factor kappa-B (NFκB), through phosphorylation and degradation of inhibitor of kappa-B (IκB). Upon nuclear translocation, IRF-3 promotes transcription production of type I and III IFN and directly activates antiviral effector gene transcription, while NFκB promotes early type I IFN induction and drives pro-inflammatory cytokine production (95-97).

***MAVS is critical for host control of WNV infection***

RLR signaling through MAVS is required for host survival during WNV infection through restriction of viral replication and programming of antiviral immunity (98, 99). During the early post-inoculation and visceral organ dissemination phases of infection, RLR signaling controls viral replication within the lymph nodes and spleen, while limiting infection of splenic DCs (16, 99). Within DCs, MAVS is critical for viral restriction through the induction of type I IFN and antiviral effector molecules (99). RLR signaling dictates viral tropism by restricting viral replication within non-permissive tissues, such as the liver and kidneys. Specifically within the liver, RLR signaling works in concert with type I IFN signaling to regulate protective NK cell responses that ultimately limit viral replication (98).

The lack of viral control in the absence of RLR signaling results in uncontrolled inflammatory immune responses, potentially due to increased viral burden, antigenic load, or tissue damage. Excessive inflammation is associated with increases in type I IFN, pro-inflammatory cytokines, and inflammatory DC populations. CD4+ T cell responses are also dysfunctional, where a lack of RLR signaling compromises Treg expansion in a T cell extrinsic manner, likely a byproduct of the inflammatory milieu (99, 100). Together, this suggests that RLR signaling is not just important for preventing virally induced pathology, but also for limiting viral burden to prevent excessive and damaging immunopathology.

During the neuroinvasive phase of infection, an absence of MAVS results in rapid neuroinvasion and enhanced viral replication within the CNS. Despite increased infiltration of WNV-specific CD8+ T cells into the brain, they are unable to clear virus from the CNS. This suggests that RLR signaling, potentially through programming of DCs, is critical for the generation of functional CNS-infiltrating anti-WNV CD8+ T cells. A neuron-intrinsic role for RLR signaling in restricting viral replication also seems likely, where MAVS-deficient primary cortical neurons exhibit enhanced viral replication due to a failure to induce type I IFN and antiviral effector molecules.

Altogether, RLR signaling through MAVS is essential for restricting viral replication and promoting viral clearance from the periphery and CNS. Restriction of viral replication prevents excessive immune activation and promotes the development of protective Treg responses, which together prevent immunopathology during WNV infection. An intriguing finding has been the cell

type specific roles of RLR signaling in programing anti-WNV immunity. Indeed, recent work using bone marrow chimeras have found that loss of MAVS expression selectively on the hematopoietic compartment is sufficient to enhance viral replication and promote immunopathology (101). Future work will need to further assess the cell intrinsic roles of RLR signaling within myeloid cell subsets (e.g. DCs, macrophages) and lymphocytes (e.g. CD8 and CD4 T cells) during WNV infection.

***Non-redundant roles of RIG-I and MDA5 during WNV infection***

RIG-I and MDA5 play non-redundant functions in controlling WNV infection and immunity, despite signaling through the shared adaptor protein MAVS (102, 103). While RIG-I signaling is required for early control of viral replication and induction of IFNβ, MDA5 is important for induction of IFNα during the late, amplification phase of the type I IFN response (102, 104). During *in vivo* infection, MDA5 is required for viral clearance from the CNS, but mostly dispensable for viral restriction within the periphery (103). MDA5 promotes viral control and induction of antiviral responses within DCs and macrophages, but is dispensable for restriction of viral replication within cortical and cerebellar granule cell neurons (102, 103). Instead, MDA5 signaling limits neuroinvasive disease by promoting efficient priming of CNS infiltrating WNV-specific CD8+ T cells (103). The requirement for MDA5 is T cell extrinsic, suggesting MDA5 signaling programs antigen presenting cells to prime protective anti-WNV CD8+ T cell responses. Future studies using cell specific deletion of MDA5 within DCs are

required to fully clarify the contributions of MDA5 during WNV infection. Despite these insights into the function of MDA5, the contributions of RIG-I during *in vivo* infection are not well understood, in part due to embryonic lethality when genetic ablation of RIG-I is maintained on a C57BL/6 background (105). The generation of cell specific knockout mice may alleviate issues of embryonic lethality and allow the clarification of the specific role of RIG-I signaling during WNV infection.

***RLR signaling during ZIKV infection***

While the role of RLR signaling during ZIKV infection remains poorly understood, a couple recent studies have shed light on their importance. Within primary human DCs, RIG-I signaling potently restricted ZIKV replication, while IFNβ signaling was significantly less effective (77). Despite viral antagonism of type I IFN responses, strong antiviral responses were observed during ZIKV infection in human DCs, including production of multiple antiviral effector molecules. This suggests that RLR signaling may play an essential role in inducing antiviral responses during ZIKV infection through a type I IFN-independent mechanism. In contrast, activation of RLR signaling by ZIKV during infection of neuroepithelial stem cells may result in mitotic arrest and apoptosis due to relocation of phosphorylated TBK1 from centrosomes to the mitochondria (106). Together, this work suggests that while RLR signaling is likely protective during ZIKV infection, RLR activation may have unintended, negative consequences in dividing cells, such as stem and progenitor cells. Future efforts will need to determine the cell intrinsic roles of RLR signaling during ZIKV

infection, including the influence of RLR and other innate immune signaling pathways on the cell cycle of stem and progenitor cells.

## B. TLR and MyD88-dependent signaling

Of the ten TLRs expressed by human cells, only a subset is specialized to recognize viral RNA, including TLR-3, TLR-7, and TLR-8 (107). In contrast to the RLRs, TLR expression is regulated in a cell-type specific manner and nucleic acid sensing occurs within endosomal compartments. Following binding of viral RNA, TLR-7 and TLR-8 signal through the shared adaptor protein myeloid differentiation primary response 88 (MyD88), while TLR-3 employs the adaptor protein TIR domain–containing adaptor-inducing IFN-β (TRIF). Although a central adaptor of TLR signaling, MyD88 is also a critical adaptor downstream of interleukin-1 (IL-1)/IL-1 receptor (IL-1R) signaling.

### *MyD88-dependent signaling restricts WNV replication within the CNS*

MyD88-dependent signaling promotes protection from lethal WNV infection, although MyD88 deficiency is notable less severe than ablation of RLR signaling (108). Signaling through MyD88 is largely dispensable for restricting viral replication during the early post-inoculation and visceral organ dissemination phases of pathogenesis, but is critical for CNS-intrinsic control of viral replication during the neuroinvasive phase. Through MyD88-dependent production of CXCL10 within the brain, viral clearance is promoted through recruitment and infiltration of macrophages and CD8+ T cells. Interestingly, MyD88 signaling also

directly restricts viral replication within cerebellar granule, but not cortical neurons. These findings suggest that MyD88-dependent restriction of WNV neuroinvasive disease is both direct, by blocking viral replication within specific neuronal subtypes, and indirect, through promoting leukocyte infiltration into the CNS.

***IL-1 signaling promotes WNV clearance from the CNS***

During human WNV infection, IL-1β secretion into the serum correlates with the kinetics of viral clearance (109). Murine models have confirmed the importance of IL-1 signaling in control of WNV infection, where deficiencies in different components of the IL-1/IL-1R1 pathway compromise host survival (109). IL-1 signaling is particularly important for CNS-intrinsic viral control, where a loss of IL-1R1 results in defective chemokine production and delayed recruitment of inflammatory immune cells into the CNS. The delayed kinetics of immune cell infiltration promotes enhanced viral burden and triggers excessive inflammation and neuropathology within the CNS. During WNV infection, the major source of IL-1β is from CNS infiltrating macrophages (110). Once secreted, IL-1β induces CXCL12 expression by the cells of the CNS microvasculature and promotes their interaction with CXCR4+ CD8+ T cells. Ablation of IL-1 signaling results in decreased CXCL12 expression, diminished CD8+ T cell interaction with the microvasculature, and excessive infiltration into the CNS parenchyma that promotes immune-mediated neuropathology. These findings suggest that the brain microvasculature, through IL-1β-dependent induction of CXCL12, serve as

a gatekeeper to limit excessive migration of CD8+ T cells into the CNS. IL-1 signaling also plays a critical role in promoting the upregulation of T cell co-stimulatory molecules (CD80, CD86, CD68) on CNS infiltrating DCs, which then provide a critical reactivation signal to CNS infiltrating CD8+ T cells (111). Together, the importance of IL-1 signaling during WNV infection highlights the delicate balance between viral control and excessive neuroinflammation.

***TLR signaling through MyD88 plays a minor role in control of WNV infection***

Mice deficient in TLR-7 have enhanced susceptibility to lethal WNV infection following infection via the intraperitoneal route (112). This was associated with increased viral burden within the systemic circulation and CNS, despite only modest increases within the spleen. Elevated expression of pro-inflammatory cytokine genes was observed within isolated blood leukocytes, with the exception of the IL-12 family members IL-12 and IL-23, both of which were modestly decreased within the circulation and in the brain. Ablation of TLR-7 or IL-23 both resulted in reduced macrophage migration into the CNS, suggesting that TLR-7-dependent production of IL-23 may promote macrophage infiltration into the brain during WNV infection. In contrast to these findings, TLR-7 was dispensable following cutaneous WNV challenge, either through intradermal injection or infected mosquito feeding (113). Combined, these studies suggest that TLR-7 signaling may play only a minor role in restricting WNV infection and programming protective immunity. This may be explained by redundancies

imposed by other innate immune signaling pathways or an absence of appropriate ligands during WNV infection.

While TLR-8 recognizes ssRNA in humans, the murine *Tlr8* gene encodes a protein that fails to respond to agonist stimulation, owing to a 5 amino acid deletion within a putative ligand-binding motif (114). While this initial work led to the conclusion that murine TLR-8 was non-functional, recent studies in *Tlr8*-/- mice have tried to challenge this paradigm. Mice deficient in *Tlr8* have elevated expression of TLR-7 and develop a TLR-7-dependent spontaneous autoimmunity, suggesting that in mice, TLR-8 may have a role in regulating TLR-7 responses (115). During murine WNV infection, TLR-8 promotes WNV infection by binding to suppressor of cytokine signaling 1 and dampening TLR-7-induced antiviral immunity (116). Whether human TLR-8 serves a dual role in virus sensing and as a regulator of TLR-7 remains unknown.

***TLR-3 plays a CNS-intrinsic role during WNV infection***

Conflicting reports exist on the role of TLR-3 during WNV infection (117-119). Early work implicated a pathogenic role for TLR-3, where ablation of TLR-3 promoted increased survival (119). TLR-3-induced pathology was attributed to excessive inflammation and enhanced blood brain barrier (BBB) permeability. A more recent study re-evaluated the role of TLR-3 during WNV infection and, in contrast, found TLR-3 played a protective role during WNV infection (118). TLR-3 signaling was dispensable for type I IFN responses and viral control within the peripheral compartment and within DCs and macrophages. Despite unaltered

BBB permeability, WNV spread more rapidly into the brain and spinal cord in the absence of TLR-3. Indeed, TLR-3 restricted WNV encephalitis in a CNS-intrinsic manner, where expression in cortical neurons was critical for restriction of viral replication. Combined, these findings suggest that TLR-3 plays a cell-type specific role during the neuroinvasive phase of WNV infection by restricting WNV replication within neurons.

***TLR-3 signaling limits neuroprogenitor growth during ZIKV infection***

While little is known about the contributions of TLR-3 signaling during ZIKV infection, a recent study argues for a potentially pathogenic role within NPCs (68). In this study, ZIKV replication within human cerebral organoid cultures was associated with decreased organoid size. Similar attenuated growth was also observed following treatment with poly(I:C), a non-specific agonist that can activate TLR-3 and RLR signaling (68, 89). Treatment of ZIKV-infected organoids with a specific TLR-3 inhibitor partially reversed the growth attenuation. Combined, these findings suggest TLR-3 signaling might play a pathogenic role in NPCs by promoting growth attenuation, potentially through regulation of pathways involved in apoptosis and neurogenesis. More rigorous study is needed to validate a role for TLR-3 signaling in regulating neural progenitor growth and apoptosis, including the use of genetic ablation and *in vivo* studies.

## D. Type I IFN signaling

### *Type I IFN signaling restricts WNV infection*

Type I IFN signaling is required for control of viral replication, restricting tissue tropism, and promoting survival during WNV infection (120). Genetic ablation of the type I IFN receptor results in rapid mortality, even with low infectious doses of WNV. A selective loss of IFNβ also severely compromises host control of WNV infection, although less severe than ablation of all type I IFN signaling (121). Interestingly, type I IFN signaling selectively on myeloid cells is required for control of viral replication and preventing lethal disease (16). When either DCs or macrophages selectively lack type I IFN signaling, viral replication is unrestricted, leading to a MAVS-dependent viral sepsis. Type I IFN signaling also promotes functional CD8+ T cell responses late during infection by preventing T cell exhaustion and dysfunction (122). Further highlighting the critical importance of type I IFN signaling for restriction of WNV replication, pathogenic strains of WNV differ from non-pathogenic strains in their ability to antagonize type I IFN signaling (123). Indeed, non-pathogenic strains of WNV promote lethal infection in the absence of type I IFN signaling.

### *Deficiency in type I IFN signaling as a mouse model for ZIKV infection*

Immune competent mice are not permissive to efficient viral replication, generating minimal viremia or disseminated infection (85). Antibody blockade of the type I IFN receptor enhances peripheral viral replication, but is not sufficient to promote severe neuroinvasive disease. A genetic deficiency in type I IFN

signaling shifts the balance to sustained viral replication and disseminated disease, promoting spread to the CNS and lethal infection (85, 124). A combined deficiency in type I and II IFN, as well as a loss of STAT2 can also promote efficient viral replication, neuroinvasion, and lethality (124, 125). Mice that are triply deficient in IRF-3, IRF-5, and IRF-7, and therefore produce minimal type I IFN, are also highly susceptible to lethal ZIKV infection (85). The lack of efficient viral replication in type I IFN-sufficient mice may be explained by the inability of ZIKV to antagonize murine STAT2, contrasting with the ability of ZIKV to target human STAT2 for degradation (126). While the IFN-deficient murine model has been of tremendous use, an immune competent small animal model of ZIKV infection is needed to better understand viral pathogenesis and the contributions of innate immune signaling to control of ZIKV infection.

**E. Type III IFN signaling**

The interferon lambda (IFNλ) family, also known as type III IFN, consists of four members, IFNλ1 (IL-29), IFNλ2 (IL-28A), IFNλ3 (IL-28B) and IFNλ4, and signal through a heterodimeric receptor (IFNLR) composed of interleukin-10 receptor β (IL-10Rβ) and IFNLR1 subunits (127, 128). Despite having a unique receptor, IFNλ signaling overlaps notably with that of type I IFN in the signaling proteins employed and the transcriptional programs induced. The most apparent divergence between type I and III IFNs is at the level of tissue receptor expression. The type I IFN receptor subunits, IFNAR1 and IFNAR2, as well as the IL-10Rβ subunit of the type III IFN receptor exhibit widespread expression,

while expression of the IFNLR1 subunit is restricted predominately to epithelial cells (127). Type III IFN signaling therefore has its most profound antiviral activity at barrier surfaces, including the respiratory tract, liver, skin, gastrointestinal tract, and the BBB.

***Type III IFN signaling regulates BBB permeability during WNV infection***

During WNV infection, IFNλ signaling limits viral burden specifically within the CNS, despite no appreciable role in direct restriction of viral replication or programming of antiviral immunity (129). The protective effect of IFNλ occurs through tightening of BBB integrity, where type III IFN signaling modulates tight junction protein localization and decreases virus movement across the BBB to limit WNV neuroinvasion. These findings suggest that antiviral therapy with IFNλ may have promise for the treatment of neurotropic viral infections, especially given the restricted IFNLR expression and potential for fewer side effects as compared with type I IFN therapy.

***Type III IFN signaling protects human placental trophoblasts from ZIKV infection***

Primary human STBs are resistant to ZIKV infection, contrasting with the permissiveness of human trophoblastic cell lines (63). Constitutive secretion of IFNλ1, and to a lesser extent IFNλ2, by STBs corresponds with their ability to restrict ZIKV replication. Treatment of permissive cells with conditioned media obtained from STBs also blocks ZIKV replication in a manner that partially

depends on the activity of IFNλ1 and IFNλ2. In contrast, less differentiated trophoblastic cells, CTBs, supported delayed and limited viral replication, and did not secrete detectable IFNλ1 secretion during ZIKV infection (61, 65). This suggests that type III IFN may serve a protective role in restricting ZIKV replication within the placenta, but further study is needed to clarify potential cell type specific roles within the placenta.

## Part 3: Systems biology approaches unravel the host antiviral response[1]

### A. The antiviral landscape

Following pathogen recognition, a series of well-orchestrated and dynamic immune responses are triggered, resulting in the rapid generation of antiviral effectors and pathogen-specific responses. The central function of these responses is to restrict viral replication and spread to neighboring uninfected cells, ultimately promoting viral clearance. Conventional approaches for investigating antiviral responses have focused on defining the mechanism of action for either a single or closely related set of genes through experimental perturbation-based studies. However, these approaches often overlook the complexities and redundancies built into the antiviral host response, providing only a narrow viewpoint. Holistic approaches, such as systems biology, instead provide a comprehensive understanding of the host response during viral

[1] This section was published in Virus Research as: “Bowen JR, Ferris MT, Suthar MS. Systems biology: A tool for charting the antiviral landscape. Virus research. 2016;218:2-9. Epub 2016/01/23. doi: 10.1016/j.virusres.2016.01.005. PubMed PMID: 26795869; PubMed Central PMCID: PMC4902762.” The content is reproduced here in whole with permission from the publisher.

infection. One of the major features of this approach is that it considers the biological system as a whole, providing a powerful tool for the unbiased and thorough analysis of the antiviral response. A unique feature of systems level approaches is their ability to reveal emergent properties that are only evident when considering the system as a whole, rather than focusing on the individual components of a system. Through this type of approach, computational and network analyses are integrated into predictive models that can be experimentally tested and refined through an iterative process. We have referred to this latter step as “biological validation” and consider it to be an integral component of any systems biology based investigation (130). The use of systems level approaches complements and guides conventional studies by revealing novel host molecules or pathways. The scope of systems biology based studies can be designed to span the organism, tissue, and cell levels, probing distinct but complementary compartments of the host response (Figure 1). We feel that it is beneficial to use the term “antiviral landscape” to represent the entire defense response process, from the onset of viral infection to clearance. In this review, we will highlight recent studies that have employed systems biology based approaches to unravel the host antiviral response, focusing on transcriptional profiling studies from whole tissues, heterogeneous cell populations, and single cells.

**B. Organism level**

Epidemiological and clinical studies have revealed that host genetics strongly influences immunity and disease severity in response to viral infection. Studies in humans infected with WNV have identified single nucleotide polymorphisms (SNPs) within *CCR5R*, *MX1*, *IRF3*, and *OAS1* as strong risk factors for enhanced susceptibility and disease severity (131, 132). Similarly, genetic risk factors have been identified for hepatitis C virus (133), Human immunodeficiency virus (134), Influenza virus (135), and other human viral pathogens. However, human genetic studies are often confounded by variable environmental factors, lack of genomic data, and difficulty in dissecting the mechanisms of a causal genetic variant on a complex trait. Inbred mouse strains have proven to be tractable models for studying viral pathogenesis. Indeed, the initial development and refinement of systems biology approaches focused on simple perturbations of classic inbred systems, such as the discovery of *Serpine-1* and the larger urokinase pathway in driving SARS-coronavirus lung injury and pathogenesis (136). While inbred mouse strains are more tractable models for studying viral pathogenesis, they often overlook the complex genetic traits that influence disease and symptomatic infection outcomes in humans. To overcome these challenges, the highly genetically diverse Collaborative Cross (CC) recombinant inbred (RI) mouse panel was generated to identify, characterize, and dissect the mechanisms of naturally occurring genetic variants (e.g. genes and gene networks) that influence diverse clinically relevant traits (137-148), including susceptibility to fungal (149), bacterial (150) and viral infections (151-

156). The CC is a multi-parental RI panel derived from eight inbred mouse strains (5 classic laboratory strains, and 3 wild-derived strains from the 3 major *Mus musculus* subspecies: *musculus, domesticus* and *castaneus*), and has >45 million naturally occurring polymorphisms (SNPs, small insertions/deletions) segregating uniformly across the genome, with minor allele frequencies of >12%, and averaging six distinct haplotypes per locus (157, 158). The generation of the CC lines eliminated long-range linkage disequilibrium within this population, removing the risk of identifying spurious associations between phenotype and genotype that plague other resources (*i.e.* no population structure) (157, 159). Furthermore, removal of long-range linkage disequilibrium breaks apart co-adapted gene complexes, resulting in the emergence of extreme phenotypes driven by epistatic interactions, such as in the development of novel models of spontaneous colitis (148) and Ebola hemorrhagic disease (160). Thus, the CC accurately mimics the complexity of genetic diversity seen within human populations and models how natural variants at loci, as opposed to the extreme abrogation that genetic knockouts create, lead to variations in phenotypes and disease outcome. The CC shows promise of bridging an important gap between mouse models and human disease, providing a useful resource for studying basic aspects of pathogenesis and serving as a platform for antiviral and vaccine development.

***Host genetics impacts Influenza A Virus pathogenesis***

Host genetics is believed to influence Influenza A virus (IAV) pathogenesis in humans, however these findings have either been correlative and unable to show direct causal relationships, or identify rare mutations found within the human population (161-164). To better model the impact of genetic diversity in influencing viral pathogenesis during IAV infection, Ferris et al (151) infected a panel of different incipient CC mice (the preCC) with IAV. A diverse range of phenotypic traits was observed, including emergent phenotypes not present within the infected founder lines, such as high viral replication with low weight loss and inflammation, as well as significant weight loss despite a lack of viral replication. Transcriptional profiling revealed that several phenotypic disease traits, including weight loss and airway inflammation, correlated with transcriptional networks corresponding to immune and inflammatory processes, suggesting a direct relationship between disease severity and genetic variation within the host response. A major strength of the CC model is the ability to track phenotypic traits back to specific genetic loci using quantitative trait locus (QTL) mapping. When combined with gene expression data (e.g. qPCR or RNAseq), genetic markers in the genomic DNA (e.g. SNPs) can be correlated to RNA transcript levels, identifying expression QTLs (eQTLs) that provide a link between genomic sequence variation and the regulation of gene expression. In this paper, several QTLs correlated with disease traits following IAV infection, including *Mx1*, a known antiviral effector gene with potent activity against IAV. Genomic sequencing of *Mx1* exons across the CC founder strains led to the discovery of a

novel allelic variant that provided protection from virus-induced weight loss, but had reduced ability to inhibit viral replication. eQTL analysis revealed that several sets of transcripts related to inflammatory and immune processes were decreased in CC mice containing this novel *Mx1* allelic variant, suggesting decreased levels of immunopathology as a potential explanation for the reduced weight loss following IAV infection. Several of the QTLs correlating to disease traits did not contain known antiviral effectors and may contain unidentified genetic factors that influence IAV infection outcome in humans. Importantly, this group identified “reactive” transcriptional networks that were dependent on genetic variants at specific loci, in particular describing three unique transcriptional profiles derived from different *Mx1* variants. Further implementation of this model across pathogenic and nonpathogenic influenza strains has the potential to drive discovery of novel host determinants of IAV pathogenesis, including potential therapeutic targets.

***Modeling determinants of symptomatic West Nile Virus infection***

The diversity of infection outcomes occurring during IAV infection is not unique, but instead a common feature with most human viral infections. Following infection with the neurotropic Flavivirus West Nile virus (WNV), 80% of cases present as asymptomatic with the remaining 20% of symptomatic cases ranging in severity from a mild febrile illness to severe encephalitis and death (13, 165, 166). In contrast to human disease, the predominant model for studying WNV infection has utilized C57BL/6J mice, where 100% of infected mice develop

neuroinvasive disease (99, 111, 118). Recently, Graham et al (165) challenged a cohort of F1 crosses of CC (CC-F1) mice with WNV and found that infection mirrored human disease phenotypes, with clinical scores stratifying mice into asymptomatic and symptomatic groups. The asymptomatic group could be further subcategorized based on the presence or absence of immune system involvement within the central nervous system (CNS), the former representing a previously unappreciated and emergent disease outcome. Analysis of innate immune responses revealed a correlation between sustained *IFNβ* and *IFIT1* expression during symptomatic disease and confirmed a previously appreciated role for genetic diversity in the *Oas1* gene in disease outcome (131). Diverse adaptive immune responses were also observed, including elevated CNS CD4+ regulatory T cells in one of the CC lines exhibiting asymptomatic disease, further highlighting the complexity of host genetics and immune regulation. While the determinants of symptomatic WNV infection remain poorly understood, this work has identified CC mouse lines with divergent infection outcomes (asymptomatic and symptomatic) that can be further studied to define host novel factors contributing to WNV pathogenesis.

***Development of an improved small animal pathogenesis model for Ebola Virus infection***

Mouse-adapted Ebola virus (EBOV) is lethal in mice, but they fail to develop the hemorrhagic fever syndrome observed during human disease. The lack of a small animal model for EBOV hemorrhagic fever has been a major

obstacle for advancing our understanding of EBOV pathogenesis and developing antiviral therapeutics. Recently, Heinz Feldmann and Michael Katze employed the CC to better understand the impact of host genetics on EBOV pathogenesis (160). Using a mouse adapted EBOV, infection of CC-F1 cohorts resulted in diverse outcomes ranging from complete protection from lethal disease ("resistant") to mice that succumbed, developing hemorrhagic fever-associated pathology prior to death ("susceptible"). The spectrum of disease phenotypes across the screened lines parallels observations in the human population during the 2014 EBOV outbreak in West Africa (167, 168), highlighting the potential of the CC to model human EBOV infection. Virologic comparison of a representative susceptible and resistant CC line revealed that, despite similar levels of EBOV genomic RNA, there was a significant increase in the production of infectious virus from the spleens and livers of susceptible mice. This was accompanied with widespread infection of hepatocytes in susceptible mice. In contrast, the livers of resistant mice exhibited restricted infection of endothelial and Kupffer cells. Transcriptional profiling of susceptible livers uncovered enrichment for genes and pathways correlating to vascular integrity, endothelial activation, and inflammation. In particular, a regulatory network centered on the endothelial kinase *Tek*, a regulator of coagulation, was found to correlate with disease severity: susceptible mice exhibited diminished expression of this *Tek*-centered network relative to naïve mice, while resistant mice had elevated expression. Interestingly, these CC-F1 animals shared one *Tek* allele with each other, while their other *Tek* alleles came from divergent subspecies, again

highlighting how divergent phenotypic outcomes can often derive from breaking apart co-adapted gene networks from divergent mouse subspecies. Further studies are needed to define the relevance of *Tek* and other positively correlating genetic loci with disease severity during human EBOV infection. Nonetheless, this work exemplifies the utility of the CC genetics resource to identify novel platforms for new viral pathogenesis models and small animal models for developing therapeutics.

**C. Tissue level**

***Transcriptomics uncovers determinants of West Nile virus tissue tropism***

WNV infects a broad range of cell types and tissues (13). The spleen is the primary permissive tissue during the visceral organ stage of WNV infection, while the liver is non-permissive to infection (98). RIG-I like receptor (RLR) signaling through MAVS and type I interferon (IFN) receptor (IFNAR) signaling are critical for protection during WNV infection (16, 98, 99, 121). To better understand the contributions of these pathways in dictating viral tropism, Suthar et al (98) infected WT, *Mavs*-/-, *Ifnar*-/-, and *Mavs*-/-*Ifnar*-/- double knock out mice with WNV and performed transcriptomics on permissive (spleen) and non-permissive (liver) tissues. Through an integrated approach, molecular signatures were defined for RLR and type I IFN signaling and used to dissect their individual contributions to host antiviral immunity during WNV infection. Network analysis revealed that RLR and type I IFN signaling trigger strong antiviral immune responses that restrict viral replication within the liver. Infected livers were also

selectively enriched for pathways associated with natural killer (NK) cell responses, uncovering a previously unappreciated protective role for NK cells during WNV infection. Biologic validation studies revealed expansion and activation of hepatic NK cells during WNV infection in a RLR and type I IFN signaling dependent manner, supporting a role for NK cell responses in restricting viral tropism within the liver. This study explored the antiviral landscape during WNV infection, uncovering critical roles for RLR and IFN signaling in dictating tissue permissiveness to infection and identifying a previously overlooked role for NK cells in dictating viral tropism within the liver.

***Transcriptomics enhances our understanding of severe Influenza A virus infection***

In immune competent individuals, infection with different strains of Influenza A virus (IAV) ranges in disease severity from mild (e.g. H3N2 seasonal strains) to severe (e.g. H5N1 and H7N9). The host factors that influence the development of these divergent disease outcomes are incompletely understood. To clarify the contributions of host immunity to disease severity during IAV infection, Ron Germain's group employed a top-down approach analyzing whole tissues and isolated cell populations from C57BL/6 mice infected over a time-course with a non-lethal strain of IAV (Tx91) and PR8 at both sub-lethal and lethal doses (169). Whole lung transcriptomics revealed similar activation of antiviral and type I IFN pathways under all infection conditions. In contrast, a unique molecular signature emerged during lethal PR8 infection that was

characterized by an early and increased enrichment for a group of genes associated with pro-inflammatory signaling pathways (e.g. neutrophil chemotaxis, NFκB, IL-1, IL-6, and TNF signaling pathways). This “fatal molecular signature” was also associated with decreased enrichment for gene clusters associated with pulmonary homeostasis and repair, consistent with the enhanced lung pathology observed during severe infection. Integration of whole organ immune profiling and transcriptomics on sorted cell populations revealed that all subpopulations of cells analyzed within the lung microenvironment contributed to the induction of antiviral and type I IFN pathways. In contrast, neutrophils were uniquely enriched for the pro-inflammatory gene clusters found with a “fatal molecular signature”. Consistent with this observation, enhanced lung infiltration of neutrophils was observed during lethal infection and partial neutrophil depletion provided a dose-dependent enhancement in survival. An integrated analysis of transcriptomes between sorted cells and whole lung immunohistochemistry revealed that neutrophils serve as a predominate source of chemotatic signals that promote neutrophil influx. Virologic analysis found that despite similar rates of viral replication during lethal and non-lethal infection, the former was associated with enhanced viral spread within the lung. Taken together, this integrated systems biology approach revealed that lethal disease outcome was associated with enhanced viral spread, leading to an early pro-inflammatory response in the lung that acts on neutrophils to trigger an inflammatory feed-forward circuit to promote pathologic neutrophil infiltration and fatal pulmonary damage.

While mice serve as a useful IAV pathogenesis model, studies in less evolutionarily distant non-human primates (NHPs) are thought to more closely model human disease (170). To better understand host determinants of severe IAV infection, Kawaoka's group infected rhesus macaques with clinical isolates of H5N1 that had caused mild or severe disease in human patients (171). While NHPs are a better model of human IAV pathogenesis, they are expensive and difficult to manipulate experimentally. To overcome these limitations and best capture the antiviral landscape, transcriptomics of bronchial brush samples was performed. Several modules, or sets of genes with similar co-expression patterns, were identified as being differentially expressed during mild and severe infection. The enrichment for a subset of these modules correlated directly with viral titers, identifying potential virus-dependent transcriptional networks. The gene sets comprising these modules were associated with immune-related processes, including inflammatory cytokine production and antiviral responses. Animals with severe disease outcomes were found to diverge from those with mild disease by having weak activation of these modules early during infection, followed by strong activation at later points during infection. These findings support a model where a lack of early viral control results in uncontrolled viral replication and immune activation.

Through the use of systems biology approaches spanning the tissue to cell levels, these papers establish a pathogenic role for excessive inflammation as a determinant of severe IAV infection in both murine and NHP pathogenesis models. This model is further reinforced by similar transcriptomic studies using

the reconstructed 1918 IAV, highlighting the power of systems biology to illuminate the antiviral landscape (172, 173). Finally, recent transcriptional profiling of monocyte derived dendritic cells following infection with seasonal or pandemic strains of IAV uncovered a molecular signature that was found to be enriched in blood samples from individuals with symptomatic, but not asymptomatic IAV infection (174). This further highlights the utility of systems biology approaches to identify disease specific molecular markers of clinical relevance.

***Transcriptomics defines human antiviral immunity to Dengue Virus***

Dengue virus (DENV) is a mosquito borne Flavivirus that is responsible for nearly 100 million infections worldwide. While monocytes and dendritic cells are early target cells of viral replication (175, 176), very little is known about the early innate immune response following human DENV infection. Given the inherent lack of manipulability in human subjects, mechanistic studies remain difficult to perform. Recently, Marcin et al (177) overcame these limitations through the use of whole blood transcriptomics, defining the antiviral landscape during acute DENV infection in humans. PBMCs from patients acutely infected with DENV displayed distinct transcriptional profiles when compared to healthy DENV seronegative controls. Gene expression patterns segregated into distinct clusters that correlated with viral load, but were independent of disease severity. Pathway analysis of top ranked genes correlating with high viral load revealed enrichment for inflammatory and innate immune pathways, suggesting viral load directly

impacts innate immune signaling. Conversely, top ranked genes correlating with low viral load revealed enrichment for stress-response related genes, including XBP-1 and associated target genes, as well as genes related to plasmablast differentiation. At the cell level, transcriptional and immune profiling revealed an expansion of CD14+CD16+ intermediate monocytes during acute DENV infection. *Ex vivo* DENV infection of monocytes isolated from healthy human donors promoted the generation of CD14+CD16+ intermediate monocytes with a potent ability to drive plasmablast differentiation and antibody production through the secretion of BAFF, APRIL and IL-10. Given the prominent plasmablast expansion observed during human DENV infection (178), these results implicate an intriguing role for CD14+CD16+ intermediate monocytes in the development of humoral immunity against DENV.

**D. Cell level**

***Single cell transcriptomics***

High-throughput genomic technologies have been invaluable tools for studying antiviral responses in recent years. While these approaches have provided novel insights into viral pathogenesis and immune signaling pathways, they have been limited to measurements from whole tissues or bulk cell populations, and thus have masked gene expression differences between infected and bystander cells. Conventional approaches to overcome this limitation have included comparison of responses between cells infected at low and high MOIs, using recombinant viruses expressing a reporter gene (e.g.

fluorescent protein) to identify or enrich for infected cells, or enriching for RNA from virally infected cells (179). Despite their historical utility, interpretations from these studies are confounded by the introduction of experimental artifacts (e.g. use of modified viruses, infection of cells with high virus doses). Recent technological advances in microfluidics and nucleic acid amplification technologies now allow for high-resolution gene expression analysis at the single cell level using qPCR (e.g. Fluidigm BioMark HD) and RNAseq (e.g. Illumina HiSeq 2000) (180). Additionally, the development of novel approaches, including droplet-based technologies (i.e. Drop-seq) (181), has increase the ease and affordability of generating single cell sequencing libraries. While these technologies have recently been utilized to characterize the heterogeneity in gene expression within individual cells in the context of embryonic development (182), cancer (183), and immunology (163, 184-186), these approaches have remained underutilized in the study of virus-host interactions.

***Single cell RNAseq reveals bimodal expression of immune response genes in dendritic cells***

Previous measures of antiviral responses within bulk DC populations have overlooked the heterogeneity present within this seemingly homogenous cell population. To determine the contributions of individual DCs to the overall antiviral landscape, Aviv Rigev's group treated bone marrow derived DCs (BMDCs) with prototypical pathogen associated molecular patterns, strong stimulators of DC activation, and performed RNAseq on isolated single cells

(185, 186). Surprisingly, transcriptomes from individual cells revealed bimodal transcript expression for subsets of genes involved in immune responses. While some of the divergence in cellular gene expression could be correlated to the developmental stage of the BMDCs, the remaining differences correlated with differential activation of *Irf7* and *Stat2* dependent regulatory networks. When observed over a 6 hour period, a small subset of “early responder cells” activated antiviral signaling and type I IFN production within the first hours of stimulation. The remaining cells were “late responders” and required cell-to-cell communication and type I IFN-signaling to activate antiviral responses, suggesting activation by type I IFN produced by “early responder cells”. While these findings highlight the individual contributions of single cells to the antiviral landscape, further work is needed to extend these findings to *in vivo* viral infection, using freshly isolated cells from infected tissues. The bimodal expression patterns of transcripts raises the question of whether genes that are lowly expressed at the population level are highly expressed within a small subset of cells and may play a greater importance than previously appreciated.

***Single cell analysis reveals subversion of type I IFN production in infected and bystander cells during rotavirus infection***

Rotavirus (RV) causes severe diarrheal disease following infection of absorptive villous enterocytes within the small intestine, replicating to high titers despite an intact type I IFN response (187). While RV is known to suppress the type I IFN response, the exact mechanisms of viral evasion during *in vivo*

infection remain unclear. To clarify how rotavirus evades host immunity, Harry Greenberg's group analyzed viral and host gene expression in single enterocytes isolated from naïve or murine rotavirus infected mice. Striking transcriptional heterogeneity existed between cells, which could be segregated into "enterocyte$^{lo}$" and "enterocyte$^{hi}$" populations based on low or high expression of enterocyte related transcripts, respectively. The enterocyte$^{hi}$ population from naïve mice displayed high levels of type I IFN transcripts, revealing that a small subset of enterocytes are responsible for maintaining homeostatic levels of type I IFN within the healthy gut. Rotavirus preferentially infected the enterocyte$^{hi}$ population and resulted in decreased type I IFN expression, while failing to trigger type I IFN production in the enterocyte$^{lo}$ population, consistent with the ability of rotavirus to antagonize type I IFN induction. Despite diminished type I IFN transcription within enterocytes, analysis of gene expression within the bulk intestine and sorted cell populations revealed type I IFN transcription is induced during RV infection by hematopoietic cells. Inhibition of NFκB, but not IRF-3, dependent transcription occurred following RV infection, suggesting that RV inhibits NFκB activation to prevent type I IFN production in infected enterocytes. To put these findings into context of the whole organism, S*tat1*$^{-/-}$ mice, which are deficient in type I and II IFN signaling, were infected with murine or simian RV, a heterologous strain whose efficient replication requires a type I IFN signaling deficiency. Heterologous RV infection triggered stronger NFκB activation within the bulk intestine as compared to murine RV, despite equivalent activation of IRF-3 dependent responses. This correlated with higher type I IFN transcription

within the intestines of heterologous RV infected mice, further suggesting that murine RV inhibits NFκB signaling to prevent type I IFN induction and promote viral replication. Thus, single cell transcriptional profiling uncovers a model where murine RV antagonizes NFκB mediated transcription of type I IFN in infected enterocytes, allowing for viral replication despite type I IFN production by intestinal hematopoietic cells.

***Outlook for the coming age of single cell analysis***

Further work is needed to better understand antiviral signaling within infected and bystander cells in the context of other relevant human viral infections using primary cells. Implementation of single cell analysis has the potential to identify novel mediators of the host response that may have low transcript expression within infected cells and have been overlooked in whole tissue or bulk cell analyses. Moving forward, it will be critical to determine the sensitivity of primer sets designed to detect viral RNA and replication intermediates to ensure reliable discrimination between infected and bystander cells. To maintain a holistic view, single cell approaches will require integration with bulk cell, whole tissue, and organism level analyses, thus providing a more complete view of the antiviral landscape at each level of complexity. The recent development of a droplet-based single cell RNAseq platform (i.e. Drop-seq) will be an invaluable tool for bridging tissue and cellular level analyses. For example, Drop-seq could be applied to profile the host response within specific cell populations of a virally infected spleen at single cell resolution. A comparison

with transcriptional profiling of sorted bulk cell populations and whole spleens would reveal the cell specific contributions to developing the antiviral landscape, while highlighting nuances to the response that may be lost within bulk measurements. Finally, existing platforms for analyzing protein expression at single cell resolution (188), along with recent technological advances in single cell ChIP-Seq (189), will allow for integrated analyses of individual cells at the epigenetic, transcript, and protein levels.

**E. Conclusion- Systems biology as a tool to chart the antiviral landscape**

Conventional approaches have been instrumental to our understanding of virus-host interactions, but new holistic approaches, such as systems biology, are necessary to appreciate the entire scope of the antiviral response. Moving forward, integration of systems biology technologies is required to comprehensively chart the antiviral landscape, combining findings from transcriptomic, proteomic, metabolomic, epigenetic, and single cell analyses into predictive models of the antiviral response. The importance of systems integration was recently highlighted by the observation of notable discordance between transcript and protein levels in peptide-stimulated antigen specific CD8+ T cells (190). Despite the utility of systems biology approaches, a notable challenge has been the extraction of meaningful information from the extensive data sets that are generated. The implementation of current and novel computation methods are required to identify and prioritize lists of top candidate molecules and signaling pathways to help drive hypothesis generation. A critical

next step is experimental testing and refinement of predictive models, a too often overlooked process referred to as biologic validation. Further application of systems biology approaches will allow for the dissection of antiviral responses within traditionally difficult to study cell populations, such as rare primary cells and human clinical samples, allowing for a much needed enhanced understanding of cell type specific antiviral responses. Finally, systems biology approaches have the potential to redefine the field of personalized medicine, allowing treatment and vaccination strategies to be designed with host genetics in mind (191). In summary, the continued implementation of systems biology approaches will be essential for improving out understanding of viral pathogenesis and antiviral immunity, revealing novel targets for therapeutic and vaccination strategies.

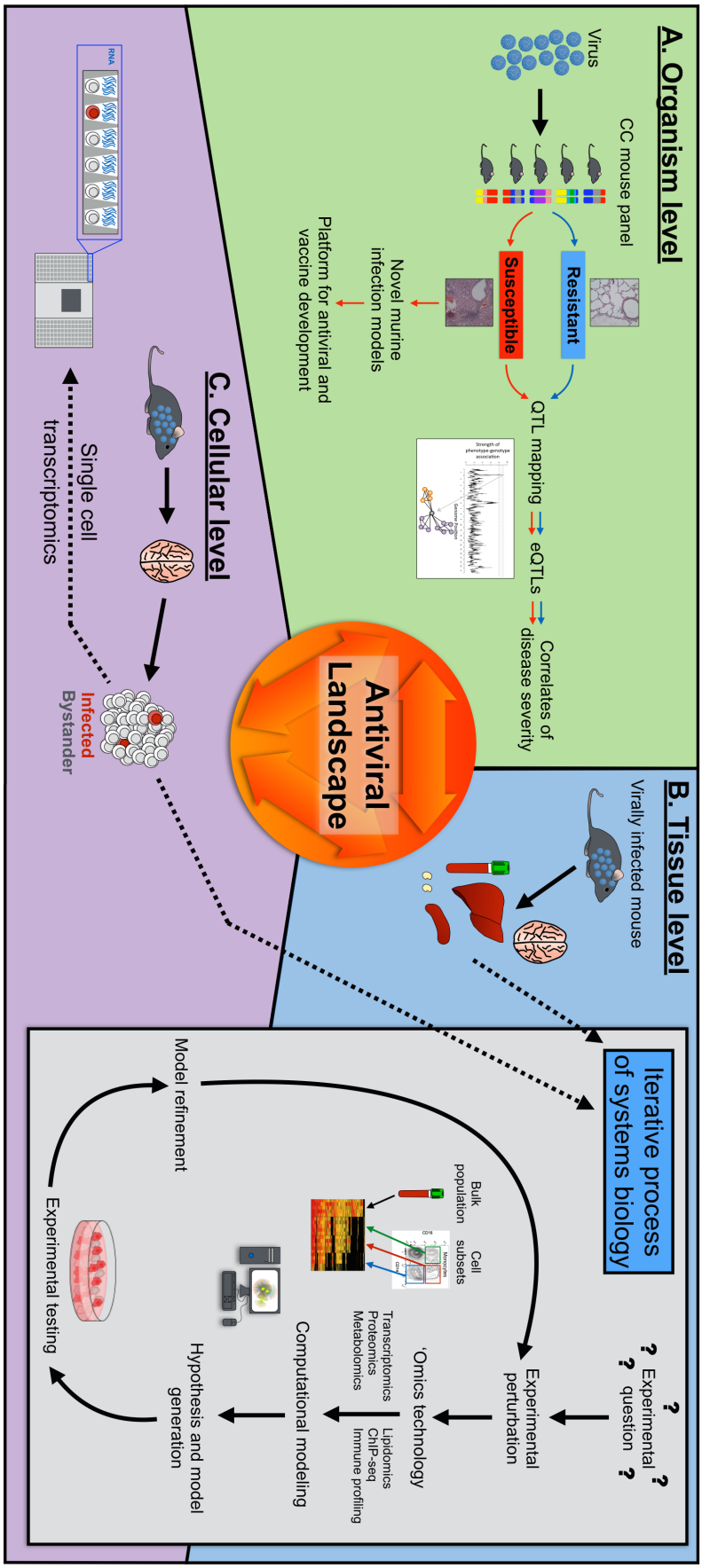
A. Organism level
Virus
CC mouse panel
Resistant
Susceptible
Novel murine infection models
Platform for antiviral and vaccine development
QTL mapping
eQTLs
Correlates of disease severity
B. Tissue level
Virally infected mouse
Iterative process of systems biology
? Experimental question ?
Experimental perturbation
'Omics technology
Transcriptomics
Proteomics
Metabolomics
Lipidomics
ChIP-seq
Immune profiling
Bulk population
Cell subsets
Computational modeling
Hypothesis and model generation
Experimental testing
Model refinement
Antiviral Landscape
C. Cellular level
Single cell transcriptomics
RNA
Infected
Bystander

**Figure 1. Systems biology: a tool for charting the antiviral landscape.** Systems biology can be employed to unravel the antiviral response at the organism (A), tissue (B), and cellular (C) levels of complexity. At the organism level (A), viral infection of a panel of collaborative cross mice probes the influence of genetic diversity on antiviral responses, identifying correlates of disease severity and improved small animal infection models. At both the tissue (B) and cellular levels (C), systems biology approaches can be utilized to uncover novel aspects of the host antiviral response through an iterative process of experimentation and computational modeling. Finally, emerging breakthroughs in single cell transcriptomics (C) can differentiate between infected and bystander cells, uncovering previously overlooked cell-specific differences in the antiviral response.

**CHAPTER 2.**

# Systems biology reveals West Nile virus antagonism of STAT5 signaling during infection of human dendritic cells

James R. Bowen, Matthew G. Zimmerman, Circe E. McDonald, Bali Pulendran, Mehul S. Suthar

The work presented in this chapter is in preparation for submission to *PLoS Pathogens*

## 2A. Abstract

West Nile virus (WNV) is a neurotropic flavivirus and the leading cause of mosquito-borne encephalitis in the United States. Studies in humans have found dysfunctional T cell responses correlate with the development of severe WNV neuroinvasive disease, however, the contributions of human dendritic cells (DCs) in priming T cell immunity remains poorly understood. Here, we utilized primary cells to demonstrate that human monocyte-derived DCs (moDCs) support productive viral replication following infection with WNV. Using mRNA sequencing combined with weighted gene co-expression network analysis (WGCNA), we defined molecular signatures of antiviral DC responses following activation of RLR and type I IFN signaling or infection with WNV. Using cis-regulatory sequence analysis, STAT5 was identified as a regulator of DC activation downstream of innate immune signaling that was not activated during WNV infection. Consequently, molecules involved in T cell activation were minimally induced during WNV infection, and functionally, WNV-infected DCs dampened allogeneic T cell proliferation. In contrast, antiviral and type I IFN responses were strongly induced, including activation of both STAT1 and STAT2 signaling. Mechanistically, WNV actively blocked STAT5 phosphorylation downstream of RIG-I, IFNβ, IL-4, and IL-13 signaling through impairment of Tyk2 and JAK1 activation. Zika virus also blocked STAT5 phosphorylation, suggesting a conserved mechanism used by pathogenic flaviviruses to subvert DC activation. Combined, we propose a model where flavivirus antagonism of

STAT5 signaling interferes with DC activation, leading to compromised T cell priming by infected DCs.

## 2B. Author summary

West Nile virus in an encephalitic flavivirus that remains endemic in the United States. Previous studies have found a correlation between dysfunctional T cell responses and severe disease outcomes during human WNV infection. In this study, we sought to better understand the ability of WNV to program human dendritic cells (DCs) to prime anti-viral T cell responses. While productive WNV infection up-regulated antiviral effector gene expression and promoted type I interferon responses, multiple groups of molecules associated with inflammation and programming of T cell responses failed to be induced. The transcription factor STAT5 was identified as an important regulator of DC responses that was minimally activated during WNV infection. Mechanistically, WNV antagonized STAT5 signaling by blocking tyrosine phosphorylation of STAT5 downstream of multiple cytokine signaling pathways through impaired activation of Tyk2 and JAK1. Zika virus was also found to block STAT5 phosphorylation, suggesting antagonism of STAT5 signaling may be a conserved strategy used by pathogenic flaviviruses to subvert DC activation and compromise subsequent anti-viral T cell priming.

## 2C. Introduction

West Nile virus (WNV) is a neurotropic flavivirus that remains the leading cause of mosquito-borne encephalitis in the United States (192). It is estimated that upwards of 6 million people have been infected by WNV in the US since its introduction in 1999, leading to over a thousand cases of neuroinvasive disease and nearly a hundred deaths each year (11). Following the bite of an infected mosquito, approximately 20% of individuals present with clinical outcomes ranging from mild febrile illness to severe neuroinvasive disease. Neuroinvasion is a serious complication with long term sequelae that includes ocular involvement, cognitive impairment, muscle weakness, and flaccid paralysis (12). The continued public health threat from WNV and other emerging flaviviruses, including Zika virus (ZIKV), underpins the need to better understand the mechanisms of protective immunity during human flavivirus infection.

The pathogenesis of human WNV infection is incompletely understood, although excellent mouse models have illuminated mechanisms of virus-induced encephalitis and critical features of immune control (13). The bite of an infected mosquito delivers high doses of WNV into the skin where keratinocytes, Langerhans cells, and dermal dendritic cells (DCs) are believed to be initial target cells of infection (15, 193). Over the next 24 hours, WNV migrates to the skin draining lymph nodes and replicates within resident DCs. Subsequent viremia promotes peripheral seeding of virus into permissive tissues such as the spleen, where viral replication occurs primarily within DCs. WNV then crosses the blood

brain barrier and infects neurons within the central nervous system (CNS), leading to viral encephalitis.

Within murine DCs, detection of WNV occurs primarily through the concerted efforts of RIG-I and MDA5 (99, 102), members of the retinoic acid inducible gene I (RIG-I) like receptor (RLR) family of cytosolic pattern recognition receptors. Signal transduction through the adaptor protein mitochondrial antiviral signaling (MAVS) triggers the nuclear factor-κB (NFκB) and interferon regulatory factor (IRF)-3, 5, and 7 dependent induction of type I interferon (IFN) and antiviral effector gene transcription (194). Following the MAVS-dependent secretion of type I IFN (99), signaling through the type I IFN receptor on DCs is required for early virus restriction and host survival (16). In addition to direct restriction of viral replication, DCs are critical for the programming of antiviral CD8+ T cell responses that are required for clearance of WNV from the peripheral tissues and CNS (195). In humans, analysis of CD4+ and CD8+ T cells from the blood of WNV-infected patients has found dysfunctional T cell responses correlate with symptomatic disease outcome (29, 30). Decreased frequencies of CD4+ regulatory T cells also correlates with symptomatic WNV infection, highlighting the importance of a balanced T cell response (28). Nevertheless, the contributions of human DCs in programming T cell immunity during human WNV infection remains poorly understood.

Here, we employed a systems biology approach to define the global antiviral response during WNV infection of human DCs, combining conventional virologic and immunologic measures with transcriptomic and computational analyses.

Using WGCNA combined with promoter scanning analysis, we identified STAT5, a critical transcription factor for regulating DC activation, downstream of RLR and type I IFN signaling. WNV infection failed to induce STAT5 signaling, corresponding with a failure to up-regulate inflammatory mediators and molecules involved in antigen presentation and T cell co-signaling. Functionally, impaired DC activation resulted in diminished T cell priming by WNV-infected moDCs during an allogeneic response. The minimal activation of WNV infected DCs reflected viral antagonism of STAT5, and to a lesser extent STAT1 and STAT2, phosphorylation through impaired Tyk2 and JAK1 activation. ZIKV also blocked STAT5 signaling, suggesting targeting STAT5 may be a common immune evasion strategy of pathogenic flaviviruses to subvert T cell immunity.

## 2D. Results

### WNV productively infects human DCs

While DCs are an important cell type during infection with multiple flaviviruses, their contributions during human WNV infection remains limited. To model viral replication in human DCs, monocyte-derived DCs (moDCs) were generated from peripheral blood CD14+ monocytes and infected with a pathogenic strain of WNV (196). Viral replication was first detected at 12hpi, as noted by increased viral RNA synthesis **(Fig 1A)**. Viral RNA levels continued to increase exponentially over the next 36hrs. Viral RNA was not detected in mock or UV inactivated virus (UV-WNV) infection controls **(S1A Fig)**. Consistent with genome replication kinetics, release of infectious virus increased exponentially

between 12 and 24hpi and plateaued at 48hpi **(Fig 1B)**. Next, infected populations of moDCs were stained for intracellular expression of a structural protein found within the virus envelope (viral E protein) (22). Corresponding with log phase viral growth, the percentage of infected cells increased exponentially between 12 and 24hpi **(Fig 1C; S1B and S1C Fig)**. Infection plateaued between 24 and 48hpi, reaching upwards of 50% of cells positive for viral E protein. E protein expression was not observed in mock or UV inactivated virus infection controls. ImageStream analysis revealed that WNV E protein was localized predominantly within the cytoplasm and did not co-localize with the cell surface marker CD11c or the nucleus. Declining percent infection at 72hpi corresponded with significant loss of cell viability **(Fig 1D)**. Combined, three complementary measures of viral replication (viral RNA, infectious virus release, and viral E protein staining) confirm that human moDCs are productively infected by WNV with log phase viral growth beginning between 12 and 24hpi.

### Innate immune signaling restricts WNV replication

Studies in mice have demonstrated the importance of RLR and type I IFN signaling in viral restriction during WNV infection, yet the contributions of innate immune signaling during infection of primary human cells remains poorly understood. Here, infected moDCs were treated with RLR agonists or IFNβ at 1hpi, after viral attachment and entry, and viral replication was assessed 24hrs later **(S2A Fig)**. To trigger RLR signaling, moDCs were transfected with a highly specific RIG-I agonist derived from the 3’ UTR of hepatitis C virus (197), or high

molecular weight poly(I:C), which preferentially activates MDA5 signaling upon delivery into the cytosol (89). Stimulation of RIG-I, MDA5, or IFNβ signaling potently restricted viral replication, with greater than 90% inhibition as measured by both infection virus release and viral E protein staining **(Fig 1E)**. Transfection reagents alone did not affect viral replication **(S2B Fig)**. To determine the role of endogenously produced type I IFN, we infected moDCs in the presence of an anti-IFNAR2 neutralizing antibody at a concentration found to block the ability of type I IFN to activate moDCs **(S2C Fig)**. Blocking type I IFN signaling showed no effect on viral replication through 24hpi, however, late viral control was compromised as shown by a 3-fold increase in the percentage of E protein+ cells and a log-fold increase in infectious virus release at 48hpi **(Fig 1F)**. RLR agonists were found to block viral replication independent of type I IFN signaling, where inclusion of an anti-IFNAR2 neutralizing antibody did not affect the potency of RIG-I or MDA5 agonist **(Fig 1G)**. These findings demonstrate that RLR and type I IFN signaling can block WNV replication in human DCs.

**Systems biology defines a molecular signature corresponding to antiviral DC responses**

Traditional studies of antiviral responses have predominantly relied on approaches involving genetic ablation, gene knockdown, or gene overexpression methodologies (198). While useful, these approaches remain difficult to perform in primary human cells and may not accurately reflect the role of a given molecule during the normal course of infection. To overcome these limitations,

we employed a systems biology approach to assess the global antiviral response during WNV infection within primary human DCs **(S3A Fig)**. We generated moDCs from 5 donors and performed messenger RNA sequencing following innate immune agonist treatment or infection with WNV. Responses were measured at 12hrs post innate immune agonist treatment, a time-point at which we observed strong and consistent induction of antiviral effector genes across the different innate immune agonists **(S3B Fig)**. To study the early antiviral response during WNV infection, transcriptional responses were measured preceding (12hpi) and during (24hpi) log phase viral replication **(Fig 1)**.

Using weighted gene co-expression network analysis (WGCNA), we defined molecular signatures following stimulation of RIG-I, MDA5, or IFNβ signaling, identifying six clusters of co-expressed genes, or modules **(Fig 2A)** (199). The module with the largest gene membership, module 5 (M5), was enriched for genes associated with the biologic process of “Defense response to virus”. Module 6 was also enriched for immune response related genes, while the remaining four modules were enriched for genes involved in biosynthetic processes, cellular metabolism, and stress responses. Given the large gene number and enrichment for antiviral response pathways, we focused our analyses to M5. We next identified differentially expressed genes (DEGs) within M5 for each treatment condition, as compared to time-matched untreated and non-infected cells (>2-fold change, significance of $p<0.01$). RIG-I agonist induced the strongest overall up-regulation of M5 genes, while both MDA5 and IFNβ stimulation induced substantial, although less profound, responses **(Fig 2B)**.

During WNV infection, there was minimal M5 gene enrichment at 12hpi, but by 24hpi, notable M5 gene up-regulation was observed, including many of the same genes induced by innate immune agonist treatment. When we performed MetaCore pathway analysis, M5 DEGs were highly enriched for pathways involved in type I IFN signaling and innate antiviral responses **(Fig 2C)**. Thus, WGCNA reveals a highly enriched cluster of genes that corresponds to antiviral DC responses during WNV infection.

**STAT5 is a regulatory node of antiviral DC responses**

WGCNA clusters together genes into modules based on co-expression, suggesting the presence of common transcriptional regulators driving gene expression within a module. To define the transcriptional regulatory network of the M5 antiviral module, we performed cis-regulatory sequence analysis to computationally predict regulatory nodes using iRegulon, which identifies enrichment of transcription factor binding motifs within the top highly connected genes comprising M5 (200). Consistent with pathway enrichment for antiviral pathways, our analysis identified STAT1, STAT2, IRF9, IRF1, and NFκB within the top predicted transcriptional regulators of M5, all well described and strong drivers of antiviral gene transcription (201-203) **(Fig 2D)**. We also found notable enrichment for STAT5, a transcriptional regulator with a previously described role in promoting DC activation (204, 205). Given that a role for STAT5 has not been previously implicated during flavivirus infection, we next looked at expression levels of predicted STAT5 target genes. While RIG-I agonist induced up-

regulation of all predicted exclusive STAT5 target genes, STAT5 signaling was substantially less enriched during WNV infection, where almost 80% of predicted exclusive STAT5 target genes were not differentially expressed **(Fig 2E)**. Combined, cis-regulatory analysis reveals STAT5 as a transcriptional regulator of M5 DEGs with minimal enrichment during WNV infection.

**STAT5 is a regulator of DC activation not activated during WNV infection**

Given recent work implicating STAT5 signaling upstream of DC activation, in part through binding to the promoter regions of CD80 and CD83, we hypothesized that STAT5 might be an important regulator of DC activation during flavivirus infection (204, 205). Consistent with this previous work, multiple predicted exclusive STAT5 target genes were involved in processes related to DC activation, including molecules involved in T cell co-signaling (e.g. *CD80*, *IDO1*, *SLAMF1*) and cytokine signaling (e.g. *CCL2*, *CCL13*, *CXCL11*, IL2RA, *JAK2, SOCS, CISH*) (**Fig 3A and 3B)**. We also found enrichment for multiple STAT5 target genes involved in innate immunity (e.g. *IRF1*, *TLR7*, *TRIM25*) **(S4A Fig)**. RIG-I agonist treatment induced significant up-regulation of STAT5 targets involved in both DC activation and innate immunity. Enrichment for STAT5 target genes corresponded with dose-dependent phosphorylation of STAT5 at tyrosine residue 694, a critical event for STAT5 dimerization and DNA binding, following 90min treatment with both RIG-I and MDA5 agonists **(Fig 3C and S4B Fig)** (206). STAT5 phosphorylation coincided with the kinetics and magnitude of IRF3

phosphorylation. STAT5 remained phosphorylated at 18hrs post RIG-I agonist treatment, suggesting sustained activation of STAT5 potentially through production of cytokines, such as IL-4 and GM-CSF, that activate STAT5 signaling **(S4C and S4D Fig)**. IFNβ signaling also promoted STAT5 phosphorylation, confirming previous work describing the activation of STAT5 by type I IFN signaling in other cell types **(Fig 3D)** (207-209).

The minimal induction of STAT5 target genes corresponded to a lack of STAT5 phosphorylation during WNV infection at 24 and 48hpi, despite increased amounts of STAT5 total protein by 48hpi **(Fig 3D)**. WNV infection also did not induce secretion of IL-4 or GM-CSF, cytokines that activate STAT5 **(S4D Fig)**. Since we did not obtain 100% infection of moDCs **(Fig 1C)**, it remained possible that STAT5 was being activated within infected cells, but the signal was being diluted out by the presence of uninfected cells. To rule this out, we employed an A549 cell infection system, a human lung carcinoma cell line previously used to study WNV infection where synchronous infection of 100% of cells can be obtained (123). WNV also failed to activate STAT5 phosphorylation at any time during an infection time course in A549 cells, despite >95% infection **(S4F Fig)**. Combined, the lack of STAT5 phosphorylation and enrichment for target genes involved in DC activation suggests that WNV might subvert STAT5 signaling to compromise human DC activation.

### WNV does not induce inflammatory cytokine responses

Given the lack of STAT5 activation and minimal enrichment for STAT5 target genes involved in DC activation, we next determined if WNV infection induced inflammatory cytokine responses, an important component of DC activation and T cell priming (210, 211). WNV infection did not promote transcription or protein secretion of multiple cytokines involved in inflammatory responses (e.g. IL-6, TNF), T cell immunity (e.g. IL-12, IL-27, IL-15, and IL-15RA), and chemotaxis (CCL2, CCL3, CCL4, CCL5, and CXCL9) **(Fig 4A and 4B)**. Importantly, RIG-I agonist induced transcriptional expression and secretion of multiple inflammatory and T cell modulatory cytokines, confirming the ability of our moDCs to mount pro-inflammatory responses upon innate immune stimulation. Indeed, while RIG-I agonist treatment induced secretion of 17 of the 25 cytokines and chemokines analyzed, only 1 was secreted at significant levels during WNV infection. *CXCR1* transcription was also selectively down-regulated during WNV infection. These findings suggest WNV-infected DCs are compromised in their ability to induce inflammatory and chemotactic mediators important for T cell priming and immune activation.

**WNV infected DCs are compromised in T cell priming**

In addition to the secretion of cytokines that modulate T cell behavior, engagement of viral associated molecular patterns increases the surface expression of T cell co-signaling and MHC molecules on activated DCs (212). MetaCore pathway analysis on M5 DEGs following RIG-I agonist treatment revealed enrichment for multiple pathways involved in T cell activation and

antigen presentation **(S5A Fig)**. In contrast, many of these pathways were not enriched during WNV infection. Indeed, WNV infection failed to induce multiple molecules associated with antigen presentation on MHC (*HLA-A, ERAP1*), *LAMP3* (213), proteasome subunits (*PSME1, PSMA2, PSMA4, PSMB10*), and *CD1D* (214) **(Fig 4A)**. WNV also failed to significantly up-regulate genes involved in T cell co-signaling (e.g. *CD80, CD86, CD40*) and selectively up-regulated expression of galectin-9 (*LGALS9*), a ligand for the T cell inhibitory receptor TIM3 (29). These findings were biologically validated by flow cytometry, where WNV infection did not up-regulate cell surface levels of CD80, CD86, CD40 or MHC class II proteins within E protein+ cells at 24hpi **(Fig 4C)** or 48hpi **(S5B Fig)**. In contrast to WNV infection, RIG-I agonist significantly up-regulated transcription of multiple molecules involved in antigen presentation and T cell co-signaling, corresponding with increased cell surface expression of CD80, CD86, CD40, and MHC II proteins. These findings demonstrate that WNV infection fails to up-regulate multiple molecules involved in antigen presentation and T cell co-signaling, despite the ability of these cells to induce DC activation upon activation of innate immune signaling.

To determine if the minimal DC activation induced during WNV infection impairs T cell priming, we assessed the capacity of WNV-infected moDCs to drive an allogeneic T cell response. Uninfected moDCs induced strong proliferation of donor mismatched CD4 and CD8 T cells in a DC:T cell ratio dependent manner **(Fig 4D)**. In contrast, WNV infected moDCs promoted diminished allogeneic CD4 and CD8 T cell proliferation. There was also

diminished up-regulation of the T cell activation markers CD38 and HLA-DR on allogeneic T cells primed by WNV infected moDCs **(S5C Fig)**. Combined, these results suggest that the lack of STAT5 activation during WNV infection compromises DC activation to subvert T cell priming.

**WNV infection activates antiviral and type I IFN responses**

Given the lack of STAT5 activation and impaired T cell priming ability of WNV-infected moDCs, we next asked whether antiviral responses were also compromised during WNV infection. Using our defined molecular signature for RIG-I signaling as a filter, we identified specific sets of antiviral genes corresponding to innate immune sensors, transcription factors, type I IFN signaling, and antiviral effectors. In contrast to our findings with DC activation, molecules involved in RNA virus sensing (e.g. *DDX58*, *IFIH1*, *PKR*, *TLR3*) and the antiviral transcription factor *IRF7* were up-regulated at 24hpi with WNV. This corresponded with up-regulation of multiple subtypes of type I IFN (*IFNB1*, *IFNA* subtypes, and *IFNW1*), type I IFN signal transducers (*STAT1* and *STAT2*), and numerous antiviral effector genes (e.g. *IFIT1, IFIT2, IFIT3, RSAD2, OASL*) at 24hpi **(Fig 5A)**. Concordantly, STAT1 and STAT2 were phosphorylated at 24 and 48hpi and secretion of both IFNβ and IFNα proteins were detected by 48hpi **(Fig 5B and 5C)**. While RIG-I agonist also induced type I IFN production, minimal to no type I IFN secretion was detected in moDCs left uninfected or infected with a UV-inactivated WNV. Combined, our data demonstrates that WNV infection of human DCs induces notable antiviral gene expression, contrasting with the

minimal enrichment of molecules involved in DC activation. Furthermore, phosphorylation of STAT1 and STAT2, but not STAT5, suggests that WNV may selectively target STAT5 to compromise DC activation.

**WNV actively antagonizes STAT5 signaling**

The lack of STAT5 activity during WNV infection strongly suggests that WNV actively inhibits STAT5 signaling. To determine if WNV can actively block STAT5 phosphorylation, we employed a Vero cell model of WNV infection, which allows for synchronous infection of 100% of cells and a lack of endogenous type I IFN signaling. Using a system that lacks type I IFN production is important to remove confounding interpretations caused by the induction of negative regulators that may down-regulate type I IFN signaling independently of viral antagonism. When we infected Vero cells with increasing MOIs of WNV (0.1, 1, and 5), we did not detected phosphorylation of STAT1, STAT2, or STAT5, consistent with the lack of an endogenous type I IFN response **(Fig 6A)**. When we pulse treated infected cells with IFNβ, we observed substantial blockade of STAT5 phosphorylation, even at an MOI were we expect a mixture of infected and uninfected cells (MOI 0.1). STAT1 and STAT2 phosphorylation were also blocked, but in contrast to STAT5, the blockade was less pronounced at MOI 0.1. This is similar to our observations in moDCs, where STAT5 was not activated during WNV infection, but both STAT1 and STAT2 were phosphorylated **(Fig 5B)**. When we next infected Vero cells with a non-pathogenic strain of WNV (WNV-MAD) previously shown to not block STAT1 or STAT2 (123), we found

STAT5 phosphorylation was not blocked **(S6A Fig)**. This suggests that STAT5 antagonism is a feature of pathogenic, but not non-pathogenic WNV strains.

We next confirmed our findings from Vero cells within primary human moDCs. STAT5 phosphorylation was potently blocked following RIG-I agonist treatment of WNV-infected moDCs **(Fig 6B)**. Given the secretion of type I IFN at 48hpi, as well as our findings in Vero cells, we hypothesized that WNV could also antagonize type I IFN-mediated STAT5 signaling. Indeed, WNV infection potently blocked STAT5 phosphorylation following IFNβ treatment **(Fig 6C and S6B Fig)**. Infection with UV-WNV failed to block RIG-I or IFNβ-mediated STAT5 phosphorylation, suggesting viral replication is required for inhibition of STAT5 signaling. Next, we asked if WNV blocked STAT5 activation downstream of additional cytokine signaling pathways. Common gamma-chain family cytokines, such as IL-4, as well as multiple growth factors, including GM-CSF, signal through their respective receptors to promote STAT5 phosphorylation (215, 216). IL-13 can also activate STAT5 phosphorylation, signaling through the shared type II IL-4 receptor complex. Here, WNV infection dampened IL-4 and IL-13 induced STAT5 phosphorylation in moDCs **(Fig 6D and S6C Fig)**. In contrast, WNV failed to antagonize GM-CSF signaling, where the increased STAT5 protein induced during infection led to increased STAT5 phosphorylation **(Fig 6E)**. Together, our findings suggest that WNV blocks STAT5 phosphorylation to antagonize STAT5-dependent gene induction in human moDCs in a pathway specific manner.

We next asked whether STAT5 antagonism was unique to WNV, or if other related flaviviruses could block STAT5 phosphorylation. Recent work has found that infection of human moDCs with ZIKV induced minimal DC activation, similar to our findings with WNV (217). Here, ZIKV infection blocked STAT5 phosphorylation downstream of RIG-I, IFNβ, and IL-4, but not GM-CSF signaling, similar to WNV **(Fig 6B-E)**. These findings demonstrate that antagonism of STAT5 might be a common strategy used by pathogenic flaviviruses to subvert DC activation and T cell immunity.

**WNV dampens activation of Tyk2 and JAK1**

The pathway specific inhibition of STAT5 provides insight into the host target of viral antagonism. The type I IFN receptor associates with JAK1 and Tyk2, which mediate tyrosine phosphorylation of STAT1 and STAT2, while Tyk2 constitutively associates with STAT5 and mediates its tyrosine phosphorylation (209). IL-4 can bind to either the type I receptor (IL-4Rα/γc), activating JAK1 and JAK3, while both IL-4 and IL-13 bind the type II receptor (IL-4Rα/IL-13Rα1) to activate Tyk2 and JAK1 (215). In contrast, GM-CSF signaling through the GM-CSF receptor predominately activates JAK2, but not JAK1 or Tyk2 (216, 218). The ability of WNV and ZIKV to block type I IFN, IL-4, and IL-13, but not GM-CSF signaling suggests Tyk2 and JAK1 may be targeted to block STAT5 phosphorylation.

To assess JAK inhibition, we infected Vero cells at MOI 0.1, 1, and 5 with WNV. Consistent with the lack of endogenous type I IFN production, WNV

infection alone did not induce Tyk2 phosphorylation. Although we did observe JAK1 phosphorylation, this is likely explained by the production of other cytokines that can activate JAK1. When we IFNβ pulse treated Vero cells infected with WNV at MOI 0.1, we observed no blockade of Tyk2 and enhanced JAK1 phosphorylation **(Fig 7A)**. When we infected with increasing MOIs of 1 and 5, we observed a MOI-dependent decrease in Tyk2 and JAK1 phosphorylation. When we instead infected Vero cells with a non-pathogenic strain of WNV (WNV-MAD), which doesn't block STAT5 **(S6A Fig)**, we did not observe decreased Tyk2 or Jak1 phosphorylation **(S7 Fig)**. Indeed, we observed increased phosphorylation of Tyk2 and JAK1 as we infected with higher MOIs. We also observed severely diminished, although not completely blocked, Tyk2 and JAK1 phosphorylation following IFN treatment of WNV-infected human moDCs **(Fig 7B)**. Combined, these findings suggest that WNV can dampen activation of Tyk2 and JAK1, which could compromise STAT5 phosphorylation.

## 2E. Discussion

In this study, we combined traditional virologic and immunologic measures with transcriptomic and computational approaches to define the global antiviral response during WNV infection in human primary cells. WNV productively infected human moDCs and induced cell death, coinciding with declining viral growth kinetics. RIG-I, MDA5, and IFNβ signaling potently restricted viral replication, corresponding with strong activation of antiviral defense response genes. Using cis-regulatory sequence analysis, STAT5, a transcription factor

previously described as a regulator of DC activation, was identified as an important regulatory node of antiviral DC responses downstream of innate immune signaling. In contrast, STAT5 signaling was not activated during WNV infection, corresponding with minimal up-regulation of inflammatory mediators or molecules involved in T cell activation. Functionally, WNV-infected moDCs primed impaired allogeneic T cell proliferation and activation. Mechanistically, WNV blocked STAT5 phosphorylation downstream of RIG-I, IFNβ, IL-4, and IL-13, but not GM-CSF signaling through diminished Tyk2 and JAK1 activation. ZIKV also blocked STAT5 phosphorylation, suggesting STAT5 antagonism is a conserved mechanism used by pathogenic flaviviruses to subvert T cell immunity.

Studies in mice have found that RLR and type I IFN signaling are critical for viral restriction and host survival during WNV infection, however, the contributions of innate immune signaling during infection of human cells remains limited (16, 98). Here, we demonstrated that RIG-I, MDA5, and IFNβ signaling potently restrict WNV replication through induction of strong antiviral gene transcription, suggesting that similar to mice, RLR and type I IFN signaling are important for viral control during human WNV infection. RIG-I and MDA5 agonists also remained efficient in blocking WNV replication independent of type I IFN signaling, consistent with the ability of RLR signaling to induce antiviral gene expression in the absence of the type I IFN receptor in mice (98). Combined, our results confirm the importance of RLR and type I IFN signaling in induction of antiviral responses and restriction of viral replication within primary human DCs.

In addition to promoting antiviral responses, cis-regulatory sequence analysis revealed STAT5 as a regulatory node of multiple components of DC activation downstream of RLR and type I IFN signaling. Indeed, we observed significant enrichment for multiple STAT5 target genes involved in DC activation, which corresponded with secretion of pro-inflammatory cytokines and up-regulation of proteins involved in T cell activation. While this confirms previous studies that have implicated STAT5 in regulation of DC activation, we have also revealed a new facet of STAT5 activation during flavivirus infection through engagement of innate immune signaling (204, 205). The rapid kinetics of STAT5 phosphorylation following RIG-I or MDA5 stimulation suggest that RLR signaling may directly induce phosphorylation of STAT5 through activation of a tyrosine kinase, such as Src or Lyn, both of which are induced by RLR signaling (219-223). Alternatively, rapid production of type I IFN, which also potently promotes STAT5 activation, may mediate STAT5 phosphorylation following RLR signaling. However, the similar kinetics of STAT5 and IRF3 phosphorylation argue against the later hypothesis, suggesting that STAT5 is phosphorylated before type I IFN has had time to be secreted. Combined, our data suggests that STAT5 is an important regulatory node of DC activation downstream of RLR and type I IFN signaling.

In contrast to RLR and IFNβ signaling, WNV infection failed to up-regulate most predicted STAT5 target genes, and STAT5 was not phosphorylated during infection, despite secretion of IFNβ and IFNα. Corresponding with minimal STAT5 enrichment, WNV infection failed to promote up-regulation of

inflammatory mediators and molecules involved in antigen presentation and T cell co-signaling. These findings are similar to previous work, where WNV infection also failed to induce inflammatory cytokine secretion (224). Infection of moDCs with a non-pathogenic WNV isolate, WNV Kunjin, also induced minimal production of IL-12, despite notable up-regulation of both CD86 and CD40 (214). This suggests that an inability to induce inflammatory cytokine responses may be shared among WNV strains, while pathogenic strains have evolved unique mechanisms to subvert antigen presentation and T cell activation. The failure of WNV to activate human moDCs is also similar to recent work with ZIKV (217). In contrast to WNV and ZIKV, infection of moDCs with the yellow fever virus vaccine strain (YFV-17D) up-regulated multiple inflammatory mediators and surface expression of CD80 and CD86 (212). The ability of YFV-17D to induce strong DC activation may reflect the loss of a viral antagonist during the attenuation process, similar to the ability of WNV Kunjin to induce up-regulation of CD86 and CD40 (214). Alternatively, the ability of YFV to induce DC activation may be an inherent property of certain flaviviruses. Indeed, DENV has also been found to activate inflammatory responses and up-regulate co-stimulatory molecules following infection (225, 226). It remains unknown whether YFV-17D or DENV can block STAT5, but our results suggest that the activation induced during YFV-17D or DENV infection may reflect an inability to block STAT5. Altogether, we demonstrate that WNV, similar to ZIKV, induces minimal DC activation during productive infection, contrasting with both DENV and YFV.

The minimal enrichment for STAT5 target genes and failure to induce DC activation during WNV infection was explained by viral blockade of STAT5 phosphorylation downstream of RIG-I, IFNβ, IL-4, IL-13, but not GM-CSF signaling. Blockade of STAT5 signaling was found to be multi-frontal, as multiple STAT5 signaling cytokines induced downstream of RIG-I signaling (GM-CSF, IL-4, IL-15) are not produced during infection with WNV. The lack of GM-CSF secretion may also overcome the need for WNV to block GM-CSF-induced STAT5 phosphorylation. ZIKV was found to similarly block STAT5 activation, which is consistent with the lack of DC activation and minimal secretion of inflammatory cytokines during ZIKV infection of human moDCs (217). Interestingly, we found a non-pathogenic strain of WNV, WNV-MAD, was unable to block STAT5 phosphorylation. This is similar to previous work, which found WNV-MAD was also unable to block STAT1 and STAT2 phosphorylation. This suggests that the ability to antagonize STAT5 signaling may be an important feature of pathogenic strains of WNV.

While STAT5 phosphorylation was not observed during WNV infection of human moDCs, both STAT1 and STAT2 were phosphorylated at 24 and 48hpi. Similarly, infection of Vero cells at an MOI where we expect to have both infected and uninfected cells, MOI 0.1, resulted in more pronounced inhibition of STAT5 phosphorylation. Indeed, while STAT5 was almost completely blocked at MOI 0.1, both STAT1 and STAT2 were phosphorylated, likely resulting from intact type I IFN signaling in uninfected cells. Importantly, UV-inactivated virus, which undergoes cellular binding and entry but is replication incompetent, failed to

inhibit STAT5. This suggests that viral replication is required for STAT5 antagonism, potentially through a secreted viral protein that would affect both infected and uninfected cells. Combined, our data suggests that STAT5 is more selectively targeted by WNV, and that antagonism of STAT5, but not STAT1 or STAT2, may occur in both productively infected and uninfected cells.

Activation of STAT1 and STAT2 corresponded with induction of antiviral and type I IFN responses, contrasting with the minimal enrichment of molecules involved in DC activation. This corresponded with late type I IFN responses during WNV infection, with protein secretion not detected until 48hpi. This is consistent with previous work that found WNV infection of moDCs at low MOIs (1 or 10) failed to induce IFNα secretion at 24hpi, while very high MOI infection (MOI 100 and 1,000) was required for detectable IFNα production (224). Infection of moDCs with WNV Kunjin, a non-pathogenic WNV isolate, also only secreted type I IFN proteins at 48hpi (214). Similar studies performed with DENV infection observed similarly late secretion of IFNα (225). This work contrasts with ZIKV infection, which has been found to block IFNβ and IFNα translation (217). Combined, this demonstrates that while WNV-infected moDCs have impaired STAT5 signaling and induction of DC activation, antiviral and type I IFN responses remain intact.

Blockade of STAT5 phosphorylation corresponded with impaired activation of Tyk2 and JAK1, members of the Janus associated kinase (JAK) family that phosphorylate STAT5 downstream of type I IFN, IL-4, IL-13, but not GM-CSF signaling. This finding is consistent with previous work with WNV, and

closely related Japanese encephalitis virus (JEV), where Tyk2 activation was blocked (123, 227). Langat virus, a tickborne flavivirus, has also been found to block Tyk2 and Jak1 activation, through the NS5 protein, to subvert JAK/STAT signaling (228). Viral antagonism of Tyk2 and JAK1 may explain how GM-CSF signaling, which predominately relies on JAK2 for downstream STAT phosphorylation, escapes viral blockade of STAT5. Nevertheless, inhibition of Tyk2 or JAK1 activation is likely not the only mechanism used by WNV to block STAT5 activation. Indeed, while STAT5 phosphorylation was completely blocked by WNV, Tyk2 and JAK1 were only partially blocked. STAT5 itself is likely not targeted directly, given that GM-CSF induced STAT5 signaling remains intact during WNV infection. It remains plausible that WNV may disrupt the interaction between STAT5 and Tyk2 or Jak1, providing a further mechanism to selectively block STAT5 activation. Another possibility is that WNV infection includes the suppressor of cytokine signaling (SOCS) family, which broadly regulate JAK/STAT signaling and can be modulated during flavivirus infection (229). The observation that a non-pathogenic strain of WNV, WNV-MAD, does not block STAT5 phosphorylation provides a valuable tool to further define the viral and host factors that mediate STAT5 blockade.

In summary, our systems biology approach identified STAT5 as a regulator of DC activation that is blocked by WNV as a mechanism to subvert DC activation and T cell priming. The inability of a non-pathogenic strain of WNV to block STAT5 suggests that antagonism of STAT5 signaling may be an important adaption of pathogenic strains of WNV. ZIKV also blocked STAT5 signaling,

suggesting that viral antagonism of STAT5 may be a common strategy of pathogenic flaviviruses to evade the pressures of host immunity. Our study advances our understanding of how pathogenic flaviviruses subvert antiviral immunity during human infection.

## 2F. Experimental Procedures

**Ethics statement.** Human peripheral blood mononuclear cells were obtained from healthy donors in accordance with the Emory University Institutional review board protocol IRB00045821.

**Cell lines.** Vero cells (WHO Reference Cell Banks) and A549 cells (ATCC) were maintained in complete DMEM. Complete DMEM was prepared as follows: DMEM medium (Corning) supplemented with 10% fetal bovine serum (Optima, Atlanta Biologics), 2mM L-Glutamine (Corning), 1mM HEPES (Corning), 1mM sodium pyruvate (Corning), 1x MEM Non-essential Amino Acids (Corning), and 1x Antibiotics/Antimycotics (Corning). Complete RPMI was prepared as follows: cRPMI; RPMI 1640 medium (Corning) supplemented with 10% fetal bovine serum (Optima, Atlanta Biologics), 2mM L-Glutamine (Corning), 1mM Sodium Pyruvate (Corning), 1x MEM Non-essential Amino Acids (Corning), and 1x Antibiotics/Antimycotics (Corning).

**Generation of monocyte derived dendritic cells.** To generate human moDCs, CD14+ monocytes were differentiated in cRPMI supplemented with 100ng/mL of

GM-CSF and IL-4 for 5-6 days, as previously described (217). In brief, freshly isolated PBMCs obtained from healthy donor peripheral blood (lymphocyte separation media; StemCell Technologies) were subjected to CD14+ magnetic bead positive selection using the MojoSort Human CD14 Selection Kit (BioLegend). Purified CD14+ monocytes were cultured in complete RPMI supplemented with 100ng/mL each of recombinant human IL-4 and GM-CSF (PeproTech) at a cell density of 2e6 cells/mL. After 24hr of culture, media and non-adherent cells were removed and replaced with fresh media and cytokines. Suspension cells ("moDCs") were harvested after 5-6 days of culture and were consistently CD14-, CD11c+, HLA-DR+, DC-SIGN+, and CD1a+ by flow cytometry. For experimentation, moDCs were maintained in complete RPMI without GM-CSF or IL-4. For experiments measuring STAT5 phosphorylation, moDCs were rested in cRPMI without GM-CSF or IL-4 for 24hrs prior to experimentation.

**Viruses.** WNV stocks were generated from an infectious clone, WNV isolate TX 2002-HC, and passaged once in Vero cells, as previously described (196). ZIKV strain PRVABC59 was obtained from the Centers for Disease Control and Prevention as previously described (230). WNV and ZIKV virus stocks were titrated on Vero cells by plaque assay. moDCs were infected with WNV or ZIKV at MOI 10 for 1hr at 37°C in cRPMI (without GM-CSF or IL-4). After 1hr, virus was washed off, cells were resuspended in fresh cRPMI, and incubated at 37°C for 3-72 hours.

**Quantitative reverse transcription-PCR (qRT-PCR).** Total RNA was purified (Quick-RNA MiniPrep Kit; Zymo Research) and viral RNA was reverse transcribed (High Capacity cDNA Kit; Applied Biosystems) using 1 pmol of a GVA tagged (underlined) primer (5'-TTTGCTAGCTTTAGGACCTACTATATCTACCTGGGTCAGCACGTTTGTCATTG-3') directed against the E gene (120, 231). Reverse transcribed viral sequences were detected by qRT-PCR (TaqMan Gene Expression Master Mix; Applied Biosystems) using 10 pmol of primers (5'-TTTGCTAGCTTTAGGACCTACTATATCTACCT3' and 5'-TCAGCGATCTCTCCACCAAAG-3') and 2.5 pmol of hydrolysis probe (5'-FAM-TGCCCGACCATGGGAGAAGCTC-3IABkFQ-3'). All custom primers and probes were obtained from Integrated DNA Technologies. All qRT-PCR was normalized to the amount of GAPDH (Hs02758991_g1; Applied Biosystems) in each respective sample.

**Quantitation of infectious virus.** Infectious virus was quantitated using a plaque assay on Vero cells with a 1% agarose overlay and crystal violet counterstain, as previously described (196).

**Innate immune agonists.** To stimulate RIG-I signaling, 100ng of RIG-I agonist derived from the 3'-UTR of hepatitis C virus (197) was transfected per 1e6 cells using TransIT-mRNA transfection kit (Mirus). For stimulation of MDA5 signaling,

100ng of high molecular weight poly-(I:C) was transfected per 1e6 cells using LyoVec transfection reagent (Invivogen). To stimulate type I IFN signaling, cells were incubated with 100 IU/mL of human recombinant IFNβ. In select experiments, different doses of agonists were used and this is indicated within the respective figure legend. To inhibit type I IFN signaling, 5μg/mL anti-human Interferon-α/β Receptor Chain 2 (MMHAR-2; EMD Milipore) blocking monoclonal antibody was used.

**RNA sequencing and bioinformatics.** moDCs were generated from 5 donors and either treated with innate immune agonists for 12hr (RIG-I, MDA5, or IFNβ) or infected with WNV (12hpi and 24hpi). Total RNA was purified (Quick-RNA MiniPrep Kit; Zymo Research) and mRNA sequencing libraries were prepared for RNA sequencing (Illumina TruSeq chemistry). RNA sequencing was performed on a Illumina HiSeq 2500 System (100bp single end reads). Sequencing reads were mapped to the human reference genome 38. Weighted gene co-expression module analysis was performed on DESeq2 normalized mapped reads (TIBCO Spotfire with Integromics Version 7.0) from RIG-I agonist, MDA5 agonist, IFNβ, and mock treated samples. First, the datasets were reduced to focus the network analysis on the 5446 most variable genes (as determined by variation value greater than 1) using the Variance function in R. We constructed a signed weighted correlation network by generating a matrix pairwise correlation between all annotated gene pairs. The resulting biweight mid-correlation matrix was transformed into an adjacency matrix using the soft thresholding power (β1) of

12. The adjacency matrix was used to define the topological overlap matrix (TOM) based on a dissimilarity measurement of 1- TO. Genes were hierarchically clustered using average linkage and modules were assigned using the dynamic tree-cutting algorithm (module eigengenes were merged if the pairwise calculation was larger than 0.75). This resulted in the construction of six modules. Transcriptional regulators within the M5 module were computationally predicted with iRegulon (200), using the top most connected M5 genes using an eigengene-based connectivity cutoff of 0.4. Differentially expressed genes within the M5 module were identified as having a >2-fold change (significance of $p<0.01$) relative to uninfected and untreated cells. Pathway analysis was performed on M5 genes using MetaCore pathway map analysis (version 6.29, Thomson Reuters). The raw data of all RNA sequencing will be deposited into the Gene Expression Omnibus (GEO) repository and the accession number will be available following acceptance of this manuscript.

**Flow cytometry.** Cells were prepared for analysis as previously described (217). In brief, cells were Fc receptor blocked for 10 min, stained for phenotypic and activation markers for 20 min, and viability stained for 20 min (Ghost Dye Violet 510, Tonbo Biosciences). For intracellular staining of WNV E protein, cells were fixed and permeabilized (Transcription Factor Staining Buffer Kit, Tonbo Biosciences) and labeled with E16-APC for 20min at room temperature (22). Flow cytometry data was analyzed using FlowJo version 10 software.

ImageStream data was analyzed using the Amnis IDEAS software. Primary antibodies are listed in S1 Table.

**T cell proliferation assay.** Freshly isolated PBMCs obtained from healthy donor peripheral blood (lymphocyte separation media; StemCell Technologies) were subjected to CD4 or CD8 T cell magnetic bead negative selection using the MojoSort Human CD4 or CD8 Selection Kit (BioLegend). Isolated CD4 or CD8 T cells were labeled with CellTrace Violet (CTV) Cell Proliferation Kit (ThermoFisher) per the manufacturer's instructions. In a 96-well U bottom plate, CTV labeled CD4 or CD8 T cells (2e5 ells) were mixed with different ratios of either uninfected moDCs, or moDCs infected with WNV for 24hr (1:4, 1:8, 1:16, 1:32, 1:64, and 1:128 DC:T cell ratios). To prevent spreading infection, we added anti-E16 neutralizing antibody at 5μg/mL throughout the DC:T cell co-culture period (22). After 6 days of co-culture, cells were stained for surface expression of CD4 or CD8, CD3, CD38, and HLA-DR and both proliferation, by CTV dilution, and T cell activation (CD38+HLA-DR+) were assessed by flow cytometry (232).

**Multiplex bead array.** Cytokine analysis was performed on supernatants using a human 25-plex panel (ThermoScientific) and a custom 2-plex panel with human IFNβ and IFNα simplex kits (eBioscience) as described previously (217). Cytokines analyzed included: IFN-α, IFNβ, GM-CSF, TNF-α, IL-4, IL-6, MIP-1α, IL-8, IL-15, IL-2R, IP-10, MIP-1β, Eotaxin, RANTES, MIG, IL-1RA, IL-12 (p40⁄p70) IL-13, IFN-γ, MCP-1, IL-7, IL-17, IL-10, IL-5, IL-2, and IL-1β.

**Western blot.** Whole-cell lysates were collected in modified radioimmunoprecipitation assay buffer (10 mM Tris [pH 7.5], 150 mM NaCl, 1% sodium deoxycholate, and 1% Triton X-100 supplemented with Halt Protease Inhibitor Cocktail [ThermoFisher] and Halt Phosphatase Inhibitor Cocktail [ThermoFisher]). Protein lysates were separated by SDS-PAGE and western blot analysis was performed using the ChemiDoc XRS+ imaging system (BioRad)**.** Western blots were analyzed using Image Lab version 5.2.1 software (BioRad) and prepared for publication using Adobe Illustrator. Primary antibodies are listed in S1 Table.

**Statistics.** All statistical analysis was performed using GraphPad Prism version 6 software. The number of donors varied by experiment and is indicated within the figure legends. Statistical significance was determined as $P<0.05$ using a Kruskal-Wallis test (when comparing more than two groups lacking paired measurements), a Wilcoxon test (when comparing two groups with paired measurements), or a 2way ANOVA (when comparing two groups across multiple independent variables). All comparisons were made between treatment or infection conditions with a time point matched, uninfected and untreated control.

## 2G. Figures and legends

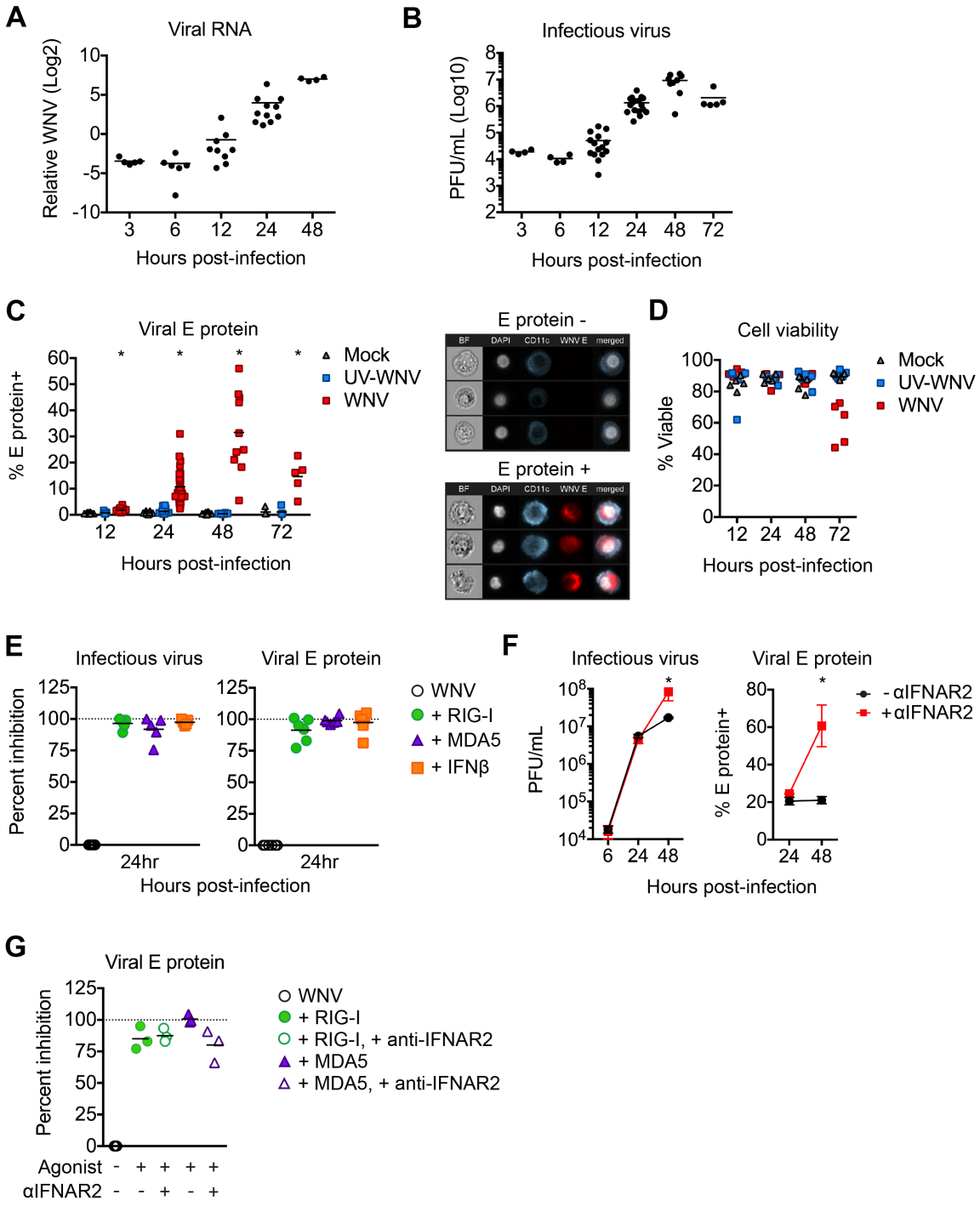


**Fig 1. WNV productively infects human moDCs and is restricted by innate immune signaling.** moDCs were infected with WNV or UV-inactivated WNV

(UV-WNV) at MOI 10 (as determined on Vero cells) and analyzed at indicated hours post-infection. **(A)** Viral RNA as quantitated in cell lysates by RT-qPCR. Shown as $\log_2$ normalized expression after normalization to *GAPDH.* Data is shown for each donor with the mean (n=5-11 donors). **(B)** Infectious virus release into the supernatant as determined by a viral plaque assay on Vero cells. Data is shown for each donor with the mean (n=4-17 donors). PFU, plaque-forming unit. **(C)** Percent E protein+ cells as determine by flow cytometry (Left panel). Data is shown for each donor with the mean (n=5-31 donors). ImageStream analysis of WNV-infected moDCs labeled for viral E protein at 24hpi (Right panel). **(D)** Percent viable cells. Data is shown for each donor with the mean (n=5 donors). **(E)** moDCs were infected with WNV at MOI 10 (as determined on Vero cells) for 1hr and then treated with RIG-I agonist (100ng/1e6 cells), MDA5 agonist (100ng/1e6 cells), IFN$\beta$ (1000 IU/mL), or left untreated ( "WNV" ). Infectious virus release into the supernatant (left panel) or viral E protein staining (right panel) was assessed at 24hpi. Data is represented as percent inhibition and shown for each donor with the mean (n= 5-6 donors). Percent inhibition was calculated as: (1 - [WNV + agonist] / [WNV alone]) * 100. Dashed line indicates 100% inhibition, or complete block of viral infection. **(F)** moDCs were infected with WNV at MOI 10 (as determined on Vero cells) in the presence or absence of anti-IFNAR2 blocking antibody (5µg/mL) and viral infection was assessed as in E. Representative donor shown with the mean +/- SD of three replicates. **(G)** moDCs treated as in E were incubated with or without anti-IFNAR2 (5µg/mL). Data is shown for each donor with the mean (n= 3 donors). Statistical

significance was determined as $P < 0.05$ using a Kruskal-Wallis test. See also S1 and S2 Fig.

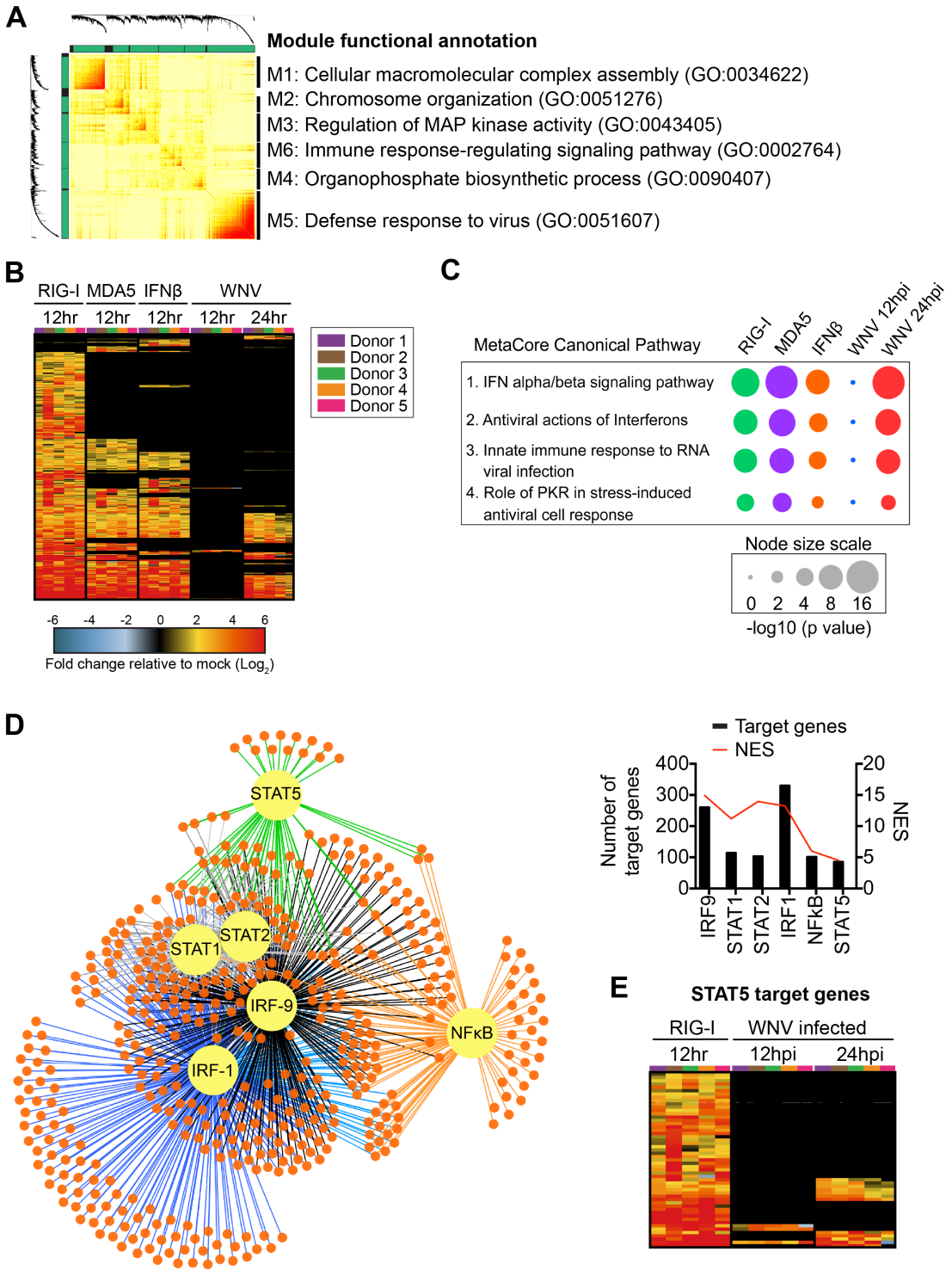


**Fig 2. Systems biology reveals STAT5 as a regulatory node of antiviral DC responses. (A)** Topologic overlap matrix showing enriched modules defined by WGCNA following 12hr treatment with RIG-I agonist (100ng/1e6 cells), MDA5

agonist (100ng/1e6 cells), or IFN $\beta$ (1000 IU/mL). Functional annotation was performed using the DAVID Bioinformatics Resource version 6.8, with the top enriched biological process shown. **(B)** Heatmap of all module 5 differentially expressed genes with the $\log_2$ normalized fold change relative to uninfected, untreated cells shown. **(C)** Top enriched MetaCore canonical pathways of module 5 differentially expressed genes relative to uninfected and untreated cells (>2-fold change, significance of $p<0.01$). Node size corresponds with the pathway enrichment significance score ($-\log_{10}$ p value) for each indicated treatment condition. **(D)** Transcription factor regulatory network of module 5 gene expression as predicted by iRegulon (left panel). The top predicted transcriptional regulators (large, yellow nodes) are shown with a connecting line to predicted target genes (small, orange nodes). The number of predicted target genes and the normalized enrichment score (NES) for a given regulator is shown below (right panel). **(E)** Heatmap of predicted STAT5 target genes with the $\log_2$ normalized fold change relative to uninfected, untreated cells is shown (>2-fold change, significance of $p<0.01$; bottom panel). For all heatmaps, each column within a treatment condition is marked by a unique color and represents a different donor (n= 5 donors). See also S2 Fig.

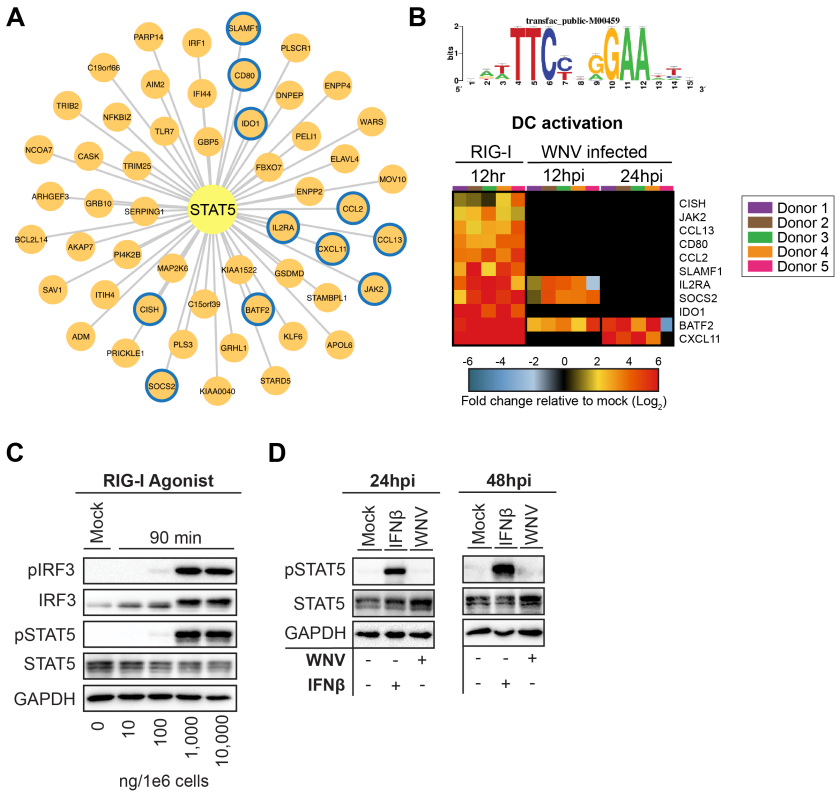


**Fig 3. STAT5 is a regulator of DC activation not activated during WNV infection. (A)** STAT5 regulatory node (large, central node) is shown with the predicted target genes indicated (small nodes), as determined by iRegulon. Genes corresponding to DC activation related processes are highlighted with a blue outline. **(B)** The position weight matrix for the STAT5 binding site from the TRANSFAC database is shown (Top panel). Heatmap of predicted STAT5 target genes involved in DC activation (as highlighted in A) with the $\log_2$ normalized fold change relative to uninfected, untreated cells is shown (>2-fold change, significance of $p<0.01$; Bottom panel). Each column within a treatment condition is marked by a unique color and represents a different donor (n= 5 donors). **(C)** moDCs were treated with RIG-I agonist for 90min (10, 100, 1,000, and

10,000ng/1e6 cells). **(D)** moDCs were treated with IFN $\beta$ for 30min (1,000 IU/mL) or infected with WNV (MOI 10, as determined on Vero cells) for 24 and 48hrs. For C and D, Western blot analysis was performed for the indicated proteins. Representative blots are shown for results obtained from 3-8 donors. See also S4 Fig.

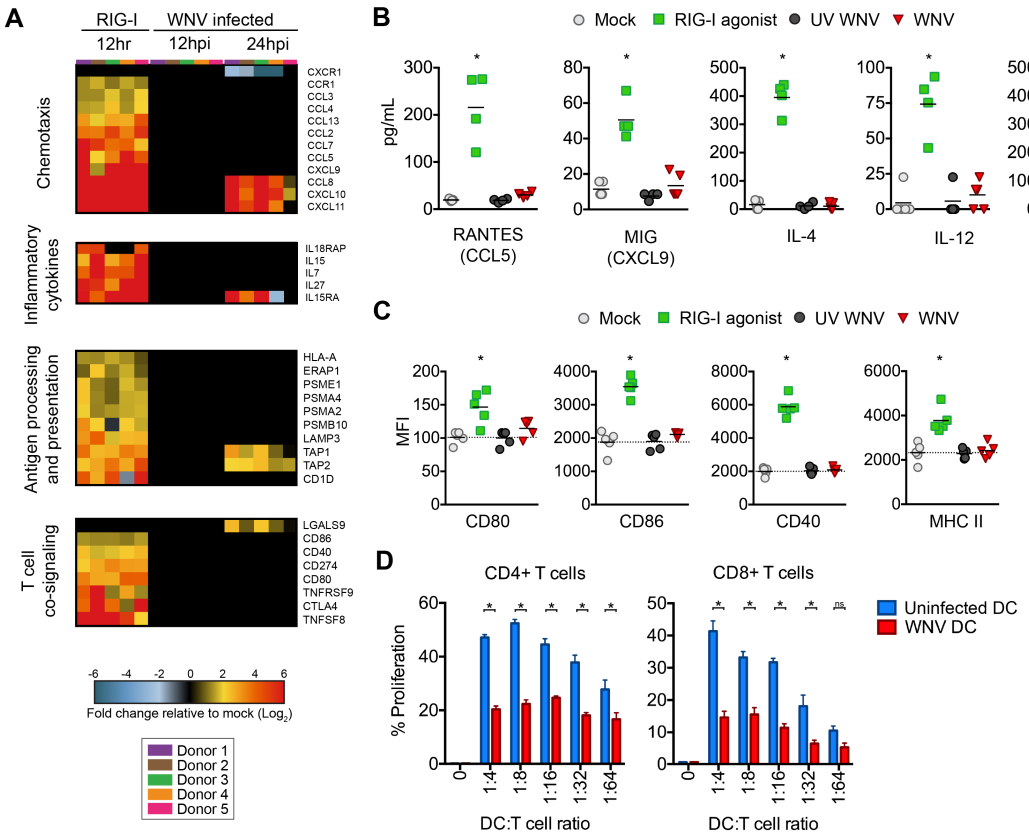


**Fig 4. WNV infected DCs are compromised in T cell priming. (A)** Heatmap of genes involved in chemotaxis, inflammatory cytokine responses, antigen processing and presentation, or T cell co-signaling. The $log_2$ normalized fold change relative to uninfected, untreated cells is shown (>2-fold change, significance of $p<0.01$). Each column within a treatment condition is marked by a unique color and represents a different donor (n= 5 donors). **(B)** Secretion of inflammatory cytokine or chemokine proteins as assessed by multiplex bead array following RIG-I agonist treatment (100ng/1e6 cells), infection with UV-inactivated WNV (MOI 10, "UV-WNV"), or infection with replication competent WNV (MOI 10, "WNV"). Responses were assessed at 24hr following treatment or infection. Data for each donor is shown with the mean (n=4-7 donors). **(C)** Cell

surface expression of CD80, CD86, CD40, or MHC II was quantitated by flow cytometry following RIG-I agonist treatment (100ng/1e6 cells), infection with UV-inactivated WNV (MOI 10, “UV-WNV”), or infection with replication competent WNV (MOI 10, “WNV”). WNV-infected moDCs were labeled for viral E protein and data is shown for the E protein+ population. Responses were assessed at 24hr following treatment or infection. Data for each donor is shown as median fluorescence intensity (MFI) with the mean (n=3-5 donors). Statistical significance ($p < 0.05$) in B and C was determined using a Kruskal-Wallis test with comparisons made to time point matched, uninfected and untreated cells. **(D)** moDCs were left uninfected or infected with WNV (MOI 10) for 24hrs. Allogeneic CD4 or CD8 T cells were labeled with CellTrace violet (CTV) and incubated with uninfected or WNV infected moDCs at the indicated DC:T cell ratios in the presence of an anti-E16 WNV blocking antibody to limit spreading infection (5μg/mL) for 6 days. Percent proliferation was defined as any cell that diluted CTV as compared to a “no DC, T cell only control”. Statistical significance ($p < 0.05$) in D was determined using a 2way ANOVA with comparisons made between T cells primed with Naïve DCs and T cells primed WNV infected DCs. See also S5 Fig.

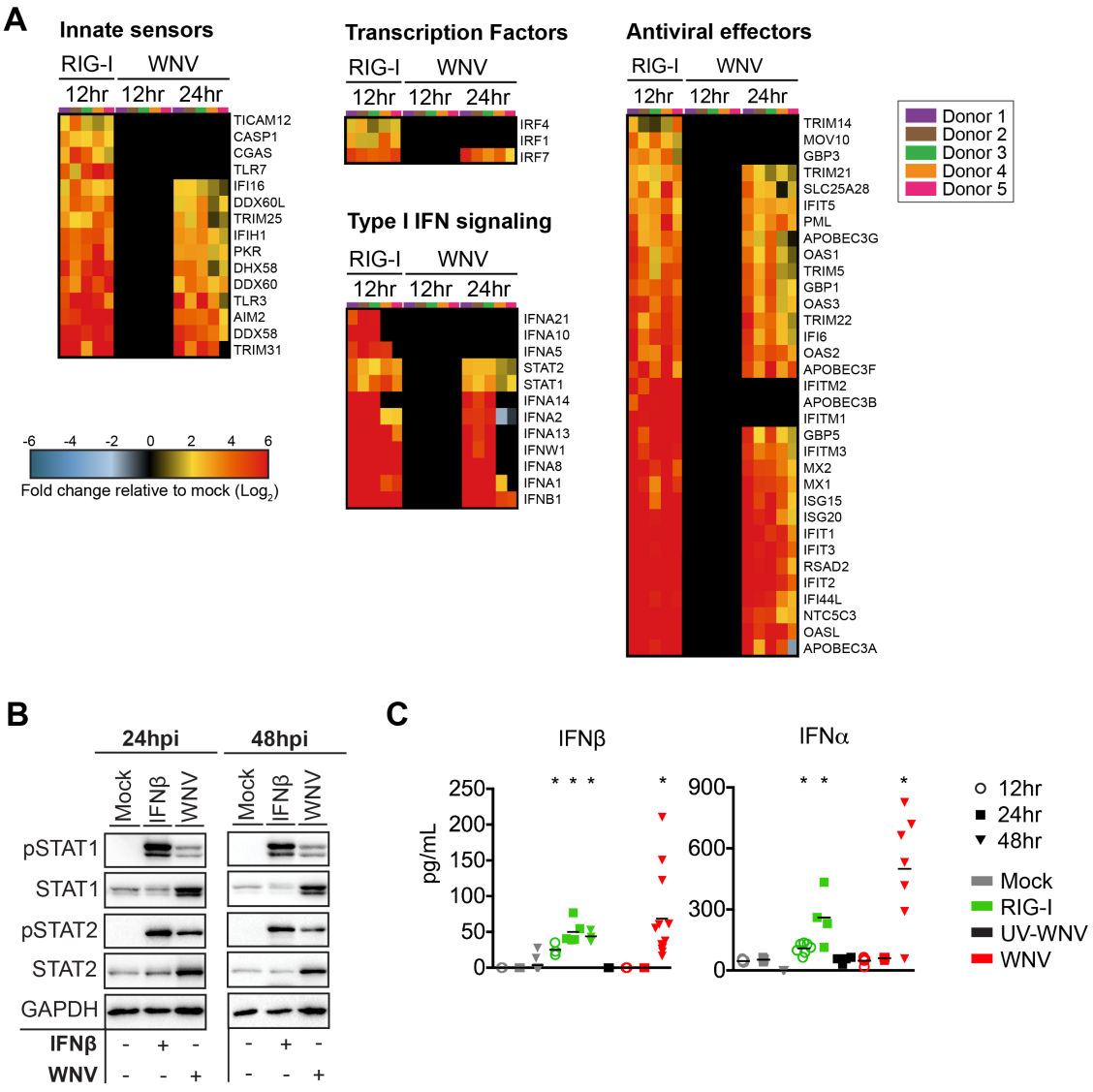


**Fig 5. WNV induces antiviral and type I IFN responses. (A)** Heatmap of differentially expressed genes related to innate immune viral sensing ("innate sensors"), antiviral transcription factors ("transcription factors"), type I IFN responses ("type I IFN signaling"), or genes with antiviral activity ("antiviral effectors"). The $\log_2$ normalized fold change relative to uninfected, untreated cells is shown (>2-fold change, significance of $p<0.01$). Each column within a treatment condition is marked by a unique color and represents a different donor

(n= 5 donors) **(C)** Secretion of IFN $\beta$ and IFN $\alpha$ proteins into the supernatant following RIG-I agonist treatment (100ng/1e6 cells), infection with UV-inactivated WNV (MOI 10, “UV-WNV”), or infection with replication competent WNV (MOI 10, “WNV”). Data is shown for each donor with the mean (n= 4-11 donors). Statistical significance ($p < 0.05$) in C was determined using a Kruskal-Wallis test with comparisons made to time point matched, uninfected and untreated cells.

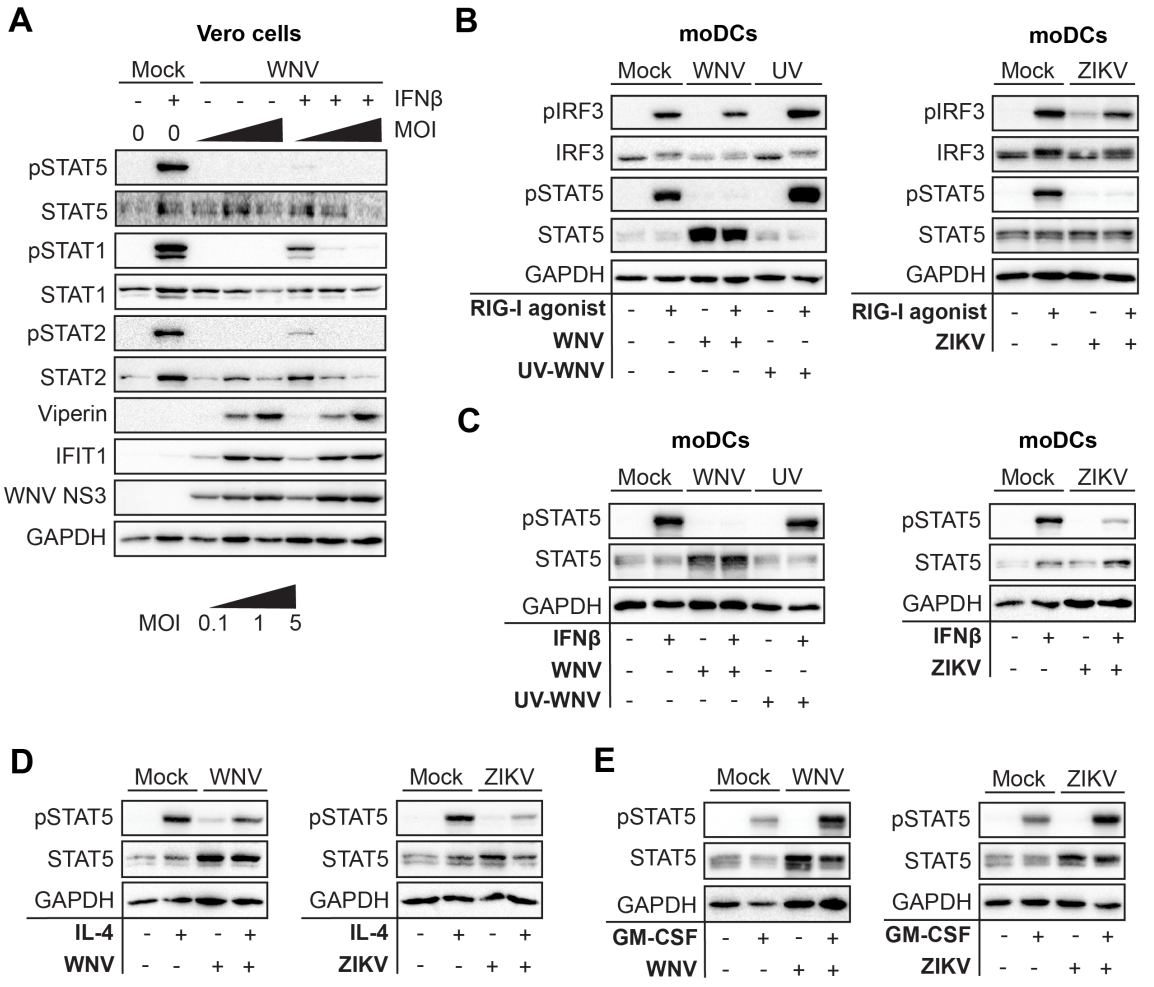


**Fig 6. WNV and ZIKV actively block STAT5 phosphorylation. (A)** Vero cells were left uninfected ( "Mock" ) or infected with WNV (MOI 0.1, 1, or 5 based on Vero titer) for 24hrs. Cells were then left untreated, or pulse treated with IFN $\beta$ (1,000 IU/mL) for 30min. **(B-E)** Human moDCs were left uninfected ("Mock") or infected with WNV, UV-WNV, or ZIKV (48hrs, MOI 10 based on Vero titer). Cells were left untreated or treated with RIG-I agonist (100ng/1e6 cells) for 90mins **(B),** IFN $\beta$ (1,000 IU/mL) for 30min **(C),** IL-4 (10 ng/mL) for 30min **(D)**, or GM-CSF (10 ng/mL) for 30min **(E)**. For A-E, Western blot analysis was performed for the

indicated proteins. Data in A is representative of results obtained from two independent experiments, while data in B-E is representative of results obtained from 3-8 donors. See also S6 Fig.

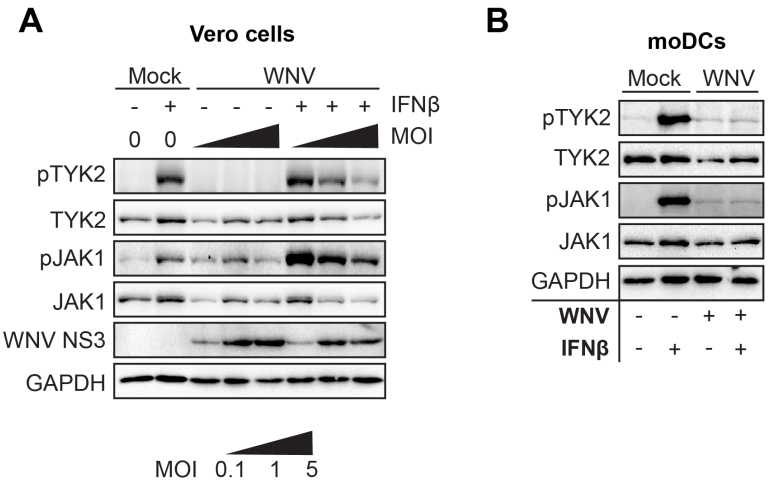


**Fig 7. WNV impairs Tyk2 and JAK1 activation to compromise STAT5 phosphorylation. (A)** Vero cells were left uninfected ( "Mock" ) or infected with WNV (MOI 0.1, 1, or 5 based on Vero titer) for 24hrs. Cells were then left untreated, or pulse treated with IFN $\beta$ (1,000 IU/mL) for 30min. **(B)** Human moDCs were left uninfected ("Mock") or infected with WNV, UV-WNV, or ZIKV (48hrs, MOI 10 based on Vero titer). Cells were left untreated or pulse treated with IFN $\beta$ (1,000 IU/mL) for 30min. For A-E, Western blot analysis was performed for the indicated proteins. Data in A is representative of results obtained from two independent experiments, while data in B is representative of results obtained from 2-3 donors. See also S7 Fig.

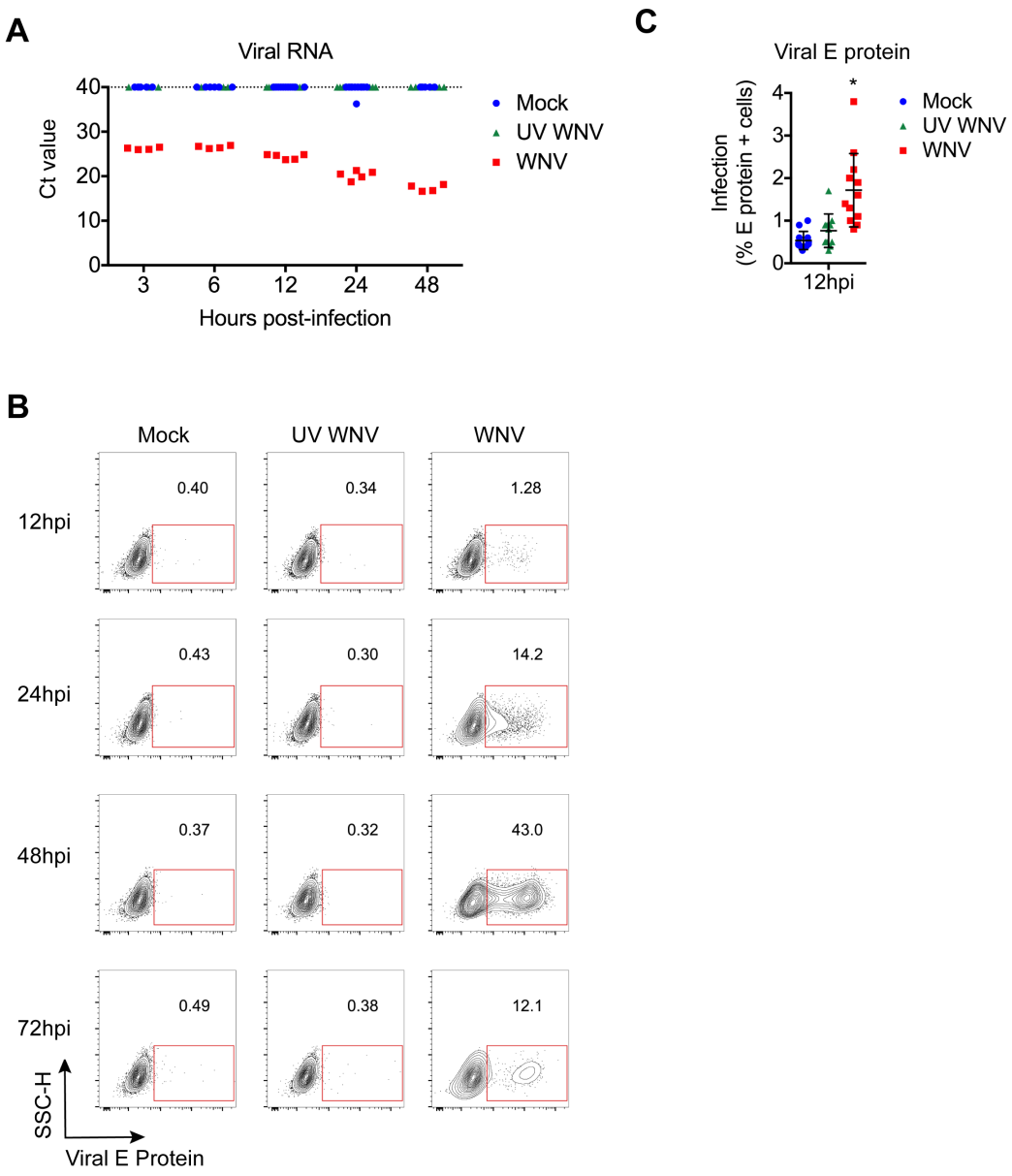


**S1 Fig. WNV productively infects human moDCs.** moDCs were infected with WNV or UV-inactivated WNV (UV-WNV) at MOI 10 (as determined on Vero cells) and analyzed at indicated hours post-infection (hpi). **(A)** Viral RNA quantitated in cell lysates. Shown as non-normalized Ct values for each donor (n=5-11 donors). A Ct value of 40 represents the assay limit of detection and indicates a lack of detectable viral RNA/cDNA amplification. **(B)** Representative flow plots from a

single donor showing the gating of viral E protein+ cells **(C)** Percent E protein+ cells at 12hpi for each donor with the mean +/- SD (n=12 donors).

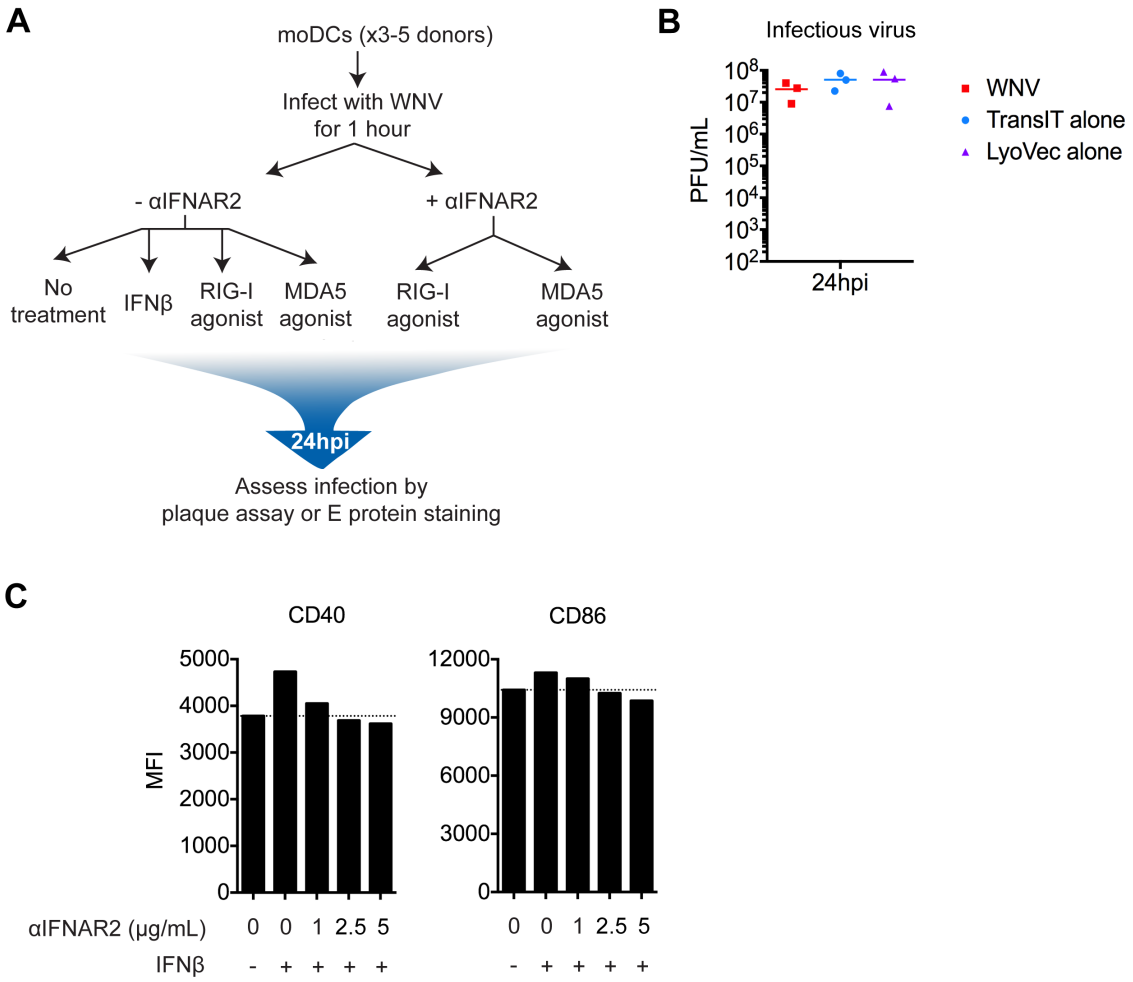


**S2 Fig. Innate immune signaling restricts WNV replication. (A)** Overview of approach used in Figure 1E-G. **(B)** moDCs were infected with WNV at MOI 10 (as determined on Vero cells) for 1hr and then treated with TransIT transfection reagent alone, LyoVec transfection reagent alone, or left untreated ("WNV"). Infectious virus release into the supernatant was assessed at 24hpi. **(C)** moDCs were pre-incubated with different doses of anti-IFNAR2 blocking antibody and then treated with IFNβ for 24hr. Cell surface expression of CD40 and CD86 was evaluated and shown as the median fluorescence intensity from a single donor.

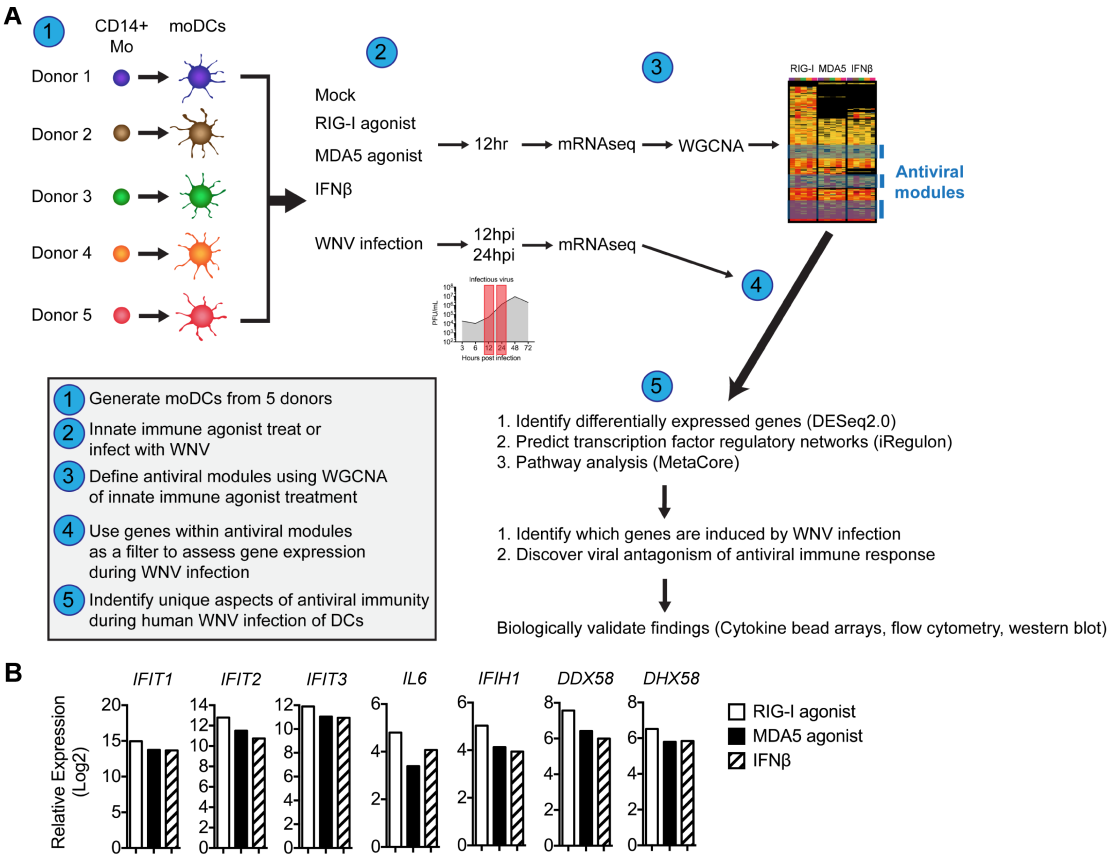


**S3 Fig. Systems biology approach to define the global antiviral response.** **(A)** Overview of systems biology approach used in this study. **(B)** qRT-PCR of antiviral gene expression was performed on cell lysates following 12hr of indicated agonist treatment. Shown as $\log_2$ normalized expression after normalization to *GAPDH* for a single donor.

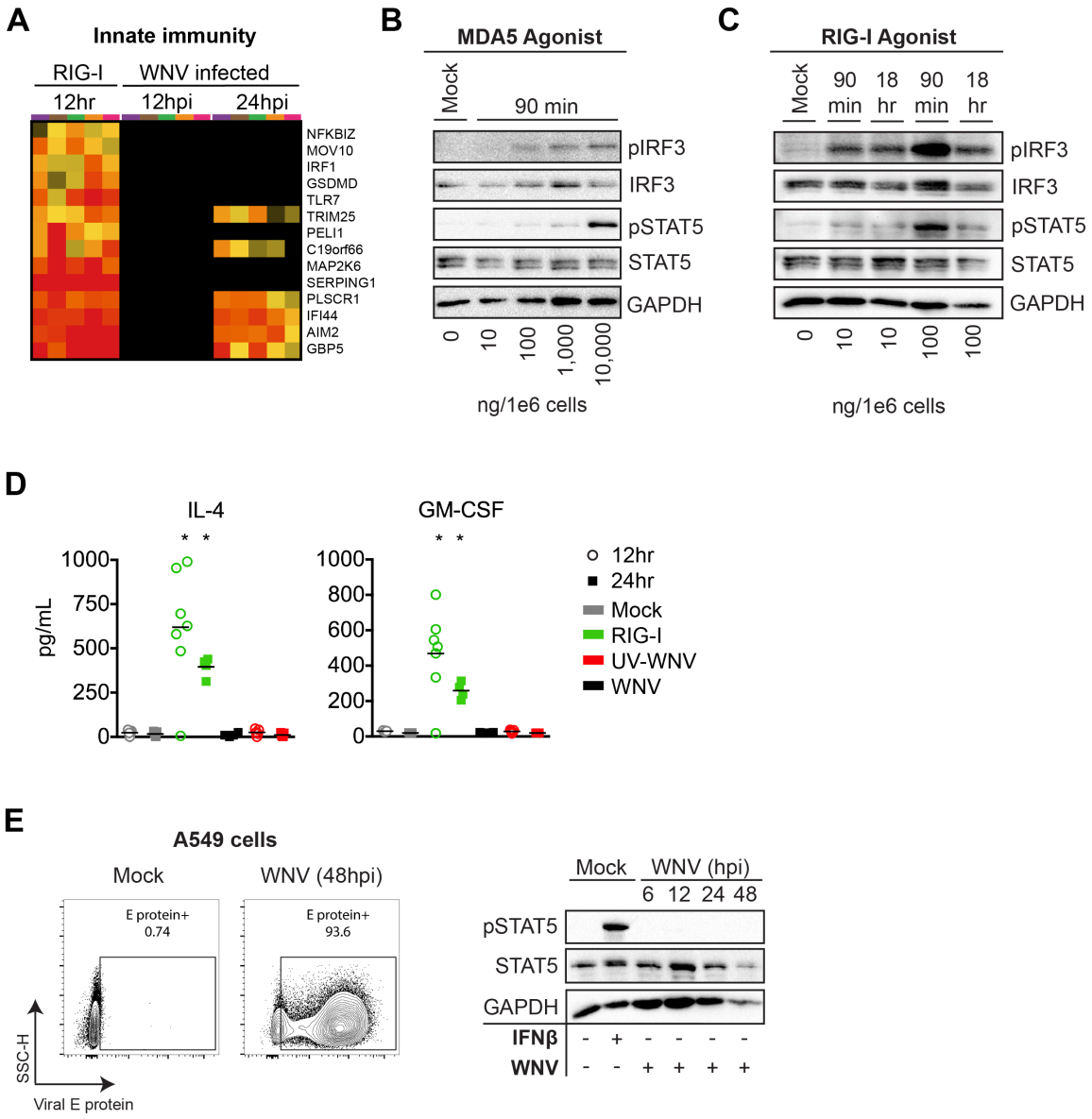


**S4 Fig. STAT5 signaling is activated by innate immune signaling, but not during WNV infection. (A)** Heatmap of predicted STAT5 target genes involved in DC activation (as highlighted in A) with the $\log_2$ normalized fold change relative to uninfected, untreated cells is shown (>2-fold change, significance of $p<0.01$; Bottom panel). Each column within a treatment condition is marked by a unique color and represents a different donor (n= 5 donors). **(B)** moDCs were treated

with MDA5 agonist for 90min (10, 100, 1,000, and 10,000ng/1e6 cells). **(C)** moDCs were treated with RIG-I agonist (10 or 100ng/1e6 cells) for 90 minutes or 18hrs. For B and C, Western blot analysis was performed for the indicated proteins. Western blots are representative of data obtained from 3-8 donors. **(D)** Secretion of IL-4 or GM-CSF as assessed by multiplex bead array following RIG-I agonist treatment (100ng/1e6 cells), infection with UV-inactivated WNV (MOI 10, “UV-WNV”), or infection with replication competent WNV (MOI 10, “WNV”). Data for each donor is shown with the mean (n=4-7 donors). **(E)** Left panel, A549 cells were infected with WNV at MOI 5 (as determined on Vero cells) for 48hrs and stained for viral E protein. Right panel, A549 cells were infected with WNV (MOI 5) and western blot analysis was performed on the indicated proteins at 6hpi, 12hpi, 24hpi, and 48hpi. Data is representative of 3 independent experiments.

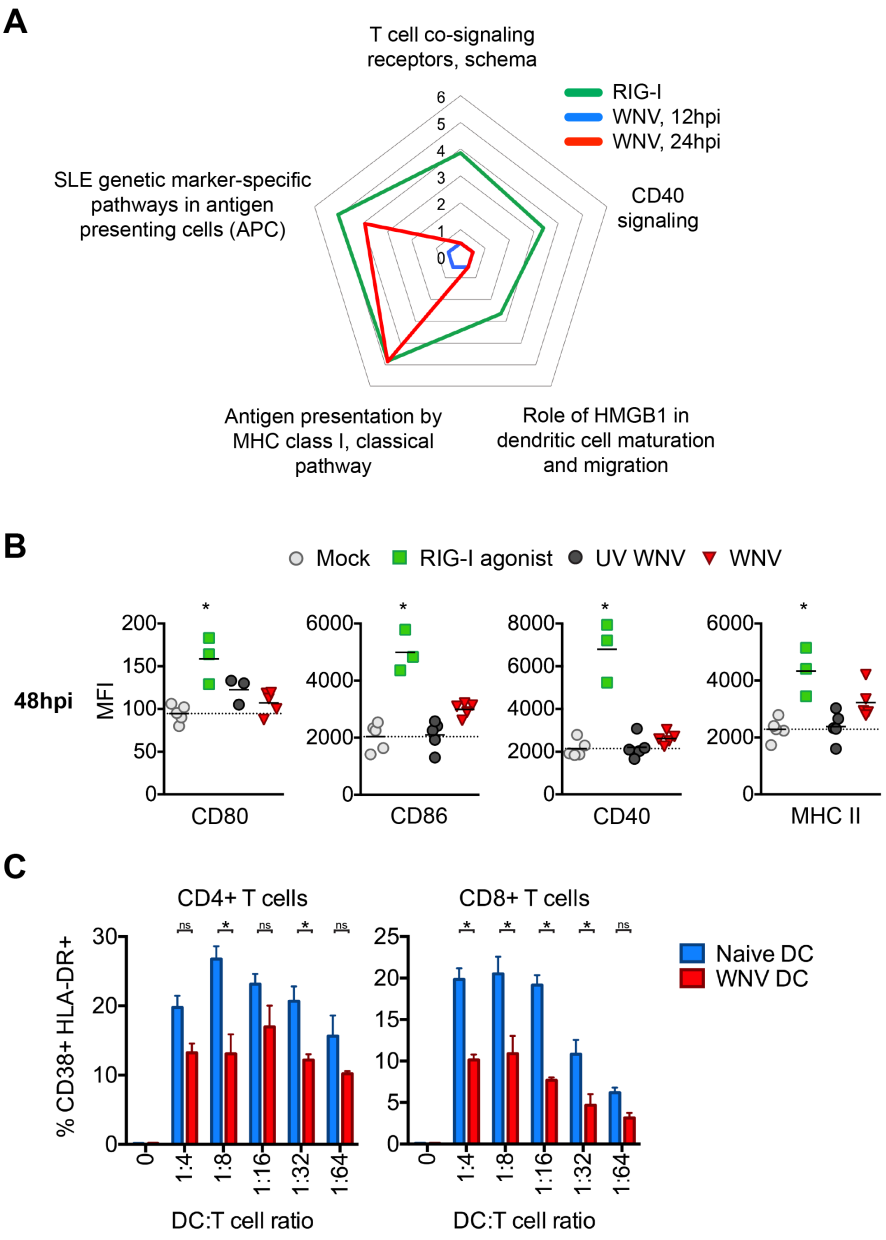


**S5 Fig. WNV induces minimal DC activation and compromises T cell priming. (A)** Top enriched MetaCore canonical pathways of module 5 differentially expressed genes that correspond to processes associated with DC function or activation. The pathway enrichment significance score ($-\log_{10}$ p value) for each indicated treatment condition is depicted as a spider plot. **(B)** Cell surface expression of CD80, CD86, CD40, or MHC II was quantitated by flow

cytometry following RIG-I agonist treatment (100ng/1e6 cells), infection with UV-inactivated WNV (MOI 10, “UV-WNV”), or infection with replication competent WNV (MOI 10, “WNV”). WNV-infected moDCs were labeled for viral E protein and data is shown for the E protein+ population. Responses were assessed at 48hr following treatment or infection. Data for each donor is shown as median fluorescence intensity (MFI) with the mean (n=3-5 donors). Statistical significance ($p < 0.05$) in B and C was determined using a Kruskal-Wallis test with comparisons made to time point matched, uninfected and untreated cells. **(C)** moDCs were left uninfected or infected with WNV (MOI 10) for 24hrs. Allogeneic CD4 or CD8 T cells were incubated with uninfected or WNV infected moDCs at the indicated DC:T cell ratios in the presence of an anti-E16 WNV blocking antibody to limit spreading infection (5μg/mL) for 6 days. The percentage of cells expressing both CD38 and HLA-DR was determined by flow cytometry. Statistical significance ($p < 0.05$) in D was determined using a 2way ANOVA with comparisons made between T cells primed with Naïve DCs and T cells primed WNV infected DCs.

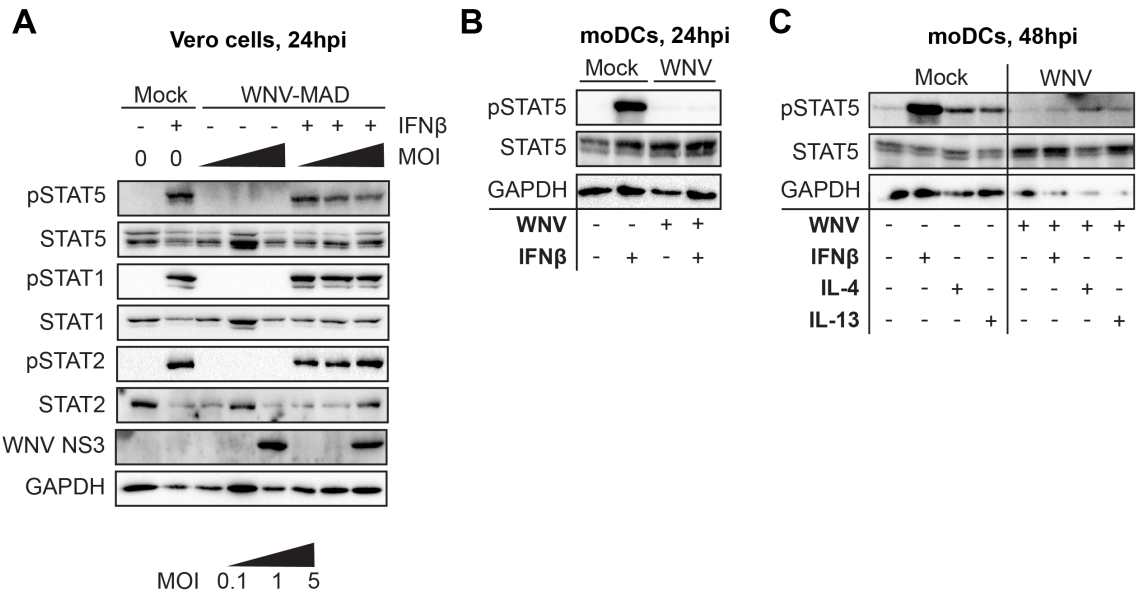


**S6 Fig. Pathogenic WNV, but not a non-pathogenic strain, blocks STAT5 signaling. (A)** Vero cells were left uninfected ("Mock") or infected with WNV-MAD (MOI 0.1, 1, or 5 based on Vero titer), a non-pathogenic WNV strain, for 24hrs. Cells were then left untreated, or pulse treated with IFNβ (1,000 IU/mL) for 30min. **(B, C)** Human moDCs were left uninfected ("Mock") or infected with WNV, UV-WNV, or ZIKV (48hrs, MOI 10 based on Vero titer). Cells were left untreated or treated with IFNβ (1,000 IU/mL), IL-4 (10 ng/mL), or IL-13 (10ng/mL) for 30min**.** For A-C, Western blot analysis was performed for the indicated proteins. Data in A is representative of results obtained from two independent experiments, while data in B and C is representative of results obtained from 2-3 donors.

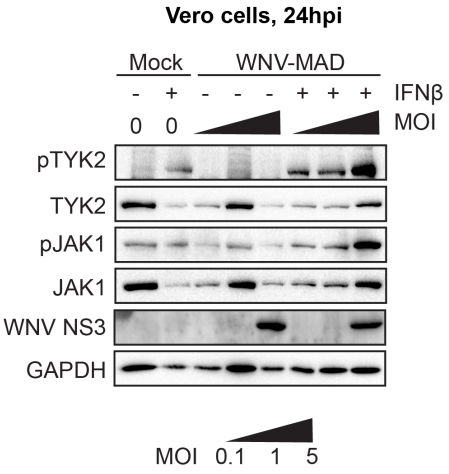


**S7 Fig. Non-pathogenic WNV does not block Tyk2 or JAK1.** Vero cells were left uninfected (“Mock”) or infected with WNV-MAD (MOI 0.1, 1, or 5 based on Vero titer), a non-pathogenic WNV strain, for 24hrs. Cells were then left untreated, or pulse treated with IFNβ (1,000 IU/mL) for 30min. Western blot analysis was performed for the indicated proteins. Data is representative of results obtained from two independent experiments.

## 2H. Tables and legends

| Primary antibody | Source | Catalog number |
|---|---|---|
| Rabbit anti-human phospho-STAT1 (Tyr701; clone D4A7) | Cell Signaling Technologies | 7649 |
| Rabbit anti-human STAT1 (clone 9172) | Cell Signaling Technologies | 9172 |
| Rabbit anti-human phospho-STAT2 (Tyr689; Upstate) | EMD Milipore | 07-224 |
| Rabbit anti-human STAT2 (clone D9J7L) | Cell Signaling Technologies | 72604 |
| Rabbit anti-human phospho-STAT5 (Tyr694; clone D47E7) | Cell Signaling Technologies | 4322 |
| Rabbit anti-human STAT5 (clone 9363) | Cell Signaling Technologies | 9363 |
| Rabbit anti-human phospho-IRF3 (Ser396; clone 4D4G) | Cell Signaling Technologies | 4947 |
| Rabbit anti-human total IRF3 (clone D83B9) | Cell Signaling Technologies | 4302 |
| Rabbit anti-human total Tyk2 (clone D4I5T) | Cell Signaling Technologies | 14193 |
| Rabbit anti-human phospho-Tyk2 (Tyr1054/1055; clone D7T8A) | Cell Signaling Technologies | 68790 |
| Rabbit anti-human total JAK1 (clone 6G4) | Cell Signaling Technologies | 3344 |
| Rabbit anti-human phospho-JAK1 (Tyr1034/1035; clone D7N4Z) | Cell Signaling Technologies | 74129 |
| Rabbit anti-human GAPDH (clone D16H11) | Cell Signaling Technologies | 5174 |
| Mouse anti-human CD11c (BV710, clone B-Ly6) | BD Biosciences | 563130 |
| Mouse anti-human HLA-DR (PE-CF594, clone G46-6) | BD Biosciences | 562304 |
| Mouse anti-human CD1a (BV421, clone HI149) | BioLegend | 300128 |
| Mouse anti-human CD209 (PE, clone 9E9A8) | BioLegend | 330106 |
| Mouse anti-human CD14 (PE, clone M5E2) | BioLegend | 301806 |
| Mouse anti-human CD80 (AF488, clone 2D10) | BioLegend | 305214 |
| Mouse anti-human CD86 (BV605, clone IT2.2) | BioLegend | 305430 |
| Mouse anti-human CD40 (PE-Cy7, clone 5C3) | BioLegend | 334322 |
| Mouse anti-human CD3 (BUV496, clone UCHT1) | BD Biosciences | 564809 |
| Mouse anti-human CD4 (FITC, clone A161A1) | BioLegend | 357406 |
| Mouse anti-human CD8 (FITC, clone HIT8a) | BioLegend | 300906 |
| Mouse anti-human HLA-DR (AF700, clone L243) | BioLegend | 307626 |
| Mouse anti-human CD38 (BUV395, clone HIT2) | BD Biosciences | 740294 |
| Unconjugated monoclonal humanized E16 antibody | Oliphant et al., 2005 | N/A |

### S1 Table. Primary antibodies used in this study

**CHAPTER 3.**

# Zika virus antagonizes type I interferon responses during infection of human dendritic cells

The work presented in this chapter was published in *PLoS Pathogens* as:

**Bowen JR***, Quicke KM*, Maddur MS, O'Neal JT, McDonald CE, Fedorova NB, Puri V, Shabman RS, Pulendran B, Suthar MS. Zika Virus Antagonizes Type I Interferon Responses during Infection of Human Dendritic Cells. PLoS Pathog. 2017;13(2):e1006164. doi: 10.1371/journal.ppat.1006164. PubMed PMID: 28152048.

*James R. Bowen and Kendra M. Quicke contributed equally to this work.

The content is reproduced here in whole with permission from the publisher.

Data not generated by the PhD candidate is indicated in the figure legends.

## 3A. Abstract

Zika virus (ZIKV) is an emerging mosquito-borne flavivirus that is causally linked to severe neonatal birth defects, including microcephaly, and is associated with Guillain-Barre syndrome in adults. Dendritic cells (DCs) are an important cell type during infection by multiple mosquito-borne flaviviruses, including dengue virus, West Nile virus, Japanese encephalitis virus, and yellow fever virus. Despite this, the interplay between ZIKV and DCs remains poorly defined. Here, we found human DCs supported productive infection by a contemporary Puerto Rican isolate with considerable variability in viral replication, but not viral binding, between DCs from different donors. Historic isolates from Africa and Asia also infected DCs with distinct viral replication kinetics between strains. African lineage viruses displayed more rapid replication kinetics and infection magnitude as compared to Asian lineage viruses, and uniquely induced cell death. Infection of DCs with both contemporary and historic ZIKV isolates led to minimal up-regulation of T cell co-stimulatory and MHC molecules, along with limited secretion of inflammatory cytokines. Inhibition of type I interferon (IFN) protein translation was observed during ZIKV infection, despite strong induction at the RNA transcript level and up-regulation of other host antiviral proteins. Treatment of human DCs with RIG-I agonist potently restricted ZIKV replication, while type I IFN had only modest effects. Mechanistically, we found all strains of ZIKV antagonized type I IFN-mediated phosphorylation of STAT1 and STAT2. Combined, our findings show that ZIKV subverts DC immunogenicity during infection, in part through evasion of type I IFN responses, but that the RLR

signaling pathway is still capable of inducing an antiviral state, and therefore may serve as an antiviral therapeutic target.

## 3B. Author Summary

Zika virus (ZIKV) is an emerging mosquito-borne flavivirus that, upon congenital infection, can cause severe neonatal birth defects. To better understand the early innate immune response to ZIKV, we compared infection of human dendritic cells (DCs) between a contemporary Puerto Rican isolate and historic isolates from Africa and Asia. Human DCs supported productive replication following infection with the contemporary strain and exhibited donor variability in viral replication, but not viral binding. While contemporary and historic Asian lineage viruses replicated similarly, the African strains displayed more rapid replication kinetics with higher infection magnitude and uniquely induced cell death. Minimal DC activation and antagonism of type I interferon (IFN) translation was observed during ZIKV infection, despite strong induction of *IFNB1* transcription and translation of other antiviral effector proteins. Treatment with a RIG-I agonist potently blocked ZIKV replication in human DCs, while type I IFN treatment was significantly less effective. Mechanistically, all ZIKV strains inhibited type I IFN receptor signaling through blockade of STAT1 and STAT2 phosphorylation. Altogether, we found that while ZIKV efficiently evades type I IFN responses during infection of human DCs, RIG-I signaling remains capable of inducing a strong antiviral state.

## 3C. Introduction

Zika virus (ZIKV) is an emerging mosquito-borne flavivirus that is causally linked to severe neonatal birth defects upon congenital infection, including microcephaly and spontaneous abortion (52, 54, 55, 58, 59), and is associated with Guillain-Barre syndrome (233) and severe thrombocytopenia (51) in adults. ZIKV was first isolated in Uganda in 1947 from a *Rhesus macaque* (34) and later isolated from the mosquito *Aedes africanus* (234). Phylogenetic analysis has identified three ZIKV lineages, the East African, West African and Asian genotypes, and suggests initial emergence from East Africa and subsequent spread to other regions (32). Humoral immunity generated against one genotype of ZIKV provides cross-protection against heterologous strains, suggesting the existence of a single ZIKV serotype (33).

For decades, ZIKV remained in Africa and Asia where it sparked local epidemics characterized by mild, self-limiting disease in humans. In recent years, Asian lineage viruses have emerged as a global public health threat with widespread epidemics in Micronesia (2007), the Pacific Islands (2013-2014), and the ongoing outbreak in the Americas (2015-2016), where over 35 countries have reported local transmission (235). In December of 2015, local transmission of ZIKV was first confirmed in Puerto Rico, where an ongoing and widespread outbreak has caused over 29,345 confirmed cases as of October 20$^{th}$, 2016 (39, 236). Of most concern, local mosquito-borne transmission of ZIKV has been reported in both Texas and Florida and has resulted in a sporadic, yet troubling increase in the number of confirmed cases (42). Recent human cases and

studies in mice have highlighted the role of sexual transmission in spreading ZIKV (45-48), and concerns of transmission through blood transfusions (237) has led to the Federal Drug Administration to advise screening of all blood and blood products for ZIKV. This growing public health crisis underpins the need to better understand viral replication dynamics and the induction of protective immune responses during ZIKV infection.

Dendritic cells (DCs) are critical immune sentinel cells, bridging pathogen detection to activation of innate and adaptive antiviral immunity. Recent studies have found that multiple subsets of murine DCs in the skin and draining lymph nodes (193), as well as human Langerhans cells, dermal DCs, and monocyte derived-DCs are important cells of dengue virus replication (175). Moreover, a selective loss of type I IFN signaling in DCs ablates host restriction of West Nile virus (WNV), resulting in lethality in a murine infection model (16). Tick-borne encephalitis virus also interferes with DC maturation through degradation of IRF-1 (238), while Japanese encephalitis virus impairs CD8 T cell immunity through depletion of cross-presenting CD8α+ DCs and impaired up-regulation of MHC class II and the T cell co-stimulatory molecule CD40 (239). Despite these studies with closely related flaviviruses, the interplay between ZIKV and DCs remains poorly defined.

The retinoic acid-inducible gene I (RIG-I)-like receptor (RLR) and type I IFN signaling axis is essential for inducing an antiviral response during flavivirus infection (98). The RLRs, which include RIG-I, MDA5, and LGP2, are a family of innate viral RNA sensors that reside in the cytoplasm of nearly every cell of the

host (86). RIG-I and MDA5, signaling through the central adaptor protein mitochondrial antiviral signaling (MAVS), act in concert to restrict flavivirus replication by triggering the production of type I IFN, antiviral effector genes, and pro-inflammatory cytokines (16, 98, 99, 102, 121). Recent work has shown evolutionarily distinct ZIKV strains antagonize innate immunity by targeting STAT2 for degradation, an essential signal transducer downstream of the type I IFN receptor (126). However, the contributions of the RLR signaling pathway in restriction of ZIKV replication remains unknown.

In this study, we demonstrate that human DCs are permissive to productive infection by a contemporary Puerto Rican ZIKV. We observed variation in virus replication between individuals, despite similar levels of viral binding to cells. Historic ZIKV isolates from Africa and Asian also infected human DCs, wherein African lineage viruses replicated more rapidly and reached a higher infection magnitude, while also uniquely inducing cell death. During infection with either contemporary or historic ZIKV strains, we observed minimal up-regulation of DC activation markers and pro-inflammatory cytokine secretion. ZIKV infection of human DCs led to significant induction of *IFNB1* at the transcript level, however, we observed impaired translation of type I IFN proteins despite induced protein expression of the RLRs (RIG-I, MDA5, and LGP2), STAT proteins (STAT1 and 2), and antiviral effectors (IFIT1, IFIT3, and viperin). Treatment with a highly specific RIG-I agonist, but not type I IFN, strongly restricted ZIKV replication in human DCs. The impaired ability of type I IFN to block infection reflected viral antagonism of type I IFN-mediated phosphorylation

of STAT1 and STAT2. Altogether, we show that human DCs have limited immunogenicity following ZIKV infection, in part due to viral antagonism of type I IFN responses.

## 3D. Results

### Contemporary Puerto Rican ZIKV isolate productively infects human DCs

To understand viral replication in human DCs, we generated monocyte derived-DCs (moDCs) from healthy donors and challenged with PRVABC59, a low passage and sequence-verified ZIKV strain isolated in December of 2015 from the serum of a patient infected while traveling in Puerto Rico (hereafter referred to as “PR-2015”). Genome sequencing and phylogenetic analysis have revealed PR-2015 is closely related to clinical isolates responsible for the 2015-2016 outbreak in Brazil (32, 38). To comprehensively profile PR-2015 replication kinetics in human moDCs, we performed parallel analyses of viral RNA synthesis and release of infectious virus. Viral replication began between 12 and 24 hours post infection (hpi), as evidenced by notable increases in viral RNA synthesis that plateaued between 48 and 72hpi (Fig 1A). No viral RNA was detected in mock-infected cells. The kinetics of viral RNA synthesis corresponded to increased release of infectious virus between 12 and 24hpi with continued log phase growth through 48hpi (Fig 1B). Together, our findings show that human moDCs support productive ZIKV replication with a contemporary Puerto Rican strain.

**Cellular level analysis of Puerto Rican ZIKV replication in human DCs**

We next determined how PR-2015 infection at the single cell level impacts viral growth kinetics in the bulk cell population. Infected moDCs were labeled for expression of ZIKV antigen using the pan-flavivirus 4G2 antibody, which recognizes a structural protein found within the virus envelope (E), and percent infection was assessed by flow cytometry. Infected cells were first detected in low numbers at 12hpi (Mock, 0.2 – 0.9%; PR-2015, 0.2 – 3.2%), increasing in percentage and staining intensity over the next 36 hours (Fig 1C). When we infected moDCs with ultraviolet (UV)-inactivated virus, we observed no E protein staining above uninfected cells, confirming detection of newly synthesized viral protein (S1A Fig). To confirm antibody staining, we performed ImageStream analysis of PR-2015-infected moDCs. ZIKV E protein was detected within the cytoplasm and did not co-localize with the cell surface marker CD11c (Fig 1D). This staining pattern is consistent with our recent observations of ZIKV E protein staining in placental macrophages, where viral protein localized to perinuclear regions within the cytoplasm and likely within an endoplasmic reticulum-derived network (2, 61). As expected, increases in the percentage of infected cells corresponded to the kinetics of viral RNA synthesis and infectious virus release.

**Variability in Puerto Rican ZIKV infection occurs after viral binding**

Notably, moDCs generated from four of the nine donors used in this analysis released lower amounts of infectious virus, and in some cases, synthesized lower amounts of viral RNA (Fig 1A and 1B). When we directly

compared infectious virus release and viral E protein staining, the same 4 donors with the lowest amount of infectious virus release at 48 and 72hpi ("low infection") also had lower percentages of E protein positive cells at 48hpi (0.4 – 3.1%) as compared to the other 5 "high infection" donors (9.8 – 18.9%) (S1B Fig). One explanation for variability in viral replication may be differences in viral binding to host receptors on moDCs generated from different donors. To test this, we developed a qRT-PCR-based viral binding assay (S1C Fig) (23, 240). To verify we were measuring bound virus, we compared viral RNA levels with and without washing, as well as after trypsin treatment, which should cleave proteinaceous cellular receptors and remove bound virus from the cell surface. Washing cells significantly reduced the amount of virus detected and trypsin treatment further diminished viral RNA levels, confirming our ability to measure cell-bound virus in the "+Wash, -Trypsin" condition (Fig 1E). In contrast to the differences observed in viral RNA synthesis, viral E protein staining, and infectious virus release, there was minimal difference in the amount of bound virus between different donors. This suggests that the variability in ZIKV infection between donors occurs after viral binding.

**Differential infection of human DCs by evolutionarily distinct ZIKV strains**

We next infected moDCs with sequence-verified ZIKV isolates spanning the evolution of the virus since its discovery, including ancestral isolates from East Africa (MR-766, "MR-1947"), West Africa (DakAr 41524, "Dak-1984"), and Asia (P6-740, "P6-1966") (31, 32). The MR-1947 strain was isolated in 1947 from

an infected sentinel *Rhesus macaque,* monkey number 766, in the Ziika forest of Uganda. The Dak-1984 strain was later isolated from an infected *Aedes africanus* mosquito in Senegal in 1984. The P6-1966 strain was isolated in 1966 from an infected *Aedes aegypti* mosquito in Malaysia, and represents the oldest known ancestor of the Asian lineage since divergence from the African lineages. Each viral isolate has different laboratory passage histories, including multiple passages in suckling mouse brains in the case of MR-1947 and P6-1966, which must also be taken into consideration (S1 Table). We independently sequenced each of the four ZIKV strains and performed nucleotide sequence alignments (see S1 Table for genome accessions), finding P6-1966 shares 95.5% of its coding region with PR-2015, while MR-1947 and Dak-1984 only share 88.6% with PR-2015 (S1 Table). This corresponded to 1.1%, 3.2%, and 3.0% differences in amino acids between PR-2015 and P6-1966, MR-1947, and Dak-1984, respectively. Of note, MR-1947 diverged from PR-2015 more notably in the structural (4.4%) than non-structural proteins (2.9%).

Using the same moDCs generated from six of the previous donors (Fig 1), we directly compared infection kinetics of the ancestral strains with that of PR-2015. The infections were performed in parallel with PR-2015 to allow for direct cross-comparison of viral growth between the different viral strains (S2A Fig). MR-1947 exhibited rapid replication kinetics with increased infectious virus release and viral RNA synthesis occurring between 12 and 24hpi (Fig 2A, 2B, and S2B Fig). The percentage of infected cells peaked at 24hpi (Fig 2C and 2D).

We next compared MR-1947 replication with Dak-1984, which is closely related to MR-1947 but has undergone less laboratory passaging. Despite reaching a similar infection magnitude, Dak-1984 exhibited slower growth kinetics as compared to MR-1947, with percent infection and release of infectious virus peaking between 48 and 72hpi. The P6-1966 strain replicated with similar kinetics and magnitude to PR-2015 through 48hpi, although we did observe subtle differences in virus infection. In particular, P6-1966 replicated to modestly higher levels at 24hpi than PR-2015. Despite this, P6-1966 replication plateaued more rapidly than PR-2015 and failed to reach a comparable magnitude of infection. These subtle differences may reflect genetic changes between ancestral Asian lineage strains and current circulating strains (S1 Table). Of note, P6-1966 was found to produce smaller viral plaques and foci on Vero cells as compared to the other three strains (S2C Fig). Given recent studies linking ZIKV to cell death of neural progenitor cells, we evaluated cell viability during ZIKV infection of human moDCs (68, 69, 71). While MR-1947 and Dak-1984 induced significant decreases in cell viability by 72hpi, neither of the Asian lineage strains resulted in loss of viability as compared to time-matched, uninfected cells (Fig 2E). Together, our data suggest that evolutionarily distinct ZIKV strains exhibit varying replicative and cell death capacities during infection of human DCs.

**Differential susceptibility of human DCs to ancestral and circulating ZIKV strains**

Given our findings that moDCs generated from different donors have differential susceptibilities to PR-2015 infection (Fig 1), we next compared replication between the four strains on a donor-by-donor basis. The MR-1947 strain replicated well within all donors, showing the least amount of variation in viral replication between donors (Fig 2B and 2D and S1B Fig). The Dak-1984 strain also replicated well in most donors, albeit to modestly diminished peak levels in donors with lower levels of PR-2015 replication. In contrast, P6-1966 replicated similarly to PR-2015 for a given donor, likely representing their shared ancestry. Together, these data suggest both viral factors, as found between different strains, as well as non-viral factors, as found between different donors, influence ZIKV replication in human DCs.

**ZIKV infection minimally activates human DCs**

A critical function of DCs is the programming of virus-specific T cell responses that are required for clearance of virally infected cells. Engagement of virus-associated molecular patterns increases the surface expression of co-stimulatory and MHC molecules on activated DCs, potently enhancing their ability to prime virus-specific T cell responses (241). To determine the ability of ZIKV infection to program DCs, we measured cell surface expression of co-stimulatory (CD80, CD86, and CD40) and MHC class II molecules at 48hpi with all four ZIKV strains. We labeled cells with 4G2 antibody and divided infected samples based on viral E protein staining (E protein-, bystander cells and E protein+, infected cells). Following infection with PR-2015, we observed

significant but modest activation in E protein+ cells only, while infection of moDCs with P6-1966 or Dak-1984 induced minimal activation (Fig 3A). In comparison, MR-1947 induced modest activation, but primarily within the E protein- cell population. This is in contrast to strong activation induced by RIG-I agonist treatment of moDCs (S3A Fig). Next, we confirmed our findings in more physiologically relevant human antigen presenting cell subsets. Similar to moDCs, *ex vivo* infection of primary monocytes, myeloid DCs, and plasmacytoid DCs from the blood of healthy donors failed to induce up-regulation of co-stimulatory or MHC molecules (S3B-D Fig).

We next asked whether the donor variability in viral replication with PR-2015 (Fig 1) corresponded to differences in DC activation during infection. We grouped samples into “low” or “high” infection donors on the basis of viral E protein staining (S1B Fig). We found no differences in the up-regulation of CD80 and CD86 when we stratified by viral replication (Fig 3B). In contrast, both CD40 and MHC class II showed greater up-regulation during infection of moDCs from donors with higher viral replication. This suggests that the induction of DC activation is influenced by the magnitude of viral replication. Altogether, these data show that ZIKV induces minimal DC activation and as a consequence, infected DCs may be compromised in their ability to prime antiviral T cell responses.

**ZIKV does not induce pro-inflammatory cytokine secretion by human DCs**

In addition to providing T cell co-stimulation, DCs promote innate and adaptive immunity through the secretion of pro-inflammatory mediators. We next assessed inflammatory cytokine and chemokine release following PR-2015 infection of moDCs. Consistent with minimal increases in surface expression of co-stimulatory molecules, PR-2015 infection failed to induce the secretion of most pro-inflammatory cytokines assayed, despite the ability of RIG-I agonist to induce their secretion (Fig 4A and S2 Table). The ancestral strains also failed to induce substantial cytokine release during infection of human moDCs. Of exception, P6-1966 induced significant IL-6 secretion, and along with MR-1947 and Dak-1984, triggered modest yet significant IP-10 secretion. Finally, to confirm these findings in more physiologically relevant myeloid cell subsets, we stimulated primary monocytes (Fig 4B and S3 Table), myeloid DCs (Fig 4C and S4 Table), and plasmacytoid DCs (Fig 4D and S5 Table) isolated from healthy human blood with PR-2015 to assess cytokine and chemokine secretion. Despite the ability of LPS (monocytes and myeloid DCs) or R848 (plasmacytoid DCs) to induce cytokine production, infection with ZIKV did not promote notable pro-inflammatory cytokine secretion. Together, our data suggests that human antigen-presenting cells exposed to ZIKV are compromised in their ability to promote inflammatory responses.

**Human DCs infected with ZIKV secrete minimal type I and III IFNs**

During viral infection, early innate immune signaling triggers the production of type I and III IFNs and antiviral effector molecules that block viral

replication (242). In particular, RLR and type I IFN signaling are essential for host restriction of flavivirus replication and ultimate control of infection (16, 98, 243). Specific to ZIKV, mice with intact type I IFN responses support only limited and low level viral replication, while genetic ablation or antibody blockade of type I IFN signaling shifts the balance towards sustained, high level ZIKV replication and pathology, including neuroinvasive disease (85, 124, 125). Moreover, mice deficient in their ability to produce type I IFN are similarly compromised in their ability to restrict viral replication (46, 85).

To determine the potential of human DCs to trigger type I IFN responses during ZIKV infection, we measured the secretion of type I IFN proteins into the supernatant by infected populations of moDCs at 48hpi. Surprisingly, all four ZIKV strains failed to induce detectable IFNβ secretion and induced only minimal secretion of IFNα (Fig 5A). Given this intriguing finding and the recently appreciated role of type III IFNs in antiviral immunity, we next measured the secretion of IFNλ1 (129). Similar to type I IFNs, ZIKV infection induced minimal secretion of type III IFN protein (Fig 5B). Treatment of the same donor cells with RIG-I agonist induced significant secretion of all three molecules, confirming these cells are capable of producing type I and type III IFNs. Similar to moDCs, pDCs produced low amounts of IFNα following ZIKV infection (S5 Table).

Next, as a complementary measurement of type I IFN secretion, we infected moDCs with ZIKV in the presence of an anti-IFNAR2 blocking antibody. Blockade of type I IFN signaling enhanced ZIKV infection modestly across all four ZIKV strains, resulting in only a 2-3 fold increase in the percentage of virally

infected cells (Fig 5C). Despite this increase in the percentage of infected cells, we observed minimal differences in the release of infectious virus in the presence of anti-IFNAR2 blocking antibody. Combined, these findings suggest that human DCs secrete type I IFN at near undetectable levels during ZIKV infection.

**ZIKV infection of human DCs induces type I IFN transcription, but not translation**

Given that multiple pathogenic human viruses have involved mechanisms to interfere with type I IFN transcription (92, 244-246), we next assessed the levels of *IFNB1* transcripts in ZIKV-infected moDCs. Despite near undetectable protein secretion, all four ZIKV strains induced notable *IFNB1* gene transcription at 48hpi, with MR-1947 showing the highest induction (Fig 5D). When we assessed *IFNB1* gene induction over an infection time-course, up-regulation of transcription occurred as early as 12hpi and remained at or near peak levels through 72hpi (S4A Fig). We also observed induction of *IFNA* transcription, but with delayed kinetics and magnitude as compared to *IFNB1*. *IFNA* transcription was up-regulated at 24hpi during infection with MR-1947, and at 48hpi during infection with the other three strains. These findings are consistent with our recent studies performed in placental macrophages, which showed minimal type I IFN protein secretion, but strong induction at the transcript level during ZIKV infection(61).

Given that RIG-I agonist induced IFNβ secretion, we directly compared *IFNB1* transcript levels in matched moDCs treated with RIG-I agonist or infected

with ZIKV PR-2015. RIG-I agonist treatment induced modestly higher, but overall similar levels of *IFNB1* transcription as compared to during ZIKV PR-2015 infection (Fig 5E). Next, to determine if there was impairment in type I IFN protein translation or secretion, we measured type I IFN protein in the supernatant and whole cell lysate from matched samples following RIG-I agonist treatment or infection with ZIKV PR-2015. We hypothesized that if ZIKV blocked protein secretion, but not translation, we would find an accumulation of type I IFN protein in the whole cell lysate. We did not detect IFNβ or IFNα protein in either the supernatants or whole cell lysates above mock levels at either low or high MOI infection (MOI 1 or 10) with ZIKV (Fig 5F). In contrast, both IFNβ and IFNα were observed in the supernatants and whole cell lysates following RIG-I agonist treatment. To determine if ZIKV could actively block type I IFN translation, we treated ZIKV PR-2015-infected moDCs with RIG-I agonist at 48hpi and measured IFNβ protein production. ZIKV infection resulted in an average 2-fold decrease in the induction of IFNβ protein translation as compared to RIG-I agonist alone (Fig 5G). Altogether, our data suggests that ZIKV antagonizes type I IFN translation during infection of human DCs.

Of relevance to our findings, protein kinase R (PKR) is important for maintaining mRNA stability of type I IFN transcripts during infection with certain RNA viruses (247). In these studies, EMCV infected cells were found to strongly induce *Ifnb1* gene expression, but in the absence of PKR these transcripts lacked poly(A) tails, leading to diminished transcript stability and minimal protein translation. To determine if a similar phenomenon occurs during ZIKV infection of

human DCs, we compared *IFNB1* transcript levels after performing cDNA synthesis with random hexamers, which will prime all RNA species, or Olido(dT), which will only prime polyadenylated transcripts. We found no differences in *IFNB1* transcript levels between the two methods, suggesting ZIKV does not influence *IFNB1* transcript stability as a mechanism to inhibit protein translation (S4B Fig).

**ZIKV infection induces an antiviral state within human DCs**

Given the minimal secretion of type I and type III IFNs, we evaluated gene expression of the RLRs and host antiviral effectors. We observed up-regulation of RIG-I (*DDX58*), MDA5 (*IFIH1*), and LGP2 (*DHX58*) in response to PR-2015 and P6-1966 at 24hpi, consistent with increases in virus load (Fig 6A). RLR expression continued to increase through 72hpi. While RLR expression was higher at 24hpi in moDCs infected with P6-1966 as compared to PR-2015, expression peaked at similar levels at 48 and 72hpi, potentially reflecting the slightly enhanced replication kinetics of P6-1966. In contrast to the Asian lineages, MR-1947 exhibited strong RLR up-regulation by 12hpi with peak expression between 24 and 48hpi. Moreover, the magnitude of RLR transcription during peak responses was notably higher for MR-1947 infection. The kinetics of RLR expression during infection with Dak-1984 was more similar to the Asian lineage strains than MR-1947, first increasing at 24hpi. Interestingly, despite reaching a similar overall magnitude of infection as MR-1947, Dak-1984 induced lower RLR transcription at all time-points.

We next evaluated expression of the IFIT gene family members, *OAS1*, and viperin (*RSAD2*), antiviral effectors with known activity against flaviviruses (248). In moDCs infected with PR-2015, we observed up-regulation of *IFIT1*, *IFIT2* and *IFIT3* beginning at 12hpi, with peak expression between 48 and 72hpi (Fig 6B). P6-1966 infection resulted in slightly delayed IFIT gene induction as compared to PR-2015. Despite this delay, P6-1966 induced stronger IFIT gene expression by 24hpi. We observed similar findings with *RSAD2* expression, with PR-1966 infection inducing lower transcript levels at 12hpi, but increased responses at 24hpi as compared to PR-2015. We found *OAS1* transcripts were up-regulated at 24hpi by both PR-2015 and P6-1966, although to higher levels during P6-1966 infection. MR-1947 infection exhibited enhanced kinetics and magnitude of antiviral effector gene transcription, with *IFIT* family members and *RSAD2* being induced as early as 12hpi. While *OAS1* was up-regulated with similar kinetics to the Asian lineage strains, the magnitude was also notably higher during MR-1947 infection. In general, Dak-1984 was transcriptionally most similar to the Asian lineage viruses, despite higher levels of viral replication during Dak-1984 infection.

Given observed differences in PR-2015 replication between donors, we compared gene expression between donors with “low” or “high” infection (S1B Fig). For all of our RNA samples, we labeled infected cells in parallel for viral E protein, allowing us to stratify our RNA data by the percentage of viral E protein+ cells. Donors with low infection had overall lower expression of RLR, type I IFN, and antiviral effector genes as compared to donors with high infection (S5 Fig).

Furthermore, there were no differences in the expression of any of the measured host genes at 3hpi between “low” and “high” infection donors, a time that likely represents basal level expression. Overall, these data show that ZIKV infection is capable of initiating antiviral responses in human DCs, with expression of certain antiviral effector genes being induced rapidly after infection, prior to log phase viral growth.

We next questioned whether the observed up-regulation of antiviral effector genes led to corresponding increases at the protein level, in light of our findings with type I IFN. As expected, overnight stimulation with RIG-I agonist induced up-regulation of the RLRs (RIG-I, MDA5, and LGP2), STAT proteins (STAT1 and STAT2), and multiple proteins directly involved in restriction of viral replication (IFIT1, IFIT3, and viperin) (Fig 6C). Notably, we observed no induction of IFIT1, IFIT3, or viperin in untreated cells. In contrast to impaired translation of type I IFN proteins, infection of moDCs for 48hrs with ZIKV PR-2015 or MR-1947 induced strong up-regulation of the RLRs, STAT proteins, and viral restriction factors to similar levels observed following RIG-I agonist treatment. We observed MOI dependent increases in many cases (STAT1, IFIT1, IFIT3, viperin) following infection with PR-2015 at MOIs of 1 and 10. Similar to what was observed at the transcript level, MR-1947 infection resulted in stronger induction of antiviral proteins as compared to PR-2015 when comparing infections at MOI of 1. This is likely explained by the higher magnitude of infection seen with MR-1947. Together, these findings suggest that ZIKV selectively inhibits in type I IFN protein translation, while translation of other antiviral host proteins remains intact.

**ZIKV replication is blocked by RIG-I, but not type I IFN signaling**

Given our findings that ZIKV infection of moDCs induced an antiviral state, and the importance of RLR and type I IFN signaling in restriction of flavivirus replication (16, 98, 99, 102), we next determined the ability of innate immune signaling pathways to restrict ZIKV replication within human DCs. At 1hpi, we treated infected moDCs with innate immune agonists and assessed viral replication at 48hpi (Fig 7A). To trigger RLR signaling, moDCs were transfected with a highly specific RIG-I agonist, derived from the 3' UTR of hepatitis C virus (197, 249). To trigger type I IFN signaling, we treated moDCs with 100 IU/mL of recombinant human IFNβ. RIG-I agonist treatment potently blocked ZIKV replication, significantly lowering infectious virus release to levels at or near the assay limit of detection (Fig 7B). Notably, the amount of infectious virus remaining after RIG-I agonist treatment was similar to levels found at 3 and 12hpi (Fig. 2A), prior to the log phase viral growth, and may represent residual input virus rather than replicated virus. Importantly, RIG-I agonist treatment restricted replication of all four ZIKV strains. In contrast, type I IFN treatment resulted in only modest, and non-significant decreases in viral replication. Altogether, RLR signaling, but not type I IFN signaling, potently blocks replication of four evolutionarily distinct ZIKV strains.

**ZIKV antagonizes type I IFN signaling by targeting STAT1 and STAT2 phosphorylation**

Secreted type I IFN binds to the type I IFN receptor, a heterodimeric complex found on the cell surface of almost all nucleated cells, triggering activation of the receptor associated kinases JAK1 and TYK2 (242). JAK1 and TYK2 phosphorylate and activate the latent transcription factors STAT1 and STAT2, which translocate to the nucleus and associate with IRF-9 to trigger antiviral gene transcription. Most flaviviruses known to infect humans have evolved mechanisms to inhibit type I IFN responses through antagonism of JAK/STAT signaling (123, 228, 250, 251). Given our finding that type I IFN treatment was not effective at blocking ZIKV replication in moDCs, we evaluated the ability of ZIKV to antagonize STAT1 and STAT2. For these studies, we utilized human A549 cells, which have been previously shown to be permissive to ZIKV infection (78) and have been employed to study antiviral innate immune signaling (123, 196, 252). We pulse treated uninfected or ZIKV-infected cells (48hpi, MOIs of 0.1 and 1) for 30 minutes with IFNβ (1000 IU/mL) and evaluated phosphorylation of STAT1 (Tyr701) and STAT2 (Tyr689) by western blot. Cells infected with any of the four ZIKV strains did not show enhanced STAT1 or STAT2 phosphorylation above untreated ZIKV-infected cells (Figs 8A and 8B, top panels). Infection alone increased the total levels of STAT1 and STAT2 protein, although notably less so at an MOI of 1 as compared to MOI 0.1. Given the different levels of total STAT proteins between conditions, we calculated the ratio of phosphorylated:total protein to allow for a better comparison of phosphorylation status (Figs 8A and 8B, bottom panels). Indeed, even in instances where ZIKV infection increased total STAT protein levels, the majority

remained in an unphosphorylated state. Interestingly, while ZIKV infection alone did induce low levels of STAT1 and STAT2 phosphorylation, in most conditions, there was a notable decrease in phosphorylation at MOIs of 1 as compared to MOIs of 0.1, a finding most profound with the African lineage viruses. We next determined the percentage of ZIKV infected cells at MOIs of 0.1 and 1 using flow cytometry. The percentage of infected cells ranged from 32.7 – 74% at an MOI of 0.1 and increased to 60.1 – 87.8% at an MOI of 1 across infection with the four strains (S6 Fig). Of note, we observed higher cytopathic effects and cell death at MO of 1 as compared to MOI of 0.1 when preparing cells for staining. Given the presence of uninfected cells, even at MOI of 1, it remains possible that the STAT1 and STAT2 phosphorylation observed during infection is from uninfected cells. Nevertheless, this confirms that the majority of cells were ZIKV-infected at the time of pulse treatment with IFNβ and inhibition of type I IFN signaling can be attributed to ZIKV infection.

We next determined whether ZIKV infection antagonizes type I IFN signaling within human DCs. ZIKV PR-2015-infected moDCs (48hpi, MOI 10) were left untreated or pulse treated with IFNβ for 30 minutes and evaluated for STAT1 and STAT2 phosphorylation. Infection with ZIKV PR-2015 in the absence of IFNβ treatment induced minimal STAT1 phosphorylation and low levels of STAT2 phosphorylation, despite notable up-regulation of STAT1 and STAT2 total proteins (Fig 8C, left panel). Treatment of ZIKV infected cells with IFNβ increased phosphorylation of STAT2, and to a lesser extent STAT1, but to notably lower levels than treatment of uninfected cells when accounting for total STAT1 and

STAT2 protein levels (Fig 8C, right panel). Combined, this shows that, similar to A549 cells, ZIKV antagonizes the phosphorylation of STAT1 and STAT2 in human DCs.

## 3E. Discussion

In our study, we show a contemporary Puerto Rican ZIKV strain, PR-2015, productively infects human DCs with notable donor variation in viral replication, despite no differences in viral binding. Ancestral ZIKV strains of the African (MR-1947 and Dak-1984) and Asian (P6-1966) lineages also infected human DCs. Each strain exhibited unique viral growth curves, with cell death only observed during infection with African lineage strains. We observed minimal up-regulation of co-stimulatory and MHC molecules, inflammatory cytokine secretion, as well as antagonism of type I IFN translation during ZIKV infection, despite notable transcriptional up-regulation of *IFNB1*. Despite this, ZIKV infection induced an antiviral state as noted by strong up-regulation of the RLRs (RIG-I, MDA5, and LGP2), STAT proteins (STAT1 and 2), and antiviral effectors (IFIT1, IFIT3, and viperin). Finally, RIG-I agonist treatment potently restricted ZIKV replication, while type I IFN was significantly less effective due to ZIKV antagonism of STAT1 and STAT2 phosphorylation.

Despite their evolutionary distance (32), minimal attention has been given to studying infection differences between African and contemporary Asian lineage strains. In general, MR-1947 and Dak-1984 replicated with more rapid kinetics and to a higher magnitude than the Asian lineage viruses. The African lineage viruses were also unique in their ability to induce cell death during

infection, potentially attributed to their replication characteristics. This raises the possibility that Asian lineage viruses may have adapted to be less cytopathic in DCs, potentially resulting from, or contributing to lower viral replication rates. Alternatively, this phenotype may be partly attributed to the extensive passage history and cell culture adaption of MR-1947, a process known to impact ZIKV and WNV glycosylation patterns (31, 253), *in vitro* replication of multiple RNA viruses (253, 254), and *in vivo* pathogenesis of hepatitis C virus (255). In support of this, MR-1947, which has undergone a multitude of passages in suckling mouse brains (S1 Table), replicated with more rapid kinetics than Dak-1984, which has been minimally passaged. Despite differences in kinetics, both viruses reach similar peak infection magnitudes and induced cell death at 72hpi, suggesting cell culture adaption alone does not explain their unique features. Future studies comparing low passaged African and Asian lineage viruses or infectious clone derived viruses (256) are needed to further study differences between these viral genotypes.

While a previous study identified as high as 60% viral E protein-positive cells at 24hr following infection of human moDCs with a French Polynesian strain of ZIKV, we did not observe infection rates this high in our study (79). This may be explained by differences in ZIKV strains, donor-to-donor variation, or technical differences in virus stock propagation or cell infections. Furthermore, our study did not rely solely on 4G2 staining, which cross-reacts with dengue virus and other flaviviruses, but also included sequence-specific detection of ZIKV RNA to verify infection.

We observed striking variability in viral replication between moDCs generated from different healthy donors. In fact, we found a subset of donors with moDCs that were less susceptible to infection with PR-2015. Although differences in receptor expression or affinity for viral proteins between donors could explain this variability, we found minimal differences in the amount of virus bound to moDCs from different donors. Instead, variability occurred after viral binding, with striking differences in the kinetics and magnitude of viral RNA synthesis, viral E protein staining, and infectious virus release between donors. One plausible explanation for infection differences is that moDCs from less susceptible donors are capable of mounting more rapid and stronger antiviral responses. However, induction of antiviral effector genes was found to be less pronounced in donors with lower viral replication. Moreover, differences in ZIKV replication did not correspond to differential DC activation or pro-inflammatory cytokine release. Of note, susceptibility to PR-2015 replication corresponded to P6-1966, where moDCs with lower PR-2015 infection rates also had lower P6-1966 replication. This raises the possibility that moDCs from some donors are better at controlling ZIKV infection. However, MR-1947 was found to replicate to high levels in moDCs from all donors, even those with low PR-2015 replication. Although this may be related to the aforementioned cell culture adaptation of MR-1947, it is possible that differential host adaption of Asian lineage strains during their evolution has resulted in differences in infection rates. Altogether, complex host factors, such as genetics, metabolism, ER stress, or redox state might explain differential susceptibility to ZIKV infection. Indeed, the collaborative

cross, a mouse model of genetic diversity, has recently revealed the importance of host genetics in influencing susceptibility to WNV infection (19). Similar donor variability in viral replication has also been observed during HIV infection of human monocyte derived macrophages (257). Although some donor variability in HIV infection was found to correspond with the presence of the CCR5 Δ32 mutation, most of the variability remained unexplained. Influenza A infection of primary human bronchial epithelial cells has also been found to vary notably between donors (258). Interestingly, cells isolated from obese donors were more susceptible to viral infection, highlighting how complex, non-genetic factors can also influence susceptibility to viral infection at the cellular level. It is interesting to speculate that differential susceptibility of DCs to ZIKV may correspond to pathogenesis during human infection, where 80% of infected individuals are asymptomatic and those with symptoms have differences in clinical presentations.

The minimal activation of DCs following exposure to ZIKV is similar to previous findings with tick-borne encephalitis virus, where DC maturation is inhibited through IRF-1 degradation (238). Diminished up-regulation of MHC class II and CD40 molecules on splenic CD8α+ DCs was also observed following Japanese encephalitis virus infection in mice (239). In contrast to our findings with ZIKV, infection of human moDCs with the yellow fever virus vaccine strain, YF-17D, promotes DC maturation (212). The ability of YF-17D to activate human DCs may be explained through the loss of a viral antagonist during its attenuation process, or could represent a unique behavior of certain flaviviruses. Indeed,

infection of human moDCs with a pathogenic dengue virus serotype 2 strain also promotes the up-regulation of co-stimulatory and MHC molecules, along with pro-inflammatory cytokine secretion (259). Combined, this work suggests members of *Flaviviridae* have evolved complementary, as well as unique strategies of targeting DCs to subvert the pressures of host immunity.

While infection with all four ZIKV strains induced type I IFN mRNA transcription, we detected minimal translation of type I or III IFN proteins. This was in contrast to RIG-I agonist treatment, which induced translation of both type I and III IFN proteins, despite similar levels of *IFNB1* transcription as observed during ZIKV infection. Indeed, ZIKV infection diminished RIG-I agonist-induced type I IFN production, suggesting ZIKV directly antagonizes type I IFN translation. We also observed a minor 2-3 fold enhancement in viral infection when type I IFN signaling was inhibited by antibody-mediated receptor blockade, further indicating type I IFN is secreted at minimal levels during ZIKV infection. Previous work with dengue virus observed secretion of IFNα protein during infection of human moDCs, suggesting our findings might be unique to ZIKV infection. Despite the antagonism of type I or III IFN production, ZIKV infection up-regulated the expression of the RLRs, STAT proteins, and multiple antiviral effector proteins to similar levels observed following RIG-I agonist treatment. This suggests that the block in type I IFN translation is selective, and that much of the antiviral response induced during ZIKV infection of human DCs occurs independent of type I IFN signaling. Indeed, in the context of WNV infection,

multiple antiviral effector genes are induced through an IFN-independent, RLR signaling-dependent manner (98).

Recent work from multiple groups has analyzed ZIKV infection and immune responses from human clinical samples and in a variety of human cell types. During the acute phase of human ZIKV infection, multiple pro-inflammatory cytokines are increased within the blood, although the cellular sources of these responses remain unknown (75). Our findings suggest that infected DCs may not be an important source of these pro-inflammatory cytokines. In contrast to our work with DCs, ZIKV infection of A549 cells has been shown to induce IFNβ secretion, further suggesting cells other than DCs may be responsible for inducing inflammatory responses during ZIKV infection (78). Indeed, *ex vivo* infection of primary human skin fibroblasts was found to induce transcriptional up-regulation of multiple pro-inflammatory mediators, although protein secretion was not explored (79). In regards to congenital ZIKV infection, recent work has found both human fetal neural progenitor cells and placental Hofbauer cells are poorly immunogenic, similar to our findings with adult DCs (61, 70). In contrast, human embryonic cranial neural crest cells secrete cytokines following ZIKV infection at levels that were found to be harmful for neurodevelopment (80). Together, different target cells of ZIKV have varying capacities to induce pro-inflammatory cytokine responses and further study is needed to determine the cell types responsible for initiating inflammatory responses during human infection.

Recent work has revealed that the NS5 protein of both MR-1947 and PR-2015 promotes the degradation of human STAT2 protein during infection, allowing ZIKV to evade type I IFN signaling downstream of the type I IFN receptor (126). In agreement with this work, we found that while RIG-I agonist treatment potently restricted viral replication, type I IFN treatment was significantly less effective at blocking ZIKV infection. Mechanistically, we found infection with both contemporary and ancestral strains of ZIKV blocked phosphorylation of STAT1 and STAT2 downstream of type I IFN signaling in both human DCs and A549 cells. In contrast to previous findings, we did not observe significant STAT2 degradation in either human DCs or A549 cells (126). In fact, in most cases, we observed up-regulation of STAT2 protein during ZIKV infection. One possibility for this discrepancy may be differences in the cell types used between the studies. Grant et al performed studies in Vero and HEK 293 cells, while we conducted experiments in A549 cells and primary human DCs. We also used lower MOIs (0.1 and 1) for our A549 cell line infections than in their studies (MOI 5, 10, and 20) and did not perform viral protein overexpression studies. Although we did use an MOI of 10 for some of our DC work, the magnitude of infection is significant lower than in Vero or HEK 293 cells and such differences in cell infectivity could also explain our differing findings. Nevertheless, we find that ZIKV antagonizes the type I IFN signaling pathway through blockade of STAT1 and STAT2 phosphorylation.

The ability of RIG-I agonist to efficiently block ZIKV replication is most likely attributed to an IFN-independent induction of antiviral effector molecules

(98, 243). Our observations that ZIKV infection induces an antiviral state in moDCs, despite viral antagonism of type I IFN responses, further suggests IFN-independent signaling pathways, such as RLR signaling through MAVS, are important for restriction of ZIKV replication. The ability of RIG-I agonist to potently restrict ZIKV replication across all four strains highlights the RLR signaling pathway as a potential target for antiviral therapy. Of note, small molecule agonists of the RLR pathway have gained recent attention as potential candidate vaccine adjuvants (260, 261) and for use in broad-spectrum antiviral therapy, including proof-of-principle studies showing potent activity against multiple flaviviruses (243, 262).

In summary, our work shows that human DCs are productively infected by currently circulating (PR-2015) and ancestral (P6-1966, MR-1947, and Dak-1984) strains of ZIKV. Each ZIKV strain exhibited unique replication kinetics and downstream effects on human DCs, including a unique ability of African lineage viruses to induce cell death. There was notable donor variability in viral replication across the ZIKV strains, highlighting the importance of both host and viral factors in influencing susceptibility during infection. We observed minimal DC activation or secretion of inflammatory cytokines, as well as viral antagonism of type I IFN translation, despite strong induction of *IFNB1* at the RNA transcript level. Nevertheless, ZIKV-infected moDCs induced an antiviral state as noted by strong up-regulation of multiple antiviral effectors. RIG-I agonist treatment potently restricted ZIKV replication in human DCs, while type I IFN treatment had minimal effects. Mechanistically, all strains of ZIKV antagonized type I IFN-

mediated phosphorylation of STAT1 and STAT2. Combined, our findings show that ZIKV efficiently evades type I IFN responses, but RLR signaling remains functional and may be a target for antiviral therapy in humans.

## 3F. Materials and Methods

**Ethics statement.** Human peripheral blood mononuclear cells (PBMCs) were obtained from healthy donors in accordance with the Emory University Institutional review board according to IRB protocol IRB00045821.

**Virus stocks.** Zika virus strains PRVABC59 (PR-2015), P6-740 (P6-1966), MR-766 (MR-1947), and DakAr 41524 (Dak-1984) were obtained from the Centers for Disease Control and Prevention. All strains were passaged once in Vero cells cultured in MEM (Life Technologies Gibco) supplemented with 10% FBS (Optima, Atlanta Biologics) to generate working viral stocks. Viral stocks were titrated by plaque assay on Vero cells as previously described (61) and stored at -80°C in MEM with 20% FBS.

**Viral stock sequencing and genome annotation.** The Zika virus isolates in this study were subjected to whole genome sequencing using previously described methods (263). Briefly, total viral RNA was subjected to next generation sequencing library construction with random hexamer-based priming methods. Libraries were sequenced on the Illumina MiSeq platform and genome assembly was performed with CLC Bio (clc_ref_assemble_long v. 3.22.55705).

Viral genome annotation was performed with VIGOR (264). The Genbank accession numbers are: KX601166.1 (Zika virus strain ZIKV/Aedes africanus/SEN/DakAr41524/1984); KX601167.1 (Zika virus strain ZIKV/Aedes sp./MYS/P6-740/1966); KX601168.1 (Zika virus strain ZIKV/Homo Sapiens/PRI/PRVABC59/2015); KX601169.1 (Zika virus strain ZIKV/Macaca mulatta/UGA/MR-766/1947).

**Cells.** Vero and A549 cells were obtained from ATCC and maintained in complete DMEM (DMEM medium [Corning] supplemented with 10% fetal bovine serum [Optima, Atlanta Biologics], 2mM L-Glutamine [Corning], 1mM HEPES [Corning], 1mM sodium pyruvate [Corning], 1x MEM Non-essential Amino Acids [Corning], and 1x Antibiotics/Antimycotics [Corning]). moDCs, monocytes, mDCs and pDCs were maintained in complete RPMI (RPMI 1640 medium [Corning] supplemented with 10% fetal bovine serum [Optima, Atlanta Biologics], 2mM L-Glutamine [Corning], 1mM Sodium Pyruvate [Corning], 1x MEM Non-essential Amino Acids [Corning], and 1x Antibiotics/Antimycotics [Corning]).

**Primary cell isolation.** PBMCs were isolated from freshly obtained healthy donor peripheral blood using lymphocyte separation media (MP Biomedicals or StemCell Technologies) per manufacturers instructions. CD14+ monocytes were magnetically purified by positive selection using the EasySep Human CD14 Positive Selection Kit (Stem Cell Technologies) per manufacturers instructions. CD14+ monocytes were resuspended in complete RPMI medium with 100ng/mL

each of recombinant human IL-4 and GM-CSF (PeproTech) at a cell density of 2e6 cells/mL. Spent media and non-adherent cells were removed 24 hours later and replaced with fresh media and cytokines. Suspension cells were harvested 5-6 days later for use in experiments. moDCs were consistently CD14-, CD11c+, HLA-DR+, DC-SIGN+, and CD1a+ by flow cytometry. To obtain mDCs and pDCs, monocytes were removed by positive selection using CD14 microbeads (Miltenyi Biotech) and the CD14- fraction was enriched for DCs using a human Pan-DC Enrichment Kit (Miltenyi Biotech). Enriched cells were surface stained to identify mDCs and pDCs for fluorescence activated cell sorting (FACS). Within the lineage-negative HLA-DR+ population, CD1c+ mDC1 and CD141+ mDC2 were collected together as CD11c+ mDCs, and CD123+ cells were collected as pDCs. Purity of microbead-sorted monocytes and FACS-sorted DC populations was >95%. Monocytes, mDCs and pDCs were maintained in complete RPMI medium. mDCs were cultured in the presence of human GM-CSF (2 ng/ml). pDC were cultured in the presence of human IL-3 (10 ng/ml).

**Cell culture infections.** moDCs were harvested after 5-6 days of differentiation and resuspended in complete RPMI (without GM-CSF or IL-4) at 1e5 cells per well of a 96-well V-bottom plate for infections. moDCs, monocytes, mDCs, and pDCs were infected with the indicated ZIKV strain at MOIs of 1 or 10 (based on Vero cell titer) for 1hr at 37°C. After 1hr, virus inoculum was washed off and cells were resuspended in 200µL fresh media and incubated at 37°C for 3-72hr.

**Viral binding assay.** moDCs were infected with ZIKV at MOI of 1 for 1hr on ice and washed 4x with cold PBS (Fig S1C). To remove bound virus, cells were then incubated with trypsin for 60 minutes on ice and washed 4x with cold PBS. Bound virus was quantitated by qRT-PCR for ZIKV RNA.

**Agonist stimulation of moDCs.** After 5-6 days of differentiation, moDCs were harvested and plated at 1e5 cells per well of a 96-well V-bottom plate in complete RPMI medium (without GM-CSF or IL-4) and stimulated with innate immune agonists. To stimulate RIG-I signaling, 10ng of a highly specific RIG-I agonist derived from the 3'-UTR of hepatitis C virus (197) was transfected per 1e5 cells using an mRNA transfection kit (Mirus). To stimulate type I IFN signaling, 1e5 cells were cultured in 200μL complete RPMI media in the presence of 100 IU/mL of human recombinant IFNβ (PBL Assay Science). To inhibit endogenous type I IFN signaling, 1e5 cells were cultured in 200μL complete RPMI media in the presence of 1.25μg/mL anti-human Interferon-α/β Receptor Chain 2 (clone MMHAR-2, EMD Milipore) blocking monoclonal antibody.

**Focus forming assay (FFA).** Supernatants collected from moDCs were diluted in DMEM supplemented with 1% FBS and used to infect Vero cells for 1hr at 37°C. Cells and inoculum were overlaid with methylcellulose (OptiMEM [Corning], 1% Antibiotic/Antimycotic [Corning], 2% FBS, and 2% methylcellulose [Sigma Aldrich]) and incubated for 72hr at 37°C. Cells were washed with PBS to remove methylcellulose and fixed with a 1:1 methanol:acetone mixture for 30min.

Cells were blocked with 5% milk in PBS at RT for 20min. Cells were incubated with primary antibody (mouse 4G2 monoclonal antibody) at 1µg/mL in 5% milk in PBS for 2hr at RT. Cells were incubated with secondary antibody (HRP-conjugated goat anti-mouse IgG) diluted 1:3000 in 5% milk in PBS for 1hr at RT. Foci were developed with TrueBlue Peroxidase Substrate (KPL). Plates were read on a CTL-ImmunoSpot S6 Micro Analyzer.

**Quantitative reverse transcription-PCR (qRT-PCR).** Total RNA was purified from 1e5 moDCs using the Quick-RNA MiniPrep kit (Zymo Research) per the manufacturer's instructions. Purified RNA was reverse transcribed using the High Capacity cDNA Reverse Transcription Kit (Applied Biosystems) using random hexamers. For quantitation of viral RNA and host gene expression, qRT-PCR was performed as previously described (61).

**Sequence Alignment.** All pairwise alignments between ZIKV PR-2015, P6-1966, MR-1947, and Dak-1984 were performed using MegAlign and the Jotun Hein method. For calculations of nucleotide sequence similarity indices, the Martinez/Needleman-Wunsch method was used, and the parameters included a minimum match of 9, gap penalty of 1.1, and gap length penalty of 0.33.

**Flow cytometry and ImageStream analysis.** The following mouse anti-human antibodies were purchased from BioLegend or Becton Dickinson: CD11c (B-Ly6), HLA-DR (G46-6), CD1a (HI149), CD209 (9E9A8), CD14 (M5E2), CD80 (2D10),

CD86 (IT2.2), and CD40 (5C3). Unconjugated monoclonal 4G2 antibody was kindly provided by Dr. Jens Wrammert (Emory University) and conjugated to APC (Novus Lightning-Link). Following 10min of Fc receptor blockade on ice (Human TruStain FcX, BioLegend), 1e5 cells were sequentially stained for surface markers and viability (Ghost Dye Red 780, Tonbo Biosciences) for 20min on ice. For intracellular staining of ZIKV E protein, cells were fixed and permeabilized (Foxp3/Transcription Factor Staining Buffer Kit, Tonbo Biosciences), blocked for 10 minutes (Human TruStain FcX and 10% normal mouse serum), and stained with 4G2-APC for 20min at room temperature. Multi-color flow cytometry acquisition was performed on a BD LSR II and data was analyzed using FlowJo version 10. ImageStream data acquisition was performed on an ImageStream X Mark II and data was analyzed using Amnis IDEAS software. Monocytes, mDCs and pDCs were stained for viability using Zombie Aqua Fixable Viability Kit in protein-free buffer. Cells for surface staining were suspended in 10% FCS/PBS and incubated with antibodies for 20min at 4°C. Cells were washed, fixed with BD Fix buffer, and acquired on a BD LSR II with all analysis performed using FlowJo version 10.

**Multiplex bead array.** Cytokine analysis was performed on supernatants obtained from 1e5 moDCs following the indicated treatment conditions using a human magnetic 25-plex panel (ThermoScientific) and a custom magnetic 3-plex panel with human IFNβ, IFNα, and IFNλ1 (eBioscience) per the manufacturer's instructions, and read on a Luminex 100 Analyzer. For cytokine analysis within

whole cell lysates, 1e5 moDCs were collected in modified radioimmunoprecipitation assay buffer (10 mM Tris [pH 7.5], 150 mM NaCl, 1% sodium deoxycholate, and 1% Triton X-100) supplemented with Halt Protease Inhibitor Cocktail (ThermoFisher) and diluted 1:5 prior to luminex analysis. Culture supernatants from monocytes, mDCs or pDCs were analyzed for cytokine and chemokines using Cytokine Bead Array (CBA) kits (BD Biosciences, San Diego, US) per the manufacturers instructions. Cytokines analyzed included: GM-CSF, TNF-α, IL-4, IL-6, MIP-1α, IL-8, IL-15, IL-2R, IP-10, MIP-1β, Eotaxin, RANTES, MIG, IL-1RA, IL-12 (p40/p70) IL-13, IFN-γ, MCP-1, IL-7, IL-17, IL-10, IL-5, IL-2, IL-1β, IFNα, IFNβ, and IFNλ1.

**Western blot analysis.** STAT1 and STAT2 signaling was studied in A549 cells as previously described (196). Briefly, A549 cells were infected with the indicated ZIKV strain at an MOI of 0.1 and 1 (based on Vero cell titration). At 48hpi, cells were pulse treated with 1000 IU/mL of recombinant human IFNβ (PBL Assay Science) for 30 minutes and whole-cell lysates were collected in modified radioimmunoprecipitation assay buffer supplemented with Halt Protease Inhibitor Cocktail (ThermoFisher) and phosphatase inhibitor cocktail II (Calbiochem). Western blot analysis was performed to detect STAT1 phosphotyrosine residue 701 (Cell Signaling), total STAT1 (Cell Signaling), STAT2 phosphotyrosine residue 689 (Upstate, EMD Milipore), total STAT2 (Cell Signaling), and glyceraldehyde 3-phosphate dehydrogenase (GAPDH; Cell Signaling). Protein expression levels were quantified using Image Lab software. For analysis of

antiviral effector proteins within human moDCs, 4e5 cells were used per condition and protein lysates were collected as described for A549 cells. The following antibodies were obtained from Cell Signaling: RIG-I, MDA5, LGP2, STAT1, STAT2, IFIT1, viperin, and GAPDH. The IFIT3 antibody was kindly provided by Dr. G. Sen.

## 3G) Figures and legends

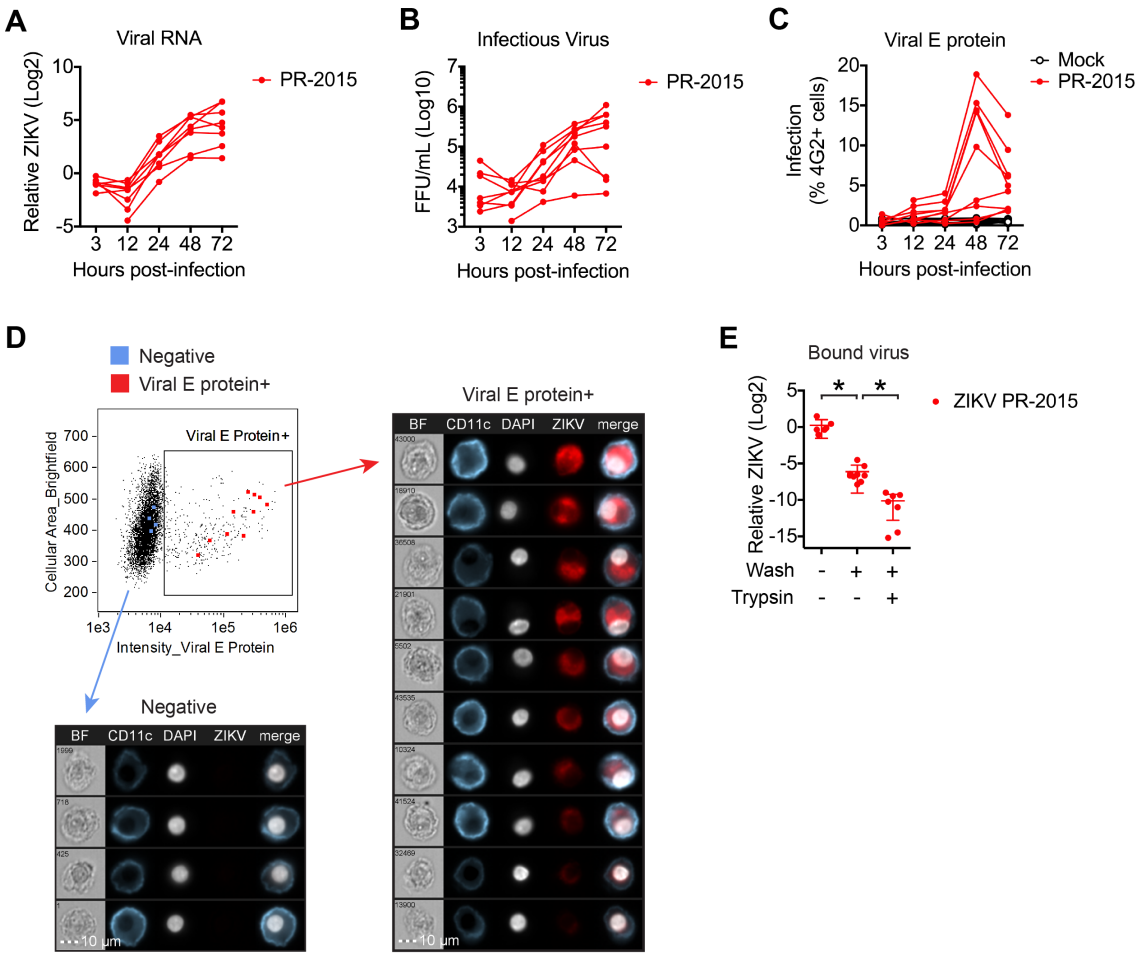


**Fig 1. Contemporary Puerto Rican ZIKV isolate productively infects human DCs.** moDCs were infected with ZIKV PR-2015 at MOI of 1 and assessed for viral replication at indicated hours post-infection. **(A)** Viral RNA was detected in cell lysates by qRT-PCR for ZIKV E protein mRNA. Gene expression is shown as relative expression after normalization to *GAPDH* levels in each respective sample (n=7 donors). **(B)** Viral titers in supernatants of ZIKV-infected moDCs as determined by focus forming assay (FFA; n=8 donors). FFU, focus forming units. **(C)** Percent infected cells as assessed by ZIKV E protein staining (4G2-APC antibody) and flow cytometry (n=9 donors). **(D)** ImageStream analysis of ZIKV-

infected moDCs labeled for viral E protein at 48hpi. Images of individual cells highlighted in the flow plot are represented and ordered according to E protein staining intensity. **(E)** moDCs were infected with ZIKV PR-2015 at MOI of 1 for 1hr on ice, washed extensively, and bound virus was quantitated by qRT-PCR for ZIKV RNA. Gene expression is represented as relative expression after normalization to *GAPDH* levels in each respective sample and shown as the mean +/- SD from 6-9 donors. See also S1 Fig.

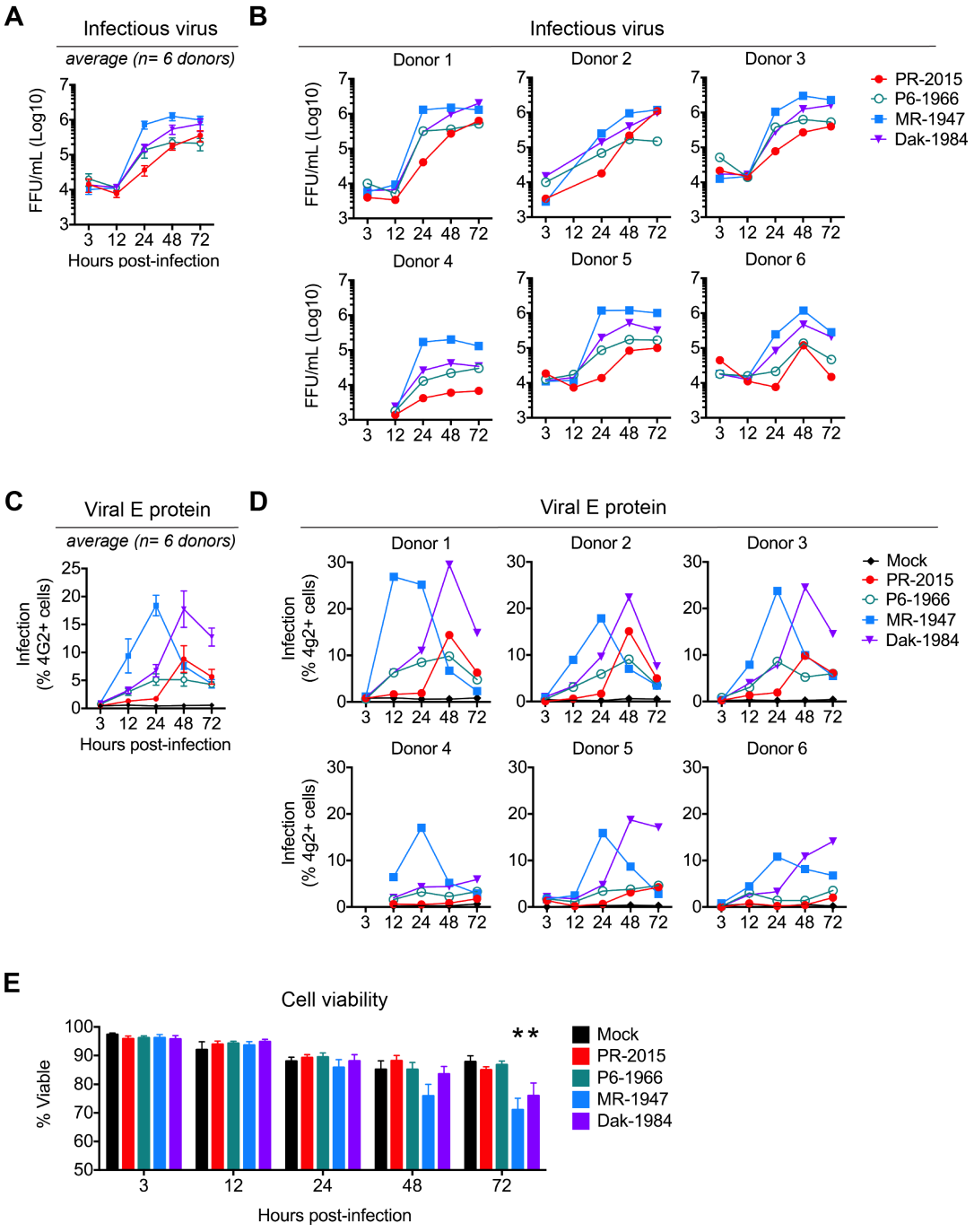


**Fig 2. Differential infection of human DCs by evolutionarily distinct ZIKV strains.** moDCs were infected with PR-2015, P6-1966, MR-1947, or Dak-1984 at MOI of 1 and assessed for viral replication at the indicated hours post-infection. **(A)** Infectious virus release into the supernatant was determined by FFA. Shown

as the mean +/- SEM from 6-9 donors. **(B)** Infectious virus release for 6 of the individual donors summarized in panel A. **(C)** Percent infected cells assessed by ZIKV E protein staining and flow cytometry. Shown as the mean +/- SEM from 6-9 donors. **(D)** Percent infected cells in 6 of the individual donors summarized in panel C. **(E)** Cell viability of infected moDCs assessed by Ghost Red 780 (Tonbo) viability staining and flow cytometry. Shown as the mean +/- SEM from 6-9 donors. Statistical significance ($p < 0.05$) was determined using a two-way ANOVA with comparisons made to mock-infected cells. See also S1 Table.

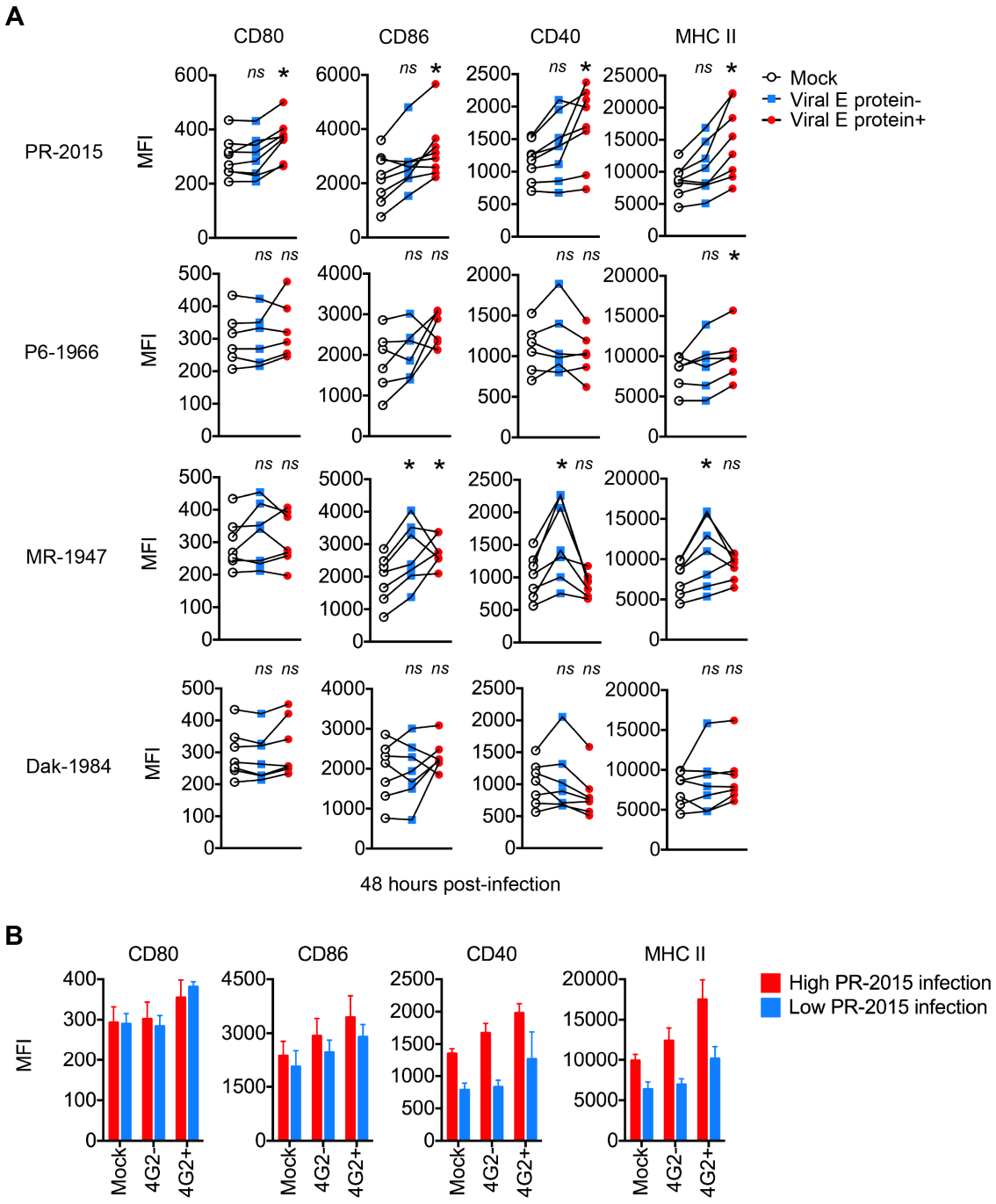


**Fig 3. ZIKV infection minimally activates human DCs. (A)** moDCs were left uninfected ("Mock") or infected with PR-2015, P6-1966, MR-1947, or Dak-1984 at MOI of 1 (n=6-8 donors). Cells were collected at 48hpi and labeled for ZIKV E protein and indicated DC activation markers. Cells were categorized as being

viral E protein- or viral E protein+ and activation marker surface expression quantitated by flow cytometry. Values are represented as median fluorescence intensity (MFI) for each individual donor with uninfected and ZIKV infected samples from the same donor connected with a line. Statistical significance ($p < 0.05$) was determined using a Friedman test with comparisons made to donor-paired, uninfected cells. **(B)** moDCs infected with PR-2015 at MOI of 1 were stratified into “low” (n=3 donors) and “high” (n=5 donors) infection on the basis of viral E protein staining. MFIs are shown as the mean +/- SD. See also S3 Fig.

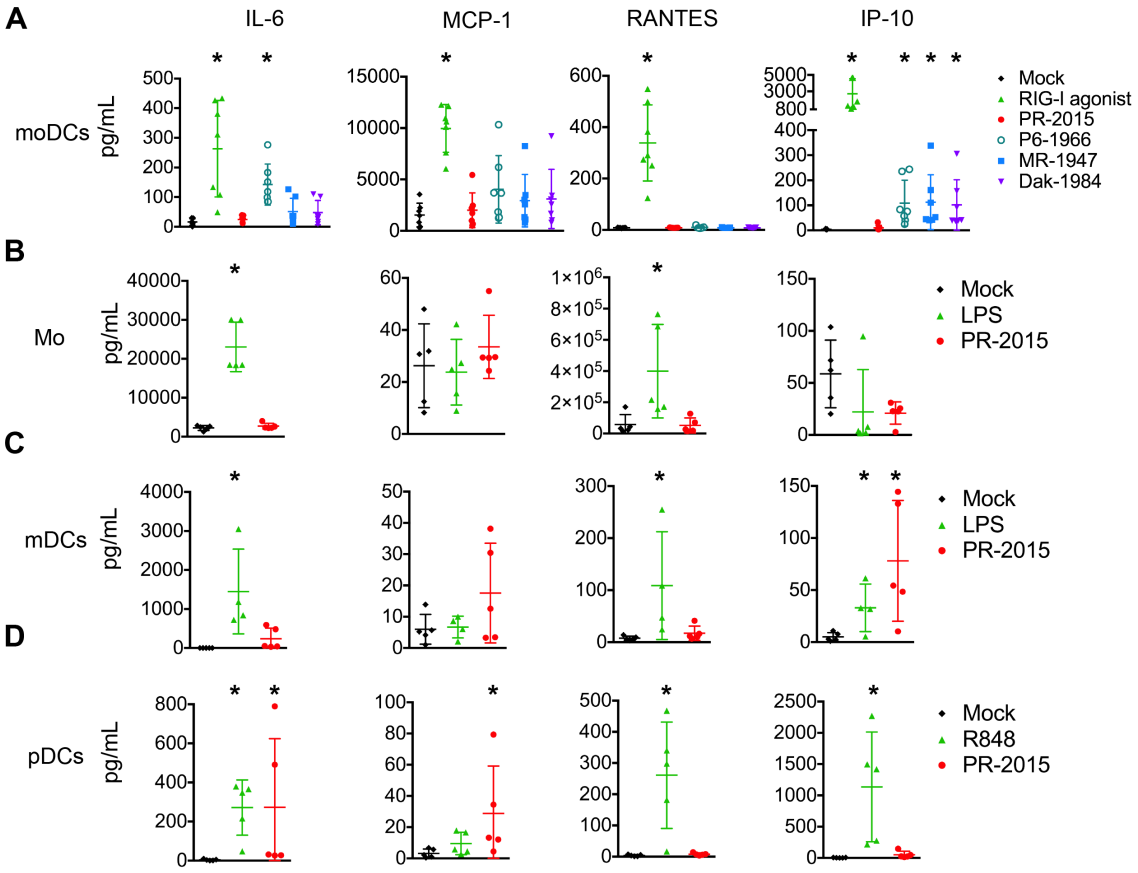


**Fig 4. ZIKV infection induces minimal pro-inflammatory cytokine production by DCs. (A)** moDCs were left untreated ("Mock"), transfected with RIG-I agonist (10ng/1e5 cells), or infected with PR-2015, P6-1966, MR-1947, or Dak-1984 at MOI of 1 (n=7 donors). Supernatants were collected at 48hpi. **(B, C)** Monocytes (Mo) and myeloid DCs (mDCs) were left untreated ("Mock"), treated with LPS (100 ng/ml), or infected with PR-2015 at MOI of 1 (n=5 donors). Supernatants were collected at 24hpi. **(D)** Plasmacytoid DCs (pDCs) were left untreated ("Mock"), treated with R848 (1 μg/ml), or infected with PR-2015 at MOI of 1 (n=5 donors). Supernatants were collected at 24hpi. Cytokine production was assessed using multiplex bead array. Values for each individual donor are shown with the mean +/- SD. Statistical significance ($p < 0.05$) was determined

using a Kruskal-Wallis test with comparisons made to untreated (“Mock”) cells. See also S2, S3, S4, and S5 Tables. Data in B-D was generated by Dr. Mohan S. Maddur and the graphs were generated by James R. Bowen.

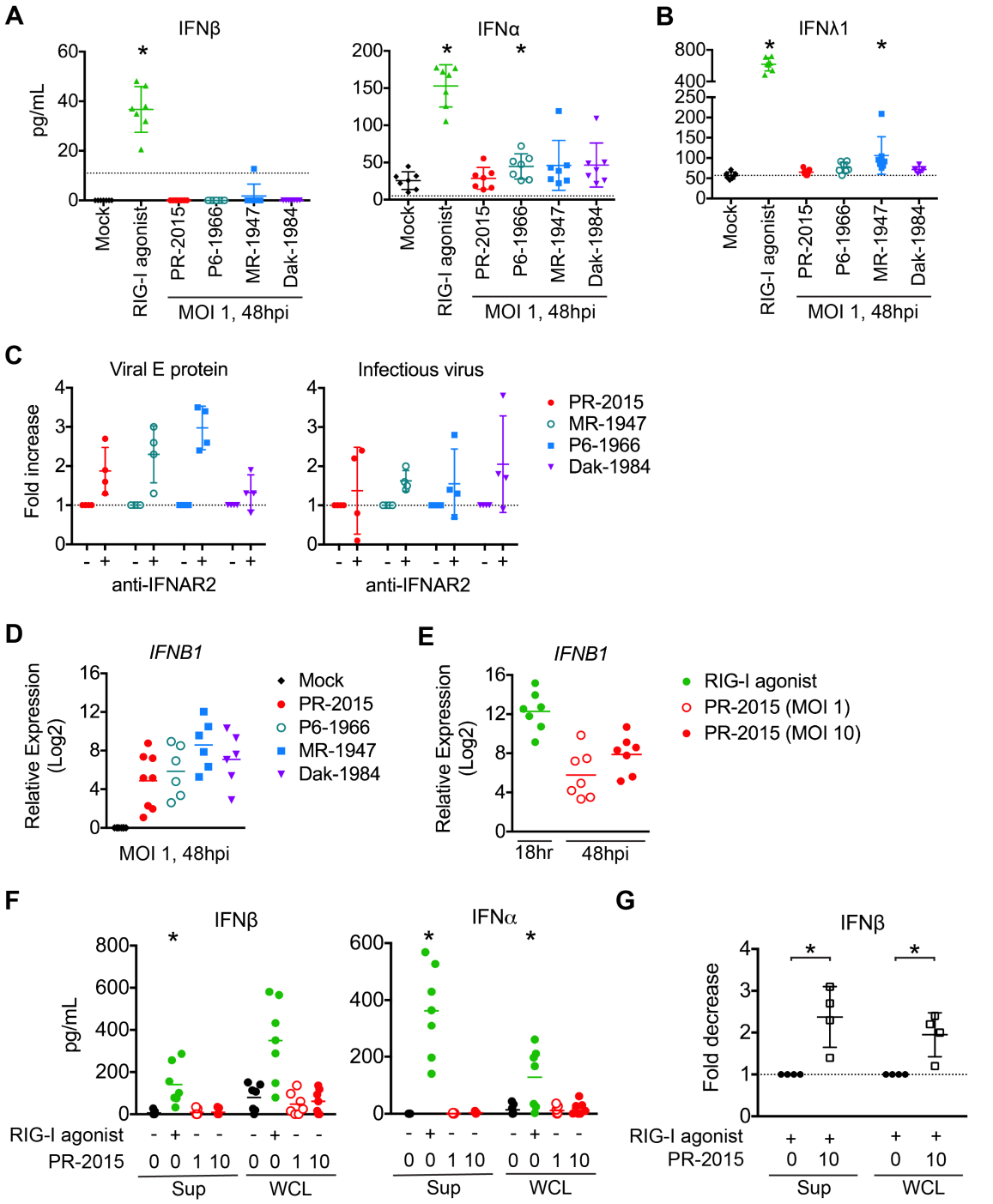


**Fig 5. ZIKV infection induces type I IFN transcription but inhibits translation.** moDCs were left untreated ("Mock"), treated with RIG-I agonist (10ng/1e5 cells), or infected with PR-2015, P6-1966, MR-1947, or Dak-1984 at MOI of 1. Supernatants were collected 24hrs (RIG-I agonist treatment) or 48hrs

(ZIKV infection) later and IFNβ and IFNα **(A)** or IFNλ1 **(B)** production was assessed via multiplex bead array. Values for each individual donor are shown with the mean +/- SD (n=7 donors). Statistical significance ($p < 0.05$) was determined using a Friedman test with comparisons made to donor-paired, mock-infected cells. A dashed line indicates the assay limit of detection. **(C)** moDCs were infected with ZIKV at MOI of 1 in the presence of anti-IFNAR2 blocking antibody. Cells were collected at 48hpi and labeled for ZIKV E protein, while release of infectious virus into the supernatants was determined by FFA. Values for each individual donor are shown with the mean +/- SD (n=4 donors). A dashed indicates no change relative to infection in the absence of anti-IFNAR2 blocking antibody. **(D)** RNA was harvested from cells treated the same as for cytokine analysis and *IFNB1* mRNA expression was determined by qRT-PCR. Gene expression was normalized to *GAPDH* transcript levels in each respective sample and represented as the $\log_2$ normalized fold increase above donor- and time point-matched untreated cells. Values for each individual donor are shown with the mean (n=6-8 donors). **(E)** moDCs were treated with RIG-I agonist (10ng/1e5 cells, 18hrs) or infected with ZIKV PR-2015 (MOI 1 and 10, 48hrs) and analyzed for *IFNB1* mRNA expression. Values for each individual donor are shown with the mean (n=7 donors) **(F)** IFNβ and IFNα were measured in the supernatant (“Sup”) and whole cell lysate (“WCL”) of moDCs treated the same as in E. Values for each individual donor are shown with the mean (n=7 donors). Statistical significance ($p < 0.05$) was determined using a Friedman test with comparisons made to donor-paired, mock-infected cells. **(G)** Uninfected or ZIKV

PR-2015-infected moDCs (MOI 10, 48hpi) were treated with RIG-I agonist (10ng/1e5 cells, 18hrs) and IFNβ and IFNα were measured as in F. The data is shown as the fold-decrease from RIG-I agonist treatment alone with significance ($P<0.05$) determined using a Mann Whitney Test (n= 4 donors). Error bars represent the mean +/- SD. See also S4 Fig.

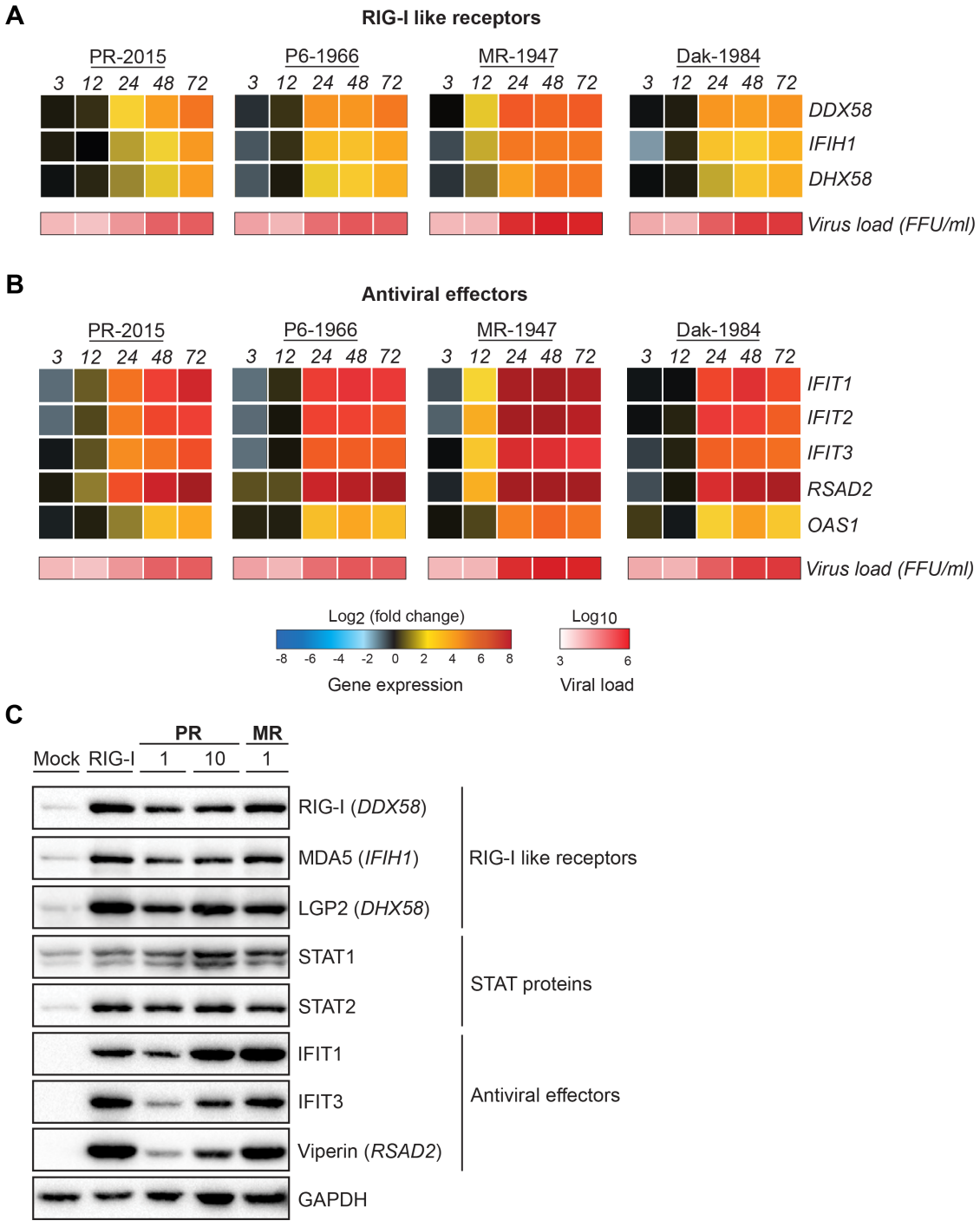


**Fig 6. ZIKV infection induces an antiviral state within human DCs.** moDCs were infected with ZIKV PR-2015, P6-1966, MR-1947, or Dak-1984 at MOI of 1 (n=6-8 donors). Cells were collected at indicated hours post-infection and antiviral gene expression was determined by qRT-PCR. Gene expression was

normalized to *GAPDH* transcript levels in each respective sample and represented as the averaged $log_2$ normalized fold increase above donor and time-point matched uninfected cells. The averaged $log_{10}$ normalized levels of infectious virus (FFU/mL) at each time point is depicted beneath the gene expression heat map. **(A)** RLR gene expression. **(B)** Antiviral effector gene expression. **(C)** moDCs were left untreated ("Mock"), treated with RIG-I agonist (10ng/1e5 cells), or infected with ZIKV PR-2015 (MOIs of 1 and 10) or MR-1947 (MOI 1). After 18hrs of agonist treatment or at 48hpi with ZIKV, whole-cell lysates were collected for western blot analysis of host antiviral effector protein expression. Western blots are shown for a single donor and are representative of data obtained from two donors. See also S5 Figure.

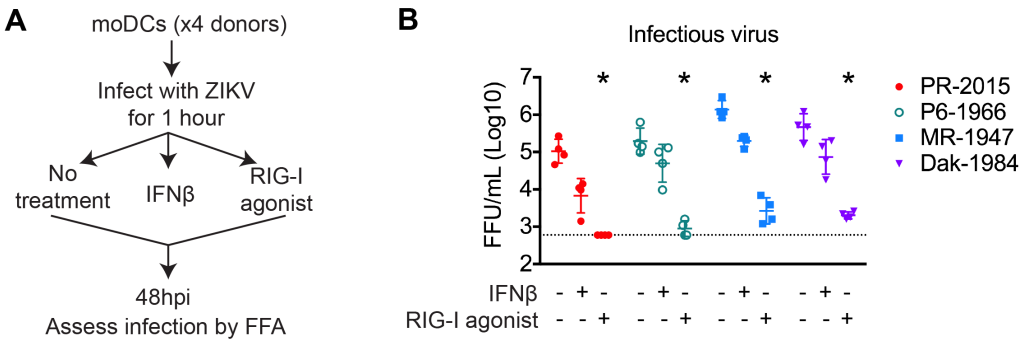


**Fig 7. Innate immune signaling restricts ZIKV viral replication within human DCs. (A)** moDCs were infected with PR-2015, P6-1966, MR-1947, or Dak-1984 at MOI of 1 (n=4 donors). After viral attachment and entry at 1hpi, cells were treated with RIG-I agonist (10ng/1e5 cells), human IFNβ (100 IU/mL), or left untreated. **(B)** Supernatants were collected at 48hpi and assessed for infectious virus release by FFA. Values for each individual donor are shown with the mean +/- SD. Statistical significance ($p < 0.05$) was determined using a Friedman test with comparisons made to donor-paired, untreated, ZIKV-infected cells. The assay limit of detection is indicated with a dashed line.

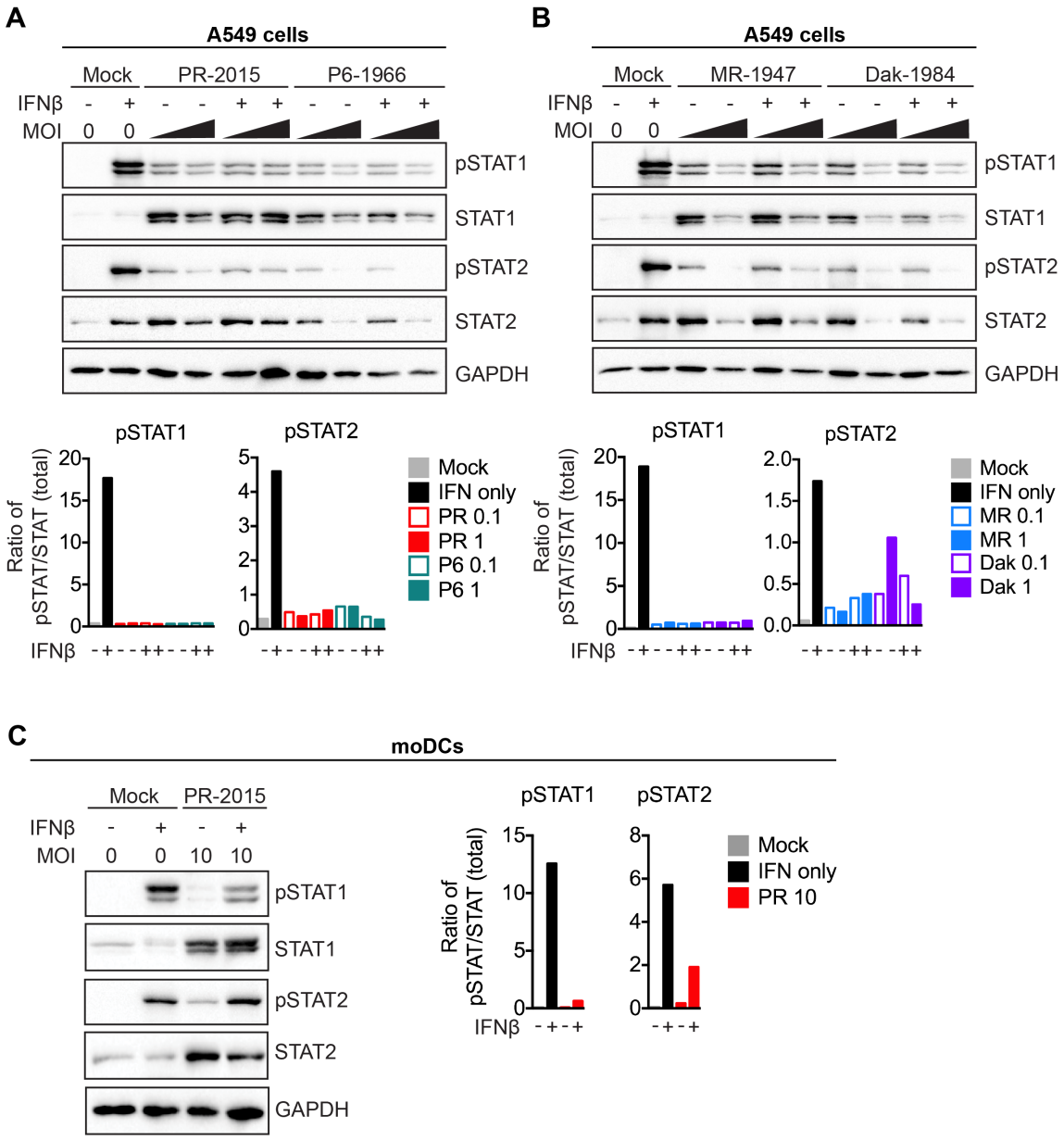


**Fig 8. ZIKV antagonizes type I IFN signaling. (A, B)** A549 cells were infected with PR-2015, P6-1966, MR-1947, or Dak-1984 at MOIs of 0.1 and 1. At 48hpi, cells were pulse treated with 1000 IU/mL of recombinant human IFNβ for 30 minutes and whole-cell lysates were collected for western blot analysis of phospho-STAT1 (Tyr701), phospho-STAT2 (Tyr689), STAT1, STAT2, and GAPDH. Representative blots are shown from one of two independent

experiments. Quantitation is shown below the representative blots, where intensity values are represented as the ratio of pSTAT:total STAT protein. **(C)** moDCs were infected with PR-2015 (MOI 10) and STAT1 and STAT2 signaling was assessed as in A and B. Data is representative of three donors from two independent experiments. Quantitation is shown to the right of the representative blots, where intensity values are represented as the ratio of pSTAT:total STAT protein.

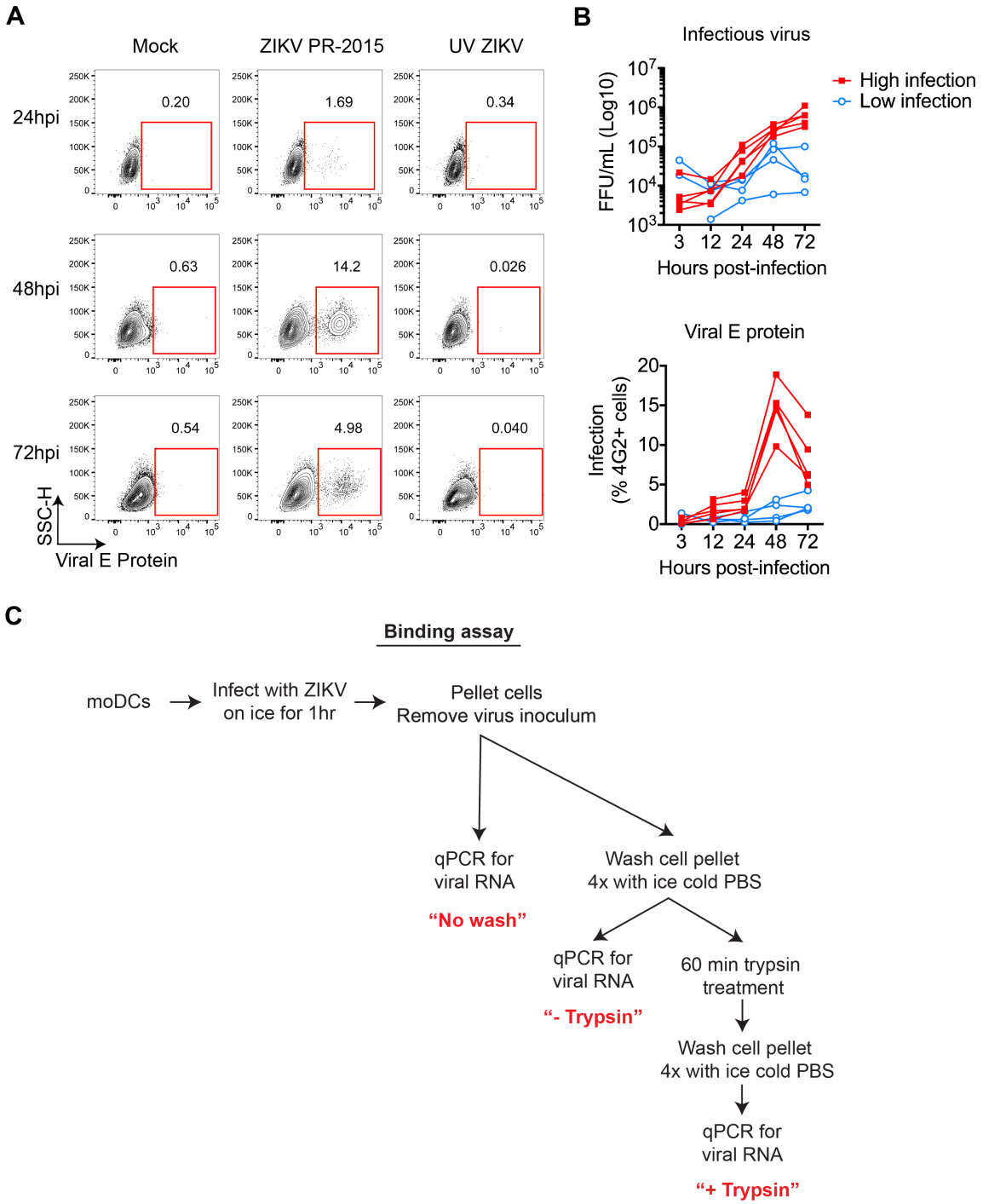


**S1 Fig. Related to Fig 1, ZIKV PR-2015 productively infects moDCs. (A)** moDCs were mock-infected, infected with ZIKV PR-2015, or UV-inactivated PR-2015 ("UV ZIKV") at MOI of 1 and the percentage of infected cells was assessed by ZIKV E protein staining. ZIKV PR-2015 was inactivated by exposure to

ultraviolet (UV) light for 1hr. hpi, hours post-infection. **(B)** Donors were stratified into “high” and “low” infection. **(C)** Experimental outline for ZIKV binding assay.

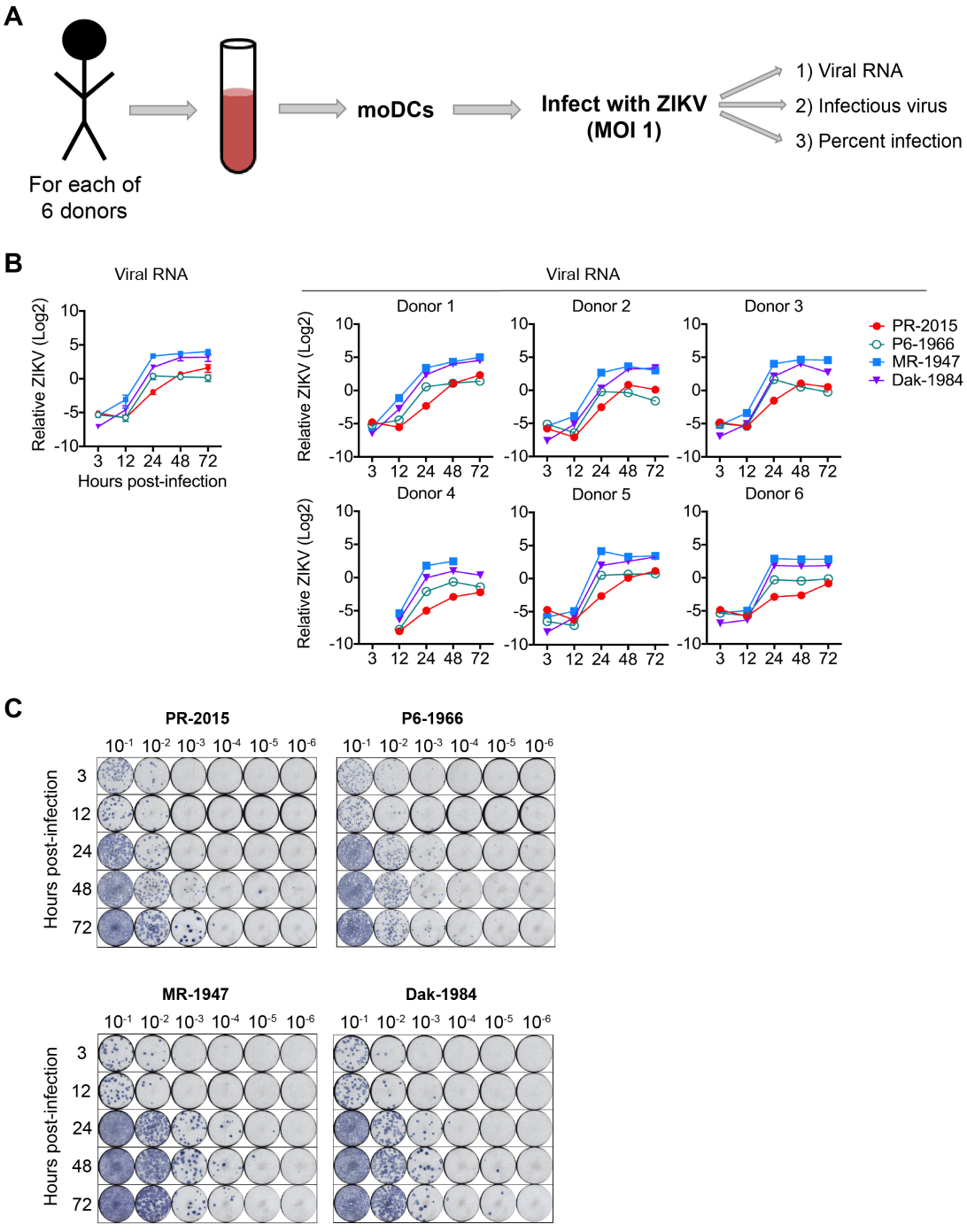


**S2 Fig. Related to Fig 2-7, ZIKV strains used in this study. (A)** Experimental outline used to obtain data in Fig 2. moDCs were generated from healthy donors and infected with all four strains of ZIKV (n=6 donors). We performed parallel analysis of viral RNA, infectious virus release, and viral E protein staining from

each of these samples. **(B)** Viral RNA was detected by qRT-PCR for ZIKV E protein mRNA. Gene expression is shown as relative expression after normalization to *GAPDH* levels in each respective sample (n=6 donors). **(C)** Representative FFA staining for the different ZIKV stains. Serial dilutions are indicated across the top.

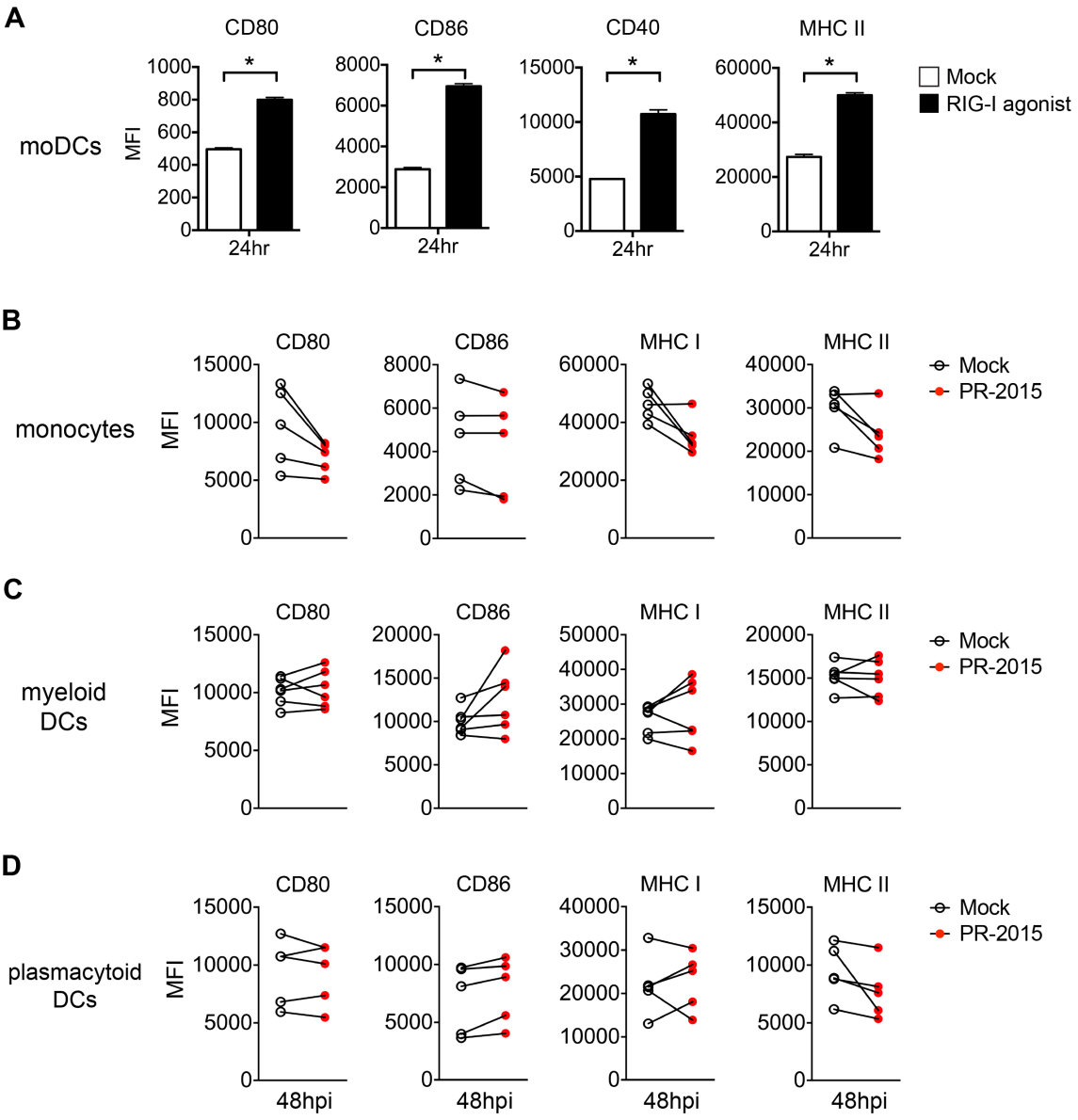


**S3 Fig. Related to Fig 3, ZIKV PR-2015 does not induce activation of human blood monocytes or DC subsets. (A)** moDCs were left untreated ("Mock") or treated with RIG-I agonist (10ng/1e5 cells) for 24hrs. Cells were labeled for indicated DC activation markers and surface expression was quantitated by flow cytometry. Values are represented as the average median fluorescence intensity (MFI) of three technical replicates. Error bars represent the SD. Statistical

significance was determined as P<0.05 by a Mann Whitney U test. **(B)** Monocytes, **(C)** myeloid DCs (mDCs) and **(D)** plasmacytoid DCs (pDCs) were left untreated ("Mock") or infected with PR-2015 at MOI of 1 (n=5 donors). Cells were collected at 24hpi and labeled for indicated DC activation markers. Surface expression was quantitated by flow cytometry. Values for each donor are represented as the median fluorescence intensity (MFI), with mock and ZIKV infected samples from the same donor connected with a line. Statistical significance was determined as p<0.05 using a Wilcoxon signed-rank test **(B-D)**. Of note, no values were statistically significant in panels B-D. Data in B-D was generated by Dr. Mohan S. Maddur and the graphs were generated by James R. Bowen.

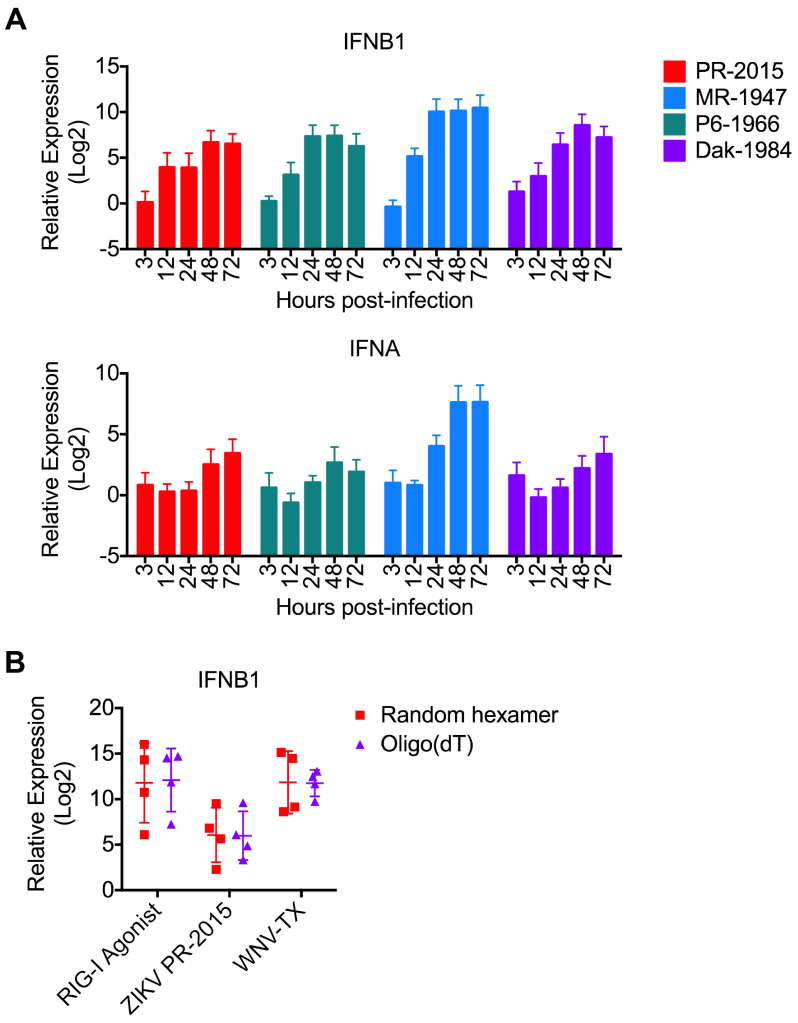


**S4 Fig. Related to Fig 5, ZIKV induces type I IFN gene transcription. (A)** moDCs were infected with ZIKV PR-2015, P6-1966, MR-1947, or Dak-1984 at MOI of 1 (n=6-8 donors). Cells were collected at indicated hours post-infection and antiviral gene expression was determined by qRT-PCR. **(B)** moDCs were treated with RIG-I agonist (10ng/1e5 cells) or virally infected with ZIKV PR-2015 at MOI of 1 (n=4 donors). At 48hpi, RNA was isolated, reverse transcribed using either random hexamer or Oligo(dT) primers, and *IFNB1* expression was determined by qRT-PCR. All gene expression was normalized to *GAPDH* transcript levels in each respective sample and represented as the $\log_2$

normalized fold increase above donor- and time point-matched uninfected cells. Error bars represent the mean +/- SD.

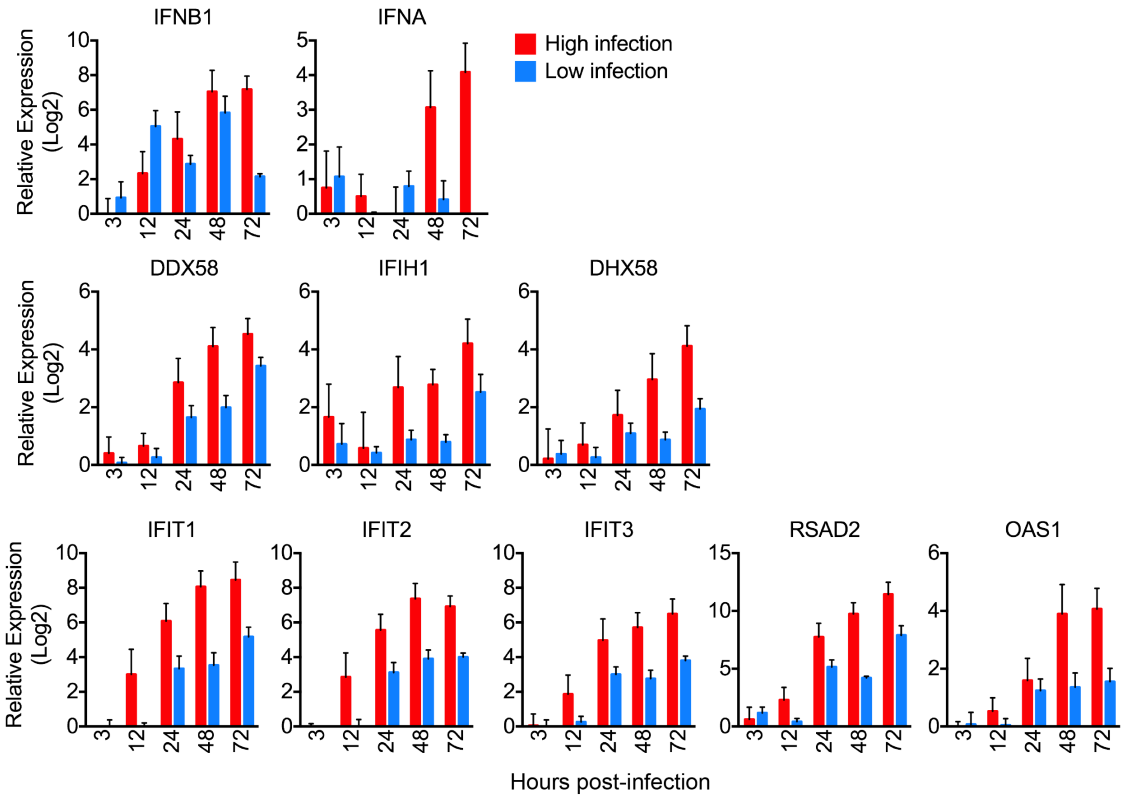


**S5 Fig. Related to Fig 5 and 6, Antiviral effector gene expression corresponds with viral replication.** moDCs from eight donors infected with ZIKV PR-2015 were separated into “high infection” (5 donors) and “low infection” (3 donors) on the basis of E protein staining as assessed by flow cytometry (see Fig 1C). Antiviral gene expression was determined by qRT-PCR. Gene expression was normalized to *GAPDH* transcript levels in each respective sample and represented as the averaged $\log_2$ normalized fold increase above donor- and time point-matched uninfected cells. Error bars represent the mean +/- SD.

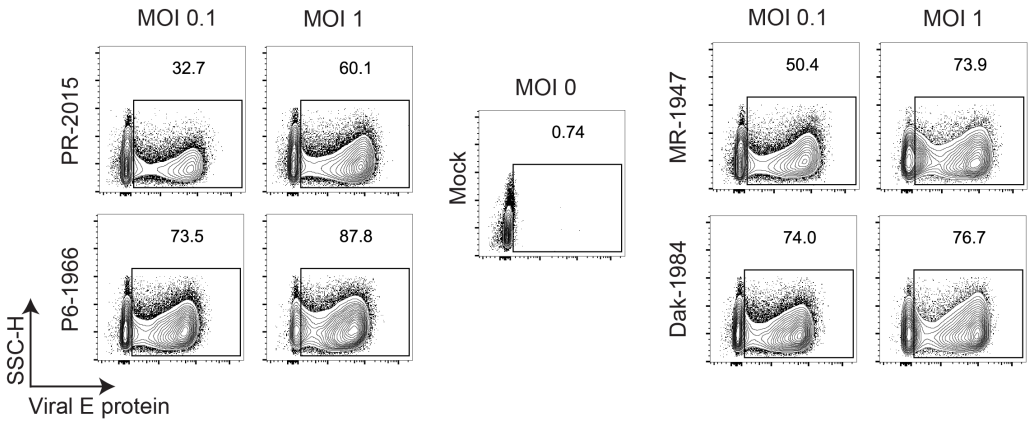


**S6 Fig. Related to Fig 8, ZIKV antagonizes type I IFN signaling.** Representative flow plots of A549 cells infected with indicated ZIKV strain at MOI of 0.1 or 1 for 48hrs and labeled for the presence of viral E protein. Data is representative of two independent experiments.

## 3H. Tables and legends

Zika virus strain information

| | PR-2015 | P6-1966 | MR-1947 | Dak-1984 |
|---|---|---|---|---|
| **Strain** | PRVABC59 | P6-740 | MR766 | DakAr 41524 |
| **Accession** | KX601168 | KX601167 | KX601169 | KX601166 |
| **Lineage** | Asian | Asian | East African | West African |
| **Country** | Puerto Rico | Malaysia | Uganda | Senegal |
| **Date** | 2015 | 1966 | 1947 | 1984 |
| **Passages** | V(4) | SM(6), V(3) | SM(149), V(3) | Ap61(1), C6(1), V(1) |

Nucleotide similarity of the CDS between strains

| | PR-2015 | P6-1966 | MR-1947 | Dak-1984 |
|---|---|---|---|---|
| **PR-2015** | 100 | 95.5 | 88.6 | 88.6 |
| **P6-1966** | 95.5 | 100 | 89.9 | 89.9 |
| **MR-1947** | 88.6 | 89.9 | 100 | 93.4 |
| **Dak-1984** | 88.6 | 89.9 | 93.4 | 100 |

Amino acid changes as compared to PR-2015

| | | P6-1966 | | MR-1947 | | Dak-1984 | |
|---|---|---|---|---|---|---|---|
| **Protein** | **Total AAs** | **# of changes** | **% changes** | **# of changes** | **% changes** | **# of changes** | **% changes** |
| **ancC** | **122** | 1 | 0.8% | 6 | 4.9% | 5 | 4.1% |
| **C** | **104** | 1 | 1.0% | 4 | 3.8% | 4 | 3.8% |
| **anc** | **18** | 0 | 0.0% | 2 | 11.1% | 1 | 5.6% |
| **preM** | **168** | 2 | 1.2% | 10 | 6.0% | 10 | 6.0% |
| **pr** | **93** | 2 | 2.2% | 7 | 7.5% | 7 | 7.5% |
| **M** | **75** | 0 | 0.0% | 3 | 4.0% | 3 | 4.0% |
| **E** | **504** | 6 | 1.2% | 19 | 3.8% | 11 | 2.2% |
| **NS1** | **352** | 2 | 0.6% | 9 | 2.6% | 7 | 2.0% |
| **NS2A** | **226** | 2 | 0.9% | 9 | 4.0% | 10 | 4.4% |
| **NS2B** | **130** | 0 | 0.0% | 2 | 1.5% | 2 | 1.5% |
| **NS3** | **617** | 3 | 0.5% | 10 | 1.6% | 13 | 2.1% |
| **NS4A** | **127** | 0 | 0.0% | 1 | 0.8% | 2 | 1.6% |
| **2K** | **23** | 0 | 0.0% | 0 | 0.0% | 0 | 0.0% |
| **NS4B** | **251** | 7 | 2.8% | 10 | 4.0% | 9 | 3.6% |
| **NS5** | **903** | 16 | 1.8% | 35 | 3.9% | 35 | 3.9% |
| **Structural** | **794** | 9 | 1.1% | 35 | 4.4% | 26 | 3.3% |
| **Non-structural** | **2629** | 30 | 1.1% | 76 | 2.9% | 78 | 3.0% |
| **Polyprotein** | **3423** | 39 | 1.1% | 111 | 3.2% | 104 | 3.0% |

**S1 Table. Related to Fig 1 and 2, ZIKV isolates used in this study.** Information about the ZIKV strains used throughout these studies, nucleotide similarity between coding regions of ZIKV strain genomes, and amino acid differences between viral proteins of ZIKV strains. CDS- coding DNA sequence,

V- Vero cell, SM- suckling mouse brain, Ap61- Aedes pseudoscutellaris cell line, C6- Aedes albopictus clone C6/36 cell line.

| | | moDCs | | | | | | | | | | | |
|---|---|---|---|---|---|---|---|---|---|---|---|---|---|
| | LLOQ | Mock | | RIG-I Agonist | | PR-2015 | | P6-1966 | | MR-1947 | | Dak-1984 | |
| | | Mean | SD | Mean | SD | Mean | SD | Mean | SD | Mean | SD | Mean | SD |
| **IL-1β** | 5 | ND | ND | ND | ND | ND | ND | ND | ND | ND | ND | ND | ND |
| **IL-10** | 1 | ND | ND | 11.1 | 6.7 | ND | ND | 7.1 | 5.8 | 6.5 | 6.9 | 5.4 | 5.9 |
| **IL-13** | 0.5 | 3.2 | 0.7 | 2.5 | 0.7 | 3.5 | 0.6 | 1.7 | 0.4 | 1.9 | 0.3 | 1.5 | 0.4 |
| **IL-6** | 0.5 | 16.3 | 10.8 | 263.3 | 162.6 | 24.8 | 12.0 | 142.5 | 69.3 | 51.4 | 44.7 | 47.8 | 40.9 |
| **IL-12** | 5 | 11.1 | 12.2 | 45.9 | 6.8 | 32.2 | 69.0 | 50.8 | 60.7 | 27.7 | 31.4 | 24.0 | 25.3 |
| **RANTES** | 10 | 8.7 | 1.0 | 338.8 | 148.2 | 8.9 | 1.0 | 10.4 | 4.1 | 8.8 | 1.2 | 8.6 | 1.2 |
| **Eotaxin** | 0.5 | ND | ND | ND | ND | ND | ND | ND | ND | ND | ND | ND | ND |
| **IL-17** | 5 | ND | ND | ND | ND | ND | ND | ND | ND | ND | ND | ND | ND |
| **MIP-1α** | 5 | 215.4 | 273.0 | 4505.2 | 1515.9 | 156.4 | 178.4 | 230.8 | 191.1 | 231.4 | 283.5 | 211.5 | 250.2 |
| **GM-CSF** | 0.5 | ND | ND | 1145.0 | 692.9 | ND | ND | ND | ND | ND | ND | ND | ND |
| **MIP-1β** | 5 | 227.2 | 136.1 | 3776.5 | 2074.6 | 158.6 | 68.2 | 164.1 | 84.4 | 161.5 | 79.7 | 150.3 | 75.8 |
| **MCP-1** | 5 | 1541.7 | 1153.6 | 9969.7 | 2321.0 | 2004.9 | 1688.8 | 4044.3 | 3278.8 | 2944.3 | 2552.6 | 3112.2 | 2872.8 |
| **IL-15** | 40 | ND | ND | 89.4 | 15.3 | ND | ND | ND | ND | ND | ND | ND | ND |
| **IL-5** | 5 | ND | ND | ND | ND | ND | ND | ND | ND | ND | ND | ND | ND |
| **IFNγ** | 1 | 3.5 | 1.7 | 9.3 | 2.7 | 3.2 | 1.4 | 5.6 | 1.6 | 5.7 | 2.8 | 5.3 | 2.8 |
| **IL-1RA** | 15 | 4988.8 | 1702.6 | 6498.4 | 2015.5 | 4952.7 | 862.0 | 8166.8 | 1551.7 | 7774.8 | 883.4 | 7571.7 | 1193.6 |
| **TNFα** | 0.5 | ND | ND | 49.8 | 36.7 | ND | ND | ND | ND | ND | ND | ND | ND |
| **IL-2** | 1 | ND | ND | ND | ND | ND | ND | ND | ND | ND | ND | ND | ND |
| **IL-7** | 10 | 27.4 | 5.0 | 52.2 | 9.1 | 25.9 | 6.2 | 20.2 | 6.1 | 17.4 | 9.3 | 14.5 | 5.7 |
| **IP-10** | 0.5 | 4.3 | 1.0 | 1257.5 | 381.9 | 10.0 | 10.1 | 108.8 | 91.5 | 112.8 | 109.4 | 101.5 | 100.3 |
| **IL-2R** | 20 | 15.6 | 8.7 | 77.1 | 8.0 | 14.8 | 8.0 | 16.2 | 6.6 | 18.4 | 9.4 | 13.6 | 10.1 |
| **MIG** | 5 | ND | ND | 27.2 | 10.2 | 13.0 | 25.5 | 27.7 | 56.9 | 30.1 | 70.2 | 31.0 | 69.5 |
| **IL-4** | 1 | ND | ND | 1689.3 | 923.3 | ND | ND | ND | ND | ND | ND | ND | ND |
| **IL-8** | 5 | 1003.6 | 1019.8 | 2183.9 | 1754.0 | 1188.1 | 1086.5 | 3057.1 | 2267.7 | 1915.4 | 1251.7 | 1891.9 | 1312.2 |
| **IFNα** | 5 | 25.5 | 11.8 | 153.0 | 28.3 | 28.7 | 14.6 | 44.7 | 16.9 | 46.1 | 33.5 | 46.6 | 29.6 |
| **IFNβ** | 11 | ND | ND | 36.7 | 9.2 | ND | ND | ND | ND | 1.8 | 4.8 | ND | ND |
| **IL-29** | 57 | 56.9 | 8.6 | 618.3 | 84.3 | 64.9 | 7.5 | 76.4 | 13.3 | 106.1 | 46.3 | 76.4 | 13.3 |

**S2 Table. Related to Fig 4, Cytokine production by monocyte derived DCs (moDCs).** moDCs were left untreated ("Mock"), transfected with RIG-I agonist (10ng/1e5 cells), or infected with ZIKV PR-2015, P6-1966, MR-1947, or Dak-1984 at MOI of 1 (n=7 donors). Cytokine levels in the supernatants were determined by multiplex bead array at 24hrs post-agonist transfection or 48hrs post-infection. All values are represented in "pg/mL". Cytokine levels that were below the lower limit of detection are indicated as not detected or "ND". LLOQ, lower limit of quantitation.

| | | | Monocytes | | | | | |
|---|---|---|---|---|---|---|---|---|
| | | | Mock | | LPS | | PR-2015 | |
| | Limit of detection (pg/ml) | Unit of expression | Mean | SD | Mean | SD | Mean | SD |
| **IL-1b** | 7.2 | pg/ml | 100.5 | 76.4 | 2372.7 | 1367.5 | 49.9 | 21.9 |
| **IL-6** | 2.5 | ng/ml | 2.3 | 0.6 | 23.1 | 6.3 | 2.7 | 0.8 |
| **IL-10** | 3.3 | pg/ml | 29.1 | 20.0 | 2077.7 | 1172.2 | 26.3 | 20.4 |
| **IL-12p70** | 1.9 | pg/ml | 1.5 | 0.7 | 33.2 | 55.9 | 1.3 | 2.0 |
| **TNF** | 3.7 | pg/ml | 12.0 | 8.3 | 2227.1 | 1416.5 | 15.5 | 12.4 |
| **IFN-a** | 1.5 | pg/ml | - | - | - | - | - | - |
| **MCP-1** | 2.7 | ng/ml | 26.3 | 16.1 | 23.8 | 12.6 | 33.5 | 12.2 |
| **Rantes** | 1.0 | pg/ml | 57.6 | 63.9 | 399.2 | 299.7 | 51.9 | 47.8 |
| **IL-8** | 0.2 | ng/ml | 67.3 | 44.1 | 172.4 | 27.0 | 81.4 | 37.4 |
| **MIG-1** | 2.5 | pg/ml | 133.2 | 156.2 | 473.8 | 409.8 | 591.9 | 681.0 |
| **IP-10** | 2.8 | pg/ml | 58.7 | 32.5 | 22.1 | 40.7 | 21.0 | 10.7 |

**S3 Table. Related to Fig 4, Cytokine production by human blood monocytes.** Monocytes were left untreated ("Mock"), treated with LPS (100ng/mL), or infected with ZIKV PR-2015 at MOI of 1 (n=4-5 donors). Cytokine levels in the supernatants were determined by multiplex bead array 24hrs later. Cytokines that were not assayed are indicated as "-". Data was generated by Dr. Mohan S. Maddur and the table was generated by James R. Bowen.

| | | | Myeloid DCs | | | | | |
|---|---|---|---|---|---|---|---|---|
| | | | Mock | | LPS | | PR-2015 | |
| | Limit of detection (pg/ml) | Unit of expression | Mean | SD | Mean | SD | Mean | SD |
| **IL-1b** | 7.2 | pg/ml | 5.0 | 5.1 | 19.8 | 5.3 | 10.5 | 9.5 |
| **IL-6** | 2.5 | ng/ml | 0.0 | 0.0 | 1.4 | 1.1 | 0.2 | 0.3 |
| **IL-10** | 3.3 | pg/ml | 1.9 | 2.5 | 20.5 | 10.6 | 6.0 | 12.0 |
| **IL-12p70** | 1.9 | pg/ml | 1.9 | 2.0 | 15.7 | 9.2 | 2.2 | 0.9 |
| **TNF** | 3.7 | pg/ml | 9.7 | 4.8 | 62.4 | 28.9 | 19.6 | 6.8 |
| **IFN-a** | 1.5 | pg/ml | - | - | - | - | - | - |
| **MCP-1** | 2.7 | ng/ml | 6.0 | 4.8 | 6.7 | 3.5 | 17.6 | 16.0 |
| **Rantes** | 1.0 | pg/ml | 7.6 | 4.1 | 108.8 | 103.7 | 17.1 | 13.9 |
| **IL-8** | 0.2 | ng/ml | 3.3 | 1.8 | 13.4 | 6.8 | 7.3 | 2.9 |
| **MIG-1** | 2.5 | pg/ml | 77.7 | 99.8 | 361.9 | 368.1 | 369.2 | 470.4 |
| **IP-10** | 2.8 | pg/ml | 4.8 | 4.4 | 32.9 | 22.9 | 78.1 | 58.0 |

**S4 Table. Related to Fig 4, Cytokine production by human blood myeloid DCs (mDCs).** mDCs were left untreated ("Mock"), treated with LPS (100ng/mL), or infected with ZIKV PR-2015 at MOI of 1 (n=4-5 donors). Cytokine levels in the supernatants were determined by multiplex bead array 24hrs later. Cytokines that were not assayed are indicated as "-". Data was generated by Dr. Mohan S. Maddur and the table was generated by James R. Bowen.

| | | | Plasmacytoid DCs | | | | | |
|---|---|---|---|---|---|---|---|---|
| | | | Mock | | R848 | | PR-2015 | |
| | Limit of detection (pg/ml) | Unit of expression | Mean | SD | Mean | SD | Mean | SD |
| **IL-1b** | 7.2 | pg/ml | 4.7 | 5.9 | 3.0 | 1.7 | 24.6 | 25.6 |
| **IL-6** | 2.5 | ng/ml | 4.2 | 4.1 | 271.6 | 141.1 | 273.3 | 351.1 |
| **IL-10** | 3.3 | pg/ml | 3.4 | 5.2 | 0.2 | 0.3 | 16.6 | 7.6 |
| **IL-12p70** | 1.9 | pg/ml | 2.8 | 2.9 | 5.0 | 3.4 | 6.3 | 6.6 |
| **TNF** | 3.7 | pg/ml | 31.2 | 19.0 | 1087.4 | 885.7 | 53.2 | 38.8 |
| **IFN-a** | 1.5 | pg/ml | 6.9 | 2.8 | 13059.4 | 8911.5 | 76.6 | 59.6 |
| **MCP-1** | 2.7 | ng/ml | 3.2 | 2.8 | 9.5 | 7.2 | 28.8 | 30.4 |
| **Rantes** | 1.0 | pg/ml | 3.3 | 3.3 | 260.9 | 170.6 | 7.9 | 3.9 |
| **IL-8** | 0.2 | ng/ml | 0.3 | 0.3 | 2.3 | 1.7 | 0.4 | 0.2 |
| **MIG-1** | 2.5 | pg/ml | 103.2 | 82.5 | 1479.1 | 1977.1 | 238.3 | 298.8 |
| **IP-10** | 2.8 | pg/ml | 4.1 | 3.2 | 1136.1 | 877.8 | 51.2 | 55.3 |

**S5 Table. Related to Fig 4. Cytokine production by human blood plasmacytoid DCs (pDCs).** pDCs were left untreated (“Mock”), treated with R848 (1µg/mL) or infected with ZIKV PR-2015 at MOI of 1 (n=4-5 donors). Cytokine levels in the supernatants were determined by multiplex bead array 24hrs later. Data was generated by Dr. Mohan S. Maddur and the table was generated by James R. Bowen.

**CHAPTER 4.**

# Zika virus infects human placental macrophages

The work presented in this chapter was published in *Cell Host Microbe* as:

Quicke KM*, **Bowen JR***, Johnson EL, McDonald CE, Ma H, O'Neal JT, Rajakumar A, Wrammert J, Rimawi BH, Pulendran B, Schinazi RF, Chakraborty R, Suthar MS. Zika Virus Infects Human Placental Macrophages. Cell host & microbe. 2016;20(1):83-90. Epub 2016/06/02. doi: 10.1016/j.chom.2016.05.015. PubMed PMID: 27247001; PubMed Central PMCID: PMC5166429.

*James R. Bowen and Kendra M. Quicke contributed equally to this work.

The content is reproduced here in whole with permission from the publisher.

Data not generated by the PhD candidate is indicated in the figure legends.

## 4A. Abstract

The recent Zika virus (ZIKV) outbreak in Brazil has been directly linked to increased cases of microcephaly in newborns. Current evidence indicates that ZIKV is transmitted vertically from mother to fetus. However, the mechanism of intrauterine transmission and the cell types involved remain unknown. We demonstrate that the contemporary ZIKV strain PRVABC59 (PR 2015) infects and replicates in primary human placental macrophages, called Hofbauer cells, and to a lesser extent cytotrophoblasts, isolated from villous tissue of full-term placentae. Viral replication coincides with induction of type I interferon (IFN), pro-inflammatory cytokines, and antiviral gene expression but with minimal cell death. Our results suggest a mechanism for intrauterine transmission in which ZIKV directly infects placental cells to cross the placental barrier.

## 4B. Introduction

Zika virus (ZIKV) is an emerging mosquito-borne flavivirus that has rapidly spread to over 30 countries in the Americas and causes illness with symptoms of fever, rash, joint pain and conjunctivitis (235, 265). ZIKV is transmitted through several routes, including mosquito bites, sexual contact, and blood transfusion (265). Most notably, ZIKV can be vertically transmitted from an infected mother to the developing fetus *in utero*, resulting in adverse pregnancy outcomes that include fetal brain abnormalities and microcephaly, a condition characterized by a reduction in head circumference that is often associated with delayed or arrested brain development (266). The mechanism by which ZIKV crosses the placenta to establish infection in the developing fetus is not well understood.

Recent studies have identified ZIKV RNA in amniotic fluid, and fetal and newborn brain tissue (52, 53, 267) and ZIKV-specific IgM antibodies have been detected in newborn cerebrospinal fluid (268). Additionally, ZIKV antigen was found in the chronic villi of a human placenta from a mother who gave birth to an infant with microcephaly, and ZIKV RNA has been isolated from placental tissue of mice infected with ZIKV (267, 269). Finally, a recent study detected ZIKV antigen in placental tissue from a mother diagnosed with ZIKV disease (270). In particular, ZIKV antigen was detected in placental macrophages and histiocytes in the intervillous space.

Vertical transmission of ZIKV from an infected mother to the developing fetus *in utero* reflects tropism for placental cells. This organ is a target for a number of viruses by direct and contiguous infection of the cell layers, virion passage through a breach or by cell-associated transport. Examples include rubella, cytomegalovirus, herpes simplex, HIV-1, hepatitis B and C virus, and parvovirus B19 (271). The placenta is characterized by contact between the maternal blood and fetal chorionic villi. Each villus is lined by trophoblasts, which encase the fetal blood supply and placental macrophages (Hofbauer cells [HCs]). Several studies have confirmed HCs are targets of viral infection *in vivo* (272) and *in vitro* (273). In contrast, syncytiotrophoblasts (differentiated cytotrophoblasts [CTBs]) have been shown to be resistant to infection by a wide range of viruses (274). A recent study showed that syncytiotrophoblasts also appear to be resistant to infection by phylogenetically-related, historic ZIKV strains at early times following infection (24 and 48hpi) (275).

Here we demonstrate that primary human HCs, and to a lesser extent CTBs, are permissive to productive infection by a contemporary strain of ZIKV, closely related to the strains currently circulating in Brazil. Upon infection, HCs are modestly activated and produce IFN-α and other pro-inflammatory cytokines. Analysis of antiviral gene expression shows up-regulation of retinoic acid-inducible gene I (RIG-I)-like receptor (RLR) transcription as well as downstream antiviral effector genes, indicating that ZIKV induces an antiviral response in HCs and CTBs. Our results suggest that ZIKV gains access to the fetal compartment by infecting and proliferating in the cells of the placenta.

## 4C. Results

### Hofbauer Cells and Cytotrophoblasts are Permissive to Productive ZIKV Infection

To determine whether human placental cells are permissive to ZIKV infection, we isolated primary HCs and CTBs from villous tissue of full-term placentae and infected with ZIKV (multiplicity of infection [MOI] 1). In this study, we used a low cell culture-passaged and sequence-verified ZIKV strain, PRVABC59 (PR 2015), isolated from the sera of an infected patient in Puerto Rico in December 2015. This strain is closely related to the epidemic strains circulating in the Americas that have been linked to *in utero* ZIKV infection (38). Through multiple virologic assays, we demonstrate that HCs, and to a lesser extent CTBs, are permissive to productive ZIKV infection (Fig. 1). Following infection of HCs, we performed a focus forming assay (FFA) on Vero cells and observed a steady decline in viral

titers from 3hpi through 24hpi that was immediately followed by log phase virus growth through 72hpi (Fig. 1A). Notably, we observed donor-to-donor variation in viral kinetics and magnitude amongst HCs isolated from five donors. Fordonor 2, we detected an approximate 35-fold increase in virus in the supernatant between 3 - 48hpi. In contrast, donor 5 showed about a 2.5-fold increase in virus in the supernatant between 48 - 96hpi. We confirmed infection of HCs with viral qRT-PCR (Fig. 1B) and immunofluorescence microscopy (Fig. 1C-E). In HCs, viral RNA substantially increased in all donors between 48 - 72hpi, reflecting an increase in virus release into the supernatant (Fig. 1A). Furthermore, we detected viral envelope (E) protein within infected HCs which localized to distinct, perinuclear regions within the cell (Fig. 1C and D). This pattern may be indicative of viral localization to the endoplasmic reticulum (ER), or ER-associated vesicles, a staining pattern consistent with virus assembly (2). Finally, we observed between 4.9 - 7.2% infected cells by immunofluorescence staining using a pan-flavivirus antibody (Fig. 1E).

In contrast, we observed minimal viral replication in CTBs at early times post-infection (3-72hpi; Fig. S1A). Of note, we found evidence of productive infection at 96hpi with all three donors exhibiting approximately 5-fold increase in viral load between 72 - 96hpi, suggesting that CTBs may support productive virus infection, albeit at lower levels compared to HCs. We observed concurrent increases in viral RNA in all three donors between 72 - 96hpi as well (Fig. S1B). Most notably, we detected persistent viral RNA in CTBs at all time points through 72hpi, further suggesting ZIKV infects and replicates in CTBs with delayed

kinetics. Collectively, these findings demonstrate that HCs are permissive to ZIKV infection and represent a key target cell of ZIKV infection within the placenta.

To assess ZIKV replication in HCs at the single cell level, flow cytometry was utilized to detect intracellular expression of viral E protein. Consistent with peak production of viral RNA and infectious virus (Fig. 1), we detected between 0.8 - 6.8% and 0.4 - 3.0% infected HCs at 48 and 72hpi, respectively (Fig. 2A). Minimal background staining was observed in donor- and time-matched uninfected cells and in ZIKV-infected cells stained with an IgG isotype control (Fig. S2B). Consistent with our FFA findings, HCs isolated from donor 2 were the most permissive to infection, with an average of 5.6% and 2.3% infected cells at 48 and 72hpi, respectively. This is consistent with infected cell counts observed by immunofluorescence microscopy (Fig. 1E). In contrast to recent studies with neuronal progenitor cells (276, 277), we did not observe a significant loss of viability during ZIKV infection through 96hpi (Fig. S2C), suggesting that these cells may be more resistant to virus-induced cell death or that ZIKV (PR 2015) is a less cytopathic virus in HCs.

Of note, percent infectivity and infectious virus production did not necessarily correspond to viral RNA levels (Fig. 1 and Fig. 2A). Specifically, while donors 1 and 2 had a 6-fold difference in cellular infectivity at 48hpi and a consistent 1-log fold difference in infectious virus release between 24-96hpi, both had similar viral RNA levels present at 48 and 72hpi. Differences in infection between donor 1 and 2 may be explained by an enhanced rate of genome

replication within HCs from donor 2, noted by an early increase in viral RNA at 24hpi in donor 2, but not donor 1 (Fig. 1). Overall, we observed variable levels of viral RNA at 24 and 48hpi, despite similar levels of viral RNA at early (3hpi) and late (48 and 72hpi) time points, further supporting differential rates of genome replication between donors. Indeed, while donors 1, 3, and 4 had similar production of infectious virus at all time points assessed, notable differences in viral RNA levels were observed at 48hpi between these donors (Fig. 1). Furthermore, while donor 5 showed minimal production of infectious virus, we observed comparable RNA levels to the more permissive donors, further highlighting discordance between genome replication and release of infectious virus. Together, these results suggest that different donors may have the capacity to differentially regulate ZIKV replication and may be restricting replication at different stages of the viral life cycle.

**ZIKV Infection Induces Modest Activation of HCs**

Next, to determine if ZIKV-infected HCs are poised to interact with T cells, we measured cell surface expression of the co-stimulatory molecules CD80, CD86, and MHC II. In ZIKV-infected HCs from all three donors, we observed minimal up-regulation of both CD80 and CD86 as compared to time-matched mock-infected cells between 48 - 72hpi (Fig. 2B and C). Consistent with enhanced virus replication, ZIKV infection of HCs from donor 2 led to up-regulation of both CD80 and CD86 by 72hpi. Additionally, significant up-regulation of MHC II was only observed with donor 2 between 48 - 72hpi (Fig. 2D). Overall, there appears

to be donor-to-donor variability in terms of up-regulation of co-stimulatory molecules, however, enhanced virus replication led to greater activation of HCs. These data suggest that ZIKV infection has the potential to program HCs for antigen presentation and T cell priming.

**Type I IFN and Pro-inflammatory Cytokines are Produced in Response to ZIKV Infection**

When cells are infected with virus, pattern recognition receptors (PRRs) within the cell recognize the viral genetic material and trigger a potent innate immune response to control viral replication and spread. Upon binding viral RNA, PRRs initiate signaling cascades that result in the production of type I interferons (IFNs), pro-inflammatory cytokines and expression of antiviral effector genes that serve to limit virus replication. In order to further assess the immunostimulatory potential of HCs, we measured pro-inflammatory cytokines and chemokines in supernatants from infected cells by multiplex bead array. Following ZIKV infection, we observed increased IFNα secretion, but not IFNβ or IFNλ1 (IL-29; Fig. 3 and Table S1). We also found increased secretion of the pro-inflammatory cytokine IL-6 and chemokines MCP-1, involved in monocyte infiltration, and IP-10, involved in recruitment of activated effector T cells. Though these cytokines were induced in all five donors, there were individual differences in the magnitude of production. Donor 2, which had the highest viral load at 48 and 72hpi (Fig. 1A), tended to exhibit the highest overall levels of IFN-α, IL-6, MCP-1 and IP-10, however, donor 2 was not consistently the lead producer of cytokines

over mock-infected controls. Of note, donor 5, which had the lowest viral load at 48 and 72hpi, did not consistently show the lowest levels of cytokines, but did exhibit reduced induction over mock-infected controls at 72hpi. No discernable patterns could be confidently drawn with CXCL-8, MIP-1α, MIP-1β or IL-1RA. In contrast to HCs, we observed limited induction of type I IFN, IL-6 and IP-10, and no detectable type III IFN in CTBs at the time points assessed (Fig. S3A and Table S2). Donor 1, while slightly less permissive to viral infection and replication (Fig. S1), did not have correspondingly lower levels of cytokine production compared to donors 2 and 3. We did observe however that donor 1 tended to have reduced production of cytokines over mock-infected control cells at 72hpi. These findings demonstrate that HCs are capable of initiating an inflammatory response to ZIKV infection.

**ZIKV Infection Provokes an Antiviral Immune Response in HCs and CTBs**

To evaluate the antiviral potential of HCs and CTBs, we examined the expression of several antiviral effector genes. We observed increased expression of *IFNA* transcripts as early as 24hpi in HCs (Fig. 4A), concordant with increased IFNα secretion (Fig. 3). While we did not observe IFNβ secretion, we detected an increase in *IFNB1* transcripts over time-matched mock cells as early as 24hpi (Fig. 4A), suggesting possible discordance between transcript levels and translation/secretion of IFNβ (247). In contrast, both *IFNA* and *IFNB1* were induced at low levels in CTBs (Fig. S3B). We next measured expression of the RIG-I-like receptors (RLRs), a family of PRRs known to recognize flavivirus RNA

and induce production of Type I IFNs and pro-inflammatory cytokines (13, 99, 278, 279). Expression of *DDX58* (RIG-I), *IFIH1* (MDA5) and *DHX58* (LGP2) transcripts are induced above time-matched mock-infected HCs across all donors by 72hpi and remain highly expressed through 96hpi (Fig. 4B). RLR expression corresponds to kinetics of virus replication, suggesting that RLRs are induced in response to ZIKV infection of HCs. In CTBs, RLR transcription is modestly induced and both *IFIH1* and *DHX58* return to near basal levels by 96hpi, though *DDX58* expression remains slightly elevated through 96hpi (Fig. S3B). We also evaluated expression of several antiviral genes produced downstream of the RLR and type I IFN signaling axes and found that *RSAD2*, *IFIT1*, *IFIT2*, *IFIT3 and OAS1* were all induced by 72hpi in HCs and remained elevated through 96hpi (Fig. 4C). In CTBs, these genes were modestly induced through 72hpi (Fig. S3B), likely corresponding to the low level of viral replication during this time period (Fig. 1). By 96hpi, a time point at which we observed productive virus replication, these cells also initiate an antiviral immune response. Importantly, we observed low levels of *IFNA* and ISG expression in mock-infected HCs and CTBs, likely induced by the cell isolation procedure, which may limit the percent of infected cells we see in our *in vitro* system. Taken together, these results show that both HCs and CTBs respond to ZIKV infection through initiation of antiviral signaling pathways.

The kinetics of the antiviral response are complex and variable and we observed donor-to-donor variation in induction of antiviral gene expression. Of note, HCs from donor 2, which exhibited the highest viral loads, and donor 5,

which exhibited the lowest viral loads, induced similar levels of antiviral effector genes by 96hpi, although genes in donor 2 were induced at a faster rate (Fig. 4). This may reflect the higher rate of replication and viral output by HCs from this donor (Fig. 1). There is likely a multifactorial rationale for why viral load does not correlate with antiviral gene expression that likely encompasses differences in individual genetics and the antagonistic capabilities of the virus.

## 4D. Discussion

The present data demonstrate that primary HCs and CTBs isolated from full-term placentae are permissive to productive ZIKV infection by a contemporary strain currently circulating in the Americas. We also found that HCs respond to infection by triggering antiviral defense programs in the absence of overt cell death. In this limited study of five donors, we observed individual variability in kinetics and magnitude of virus replication, inflammation and antiviral gene expression, likely reflecting differences in individual genetics (280, 281). Though unlikely given the low number of cell passages PR 2015 has undergone, it is possible that minor cell culture adaptations or quasi species may also be playing a role in donor-to-donor variability. These observations suggest that donors may have the capacity to restrict ZIKV at different stages of the viral replication cycle. This may also relate to observed differences in intrauterine transmission efficiency, where more susceptible HCs from a pregnant mother may support higher levels of virus replication and subsequent spread to the developing fetal nervous system. Additionally, it will be important in future studies to characterize when HCs and CTBs are most susceptible to ZIKV infection (i.e. first, second or

third trimester). Recent projections from the CDC based on data from Brazil indicate that virus infection during the first trimester or early in the second trimester of pregnancy is temporally associated with the observed increase in infants born with microcephaly (282).

A recent study reported that primary syncytiotrophoblasts isolated from full-term placentae are resistant to ZIKV infection through a potential mechanism involving type III IFN-mediated antiviral immunity (275). Similarly, in CTBs we observed a lack of productive virus replication through 48hpi, however, we did observe persistent viral RNA through 72hpi. By 96hpi, we observed low level virus replication as well as induction of antiviral effector genes, suggesting that ZIKV infects and persists in CTBs but is efficiently controlled at early times post-infection. Additionally, while Bayer et al. was able to identify IFN-λ (Type III IFN) in the supernatant of uninfected syncytiotrophoblasts, we did not detect the presence of IFN-λ in the supernatants of ZIKV-infected HCs or CTBs. The discordance between these two studies may be attributed to differences in time points assessed and viral isolates used in each study (FSS13025 and MR766 as compared to PR 2015).

What are the possible mechanisms by which ZIKV crosses the placental barrier and infects HCs? One explanation is that ZIKV may initially infect trophoblasts and productively replicate and disseminate locally within the placenta to involve HCs, which then support more efficient ZIKV replication than CTBs. An alternative hypothesis is that non-neutralizing, cross-reactive antibodies bind ZIKV and traffic across the placenta, through a neonatal Fc-

receptor-mediated mechanism, to infect placental macrophages. ZIKV crossing the placenta and replication in/release from HCs likely results in viral dissemination through the cord blood with subsequent infection of neural progenitor cells. At this time, it is uncertain whether maternal macrophages are infected or play a role in allowing ZIKV to cross the placental barrier. However, a recent report has directly identified the presence of viral antigen through immunohistochemistry in the placenta from a mother with an infant who developed ZIKV-related fetal anomalies (267). Of note, ZIKV viral antigen was detected within the chorionic villi and not in the maternal decidua. Based on these findings, it does not appear that decidual macrophages are key players in ZIKV transmission at the placenta.

HCs are likely programmed to limit inflammation following virus infection, a mechanism that is consistent with the immune tolerant environment of the placenta and which would support higher infection of HCs compared to maternal macrophages. An alternative hypothesis is that the relative paucity of effector cells in the placenta that would otherwise readily kill infected macrophages (e.g. CD8+ T cells), contributes to a permissive environment for ZIKV infection and replication in HCs. Altogether, our data support the notion that HCs represent a key target cell within the placenta. These findings stress the importance of developing antiviral therapies directed against ZIKV replication within placental cells as a means to reduce vertical transmission in the mother-infant dyad and the incidence of adverse pregnancy outcomes and fetal abnormalities.

## 4E. Experimental procedures

**Ethics statement.** Human Placenta: Term (>37 weeks gestation) placentae from HIV-1 seronegative and hepatitis B-uninfected women (>18 years of age) were obtained immediately following elective caesarian section without labor from Grady Memorial and Emory Midtown Hospitals in Atlanta, GA. Approval of the study was granted from the Emory University Institutional Review Board (IRB 00021715) and the Grady Research Oversight Committee. Written informed consent was obtained from donors before collection, and samples were de-identified prior to handling by laboratory personnel.

**Isolation of primary placental cells.** Hofbauer cells (HCs) and cytotrophoblasts (CTBs), were dissected from membrane-free villous placenta, as previously described (273). HCs were isolated and purified by positive selection with anti-CD14 magnetic beads per the manufacturer's instructions. The purity of the HC population was assessed by CD14 staining and was on average greater than 97% (Fig. S2A). CTBs were isolated and purified by negative selection with magnetic beads (Miltenyi Biotech). The purity of the CTB population was assessed by cytokeratin-7 staining and was on average greater than 97% (283). HCs were maintained in complete RPMI medium and CTBs were maintained in complete DMEM medium. A detailed protocol can be found in Supplemental Experimental Procedures.

**Viruses and infections.** Zika virus strain PRVABC59 (ZIKV [PR 2015]) was isolated in 2015 from the serum of a patient who traveled to Puerto Rico, and passaged three times in Vero cells. PRVABC59 was obtained from the Centers for Disease Control and Prevention in Fort Collins, CO and passaged twice in Vero cells cultured in MEM (Gibco) supplemented with 10% FBS (Optima, Atlanta Biologics) to generate working viral stocks. Viral stocks were titered by plaque assay on Vero cells and stored in MEM with 20% FBS. Vero cells (ATCC) were maintained in complete DMEM medium (Supplemental Experimental Procedures). HCs or CTBs were allowed to rest for ~24h before infecting with ZIKV (PR 2015) at an MOI of 1 for 1hr at 37°C. Virus was washed off, cells were resuspended in fresh complete media and incubated at 37°C for 3-96hr. MOI of 1 was based on results of plaque assays as well as a recent paper where DCs (a similar cell type to macrophages) were infected with ZIKV at an MOI of 1 (79). All work with infectious ZIKV was performed in an approved BSL-3 facility.

**Quantitative reverse transcription-PCR (qRT-PCR).** Total RNA was purified from mock- or ZIKV-infected HCs or CTBs ($2x10^5$ cells per condition) using the ZR-96 Quick-RNA Kit (Zymo Research) per the manufacturer's instructions. Purified RNA was reverse transcribed using the High Capacity cDNA Reverse Transcription Kit (Applied Biosystems) using random hexamers. For quantitation of viral RNA and analysis of host gene expression, qRT-PCR was performed using TaqMan Gene Expression Master Mix (Applied Biosystems) per the manufactures instructions. For quantitation of viral RNA, each 12.5µl reaction

contained 2.5pmol of TaqMan probe directed against the amplified ZIKV E gene region. Host gene expression was performed using SYBR green with appropriate primer sets (Supplemental Experimental Procedures). All qRT-PCR results were normalized to GAPDH.

**Flow cytometry.** The following mouse anti-human antibodies were purchased from BioLegend or Becton Dickinson: CD14 (M5E2), CD80 (2D10), CD86 (IT2.2), and HLA-DR (G46-6). Unconjugated 4G2 monoclonal antibody was kindly provided by Jens Wrammert and subsequently conjugated with APC (Novus Lightning-Link). $2x10^5$ HCs or CTBs were used per condition. Cells were stained for surface markers and permeablized to stain for ZIKV E protein. A detailed protocol can be found in Supplemental Experimental Procedures.

**Multiplex bead array.** Cytokine analysis was performed on supernatants from mock- or ZIKV-infected HCs or CTBs ($2x10^5$ cells per condition) using a human cytokine 25-plex panel (ThermoScientific), and a custom 2-plex panel with human IFNβ and IFNλ1 (eBioscience) per the manufacturer's instructions, and read on a Luminex 100 Analyzer.

**Statistical analysis.** Sample size was dependent on the number of donors. HCs were isolated from 5 donors and CTBs were isolated from 3 of these donors. Experiments with HCs were repeated twice (3 donors in the first experiment, 2 donors in the second). Experiments with CTBs were repeated once (3 donors in

1 experiment). All statistical analysis was performed in GraphPad Prism 6, with significance assessed by Mann Whitney U test with $p<0.05$. Infectivity as assessed by 4G2 staining utilized a 1-tailed test. Cell activation as assessed by surface staining utilized a 2-tailed test.

## 4F. Figures and legends

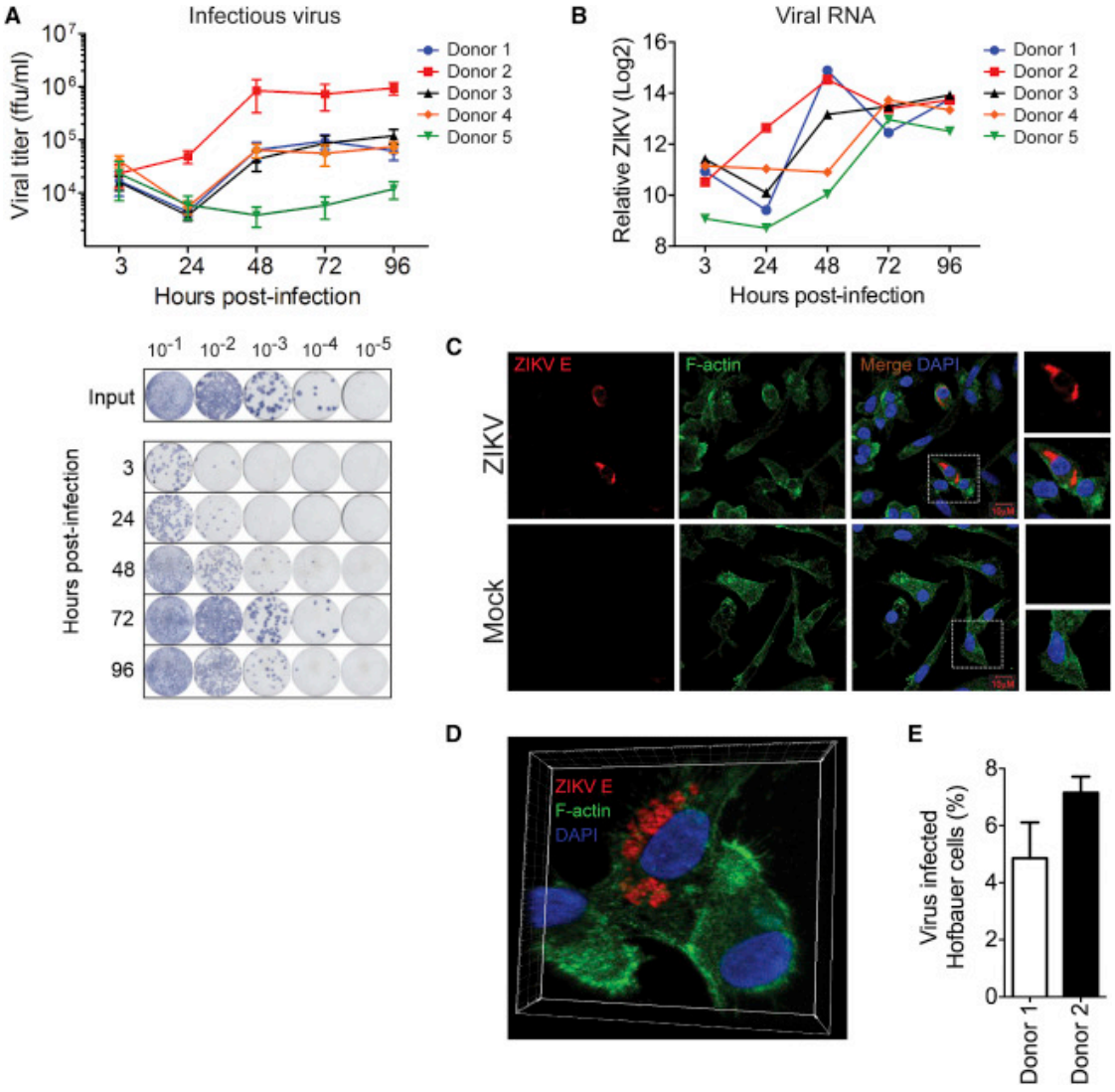


**Figure 1. Hofbauer cells are permissive to ZIKV infection. (A)** HCs from five donors were infected with ZIKV (PR 2015) at an MOI of 1 and viral titers in supernatants determined by FFA. Viral inoculum for all donors was $1x10^6$ffu/ml. Data are represented as the mean of four technical replicates +/- SD (top). Representative FFA staining (bottom). ffu, focus forming units. **(B)** Viral RNA detected by qRT-PCR in HCs infected with ZIKV (PR 2015). Data are relative to

GAPDH control and mock-infected cells ($\Delta\Delta C_T$). **(C, D, E)** Confocal microscopy of mock- and ZIKV (PR 2015)-infected HCs at 72hpi. **(D)** 3D reconstruction. **(E)** Percent infected cells determined from 5 fields of view. Data are represented as mean +/- SD. See also Figure S2. Data in C-E was generated by Dr. Huailiang Ma.

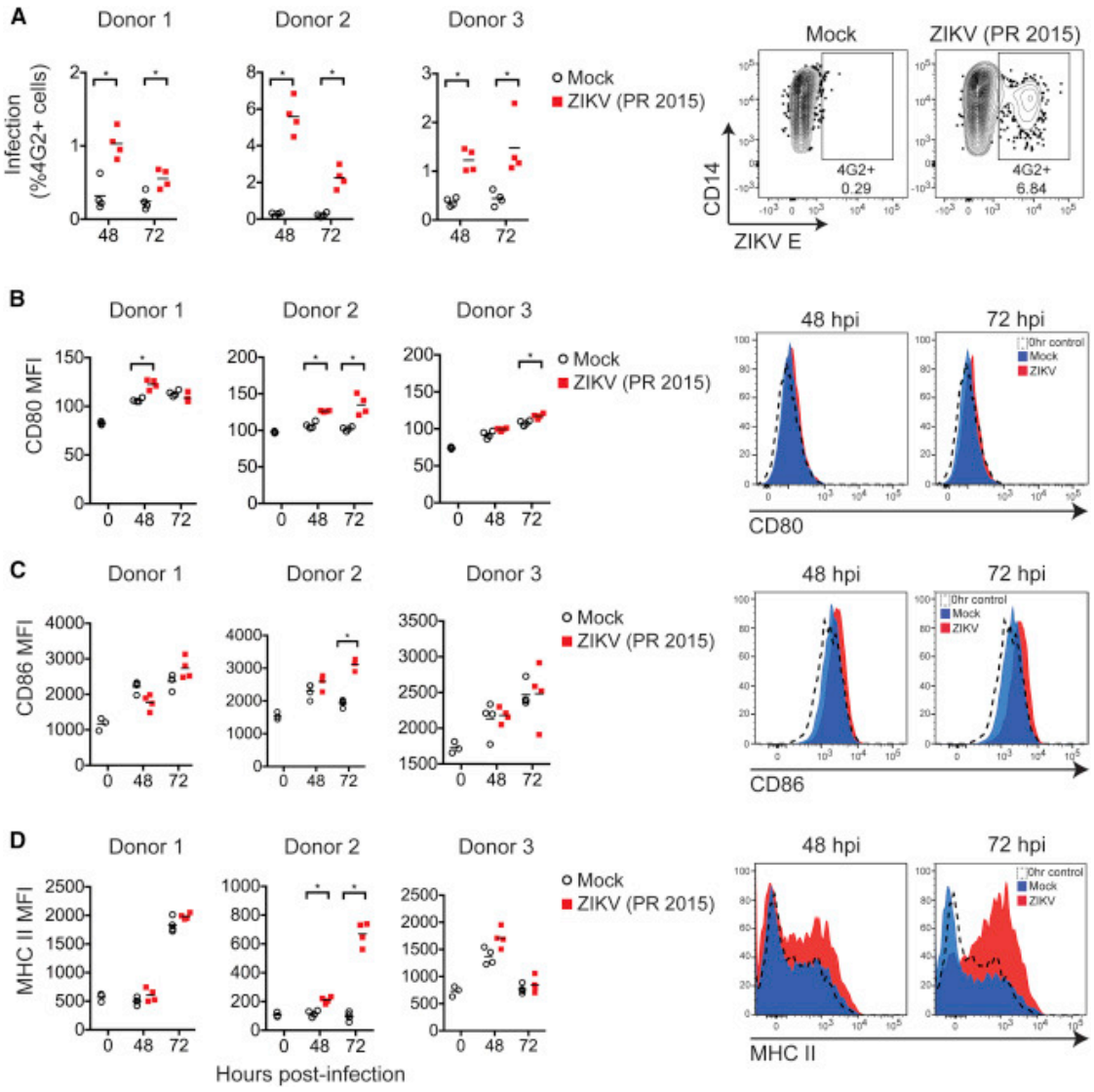


**Figure 2. ZIKV infection induces activation of HCs. (A)** HCs from three donors were infected with ZIKV (PR 2015) at an MOI of 1 or mock-infected. Percentages of infected cells at 48 and 72hpi were determined by intracellular viral E protein staining and flow cytometry (left panels). Horizontal bars indicate the mean of four technical replicates. (**B, C, D**) Surface expression of CD80, CD86, and MHC II was determined by flow cytometry. Data are represented as median fluorescence intensity (MFI). Horizontal bars indicate the mean of four

technical replicates. Representative histograms are provided (right panels). hpi, hours post-infection. See also Figure S2.

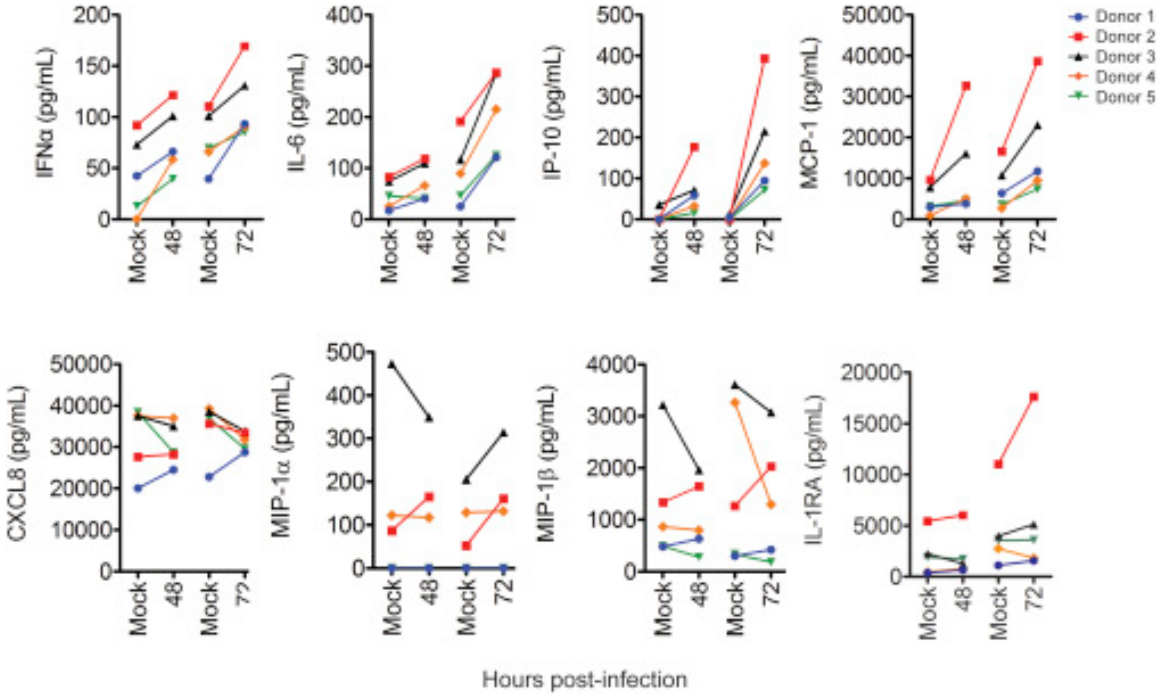


**Figure 3. ZIKV infection of HCs induces type I IFN and inflammatory cytokines.** HCs from five donors were infected with ZIKV (PR 2015) at an MOI of 1 or mock-infected. Cytokine levels in the supernatants were determined by multiplex bead array. All values are represented in “pg/ml” and shown with a connecting line between ZIKV-infected samples (48 and 72hpi) and their respective donor- and time-matched mock-infected samples. See also Table S1.

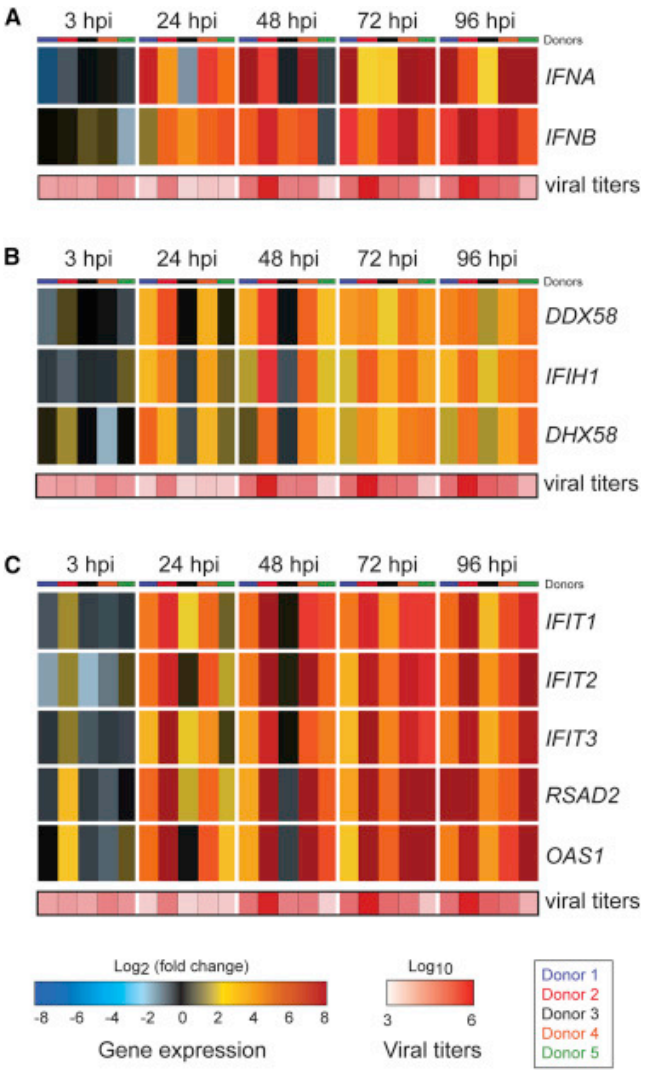


**Figure 4. ZIKV infection induces an antiviral response in HCs.** HCs from five donors were infected with ZIKV (PR 2015) at an MOI of 1 and antiviral gene expression determined by qRT-PCR. Gene expression data are represented as fold change relative to time-matched mock-infected controls (gene expression normalized to GAPDH - $\Delta\Delta C_T$ method). Individual donors are depicted as separate bars, organized from donor 1 to donor 5, within each time point block. Viral titers determined in Fig. 1 are represented as a separate heat map below

each group of genes. **(A)** Type I IFNs. **(B)** RIG-I-like receptors. **(C)** Antiviral effector genes. hpi, hours post-infection.

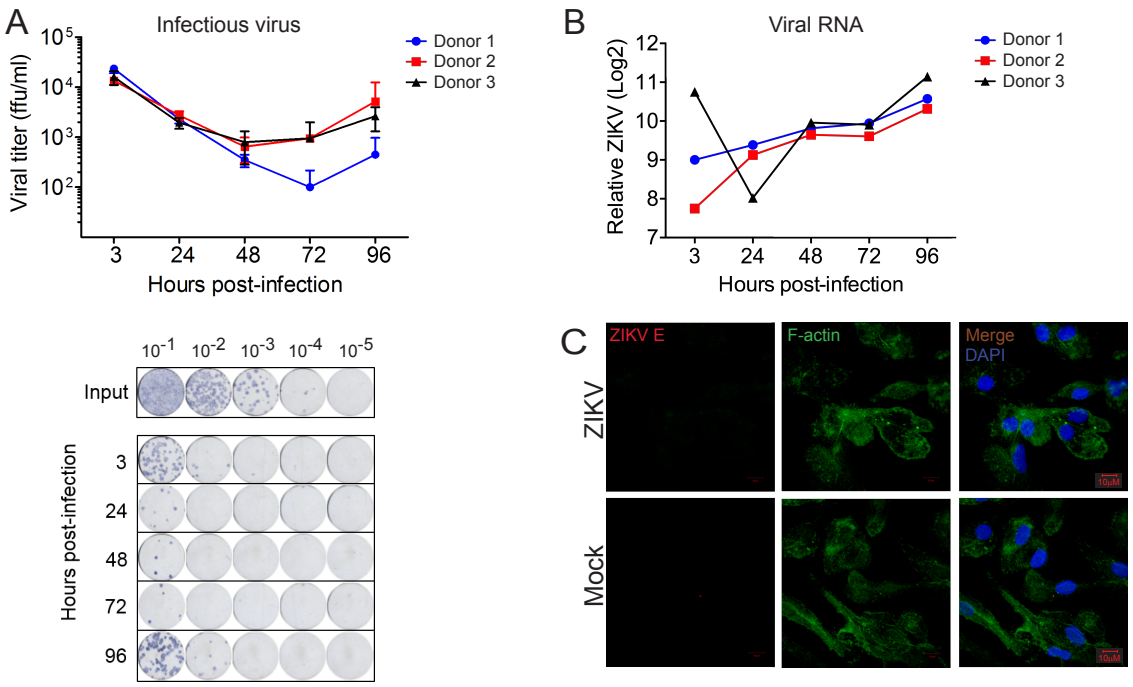


**Figure S1. Related to Figure 1. Cytotrophoblasts are permissive to ZIKV infection. (A)** CTBs from three donors were infected with ZIKV (PR 2015) at an MOI of 1 and viral titers in supernatants determined by FFA. Data are represented as the mean of four technical replicates +/- SD (top). Representative FFA staining (bottom). ffu, focus forming units. **(B)** Viral RNA detected by qRT-PCR in CTBs infected with ZIKV (PR 2015). Data are relative to GAPDH control and mock-infected cells ($\Delta\Delta C_T$). **(C)** Confocal microscopy of mock- and ZIKV (PR 2015)-infected CTBs at 72hpi. Data in C was generated by Dr. Huailiang Ma.

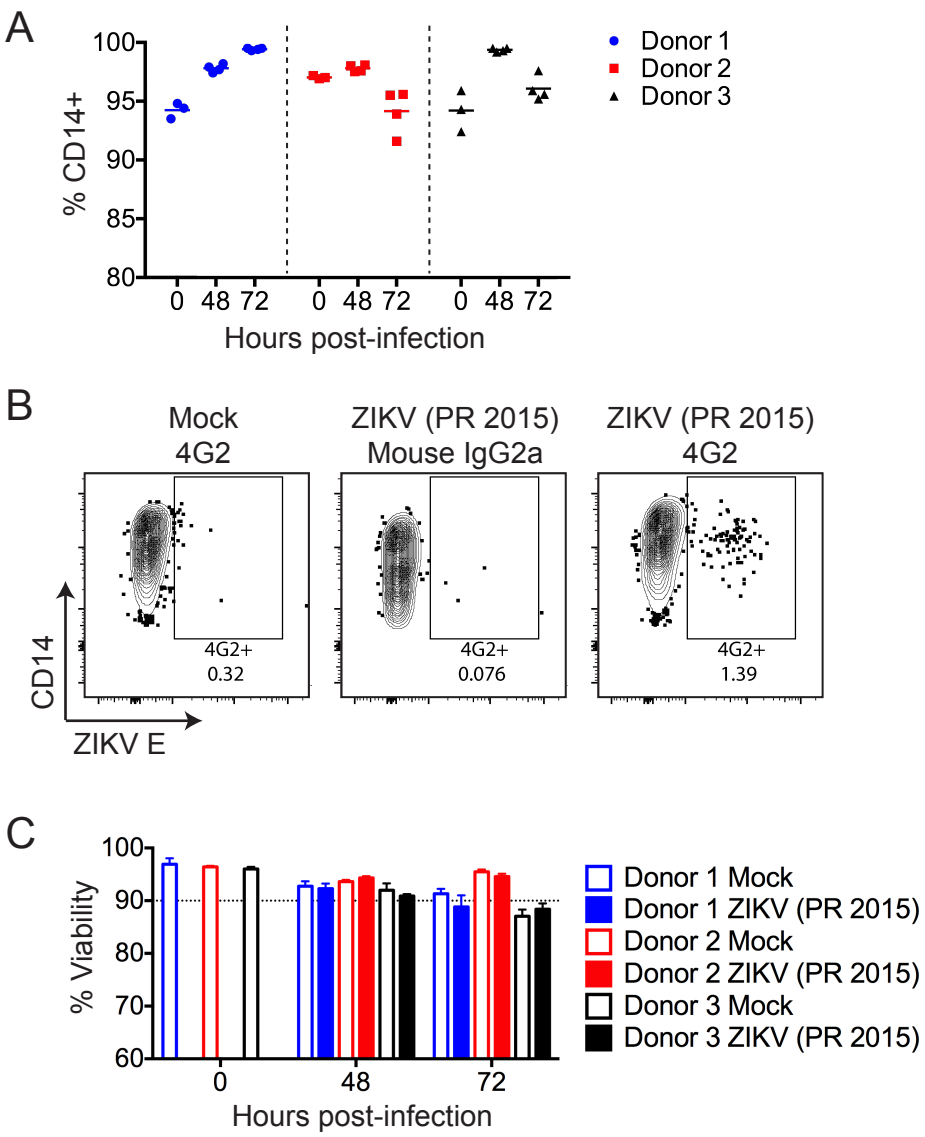


**Figure S2. Related to Figures 1-4. Controls for HC flow cytometry analysis.** **(A)** HCs used in these experiments were on average >95% pure by CD14 staining. Horizontal bars indicate the mean. For 0hpi, n=3; for 48 and 72hpi, n=4. **(B)** No ZIKV E protein was detected by mouse 4G2 antibody in mock-infected cells, or by mouse IgG2A isotype control in ZIKV-infected cells. **(C)** Both mock- and ZIKV-infected HCs retained ~90% or better viability over the time course as

determined by Ghost Dye Red 780 staining. Data are represented as the mean +/- SD.

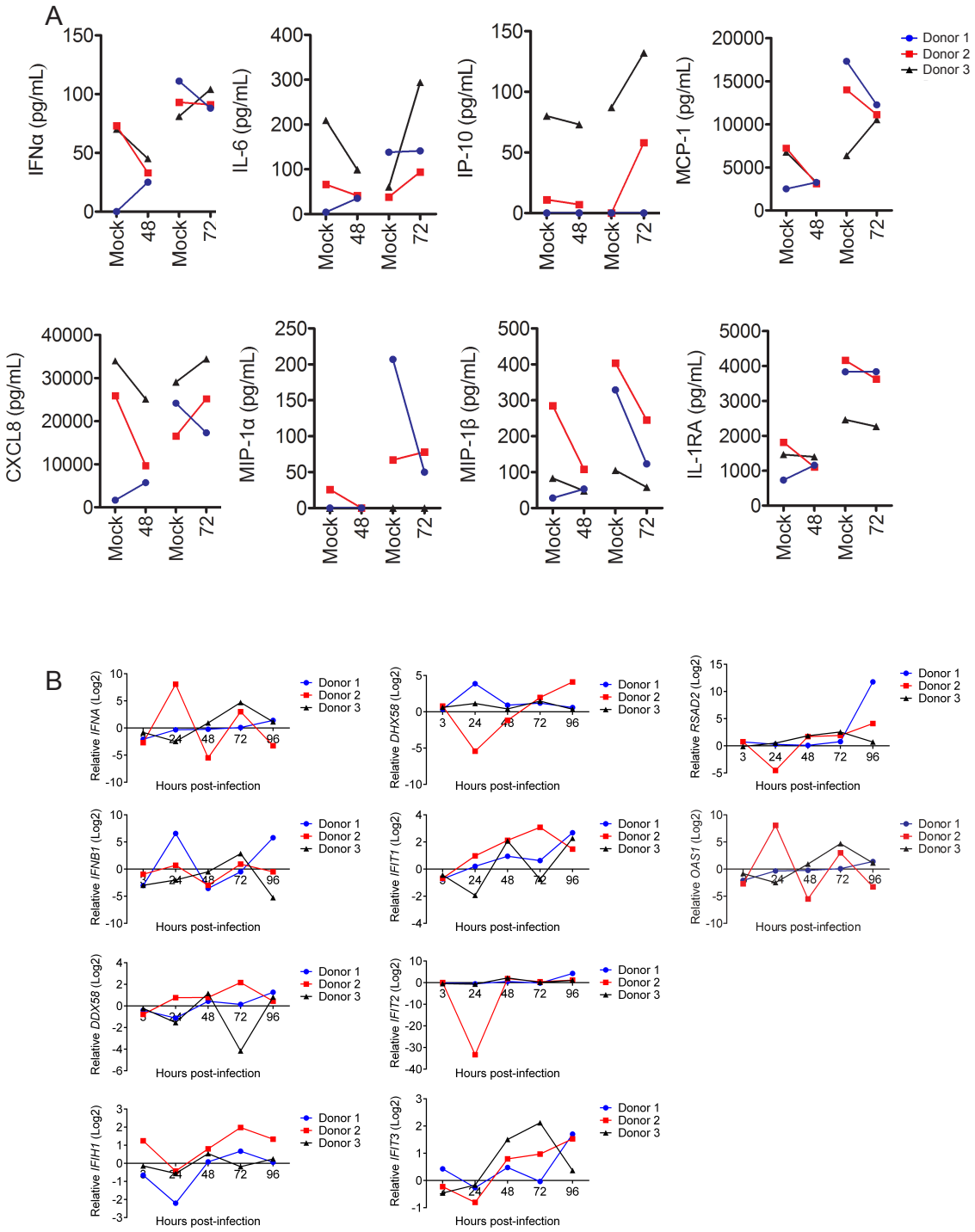


**Figure S3. Related to Figures 3 and 4. ZIKV infection of CTBs induces limited type I IFN and proinflammatory cytokine response.** (**A**) CTBs isolated

from three donors were infected with ZIKV (PR 2015) at an MOI of 1 or mock-infected. Cytokine levels in the supernatants were determined by multiplex bead array. All values are represented in “pg/ml” and shown with a connecting line between ZIKV-infected samples (48 and 72hpi) and their respective donor- and time-matched mock-infected samples. See also Table S2, (**B**) Antiviral gene expression determined by qRT-PCR in CTBs (three donors) infected with ZIKV (PR 2015). Gene expression data are represented as fold change relative to time-matched mock-infected controls (gene expression normalized to GAPDH - $\Delta\Delta C_T$ method).

# 4G. Tables and legends

| | Mock | | | | | 48hpi ZIKV (PR 2015) | | | | |
|---|---|---|---|---|---|---|---|---|---|---|
| | **Donor 1** | **Donor 2** | **Donor 3** | **Donor 4** | **Donor 5** | **Donor 1** | **Donor 2** | **Donor 3** | **Donor 4** | **Donor 5** |
| **IL-1β** | ND | ND | ND | ND | ND | ND | ND | ND | ND | ND |
| **IL-10** | ND | ND | ND | ND | ND | ND | ND | ND | ND | ND |
| **IL-13** | ND | ND | ND | ND | ND | ND | ND | ND | ND | ND |
| **IL-6** | 17 | 83 | 74 | 25 | 46 | 40 | 119 | 110 | 66 | 41 |
| **IL-12** | ND | ND | ND | ND | ND | ND | ND | ND | ND | ND |
| **RANTES** | ND | ND | ND | ND | ND | ND | ND | ND | ND | ND |
| **Eotaxin** | ND | ND | ND | ND | ND | ND | ND | ND | ND | ND |
| **IL-17** | ND | ND | ND | ND | ND | ND | ND | ND | ND | ND |
| **MIP-1α** | ND | 87 | 473 | 123 | ND | ND | 166 | 349 | 117 | ND |
| **GM-CSF** | ND | ND | ND | ND | ND | ND | ND | ND | ND | ND |
| **MIP-1β** | 481 | 1333 | 3218 | 864 | 490 | 630 | 1646 | 1962 | 798 | 278 |
| **MCP-1** | 3005 | 9691 | 7852 | 927 | 3173 | 6340 | 16624 | 10744 | 2711 | 3621 |
| **IL-15** | ND | ND | ND | ND | ND | ND | ND | ND | ND | ND |
| **IL-5** | ND | ND | ND | ND | ND | ND | ND | ND | ND | ND |
| **IFNγ** | ND | ND | ND | ND | ND | ND | ND | ND | ND | ND |
| **IL-1RA** | 372 | 5437 | 2249 | 465 | 1915 | 666 | 6029 | 1268 | 776 | 1721 |
| **TNFα** | ND | ND | ND | ND | ND | ND | ND | ND | ND | ND |
| **IL-2** | ND | ND | ND | ND | ND | ND | ND | ND | ND | ND |
| **IL-7** | ND | ND | ND | ND | ND | ND | ND | ND | ND | ND |
| **IP-10** | ND | ND | 36 | ND | ND | 59 | 177 | 71 | 33 | 16 |
| **IL-2R** | ND | ND | 56 | ND | ND | ND | 41 | 22 | ND | ND |
| **MIG** | ND | ND | ND | 4 | ND | ND | ND | ND | 4 | ND |
| **IL-4** | ND | ND | ND | ND | ND | ND | ND | ND | ND | ND |
| **IL-8** | 20060 | 27644 | 37556 | 37510 | 38402 | 24535 | 28257 | 35014 | 36993 | 28748 |
| **IFNα** | 42 | 92 | 73 | ND | 13 | 66 | 122 | 101 | 59 | 40 |
| **IFNβ** | ND | ND | ND | ND | ND | ND | ND | ND | ND | ND |
| **IFNλ1** | ND | ND | ND | ND | ND | ND | ND | ND | ND | ND |

| | **Mock** | | | | | **72hpi ZIKV (PR 2015)** | | | | |
|---|---|---|---|---|---|---|---|---|---|---|
| | **Donor 1** | **Donor 2** | **Donor 3** | **Donor 4** | **Donor 5** | **Donor 1** | **Donor 2** | **Donor 3** | **Donor 4** | **Donor 5** |
| **IL-1β** | ND | ND | ND | ND | ND | ND | ND | ND | ND | ND |
| **IL-10** | ND | ND | ND | ND | ND | ND | ND | ND | ND | ND |
| **IL-13** | ND | ND | ND | ND | ND | ND | ND | ND | ND | ND |
| **IL-6** | 25 | 192 | 117 | 90 | 46 | 121 | 287 | 286 | 215 | 126 |
| **IL-12** | ND | ND | ND | ND | ND | ND | ND | ND | ND | ND |
| **RANTES** | ND | ND | ND | ND | ND | ND | ND | ND | ND | ND |
| **Eotaxin** | ND | ND | ND | ND | ND | ND | ND | ND | ND | ND |
| **IL-17** | ND | ND | ND | ND | ND | ND | ND | ND | ND | ND |
| **MIP-1α** | ND | 52 | 206 | 129 | ND | ND | 161 | 314 | 132 | ND |
| **GM-CSF** | ND | ND | ND | ND | ND | ND | ND | ND | ND | ND |
| **MIP-1β** | 302 | 1267 | 3613 | 3269 | 334 | 421 | 2028 | 3076 | 1297 | 182 |
| **MCP-1** | 3826 | 32675 | 16101 | 5078 | 4644 | 11758 | 38672 | 23022 | 9512 | 7399 |
| **IL-15** | ND | ND | ND | ND | ND | ND | ND | ND | ND | ND |
| **IL-5** | ND | ND | ND | ND | ND | ND | ND | ND | ND | ND |
| **IFNγ** | ND | 4 | ND | ND | ND | ND | 4 | ND | ND | ND |
| **IL-1RA** | 1105 | 11027 | 3983 | 2745 | 3563 | 1565 | 17634 | 5120 | 1818 | 3575 |
| **TNFα** | ND | ND | ND | ND | ND | ND | ND | ND | ND | ND |
| **IL-2** | ND | ND | ND | ND | ND | ND | ND | ND | ND | ND |
| **IL-7** | ND | ND | ND | ND | ND | ND | ND | ND | ND | ND |

| | | | | | | | | | | |
|---|---|---|---|---|---|---|---|---|---|---|
| **IP-10** | 4 | ND | 12 | ND | ND | 95 | 394 | 215 | 137 | 72 |
| **IL-2R** | ND | ND | ND | 22 | 22 | ND | 56 | ND | ND | ND |
| **MIG** | ND | ND | ND | 23 | ND | ND | 4 | ND | 4 | ND |
| **IL-4** | ND | ND | ND | ND | ND | ND | ND | ND | ND | ND |
| **IL-8** | 22801 | 35633 | 38583 | 39257 | 36938 | 28784 | 33427 | 33837 | 31804 | 29587 |
| **IFNα** | 40 | 111 | 101 | 66 | 70 | 93 | 169 | 131 | 91 | 85 |
| **IFNβ** | ND | ND | ND | ND | ND | ND | ND | ND | ND | ND |
| **IFNλ1** | ND | ND | ND | ND | ND | ND | ND | ND | ND | ND |

**Table S1. Related to Figures 3 and S3. Cytokine analysis of Hofbauer cells at 48 and 72 hours post infection with ZIKV (PR 2015).** Cytokine levels in the supernatants of mock or ZIKV (PR 2015) infected HCs at 48 and 72 hours post infection as determined by multiplex bead array. All values are represented in “pg/mL”. Cytokine levels that were below the lower limit of detection are indicated as not detected or “ND”. hpi, hours post-infection.

| | Mock | | | 48hpi ZIKV (PR 2015) | | |
|---|---|---|---|---|---|---|
| | Donor 1 | Donor 2 | Donor 3 | Donor 1 | Donor 2 | Donor 3 |
| IL-1β | ND | ND | ND | ND | ND | ND |
| IL-10 | ND | ND | 2 | ND | ND | ND |
| IL-13 | ND | ND | ND | ND | ND | ND |
| IL-6 | 4 | 66 | 209 | 35 | 41 | 99 |
| IL-12 | ND | ND | ND | ND | ND | ND |
| RANTES | ND | ND | ND | ND | ND | ND |
| Eotaxin | ND | ND | ND | ND | ND | ND |
| IL-17 | ND | ND | ND | ND | ND | ND |
| MIP-1α | ND | 26 | ND | ND | ND | ND |
| GM-CSF | ND | ND | ND | ND | ND | ND |
| MIP-1β | 28 | 285 | 83 | 53 | 108 | 48 |
| MCP-1 | 2505 | 7234 | 6766 | 3256 | 3103 | 3273 |
| IL-15 | ND | ND | ND | ND | ND | ND |
| IL-5 | ND | ND | ND | ND | ND | ND |
| IFNγ | ND | ND | ND | ND | ND | ND |
| IL-1RA | 733 | 1815 | 1459 | 1157 | 1102 | 1397 |
| TNFα | ND | ND | ND | ND | ND | ND |
| IL-2 | ND | ND | ND | ND | ND | ND |
| IL-7 | ND | ND | ND | ND | ND | ND |
| IP-10 | ND | 11 | 80 | ND | 7 | 73 |
| IL-2R | ND | ND | ND | ND | ND | ND |
| MIG | ND | ND | 56 | ND | ND | 37 |
| IL-4 | ND | ND | ND | ND | ND | ND |
| IL-8 | 1663 | 25899 | 33972 | 5729 | 9672 | 25122 |
| IFNα | ND | 73 | 70 | 25 | 33 | 45 |
| IFNβ | ND | ND | ND | ND | ND | ND |
| IFNλ1 | ND | ND | ND | ND | ND | ND |

| | Mock | | | 72hpi ZIKV (PR 2015) | | |
|---|---|---|---|---|---|---|
| | Donor 1 | Donor 2 | Donor 3 | Donor 1 | Donor 2 | Donor 3 |
| IL-1β | ND | ND | ND | ND | ND | ND |
| IL-10 | ND | 2 | 5 | ND | ND | 14 |
| IL-13 | ND | ND | ND | ND | ND | ND |
| IL-6 | 138 | 38 | 60 | 141 | 94 | 294 |
| IL-12 | ND | ND | ND | ND | ND | ND |
| RANTES | ND | ND | ND | ND | ND | ND |
| Eotaxin | ND | ND | ND | ND | ND | ND |
| IL-17 | ND | ND | ND | ND | ND | ND |
| MIP-1α | 207 | 67 | ND | 50 | 78 | ND |
| GM-CSF | ND | ND | ND | ND | ND | ND |
| MIP-1β | 329 | 404 | 105 | 123 | 245 | 58 |
| MCP-1 | 17312 | 14016 | 6359 | 12257 | 11117 | 10534 |
| IL-15 | ND | ND | ND | ND | ND | ND |
| IL-5 | ND | ND | ND | ND | ND | ND |
| IFNγ | ND | ND | ND | ND | ND | ND |
| IL-1RA | 3833 | 4162 | 2461 | 3837 | 3623 | 2264 |
| TNFα | ND | ND | ND | ND | ND | ND |
| IL-2 | ND | ND | ND | ND | ND | ND |
| IL-7 | ND | ND | ND | ND | ND | ND |
| IP-10 | ND | ND | 87 | ND | 58 | 132 |
| IL-2R | ND | ND | 22 | ND | ND | ND |
| MIG | ND | ND | 82 | ND | ND | 94 |
| IL-4 | ND | ND | ND | ND | ND | ND |
| IL-8 | 24157 | 16535 | 29035 | 17273 | 25173 | 34423 |
| IFNα | 111 | 93 | 81 | 88 | 91 | 104 |
| IFNβ | ND | ND | ND | ND | ND | ND |
| IFNλ1 | ND | ND | ND | ND | ND | ND |

**Table S2. Related to Figures 3 and S3. Cytokine analysis of cytotrophoblasts at 48 and 72 hours post infection with ZIKV (PR 2015).** Cytokine levels in the supernatants of mock or ZIKV (PR 2015) infected CTBs at 48 and 72 hours post infection as determined by multiplex bead array. All values are represented in “pg/mL”. Cytokine levels that were below the lower limit of detection are indicated as not detected or “ND”. hpi, hours post-infection.

**CHAPTER 5.**

# General discussion and future directions

Vaccines against WNV and ZIKV are in various stages of clinical development for use in humans, but currently lack FDA-approval (40, 284). Despite vaccine efforts, little progress has been made in the development of specific antivirals that target flaviviruses. The lack of approved vaccines and specific antivirals underpins the need to better understand the human immune response during WNV and ZIKV infection. While the use of murine infection models have provided valuable insight into critical aspects of immunity during WNV and ZIKV infection, studies in mice don't accurately reflect human pathogenesis or immunity. Furthermore, efficient viral replication of ZIKV in mice requires deficiency in type I IFN signaling, limiting our understanding of how innate immunity restricts viral replication during ZIKV infection. The use of human primary cells offers many opportunities to overcome the limitations of murine models, without the difficulty of studying infection directly within humans. Through infection of primary human myeloid cells, the work presented in this dissertation has contributed to our understanding of how WNV and ZIKV evade innate immune barriers of infection. In Chapter 2, we employed a systems biology approach to reveal that WNV and ZIKV antagonize phosphorylation of STAT5 to subvert DC activation. In Chapter 3, we revealed that ZIKV antagonizes type I IFN responses to subvert antiviral immunity by blocking type I

IFN translation and downstream JAK/STAT signaling. In Chapter 4, we revealed that placental macrophages, known as Hofbauer cells, are susceptible to productive viral replication, providing support for a model of transplacental transmission where ZIKV crosses the placental barrier through direct infection of placental myeloid cells. Combined, the work presented in Chapters 2, 3, and 4 have advanced our understanding of how WNV and ZIKV evade host antiviral responses and barriers to promote viral replication and spread.

**Human DCs are targeted by WNV and ZIKV for productive viral replication**

Studies in mice have suggested that DCs are critical targets of viral replication during WNV infection (16, 99, 111). The most compelling evidence comes from work demonstrating that a selective loss of type I IFN signaling on CD11c+ cells, a majority of which are DCs, results in uncontrolled viral replication and lethal infection (16). While it has been speculated that WNV also replicates within DCs during human WNV infection, this has yet to be formally proven. In Chapter 2, we used primary human monocyte-derived DCs (moDCs) to demonstrate that human DCs have the capacity to support productive viral replication during infection by WNV. Our findings are similar to previous work with dengue and yellow fever viruses, both of which productively infect human moDCs (175, 225, 285, 286). Our findings suggest that similar to studies in mice, human DCs may be important targets of viral replication. To confirm the *in vivo* relevance of human DCs as targets of viral replication, future work will need to identify WNV-infected DCs within the blood of acutely infected patients. To verify

productive infection, it will be important to recover infectious virus from *in vivo* DC populations.

Our insights with WNV in Chapter 2 guided our studies in Chapter 3, where we next demonstrated that ZIKV also productively infects human moDCs. While previous work had shown human moDCs harbor viral antigen upon exposure to ZIKV, our work was the first demonstration of productive viral replication with human moDCs (79). To determine if replication within DCs was a recent adaptation of Asian lineage strains, we infected moDCs with four ZIKV strains spanning the evolution of the virus since its first discovery in 1947, including two historic African lineage viruses, an ancestral Asian lineage virus, and a contemporary Asian lineage virus. All four strains of ZIKV productively infected human moDCs, suggesting that the ability to target human DCs for infection evolved prior to 1947. Although all four strains could replicate within human moDCs, African linage viruses replicated to a higher magnitude than Asian lineage viruses. Differences in replication may also explain why we observed cell death following moDC infection with African, but not Asian lineage viruses. This raises the possibility that following their divergence from the African lineage, the Asian lineage viruses have evolved to replicate less efficiently in DCs, potentially to evade immune detection. Identification of specific mutations that may have altered the infectivity or replicative capacity of Asian lineage viruses is required to better understand the relevance of these findings.

**WNV and ZIKV differentially induce type I IFN responses during infection of human DCs**

Systemic type I IFN responses are associated with viral control during human WNV infection, although the cellular sources of type I IFN remains unclear (287). In Chapter 2, we demonstrated that WNV infection of human moDCs induces type I IFN secretion and antiviral responses. These findings are consistent with previous work where exposure of different human DC subsets to WNV induced IFNα secretion, and also similar to studies with DENV (224, 225). While it remains difficult to speculate on the relative contributions of human DCs during *in vivo* infection, our findings suggest that infected DCs may be important producers of type I IFN during human WNV infection (287).

Our findings in Chapter 3 revealed that ZIKV differs from WNV and DENV, inducing notable type I IFN gene transcription, but selectively blocking protein translation. While blockade of type I IFN transcription has been described as a mechanism used by DENV to evade type I IFN responses, selective blockade of type I IFN protein translation has not been previously described during flavivirus infection (225). The mechanism used by ZIKV to selectively block type I IFN protein translation remains unknown, but several possibilities exist. While type I IFN mRNA may be transcribed, the transcripts may exhibit decreased stability due to a impaired polyadenylation or the presence of microRNAs. Decreased transcript stability resulting from defective polyadenylation seems unlikely, given our findings that there were no differences between the quantity of total *IFNB1* and poly-adenylated *IFNB1* mRNA transcripts. It remains possible that miRNAs

that target type I IFN transcripts may alter mRNA stability after polyadenylation. Another possibility is that there is a block in nuclear export or sequestration of type I IFN transcripts away from the host translation machinery. Future studies will be focused on addressing these possibilities to fully elucidate the mechanism of selective inhibition of type I IFN protein translation by ZIKV.

**Innate immune signaling restricts WNV and ZIKV replication**

While studies in mice have found that both RLR and type I IFN signaling are critical for restricting WNV replication, the contributions of these pathways during human infection is less clear. In addition, the lack of an immune competent murine model of ZIKV infection has limited our understanding of the role of innate immune signaling during ZIKV infection, within mice or humans. In Chapters 2 and 3, we utilized a primary human moDC infection system and specific innate immune agonist treatment to demonstrate that activation of RLR signaling potently blocks replication of both WNV and ZIKV. In contrast, while IFNβ signaling strongly blocked WNV replication, ZIKV was notably more resistant. When we compared the ability of IFNβ treatment to restrict WNV or ZIKV replication using moDCs generated from the same donor, notably higher doses of IFNβ were required to restrict ZIKV than WNV (Fig. 1). While we found that WNV and ZIKV differed in their ability to induce type I IFN protein translation, this does not explain why ZIKV is more resistant to IFNβ treatment. We also found that both WNV and ZIKV block STAT1 and STAT2 phosphorylation to evade type I IFN signaling, suggesting that differential antagonism of type I IFN

signaling likely does not explain why ZIKV is more resistant to IFNβ treatment. Furthermore, the IFNβ treatment occurs at 1hr post infection, before the virus has had a chance to replicate and synthesize antagonistic viral proteins. Consequently, the ability of ZIKV to resist IFNβ treatment more likely represents evasion of the type I IFN-induced antiviral state, rather than direct inhibition of type I IFN signal transduction. To do so, ZIKV may uniquely antagonize the actions of one or more antiviral effector molecules. Direct evasion of antiviral effectors has been described for WNV, DENV, and JEV, all of which encode a 2'-*O*-methyltransferase within their NS5 protein that adds a methyl group to the 2'-O site within the 5' guanosine cap, evading protein translation inhibition by the IFIT family (288, 289). Whether ZIKV similarly blocks the antiviral activity of the IFITs remains to be determined. Nevertheless, ZIKV may block different antiviral effectors than WNV, and this could explain their differential susceptibility to IFNβ treatment.

The historic African lineage virus (MR-1947) was more efficient at evading the IFNβ-induced antiviral state than a contemporary Asian lineage ZIKV (PR-2015) (Fig. 1). This suggests that African and Asian lineage viruses may have a differential capacity to block antiviral immunity, which may also relate to the more rapid replication kinetics and enhanced infection magnitude observed with African lineage ZIKVs in Chapter 3. This also suggests that comparing the differences between African and Asian lineage viruses may provide clues to the mechanisms by which ZIKV blocks the IFNβ-induced antiviral state. Recent

development of infectious clones spanning the evolution of ZIKV will be a useful tool for these studies (290).

**RLR signaling restricts viral replication in a type I IFN independent manner**

Findings in Chapters 2 and 3 suggest that RIG-I signaling is capable of programming protective antiviral immunity within DCs in a type I IFN independent manner. Despite viral antagonism of type I IFN signaling by WNV (chapter 2) and ZIKV (chapter 3), strong antiviral responses are observed during infection of human moDCs, including production of multiple antiviral effector molecules. Activation of RLR signaling also remained effective in blocking WNV replication, even in the presence of an anti-IFNAR blocking antibody. This is consistent with previous work that identified multiple antiviral effector genes as direct targets of IRF-3, independent of the type I IFN receptor (96, 291, 292). Other work has also demonstrated that multiple antiviral effector genes are induced during WNV infection of mice that lack type I IFN signaling, and that much of this is lost when both RLR and type I IFN signaling are removed (98).

**ZIKV antagonizes type I IFN signaling through blockade of STAT1 and STAT2**

Our findings in Chapter 3 were the first report of ZIKV antagonizing STAT1, and the first description of ZIKV blocking STAT2 phosphorylation. A study published shortly before our own had found that the ZIKV NS5 protein binds to human STAT2, but not the murine homolog, and promotes STAT2

degradation (126). In our study, we did not observe degradation of STAT2 during ZIKV infection of either human DCs or A549 cells. Instead, we found up-regulation of STAT2 total protein levels during ZIKV infection. STAT2 expression is up-regulated in a manner that depends on either type I IFN or RLR signaling, where it is important to note that RLR signaling alone can induce STAT2 up-regulation (98). The differences in STAT2 degradation between studies may therefore reflect important cell type specific differences in the antiviral response during ZIKV infection. The studies in which STAT2 degradation was observed were performed in Vero and HEK 293T cells. Vero cells are defective in type I IFN production and RLR signaling, explained by defective IRF-3 activity and deletion of the type I IFN gene locus, and therefore have a severely diminished capacity to up-regulate STAT2 expression during viral infection (293-295). In contrast, both moDCs and A549 cells induce rigorous antiviral responses during ZIKV infection, resulting in STAT2 up-regulation, likely through both type I IFN and RLR signaling. The increased expression of STAT2 protein in systems with an intact antiviral response likely masks any degradation that may occur within infected cells. Therefore, the consequences of virally induced STAT2 degradation in systems were STAT2 is up-regulated remains unclear. Nevertheless, our work in Chapter 3, combined with current evidence suggests that ZIKV antagonizes type I IFN signaling through multiple mechanisms, including STAT2 degradation and blockade of STAT1 and STAT2 phosphorylation.

**STAT5 is a regulatory node of DC activation**

STAT5 has recently been defined as a regulator of DC activation in both murine and human systems, where STAT5 was found to bind to the promoter regions of CD80 and CD83 (204, 205). However, while activation of STAT5 by type I IFN signaling has been described, the role of innate immune signaling in driving STAT5-mediated DC activation is unclear (209, 296). In Chapter 2, using cis-regulatory sequence analysis, we identified STAT5 as a regulatory node upstream of multiple components of DC activation following RLR and IFNβ stimulation. This suggests that STAT5 signaling may play an important role in enhancing DC activation downstream of innate immune signaling. Future work will need to confirm the role of STAT5 in driving DC activation through the use of specific inhibitors and genetic ablation of STAT5.

Treatment with RIG-I and MDA5 agonists induced STAT5 phosphorylation within 90mins, coinciding with IRF3 phosphorylation kinetics. How RLR signaling activates STAT5 signaling remains unclear, but multiple possibilities exist. One possibility is that RLR agonist treatment induces rapid secretion of type I IFN, which then promotes STAT5 phosphorylation. Alternatively, STAT5 might be phosphorylated by a tyrosine kinase, such as Src or Lyn, that is activated directly downstream of RLR signaling (219, 220). Future studies within murine bone marrow derived DCs generated from mice with genetic knockouts of different components of innate immune signaling (e.g. *Ifnar1*-/-, *Mavs*-/-, *Tbk1*-/-) will be needed to fully parse this out.

**WNV and ZIKV subvert DC activation through blockade of STAT activation**

In Chapters 2 and 3, we found WNV and ZIKV infection did not activate human DCs, as noted by minimal up-regulation of pro-inflammatory cytokines, chemokines, or molecules involved in T cell activation. WNV infected DCs were also found to dampen allogeneic CD4 and CD8 T cell proliferation, suggesting that WNV, and likely ZIKV, subvert DC activation to compromise efficient T cell priming. Mechanistically, subversion of DC activation was explained by viral antagonism of STAT5, and to a lesser degree STAT1 and STAT2 signaling. While multiple groups have described flavivirus antagonism of STAT1 and STAT2, including our own work with ZIKV in Chapter 3, our findings in Chapter 2 are the first description of STAT5 being a target of viral antagonism during flavivirus infection.

Our findings in Chapter 2 of impaired DC activation are consistent with previous work, where WNV infection promotes only limited secretion of pro-inflammatory chemokines (224). Studies with a non-pathogenic subtype of WNV, WNV Kunjin, also found minimal secretion of IL-12, although in contrast to our work with a pathogenic WNV strain, there was notable up-regulation of CD86 and CD40 (214). The ability of pathogenic strains of WNV to antagonize the up-regulation of T cell co-stimulatory molecules may be a critical determinant for viral pathogenesis. Consistent with this idea, the YFV vaccine strain (YFV-17D) strongly up-regulates T cell co-stimulatory molecules on human DCs, which contributes to its efficacy as a vaccine (212). It would be interesting to compare YFV-17D with its non-attenuated parental strain, YFV Asibi (297). Based on our

studies with WNV and ZIKV, we would predict that YFV Asibi would not block STAT5 phosphorylation and fail to activate human DCs. Similar to our work with WNV and ZIKV, tick-borne flaviviruses have also been found to subvert DC activation within murine DCs through blockade of both IRF-1 and type I IFN signaling (238). In contrast with WNV and ZIKV, DENV activates pro-inflammatory responses and up-regulates T cell co-stimulatory molecules during infection of human DCs (225, 226). This suggests that WNV and ZIKV may have evolved unique mechanisms from DENV to evade antiviral immunity.

**WNV dampens Tyk2 and JAK1 activation**

The mechanism behind viral antagonism of STAT5, STAT1, and STAT2 phosphorylation remains unclear, but a few hypotheses can be made from our work in Chapter 2. Previous studies with WNV and other flaviviruses has implicated members of the Janus associated kinase (JAK) family as targets of viral antagonism. The type I IFN receptor associates with JAK1 and Tyk2, which mediate tyrosine phosphorylation of STAT1 and STAT2, while Tyk2 mediates tyrosine phosphorylation of STAT5 (209). Similar to type I IFN signaling, IL-4 and IL-13 can both signal through the shared type II IL-4 receptor, activating JAK1 and Tyk2 to mediate STAT5 phosphorylation (215). To determine if WNV blocks Tyk2 or JAK1 activation, we employed a Vero cell model of infection where we can achieve synchronous infection of 100% of cells in the absence of an endogenous type I IFN response. Similar to moDCs, WNV infection was able to block IFNβ-induced STAT5, as well as STAT1 and STAT2 phosphorylation in a

MOI-dependent manner. We did observe differences in STAT inhibition when we infected at an MOI of 0.1, where we likely have a mixed population of infected and uninfected cells, where STAT5 phosphorylation was more strongly inhibited than STAT1 or STAT2. This suggests that STAT5 may be more efficiently blocked by WNV than STAT1 or STAT2. Consistent with this, we observed no STAT5 phosphorylation during WNV infection of moDCs in Chapter 2, but did observe STAT1 and STAT2 phosphorylation. We did observe induction of antiviral effector molecules, demonstrating that the STAT blockade is specific. Despite the strong blockade in STAT phosphorylation, we observed a less pronounced blockade of Tyk2 and JAK1 phosphorylation at high MOI infection (MOI 1 and 5), but not at an MOI of 0.1. While previous work with WNV found a more profound blockade of Tyk2 phosphorylation than we observed in our own study, this previous work employed a cell system (A549 cells) that has an intact endogenous type I IFN response, which may explain the observed differences (123). Interestingly, work with the tick-borne flavivirus Langat virus (LGTV) differs from our own, where LGTV strongly block Tyk2 and JAK1 phosphorylation in Vero cells (228). Combined, this suggests that antagonism of JAK/STAT signaling is partially explained by inhibition of Tyk2 and JAK1 activation, but that further antagonism likely occurs after JAK activation. Furthermore, WNV and ZIKV likely differ from other flaviviruses in how they antagonize JAK/STAT signaling.

Our findings in Chapter 2 suggest that while WNV may dampen Tyk2 and JAK1 activation, this does not fully explain the potent blockade in STAT

phosphorylation. One possible mechanism for STAT blockade is that a viral protein may bind to the STAT proteins through a conserved sequence and sequester the STATs away from the activated JAKs. A similar phenomenon has been described during blue tongue virus infection, where STAT1 is sequestered within the cytosol and does not translocate to the nucleus (298). This possibility does not seem likely, at least for STAT5, since we found that both WNV and ZIKV fail to block GM-CSF induced STAT5 phosphorylation. This finding demonstrates that STAT5 itself is likely not targeted. Importantly, GM-CSF signaling does not involve activation of Tyk2, contrasting with type I IFN, IL-4, and IL-13 signaling. This suggests that WNV and ZIKV may block STAT phosphorylation by interfering with the interaction between Tyk2 and downstream STAT proteins. A final possibility that cannot be ruled out is that WNV and ZIKV may activate the suppressor of cytokine signaling (SOCS) protein family, which broadly regulate JAK/STAT signaling through binding to cytokine receptors, including IFNAR1, and activated JAKs (299). Indeed, SOCS proteins can be modulated during flavivirus infection (229). A better understanding of the mechanism used by WNV and ZIKV to block STAT phosphorylation will reveal a novel mechanism of immune antagonism during flavivirus infection.

**Transplacental transmission of ZIKV**

An unexpected and unique feature of ZIKV has been the ability to cross the placental barrier and cause perinatal infection. While multiple other human pathogens, including several viruses (human cytomegalovirus/CMV, rubella virus, and herpes simplex virus/HSV), are known to cause *in utero* infection,

ZIKV is the first flavivirus to exhibit this behavior. These recent findings have led to the suggestion by multiple groups that ZIKV should be included as a TORCH pathogen, which already includes *Toxoplasma gondii*, rubella virus, CMV, and HSV, and collectively refers to pathogens that can cause congenital infection (62). How readily ZIKV can reach the fetal compartment during human *in utero* infection is not clear, but studies in pregnant non-human primates infected with ZIKV suggests it may be an efficient process (57, 60). While the primary route of transplacental ZIKV transmission remains unclear, recent work, including our own work in Chapter 4, has provided valuable insight into potential mechanisms underlying transplacental ZIKV transmission.

Previous work by Carolyn Coyne's group found that primary STBs resist infection by ZIKV through constitutive production of type III IFN. These findings raised an important question of whether other placental cell types, including myeloid cells, could support viral replication. In Chapter 4 we demonstrated that HCs support productive viral replication during *ex vivo* infection, a finding that has since been confirmed by several other groups (65, 300). In addition to HCs, progenitor trophoblasts have also been reported as potential targets of ZIKV infection (61, 65). This includes our own work in Chapter 4, where we demonstrate that CTBs supported delayed and limited viral replication. Progenitor trophoblasts are also infected within a murine model of intrauterine transmission, while STBs were described as less susceptible (58). To confirm the relevance of placental cell types during human *in vivo* congenital infection, Sherif Zaki's group performed *in situ* hybridization for ZIKV RNA within placental tissue

obtained from pregnant mothers with confirmed ZIKV infection (64). ZIKV plus strand genomic RNA and minus strand RNA, a replication intermediate, were both detected in placental tissue and were predominately found within HCs. These *in vivo* findings, combined with our own work suggest that HCs, and not trophoblasts, are the more important target of ZIKV replication within the placenta during congenital infection.

Identification of HCs as targets of ZIKV infection raises a critical question: how does ZIKV cross the placental STB barrier to access the underlying susceptible HCs? Given the resistance of STBs to infection, it seem unlikely that ZIKV can cross the placenta through direct viral replication within the STB layer. There are at least three possible mechanisms by which ZIKV could cross the placenta without infecting STBs: 1) antibody mediated transcytosis through the neonatal Fc receptor (FcRn); 2) transmigration of infected maternal immune cells; or 3) immune-mediated placenta damage, leading to breaks in the STB layer. Antibody mediated transcytosis raises the possibility that cross-reacting, non-neutralizing anti-DENV antibodies may enhance transplacental transmission of ZIKV (66). These cross-reactive anti-DENV antibodies may also promote more efficient ZIKV infection of HCs, given their abundant expression of Fc receptors. Once ZIKV infects and replicates within HCs, the virus must then reach the developing fetus. Amniotic epithelial cells, the cells that make up the amniochorionic membrane that surround the fetus, support ZIKV replication during *ex vivo* infection (65). Direct infection of amniotic epithelial cells might allow the virus to spread across the amniochorionic membrane after viral

amplification within HCs. Despite these insights, including our own in Chapter 4, the exact mechanism by which ZIKV crosses the placenta and reaches the developing fetus remains an open question.

**Conclusion**

The work presented in Chapters 2, 3, and 4 have contributed to our understanding of how WNV and ZIKV evade human antiviral responses and barriers to infection. Many questions remain in Chapters 2 and 3, including the identity of the virally encoded factors that mediate subversion of DC activation. Future work that identifies the viral antagonist of STAT phosphorylation will be important to fully understand the mechanisms underlying WNV and ZIKV subversion of type I IFN signaling and DC activation. Further elucidation of the mechanism used by ZIKV to selectively block type I IFN translation will also be important to understanding ZIKV pathogenesis and immunity. Our work in Chapter 4 demonstrated that placental macrophages can support productive viral replication by ZIKV, however, how ZIKV reaches these susceptible cell types during perinatal infection remains unknown. A clearer understanding of how ZIKV crosses the placenta will be important for fully elucidating the pathogenesis of congenital infection. In conclusion, our work suggests that human DCs may be important targets of viral replication and immune subversion during infection by WNV and ZIKV, while placental macrophages may be important viral targets used by ZIKV during congenital infection.

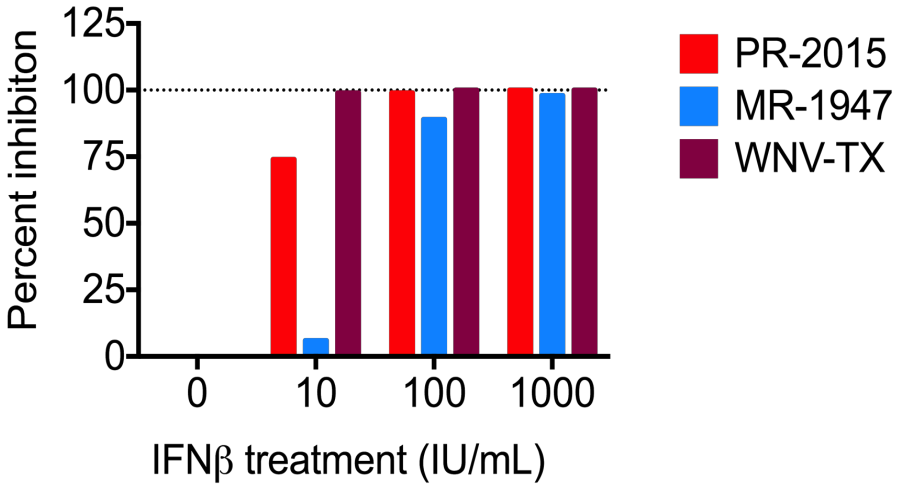


**Figure 1. IFNβ treatment is less effective at blocking ZIKV replication than WNV.** moDCs were infected with ZIKV PR-2015, ZIKV MR-1947, or WNV-TX at MOI 10 (as determined on Vero cells) for 1hr and then treated with IFNβ (10, 100, or 1000 IU/mL), or left untreated (0 IU/mL). Infectious virus release into the supernatant was assessed at 24hpi. Data is represented as percent inhibition, which was calculated as: (1 - [WNV + agonist] / [WNV alone]) * 100. Dashed line indicates 100% inhibition, or complete block of viral infection.

## REFERENCES

1. Mukhopadhyay S, Kuhn RJ, Rossmann MG. A structural perspective of the flavivirus life cycle. Nat Rev Microbiol. 2005;3(1):13-22. Epub 2004/12/21. doi: 10.1038/nrmicro1067. PubMed PMID: 15608696.
2. Welsch S, Miller S, Romero-Brey I, Merz A, Bleck CK, Walther P, Fuller SD, Antony C, Krijnse-Locker J, Bartenschlager R. Composition and three-dimensional architecture of the dengue virus replication and assembly sites. Cell Host Microbe. 2009;5(4):365-75. Epub 2009/04/22. doi: 10.1016/j.chom.2009.03.007. PubMed PMID: 19380115.
3. Brass AL, Huang IC, Benita Y, John SP, Krishnan MN, Feeley EM, Ryan BJ, Weyer JL, van der Weyden L, Fikrig E, Adams DJ, Xavier RJ, Farzan M, Elledge SJ. The IFITM proteins mediate cellular resistance to influenza A H1N1 virus, West Nile virus, and dengue virus. Cell. 2009;139(7):1243-54. Epub 2010/01/13. doi: 10.1016/j.cell.2009.12.017. PubMed PMID: 20064371; PMCID: PMC2824905.
4. Gorman MJ, Poddar S, Farzan M, Diamond MS. The Interferon-Stimulated Gene Ifitm3 Restricts West Nile Virus Infection and Pathogenesis. J Virol. 2016;90(18):8212-25. Epub 2016/07/08. doi: 10.1128/JVI.00581-16. PubMed PMID: 27384652; PMCID: PMC5008082.
5. Kajaste-Rudnitski A, Mashimo T, Frenkiel MP, Guenet JL, Lucas M, Despres P. The 2',5'-oligoadenylate synthetase 1b is a potent inhibitor of West Nile virus replication inside infected cells. J Biol Chem. 2006;281(8):4624-37. Epub 2005/12/24. doi: 10.1074/jbc.M508649200. PubMed PMID: 16371364.
6. Samuel MA, Whitby K, Keller BC, Marri A, Barchet W, Williams BR, Silverman RH, Gale M, Jr., Diamond MS. PKR and RNase L contribute to protection against lethal West Nile Virus infection by controlling early viral spread in the periphery and replication in neurons. J Virol. 2006;80(14):7009-19. Epub 2006/07/01. doi: 10.1128/JVI.00489-06. PubMed PMID: 16809306; PMCID: PMC1489062.
7. Cho H, Shrestha B, Sen GC, Diamond MS. A role for Ifit2 in restricting West Nile virus infection in the brain. J Virol. 2013;87(15):8363-71. Epub 2013/06/07. doi: 10.1128/JVI.01097-13. PubMed PMID: 23740986; PMCID: PMC3719802.
8. Szretter KJ, Brien JD, Thackray LB, Virgin HW, Cresswell P, Diamond MS. The interferon-inducible gene viperin restricts West Nile virus pathogenesis. J Virol. 2011;85(22):11557-66. Epub 2011/09/02. doi: 10.1128/JVI.05519-11. PubMed PMID: 21880757; PMCID: PMC3209274.
9. Ma DY, Suthar MS. Mechanisms of innate immune evasion in re-emerging RNA viruses. Curr Opin Virol. 2015;12:26-37. Epub 2015/03/15. doi: 10.1016/j.coviro.2015.02.005. PubMed PMID: 25765605; PMCID: PMC4470747.
10. Gack MU, Diamond MS. Innate immune escape by Dengue and West Nile viruses. Curr Opin Virol. 2016;20:119-28. Epub 2016/10/30. doi: 10.1016/j.coviro.2016.09.013. PubMed PMID: 27792906.
11. Chancey C, Grinev A, Volkova E, Rios M. The global ecology and epidemiology of West Nile virus. Biomed Res Int. 2015;2015:376230. Epub

2015/04/14. doi: 10.1155/2015/376230. PubMed PMID: 25866777; PMCID: 4383390.
12. Patel H, Sander B, Nelder MP. Long-term sequelae of West Nile virus-related illness: a systematic review. Lancet Infect Dis. 2015;15(8):951-9. doi: 10.1016/S1473-3099(15)00134-6. PubMed PMID: 26163373.
13. Suthar MS, Diamond MS, Gale M, Jr. West Nile virus infection and immunity. Nat Rev Microbiol. 2013;11(2):115-28. Epub 2013/01/17. doi: 10.1038/nrmicro2950. PubMed PMID: 23321534.
14. Styer LM, Kent KA, Albright RG, Bennett CJ, Kramer LD, Bernard KA. Mosquitoes inoculate high doses of West Nile virus as they probe and feed on live hosts. PLoS Pathog. 2007;3(9):1262-70. Epub 2007/10/19. doi: 10.1371/journal.ppat.0030132. PubMed PMID: 17941708; PMCID: PMC1976553.
15. Lim PY, Behr MJ, Chadwick CM, Shi PY, Bernard KA. Keratinocytes are cell targets of West Nile virus in vivo. J Virol. 2011;85(10):5197-201. Epub 2011/03/04. doi: 10.1128/JVI.02692-10. PubMed PMID: 21367890; PMCID: 3126165.
16. Pinto AK, Ramos HJ, Wu X, Aggarwal S, Shrestha B, Gorman M, Kim KY, Suthar MS, Atkinson JP, Gale M, Jr., Diamond MS. Deficient IFN signaling by myeloid cells leads to MAVS-dependent virus-induced sepsis. PLoS Pathog. 2014;10(4):e1004086. Epub 2014/04/20. doi: 10.1371/journal.ppat.1004086. PubMed PMID: 24743949; PMCID: PMC3990718.
17. Shrestha B, Gottlieb D, Diamond MS. Infection and injury of neurons by West Nile encephalitis virus. J Virol. 2003;77(24):13203-13. Epub 2003/12/04. doi: 10.1128/JVI.77.24.13203-13213.2003. PubMed PMID: 14645577; PMCID: PMC296085.
18. Agamanolis DP, Leslie MJ, Caveny EA, Guarner J, Shieh WJ, Zaki SR. Neuropathological findings in West Nile virus encephalitis: a case report. Ann Neurol. 2003;54(4):547-51. Epub 2003/10/02. doi: 10.1002/ana.10731. PubMed PMID: 14520673.
19. Graham JB, Thomas S, Swarts J, McMillan AA, Ferris MT, Suthar MS, Treuting PM, Ireton R, Gale M, Jr., Lund JM. Genetic diversity in the collaborative cross model recapitulates human West Nile virus disease outcomes. MBio. 2015;6(3):e00493-15. Epub 2015/05/07. doi: 10.1128/mBio.00493-15. PubMed PMID: 25944860; PMCID: PMC4436067.
20. Diamond MS, Shrestha B, Marri A, Mahan D, Engle M. B cells and antibody play critical roles in the immediate defense of disseminated infection by West Nile encephalitis virus. J Virol. 2003;77(4):2578-86. Epub 2003/01/29. doi: 10.1128/JVI.77.4.2578-2586.2003. PubMed PMID: 12551996; PMCID: PMC141119.
21. Diamond MS, Sitati EM, Friend LD, Higgs S, Shrestha B, Engle M. A critical role for induced IgM in the protection against West Nile virus infection. J Exp Med. 2003;198(12):1853-62. Epub 2003/12/10. doi: 10.1084/jem.20031223. PubMed PMID: 14662909; PMCID: PMC2194144.
22. Oliphant T, Engle M, Nybakken GE, Doane C, Johnson S, Huang L, Gorlatov S, Mehlhop E, Marri A, Chung KM, Ebel GD, Kramer LD, Fremont DH,

Diamond MS. Development of a humanized monoclonal antibody with therapeutic potential against West Nile virus. Nat Med. 2005;11(5):522-30. Epub 2005/04/27. doi: 10.1038/nm1240. PubMed PMID: 15852016; PMCID: PMC1458527.
23. Nybakken GE, Oliphant T, Johnson S, Burke S, Diamond MS, Fremont DH. Structural basis of West Nile virus neutralization by a therapeutic antibody. Nature. 2005;437(7059):764-9. Epub 2005/09/30. doi: 10.1038/nature03956. PubMed PMID: 16193056.
24. Busch MP, Kleinman SH, Tobler LH, Kamel HT, Norris PJ, Walsh I, Matud JL, Prince HE, Lanciotti RS, Wright DJ, Linnen JM, Caglioti S. Virus and antibody dynamics in acute west nile virus infection. J Infect Dis. 2008;198(7):984-93. Epub 2008/08/30. doi: 10.1086/591467. PubMed PMID: 18729783.
25. Shrestha B, Diamond MS. Role of CD8+ T cells in control of West Nile virus infection. J Virol. 2004;78(15):8312-21. Epub 2004/07/16. doi: 10.1128/JVI.78.15.8312-8321.2004. PubMed PMID: 15254203; PMCID: PMC446114.
26. Shrestha B, Samuel MA, Diamond MS. CD8+ T cells require perforin to clear West Nile virus from infected neurons. J Virol. 2006;80(1):119-29. Epub 2005/12/15. doi: 10.1128/JVI.80.1.119-129.2006. PubMed PMID: 16352536; PMCID: PMC1317548.
27. Sitati EM, Diamond MS. CD4+ T-cell responses are required for clearance of West Nile virus from the central nervous system. J Virol. 2006;80(24):12060-9. Epub 2006/10/13. doi: 10.1128/JVI.01650-06. PubMed PMID: 17035323; PMCID: PMC1676257.
28. Lanteri MC, O'Brien KM, Purtha WE, Cameron MJ, Lund JM, Owen RE, Heitman JW, Custer B, Hirschkorn DF, Tobler LH, Kiely N, Prince HE, Ndhlovu LC, Nixon DF, Kamel HT, Kelvin DJ, Busch MP, Rudensky AY, Diamond MS, Norris PJ. Tregs control the development of symptomatic West Nile virus infection in humans and mice. J Clin Invest. 2009;119(11):3266-77. Epub 2009/10/27. doi: 10.1172/JCI39387. PubMed PMID: 19855131; PMCID: PMC2769173.
29. Lanteri MC, Diamond MS, Law JP, Chew GM, Wu S, Inglis HC, Wong D, Busch MP, Norris PJ, Ndhlovu LC. Increased frequency of Tim-3 expressing T cells is associated with symptomatic West Nile virus infection. PLoS One. 2014;9(3):e92134. Epub 2014/03/20. doi: 10.1371/journal.pone.0092134. PubMed PMID: 24642562; PMCID: PMC3958446.
30. James EA, Gates TJ, LaFond RE, Yamamoto S, Ni C, Mai D, Gersuk VH, O'Brien K, Nguyen QA, Zeitner B, Lanteri MC, Norris PJ, Chaussabel D, Malhotra U, Kwok WW. Neuroinvasive West Nile Infection Elicits Elevated and Atypically Polarized T Cell Responses That Promote a Pathogenic Outcome. PLoS Pathog. 2016;12(1):e1005375. doi: 10.1371/journal.ppat.1005375. PubMed PMID: 26795118; PMCID: PMC4721872.
31. Haddow AD, Schuh AJ, Yasuda CY, Kasper MR, Heang V, Huy R, Guzman H, Tesh RB, Weaver SC. Genetic characterization of Zika virus strains: geographic expansion of the Asian lineage. PLoS Negl Trop Dis.

2012;6(2):e1477. Epub 2012/03/06. doi: 10.1371/journal.pntd.0001477. PubMed PMID: 22389730; PMCID: PMC3289602.
32. Lanciotti RS, Lambert AJ, Holodniy M, Saavedra S, Signor Ldel C. Phylogeny of Zika Virus in Western Hemisphere, 2015. Emerg Infect Dis. 2016;22(5):933-5. Epub 2016/04/19. doi: 10.3201/eid2205.160065. PubMed PMID: 27088323; PMCID: PMC4861537.
33. Dowd KA, DeMaso CR, Pelc RS, Speer SD, Smith AR, Goo L, Platt DJ, Mascola JR, Graham BS, Mulligan MJ, Diamond MS, Ledgerwood JE, Pierson TC. Broadly Neutralizing Activity of Zika Virus-Immune Sera Identifies a Single Viral Serotype. Cell Rep. 2016;16(6):1485-91. Epub 2016/08/03. doi: 10.1016/j.celrep.2016.07.049. PubMed PMID: 27481466; PMCID: PMC5004740.
34. Dick GW, Kitchen SF, Haddow AJ. Zika virus. I. Isolations and serological specificity. Trans R Soc Trop Med Hyg. 1952;46(5):509-20. Epub 1952/09/01. PubMed PMID: 12995440.
35. Duffy MR, Chen TH, Hancock WT, Powers AM, Kool JL, Lanciotti RS, Pretrick M, Marfel M, Holzbauer S, Dubray C, Guillaumot L, Griggs A, Bel M, Lambert AJ, Laven J, Kosoy O, Panella A, Biggerstaff BJ, Fischer M, Hayes EB. Zika virus outbreak on Yap Island, Federated States of Micronesia. N Engl J Med. 2009;360(24):2536-43. Epub 2009/06/12. doi: 10.1056/NEJMoa0805715. PubMed PMID: 19516034.
36. Cao-Lormeau VM, Roche C, Teissier A, Robin E, Berry AL, Mallet HP, Sall AA, Musso D. Zika virus, French polynesia, South pacific, 2013. Emerg Infect Dis. 2014;20(6):1085-6. Epub 2014/05/27. doi: 10.3201/eid2006.140138. PubMed PMID: 24856001; PMCID: PMC4036769.
37. Musso D, Nilles EJ, Cao-Lormeau VM. Rapid spread of emerging Zika virus in the Pacific area. Clin Microbiol Infect. 2014;20(10):O595-6. Epub 2014/06/10. doi: 10.1111/1469-0691.12707. PubMed PMID: 24909208.
38. Faria NR, Azevedo Rdo S, Kraemer MU, Souza R, Cunha MS, Hill SC, Theze J, Bonsall MB, Bowden TA, Rissanen I, Rocco IM, Nogueira JS, Maeda AY, Vasami FG, Macedo FL, Suzuki A, Rodrigues SG, Cruz AC, Nunes BT, Medeiros DB, Rodrigues DS, Nunes Queiroz AL, da Silva EV, Henriques DF, Travassos da Rosa ES, de Oliveira CS, Martins LC, Vasconcelos HB, Casseb LM, Simith Dde B, Messina JP, Abade L, Lourenco J, Carlos Junior Alcantara L, de Lima MM, Giovanetti M, Hay SI, de Oliveira RS, Lemos Pda S, de Oliveira LF, de Lima CP, da Silva SP, de Vasconcelos JM, Franco L, Cardoso JF, Vianez-Junior JL, Mir D, Bello G, Delatorre E, Khan K, Creatore M, Coelho GE, de Oliveira WK, Tesh R, Pybus OG, Nunes MR, Vasconcelos PF. Zika virus in the Americas: Early epidemiological and genetic findings. Science. 2016;352(6283):345-9. Epub 2016/03/26. doi: 10.1126/science.aaf5036. PubMed PMID: 27013429; PMCID: PMC4918795.
39. Adams L, Bello-Pagan M, Lozier M, Ryff KR, Espinet C, Torres J, Perez-Padilla J, Febo MF, Dirlikov E, Martinez A, Munoz-Jordan J, Garcia M, Segarra MO, Malave G, Rivera A, Shapiro-Mendoza C, Rosinger A, Kuehnert MJ, Chung KW, Pate LL, Harris A, Hemme RR, Lenhart A, Aquino G, Zaki S, Read JS, Waterman SH, Alvarado LI, Alvarado-Ramy F, Valencia-Prado M, Thomas D, Sharp TM, Rivera-Garcia B. Update: Ongoing Zika Virus Transmission - Puerto

Rico, November 1, 2015-July 7, 2016. MMWR Morb Mortal Wkly Rep. 2016;65(30):774-9. Epub 2016/08/05. doi: 10.15585/mmwr.mm6530e1. PubMed PMID: 27490087.

40. Aliota MT, Bassit L, Bradrick SS, Cox B, Garcia-Blanco MA, Gavegnano C, Friedrich TC, Golos TG, Griffin DE, Haddow A, Kallas EG, Kitron U, Lecuit M, Magnani DM, Marrs C, Mercer N, McSweegan E, Ng L, O'Connor DH, Osorio JE, Ribeiro GS, Ricciardi M, Rossi SL, Saade G, Schinazi RF, Schott-Lerner GO, Shan C, Shi PY, Watkins DI, Vasilakis N, Weaver SC. Zika in the Americas, year 2: What have we learned? What gaps remain? A report from the Global Virus Network. Antiviral Res. 2017. Epub 2017/06/10. doi: 10.1016/j.antiviral.2017.06.001. PubMed PMID: 28595824.

41. Grubaugh ND, Ladner JT, Kraemer MUG, Dudas G, Tan AL, Gangavarapu K, Wiley MR, White S, Theze J, Magnani DM, Prieto K, Reyes D, Bingham AM, Paul LM, Robles-Sikisaka R, Oliveira G, Pronty D, Barcellona CM, Metsky HC, Baniecki ML, Barnes KG, Chak B, Freije CA, Gladden-Young A, Gnirke A, Luo C, MacInnis B, Matranga CB, Park DJ, Qu J, Schaffner SF, Tomkins-Tinch C, West KL, Winnicki SM, Wohl S, Yozwiak NL, Quick J, Fauver JR, Khan K, Brent SE, Reiner RC, Jr., Lichtenberger PN, Ricciardi MJ, Bailey VK, Watkins DI, Cone MR, Kopp EWt, Hogan KN, Cannons AC, Jean R, Monaghan AJ, Garry RF, Loman NJ, Faria NR, Porcelli MC, Vasquez C, Nagle ER, Cummings DAT, Stanek D, Rambaut A, Sanchez-Lockhart M, Sabeti PC, Gillis LD, Michael SF, Bedford T, Pybus OG, Isern S, Palacios G, Andersen KG. Genomic epidemiology reveals multiple introductions of Zika virus into the United States. Nature. 2017;546(7658):401-5. Epub 2017/05/26. doi: 10.1038/nature22400. PubMed PMID: 28538723.

42. Likos A, Griffin I, Bingham AM, Stanek D, Fischer M, White S, Hamilton J, Eisenstein L, Atrubin D, Mulay P, Scott B, Jenkins P, Fernandez D, Rico E, Gillis L, Jean R, Cone M, Blackmore C, McAllister J, Vasquez C, Rivera L, Philip C. Local Mosquito-Borne Transmission of Zika Virus - Miami-Dade and Broward Counties, Florida, June-August 2016. MMWR Morb Mortal Wkly Rep. 2016;65(38):1032-8. Epub 2016/09/30. doi: 10.15585/mmwr.mm6538e1. PubMed PMID: 27684886.

43. Monaghan AJ, Morin CW, Steinhoff DF, Wilhelmi O, Hayden M, Quattrochi DA, Reiskind M, Lloyd AL, Smith K, Schmidt CA, Scalf PE, Ernst K. On the Seasonal Occurrence and Abundance of the Zika Virus Vector Mosquito Aedes Aegypti in the Contiguous United States. PLoS Curr. 2016;8. Epub 2016/04/12. doi: 10.1371/currents.outbreaks.50dfc7f46798675fc63e7d7da563da76. PubMed PMID: 27066299; PMCID: PMC4807952.

44. Wong PS, Li MZ, Chong CS, Ng LC, Tan CH. Aedes (Stegomyia) albopictus (Skuse): a potential vector of Zika virus in Singapore. PLoS Negl Trop Dis. 2013;7(8):e2348. Epub 2013/08/13. doi: 10.1371/journal.pntd.0002348. PubMed PMID: 23936579; PMCID: PMC3731215.

45. D'Ortenzio E, Matheron S, Yazdanpanah Y, de Lamballerie X, Hubert B, Piorkowski G, Maquart M, Descamps D, Damond F, Leparc-Goffart I. Evidence of Sexual Transmission of Zika Virus. N Engl J Med. 2016;374(22):2195-8. Epub 2016/04/14. doi: 10.1056/NEJMc1604449. PubMed PMID: 27074370.

46. Yockey LJ, Varela L, Rakib T, Khoury-Hanold W, Fink SL, Stutz B, Szigeti-Buck K, Van den Pol A, Lindenbach BD, Horvath TL, Iwasaki A. Vaginal Exposure to Zika Virus during Pregnancy Leads to Fetal Brain Infection. Cell. 2016;166(5):1247-56 e4. Epub 2016/08/28. doi: 10.1016/j.cell.2016.08.004. PubMed PMID: 27565347; PMCID: PMC5006689.
47. Davidson A, Slavinski S, Komoto K, Rakeman J, Weiss D. Suspected Female-to-Male Sexual Transmission of Zika Virus - New York City, 2016. MMWR Morb Mortal Wkly Rep. 2016;65(28):716-7. Epub 2016/07/22. doi: 10.15585/mmwr.mm6528e2. PubMed PMID: 27442327.
48. Govero J, Esakky P, Scheaffer SM, Fernandez E, Drury A, Platt DJ, Gorman MJ, Richner JM, Caine EA, Salazar V, Moley KH, Diamond MS. Zika virus infection damages the testes in mice. Nature. 2016;540(7633):438-42. Epub 2016/11/01. doi: 10.1038/nature20556. PubMed PMID: 27798603; PMCID: PMC5432198.
49. Oehler E, Watrin L, Larre P, Leparc-Goffart I, Lastere S, Valour F, Baudouin L, Mallet H, Musso D, Ghawche F. Zika virus infection complicated by Guillain-Barre syndrome--case report, French Polynesia, December 2013. Euro Surveill. 2014;19(9). Epub 2014/03/15. PubMed PMID: 24626205.
50. Parra B, Lizarazo J, Jimenez-Arango JA, Zea-Vera AF, Gonzalez-Manrique G, Vargas J, Angarita JA, Zuniga G, Lopez-Gonzalez R, Beltran CL, Rizcala KH, Morales MT, Pacheco O, Ospina ML, Kumar A, Cornblath DR, Munoz LS, Osorio L, Barreras P, Pardo CA. Guillain-Barre Syndrome Associated with Zika Virus Infection in Colombia. N Engl J Med. 2016;375(16):1513-23. Epub 2016/11/01. doi: 10.1056/NEJMoa1605564. PubMed PMID: 27705091.
51. Sharp TM, Munoz-Jordan J, Perez-Padilla J, Bello-Pagan MI, Rivera A, Pastula DM, Salinas JL, Martinez Mendez JH, Mendez M, Powers AM, Waterman S, Rivera-Garcia B. Zika Virus Infection Associated With Severe Thrombocytopenia. Clin Infect Dis. 2016;63(9):1198-201. Epub 2016/07/16. doi: 10.1093/cid/ciw476. PubMed PMID: 27418575; PMCID: PMC5176332.
52. Driggers RW, Ho CY, Korhonen EM, Kuivanen S, Jaaskelainen AJ, Smura T, Rosenberg A, Hill DA, DeBiasi RL, Vezina G, Timofeev J, Rodriguez FJ, Levanov L, Razak J, Iyengar P, Hennenfent A, Kennedy R, Lanciotti R, du Plessis A, Vapalahti O. Zika Virus Infection with Prolonged Maternal Viremia and Fetal Brain Abnormalities. N Engl J Med. 2016;374(22):2142-51. Epub 2016/03/31. doi: 10.1056/NEJMoa1601824. PubMed PMID: 27028667.
53. Calvet G, Aguiar RS, Melo AS, Sampaio SA, de Filippis I, Fabri A, Araujo ES, de Sequeira PC, de Mendonca MC, de Oliveira L, Tschoeke DA, Schrago CG, Thompson FL, Brasil P, Dos Santos FB, Nogueira RM, Tanuri A, de Filippis AM. Detection and sequencing of Zika virus from amniotic fluid of fetuses with microcephaly in Brazil: a case study. Lancet Infect Dis. 2016;16(6):653-60. Epub 2016/02/22. doi: 10.1016/S1473-3099(16)00095-5. PubMed PMID: 26897108.
54. Brasil P, Pereira JP, Jr., Moreira ME, Ribeiro Nogueira RM, Damasceno L, Wakimoto M, Rabello RS, Valderramos SG, Halai UA, Salles TS, Zin AA, Horovitz D, Daltro P, Boechat M, Raja Gabaglia C, Carvalho de Sequeira P, Pilotto JH, Medialdea-Carrera R, Cotrim da Cunha D, Abreu de Carvalho LM, Pone M, Machado Siqueira A, Calvet GA, Rodrigues Baiao AE, Neves ES,

Nassar de Carvalho PR, Hasue RH, Marschik PB, Einspieler C, Janzen C, Cherry JD, Bispo de Filippis AM, Nielsen-Saines K. Zika Virus Infection in Pregnant Women in Rio de Janeiro. N Engl J Med. 2016;375(24):2321-34. Epub 2016/03/05. doi: 10.1056/NEJMoa1602412. PubMed PMID: 26943629; PMCID: PMC5323261.

55. Mlakar J, Korva M, Tul N, Popovic M, Poljsak-Prijatelj M, Mraz J, Kolenc M, Resman Rus K, Vesnaver Vipotnik T, Fabjan Vodusek V, Vizjak A, Pizem J, Petrovec M, Avsic Zupanc T. Zika Virus Associated with Microcephaly. N Engl J Med. 2016;374(10):951-8. Epub 2016/02/11. doi: 10.1056/NEJMoa1600651. PubMed PMID: 26862926.

56. de Paula Freitas B, de Oliveira Dias JR, Prazeres J, Sacramento GA, Ko AI, Maia M, Belfort R, Jr. Ocular Findings in Infants With Microcephaly Associated With Presumed Zika Virus Congenital Infection in Salvador, Brazil. JAMA Ophthalmol. 2016. Epub 2016/02/13. doi: 10.1001/jamaophthalmol.2016.0267. PubMed PMID: 26865554; PMCID: PMC5444996.

57. Adams Waldorf KM, Stencel-Baerenwald JE, Kapur RP, Studholme C, Boldenow E, Vornhagen J, Baldessari A, Dighe MK, Thiel J, Merillat S, Armistead B, Tisoncik-Go J, Green RR, Davis MA, Dewey EC, Fairgrieve MR, Gatenby JC, Richards T, Garden GA, Diamond MS, Juul SE, Grant RF, Kuller L, Shaw DW, Ogle J, Gough GM, Lee W, English C, Hevner RF, Dobyns WB, Gale M, Jr., Rajagopal L. Fetal brain lesions after subcutaneous inoculation of Zika virus in a pregnant nonhuman primate. Nat Med. 2016;22(11):1256-9. Epub 2016/11/01. doi: 10.1038/nm.4193. PubMed PMID: 27618651; PMCID: PMC5365281.

58. Miner JJ, Cao B, Govero J, Smith AM, Fernandez E, Cabrera OH, Garber C, Noll M, Klein RS, Noguchi KK, Mysorekar IU, Diamond MS. Zika Virus Infection during Pregnancy in Mice Causes Placental Damage and Fetal Demise. Cell. 2016;165(5):1081-91. Epub 2016/05/18. doi: 10.1016/j.cell.2016.05.008. PubMed PMID: 27180225; PMCID: PMC4874881.

59. Cugola FR, Fernandes IR, Russo FB, Freitas BC, Dias JL, Guimaraes KP, Benazzato C, Almeida N, Pignatari GC, Romero S, Polonio CM, Cunha I, Freitas CL, Brandao WN, Rossato C, Andrade DG, Faria Dde P, Garcez AT, Buchpigel CA, Braconi CT, Mendes E, Sall AA, Zanotto PM, Peron JP, Muotri AR, Beltrao-Braga PC. The Brazilian Zika virus strain causes birth defects in experimental models. Nature. 2016;534(7606):267-71. Epub 2016/06/10. doi: 10.1038/nature18296. PubMed PMID: 27279226; PMCID: PMC4902174.

60. Nguyen SM, Antony KM, Dudley DM, Kohn S, Simmons HA, Wolfe B, Salamat MS, Teixeira LBC, Wiepz GJ, Thoong TH, Aliota MT, Weiler AM, Barry GL, Weisgrau KL, Vosler LJ, Mohns MS, Breitbach ME, Stewart LM, Rasheed MN, Newman CM, Graham ME, Wieben OE, Turski PA, Johnson KM, Post J, Hayes JM, Schultz-Darken N, Schotzko ML, Eudailey JA, Permar SR, Rakasz EG, Mohr EL, Capuano S, 3rd, Tarantal AF, Osorio JE, O'Connor SL, Friedrich TC, O'Connor DH, Golos TG. Highly efficient maternal-fetal Zika virus transmission in pregnant rhesus macaques. PLoS Pathog. 2017;13(5):e1006378. Epub 2017/05/26. doi: 10.1371/journal.ppat.1006378. PubMed PMID: 28542585; PMCID: PMC5444831.

61. Quicke KM, Bowen JR, Johnson EL, McDonald CE, Ma H, O'Neal JT, Rajakumar A, Wrammert J, Rimawi BH, Pulendran B, Schinazi RF, Chakraborty R, Suthar MS. Zika Virus Infects Human Placental Macrophages. Cell Host Microbe. 2016;20(1):83-90. Epub 2016/06/02. doi: 10.1016/j.chom.2016.05.015. PubMed PMID: 27247001; PMCID: PMC5166429.
62. Coyne CB, Lazear HM. Zika virus - reigniting the TORCH. Nat Rev Microbiol. 2016;14(11):707-15. Epub 2016/08/31. doi: 10.1038/nrmicro.2016.125. PubMed PMID: 27573577.
63. Bayer A, Lennemann NJ, Ouyang Y, Bramley JC, Morosky S, Marques ET, Jr., Cherry S, Sadovsky Y, Coyne CB. Type III Interferons Produced by Human Placental Trophoblasts Confer Protection against Zika Virus Infection. Cell Host Microbe. 2016;19(5):705-12. Epub 2016/04/14. doi: 10.1016/j.chom.2016.03.008. PubMed PMID: 27066743; PMCID: PMC4866896.
64. Bhatnagar J, Rabeneck DB, Martines RB, Reagan-Steiner S, Ermias Y, Estetter LB, Suzuki T, Ritter J, Keating MK, Hale G, Gary J, Muehlenbachs A, Lambert A, Lanciotti R, Oduyebo T, Meaney-Delman D, Bolanos F, Saad EA, Shieh WJ, Zaki SR. Zika Virus RNA Replication and Persistence in Brain and Placental Tissue. Emerg Infect Dis. 2017;23(3):405-14. Epub 2016/12/14. doi: 10.3201/eid2303.161499. PubMed PMID: 27959260; PMCID: PMC5382738.
65. Tabata T, Petitt M, Puerta-Guardo H, Michlmayr D, Wang C, Fang-Hoover J, Harris E, Pereira L. Zika Virus Targets Different Primary Human Placental Cells, Suggesting Two Routes for Vertical Transmission. Cell Host Microbe. 2016;20(2):155-66. Epub 2016/07/23. doi: 10.1016/j.chom.2016.07.002. PubMed PMID: 27443522; PMCID: PMC5257282.
66. Priyamvada L, Quicke KM, Hudson WH, Onlamoon N, Sewatanon J, Edupuganti S, Pattanapanyasat K, Chokephaibulkit K, Mulligan MJ, Wilson PC, Ahmed R, Suthar MS, Wrammert J. Human antibody responses after dengue virus infection are highly cross-reactive to Zika virus. Proceedings of the National Academy of Sciences of the United States of America. 2016;113(28):7852-7. Epub 2016/06/30. doi: 10.1073/pnas.1607931113. PubMed PMID: 27354515; PMCID: PMC4948328.
67. Tang H, Hammack C, Ogden SC, Wen Z, Qian X, Li Y, Yao B, Shin J, Zhang F, Lee EM, Christian KM, Didier RA, Jin P, Song H, Ming GL. Zika Virus Infects Human Cortical Neural Progenitors and Attenuates Their Growth. Cell Stem Cell. 2016;18(5):587-90. Epub 2016/03/10. doi: 10.1016/j.stem.2016.02.016. PubMed PMID: 26952870; PMCID: PMC5299540.
68. Dang J, Tiwari SK, Lichinchi G, Qin Y, Patil VS, Eroshkin AM, Rana TM. Zika Virus Depletes Neural Progenitors in Human Cerebral Organoids through Activation of the Innate Immune Receptor TLR3. Cell Stem Cell. 2016;19(2):258-65. Epub 2016/05/11. doi: 10.1016/j.stem.2016.04.014. PubMed PMID: 27162029; PMCID: PMC5116380.
69. Garcez PP, Loiola EC, Madeiro da Costa R, Higa LM, Trindade P, Delvecchio R, Nascimento JM, Brindeiro R, Tanuri A, Rehen SK. Zika virus impairs growth in human neurospheres and brain organoids. Science. 2016;352(6287):816-8. Epub 2016/04/12. doi: 10.1126/science.aaf6116. PubMed PMID: 27064148.

70. Hanners NW, Eitson JL, Usui N, Richardson RB, Wexler EM, Konopka G, Schoggins JW. Western Zika Virus in Human Fetal Neural Progenitors Persists Long Term with Partial Cytopathic and Limited Immunogenic Effects. Cell Rep. 2016;15(11):2315-22. Epub 2016/06/09. doi: 10.1016/j.celrep.2016.05.075. PubMed PMID: 27268504.
71. Li C, Xu D, Ye Q, Hong S, Jiang Y, Liu X, Zhang N, Shi L, Qin CF, Xu Z. Zika Virus Disrupts Neural Progenitor Development and Leads to Microcephaly in Mice. Cell Stem Cell. 2016;19(1):120-6. Epub 2016/05/18. doi: 10.1016/j.stem.2016.04.017. PubMed PMID: 27179424.
72. Souza BS, Sampaio GL, Pereira CS, Campos GS, Sardi SI, Freitas LA, Figueira CP, Paredes BD, Nonaka CK, Azevedo CM, Rocha VP, Bandeira AC, Mendez-Otero R, Dos Santos RR, Soares MB. Zika virus infection induces mitosis abnormalities and apoptotic cell death of human neural progenitor cells. Sci Rep. 2016;6(1):39775. Epub 2016/12/23. doi: 10.1038/srep39775. PubMed PMID: 28008958; PMCID: PMC5180086.
73. Gabriel E, Ramani A, Karow U, Gottardo M, Natarajan K, Gooi LM, Goranci-Buzhala G, Krut O, Peters F, Nikolic M, Kuivanen S, Korhonen E, Smura T, Vapalahti O, Papantonis A, Schmidt-Chanasit J, Riparbelli M, Callaini G, Kronke M, Utermohlen O, Gopalakrishnan J. Recent Zika Virus Isolates Induce Premature Differentiation of Neural Progenitors in Human Brain Organoids. Cell Stem Cell. 2017;20(3):397-406 e5. Epub 2017/01/31. doi: 10.1016/j.stem.2016.12.005. PubMed PMID: 28132835.
74. Li H, Saucedo-Cuevas L, Regla-Nava JA, Chai G, Sheets N, Tang W, Terskikh AV, Shresta S, Gleeson JG. Zika Virus Infects Neural Progenitors in the Adult Mouse Brain and Alters Proliferation. Cell Stem Cell. 2016;19(5):593-8. Epub 2016/08/23. doi: 10.1016/j.stem.2016.08.005. PubMed PMID: 27545505; PMCID: PMC5097023.
75. Tappe D, Perez-Giron JV, Zammarchi L, Rissland J, Ferreira DF, Jaenisch T, Gomez-Medina S, Gunther S, Bartoloni A, Munoz-Fontela C, Schmidt-Chanasit J. Cytokine kinetics of Zika virus-infected patients from acute to reconvalescent phase. Med Microbiol Immunol. 2016;205(3):269-73. Epub 2015/12/26. doi: 10.1007/s00430-015-0445-7. PubMed PMID: 26702627; PMCID: PMC4867002.
76. Tripathi S, Balasubramaniam VR, Brown JA, Mena I, Grant A, Bardina SV, Maringer K, Schwarz MC, Maestre AM, Sourisseau M, Albrecht RA, Krammer F, Evans MJ, Fernandez-Sesma A, Lim JK, Garcia-Sastre A. A novel Zika virus mouse model reveals strain specific differences in virus pathogenesis and host inflammatory immune responses. PLoS Pathog. 2017;13(3):e1006258. Epub 2017/03/10. doi: 10.1371/journal.ppat.1006258. PubMed PMID: 28278235; PMCID: PMC5373643.
77. Bowen JR, Quicke KM, Maddur MS, O'Neal JT, McDonald CE, Fedorova NB, Puri V, Shabman RS, Pulendran B, Suthar MS. Zika Virus Antagonizes Type I Interferon Responses during Infection of Human Dendritic Cells. PLoS Pathog. 2017;13(2):e1006164. Epub 2017/02/06. doi: 10.1371/journal.ppat.1006164. PubMed PMID: 28152048; PMCID: PMC5289613.

78. Frumence E, Roche M, Krejbich-Trotot P, El-Kalamouni C, Nativel B, Rondeau P, Misse D, Gadea G, Viranaicken W, Despres P. The South Pacific epidemic strain of Zika virus replicates efficiently in human epithelial A549 cells leading to IFN-beta production and apoptosis induction. Virology. 2016;493:217-26. Epub 2016/04/10. doi: 10.1016/j.virol.2016.03.006. PubMed PMID: 27060565.
79. Hamel R, Dejarnac O, Wichit S, Ekchariyawat P, Neyret A, Luplertlop N, Perera-Lecoin M, Surasombatpattana P, Talignani L, Thomas F, Cao-Lormeau VM, Choumet V, Briant L, Despres P, Amara A, Yssel H, Misse D. Biology of Zika Virus Infection in Human Skin Cells. J Virol. 2015;89(17):8880-96. Epub 2015/06/19. doi: 10.1128/JVI.00354-15. PubMed PMID: 26085147; PMCID: PMC4524089.
80. Bayless NL, Greenberg RS, Swigut T, Wysocka J, Blish CA. Zika Virus Infection Induces Cranial Neural Crest Cells to Produce Cytokines at Levels Detrimental for Neurogenesis. Cell Host Microbe. 2016;20(4):423-8. Epub 2016/10/04. doi: 10.1016/j.chom.2016.09.006. PubMed PMID: 27693308; PMCID: PMC5113290.
81. Bardina SV, Bunduc P, Tripathi S, Duehr J, Frere JJ, Brown JA, Nachbagauer R, Foster GA, Krysztof D, Tortorella D, Stramer SL, Garcia-Sastre A, Krammer F, Lim JK. Enhancement of Zika virus pathogenesis by preexisting antiflavivirus immunity. Science. 2017;356(6334):175-80. Epub 2017/04/01. doi: 10.1126/science.aal4365. PubMed PMID: 28360135.
82. Elong Ngono A, Vizcarra EA, Tang WW, Sheets N, Joo Y, Kim K, Gorman MJ, Diamond MS, Shresta S. Mapping and Role of the CD8+ T Cell Response During Primary Zika Virus Infection in Mice. Cell Host Microbe. 2017;21(1):35-46. Epub 2017/01/13. doi: 10.1016/j.chom.2016.12.010. PubMed PMID: 28081442; PMCID: PMC5234855.
83. Manangeeswaran M, Ireland DD, Verthelyi D. Zika (PRVABC59) Infection Is Associated with T cell Infiltration and Neurodegeneration in CNS of Immunocompetent Neonatal C57Bl/6 Mice. PLoS Pathog. 2016;12(11):e1006004. Epub 2016/11/18. doi: 10.1371/journal.ppat.1006004. PubMed PMID: 27855206; PMCID: PMC5113993.
84. Wen J, Tang WW, Sheets N, Ellison J, Sette A, Kim K, Shresta S. Identification of Zika virus epitopes reveals immunodominant and protective roles for dengue virus cross-reactive CD8+ T cells. Nat Microbiol. 2017;2:17036. Epub 2017/03/14. doi: 10.1038/nmicrobiol.2017.36. PubMed PMID: 28288094.
85. Lazear HM, Govero J, Smith AM, Platt DJ, Fernandez E, Miner JJ, Diamond MS. A Mouse Model of Zika Virus Pathogenesis. Cell Host Microbe. 2016;19(5):720-30. Epub 2016/04/14. doi: 10.1016/j.chom.2016.03.010. PubMed PMID: 27066744; PMCID: PMC4866885.
86. Loo YM, Gale M, Jr. Immune signaling by RIG-I-like receptors. Immunity. 2011;34(5):680-92. Epub 2011/05/28. doi: 10.1016/j.immuni.2011.05.003. PubMed PMID: 21616437; PMCID: PMC3177755.
87. Vazquez C, Horner SM. MAVS Coordination of Antiviral Innate Immunity. Journal of virology. 2015;89(14):6974-7. Epub 2015/05/08. doi: 10.1128/JVI.01918-14. PubMed PMID: 25948741; PMCID: 4473567.

88. Quicke KM, Diamond MS, Suthar MS. Negative regulators of the RIG-I-like receptor signaling pathway. Eur J Immunol. 2017;47(4):615-28. Epub 2017/03/16. doi: 10.1002/eji.201646484. PubMed PMID: 28295214.
89. Kato H, Takeuchi O, Mikamo-Satoh E, Hirai R, Kawai T, Matsushita K, Hiiragi A, Dermody TS, Fujita T, Akira S. Length-dependent recognition of double-stranded ribonucleic acids by retinoic acid-inducible gene-I and melanoma differentiation-associated gene 5. J Exp Med. 2008;205(7):1601-10. doi: 10.1084/jem.20080091. PubMed PMID: 18591409; PMCID: PMC2442638.
90. Wies E, Wang MK, Maharaj NP, Chen K, Zhou S, Finberg RW, Gack MU. Dephosphorylation of the RNA sensors RIG-I and MDA5 by the phosphatase PP1 is essential for innate immune signaling. Immunity. 2013;38(3):437-49. Epub 2013/03/19. doi: 10.1016/j.immuni.2012.11.018. PubMed PMID: 23499489; PMCID: PMC3616631.
91. Gack MU, Shin YC, Joo CH, Urano T, Liang C, Sun L, Takeuchi O, Akira S, Chen Z, Inoue S, Jung JU. TRIM25 RING-finger E3 ubiquitin ligase is essential for RIG-I-mediated antiviral activity. Nature. 2007;446(7138):916-20. Epub 2007/03/30. doi: 10.1038/nature05732. PubMed PMID: 17392790.
92. Horner SM, Park HS, Gale M, Jr. Control of innate immune signaling and membrane targeting by the Hepatitis C virus NS3/4A protease are governed by the NS3 helix alpha0. J Virol. 2012;86(6):3112-20. Epub 2012/01/13. doi: 10.1128/JVI.06727-11. PubMed PMID: 22238314; PMCID: PMC3302330.
93. Dixit E, Boulant S, Zhang Y, Lee AS, Odendall C, Shum B, Hacohen N, Chen ZJ, Whelan SP, Fransen M, Nibert ML, Superti-Furga G, Kagan JC. Peroxisomes are signaling platforms for antiviral innate immunity. Cell. 2010;141(4):668-81. Epub 2010/05/11. doi: 10.1016/j.cell.2010.04.018. PubMed PMID: 20451243; PMCID: PMC3670185.
94. Hou F, Sun L, Zheng H, Skaug B, Jiang QX, Chen ZJ. MAVS forms functional prion-like aggregates to activate and propagate antiviral innate immune response. Cell. 2011;146(3):448-61. Epub 2011/07/26. doi: 10.1016/j.cell.2011.06.041. PubMed PMID: 21782231; PMCID: PMC3179916.
95. Brownell J, Bruckner J, Wagoner J, Thomas E, Loo YM, Gale M, Jr., Liang TJ, Polyak SJ. Direct, interferon-independent activation of the CXCL10 promoter by NF-kappaB and interferon regulatory factor 3 during hepatitis C virus infection. J Virol. 2014;88(3):1582-90. Epub 2013/11/22. doi: 10.1128/JVI.02007-13. PubMed PMID: 24257594; PMCID: PMC3911583.
96. Daffis S, Samuel MA, Keller BC, Gale M, Jr., Diamond MS. Cell-specific IRF-3 responses protect against West Nile virus infection by interferon-dependent and -independent mechanisms. PLoS Pathog. 2007;3(7):e106. Epub 2007/08/07. doi: 10.1371/journal.ppat.0030106. PubMed PMID: 17676997; PMCID: PMC1933455.
97. Wang J, Basagoudanavar SH, Wang X, Hopewell E, Albrecht R, Garcia-Sastre A, Balachandran S, Beg AA. NF-kappa B RelA subunit is crucial for early IFN-beta expression and resistance to RNA virus replication. J Immunol. 2010;185(3):1720-9. Epub 2010/07/09. doi: 10.4049/jimmunol.1000114. PubMed PMID: 20610653; PMCID: PMC2910841.

98. Suthar MS, Brassil MM, Blahnik G, McMillan A, Ramos HJ, Proll SC, Belisle SE, Katze MG, Gale M, Jr. A systems biology approach reveals that tissue tropism to West Nile virus is regulated by antiviral genes and innate immune cellular processes. PLoS Pathog. 2013;9(2):e1003168. Epub 2013/04/02. doi: 10.1371/journal.ppat.1003168. PubMed PMID: 23544010; PMCID: PMC3567171.
99. Suthar MS, Ma DY, Thomas S, Lund JM, Zhang N, Daffis S, Rudensky AY, Bevan MJ, Clark EA, Kaja MK, Diamond MS, Gale M, Jr. IPS-1 is essential for the control of West Nile virus infection and immunity. PLoS Pathog. 2010;6(2):e1000757. Epub 2010/02/09. doi: 10.1371/journal.ppat.1000757. PubMed PMID: 20140199; PMCID: PMC2816698.
100. Da Costa A, Garza E, Graham JB, Swarts JL, Soerens AG, Gale M, Lund JM. Extrinsic MAVS signaling is critical for Treg maintenance of Foxp3 expression following acute flavivirus infection. Sci Rep. 2017;7:40720. Epub 2017/01/18. doi: 10.1038/srep40720. PubMed PMID: 28094802; PMCID: PMC5240555.
101. Zhao J, Vijay R, Zhao J, Gale M, Jr., Diamond MS, Perlman S. MAVS Expressed by Hematopoietic Cells Is Critical for Control of West Nile Virus Infection and Pathogenesis. J Virol. 2016;90(16):7098-108. Epub 2016/05/27. doi: 10.1128/JVI.00707-16. PubMed PMID: 27226371; PMCID: PMC4984631.
102. Errett JS, Suthar MS, McMillan A, Diamond MS, Gale M, Jr. The essential, nonredundant roles of RIG-I and MDA5 in detecting and controlling West Nile virus infection. J Virol. 2013;87(21):11416-25. Epub 2013/08/24. doi: 10.1128/JVI.01488-13. PubMed PMID: 23966395; PMCID: 3807316.
103. Lazear HM, Pinto AK, Ramos HJ, Vick SC, Shrestha B, Suthar MS, Gale M, Jr., Diamond MS. Pattern recognition receptor MDA5 modulates CD8+ T cell-dependent clearance of West Nile virus from the central nervous system. J Virol. 2013;87(21):11401-15. Epub 2013/08/24. doi: 10.1128/JVI.01403-13. PubMed PMID: 23966390; PMCID: PMC3807324.
104. Fredericksen BL, Keller BC, Fornek J, Katze MG, Gale M, Jr. Establishment and maintenance of the innate antiviral response to West Nile Virus involves both RIG-I and MDA5 signaling through IPS-1. J Virol. 2008;82(2):609-16. Epub 2007/11/06. doi: 10.1128/JVI.01305-07. PubMed PMID: 17977974; PMCID: PMC2224571.
105. Kato H, Takeuchi O, Sato S, Yoneyama M, Yamamoto M, Matsui K, Uematsu S, Jung A, Kawai T, Ishii KJ, Yamaguchi O, Otsu K, Tsujimura T, Koh CS, Reis e Sousa C, Matsuura Y, Fujita T, Akira S. Differential roles of MDA5 and RIG-I helicases in the recognition of RNA viruses. Nature. 2006;441(7089):101-5. Epub 2006/04/21. doi: 10.1038/nature04734. PubMed PMID: 16625202.
106. Onorati M, Li Z, Liu F, Sousa AM, Nakagawa N, Li M, Dell'Anno MT, Gulden FO, Pochareddy S, Tebbenkamp AT, Han W, Pletikos M, Gao T, Zhu Y, Bichsel C, Varela L, Szigeti-Buck K, Lisgo S, Zhang Y, Testen A, Gao XB, Mlakar J, Popovic M, Flamand M, Strittmatter SM, Kaczmarek LK, Anton ES, Horvath TL, Lindenbach BD, Sestan N. Zika Virus Disrupts Phospho-TBK1 Localization and Mitosis in Human Neuroepithelial Stem Cells and Radial Glia. Cell Rep.

2016;16(10):2576-92. Epub 2016/08/29. doi: 10.1016/j.celrep.2016.08.038. PubMed PMID: 27568284; PMCID: PMC5135012.
107. Brubaker SW, Bonham KS, Zanoni I, Kagan JC. Innate immune pattern recognition: a cell biological perspective. Annu Rev Immunol. 2015;33(1):257-90. Epub 2015/01/13. doi: 10.1146/annurev-immunol-032414-112240. PubMed PMID: 25581309.
108. Szretter KJ, Daffis S, Patel J, Suthar MS, Klein RS, Gale M, Jr., Diamond MS. The innate immune adaptor molecule MyD88 restricts West Nile virus replication and spread in neurons of the central nervous system. Journal of virology. 2010;84(23):12125-38. Epub 2010/10/01. doi: 10.1128/JVI.01026-10. PubMed PMID: 20881045; PMCID: 2976388.
109. Ramos HJ, Lanteri MC, Blahnik G, Negash A, Suthar MS, Brassil MM, Sodhi K, Treuting PM, Busch MP, Norris PJ, Gale M, Jr. IL-1beta signaling promotes CNS-intrinsic immune control of West Nile virus infection. PLoS Pathog. 2012;8(11):e1003039. Epub 2012/12/05. doi: 10.1371/journal.ppat.1003039. PubMed PMID: 23209411; PMCID: PMC3510243.
110. Durrant DM, Daniels BP, Klein RS. IL-1R1 signaling regulates CXCL12-mediated T cell localization and fate within the central nervous system during West Nile Virus encephalitis. J Immunol. 2014;193(8):4095-106. Epub 2014/09/10. doi: 10.4049/jimmunol.1401192. PubMed PMID: 25200953; PMCID: 4340598.
111. Durrant DM, Robinette ML, Klein RS. IL-1R1 is required for dendritic cell-mediated T cell reactivation within the CNS during West Nile virus encephalitis. J Exp Med. 2013;210(3):503-16. Epub 2013/03/06. doi: 10.1084/jem.20121897. PubMed PMID: 23460727; PMCID: PMC3600909.
112. Town T, Bai F, Wang T, Kaplan AT, Qian F, Montgomery RR, Anderson JF, Flavell RA, Fikrig E. Toll-like receptor 7 mitigates lethal West Nile encephalitis via interleukin 23-dependent immune cell infiltration and homing. Immunity. 2009;30(2):242-53. Epub 2009/02/10. doi: 10.1016/j.immuni.2008.11.012. PubMed PMID: 19200759; PMCID: 2707901.
113. Welte T, Reagan K, Fang H, Machain-Williams C, Zheng X, Mendell N, Chang GJ, Wu P, Blair CD, Wang T. Toll-like receptor 7-induced immune response to cutaneous West Nile virus infection. J Gen Virol. 2009;90(Pt 11):2660-8. Epub 2009/07/31. doi: 10.1099/vir.0.011783-0. PubMed PMID: 19641044; PMCID: 2771433.
114. Liu J, Xu C, Hsu LC, Luo Y, Xiang R, Chuang TH. A five-amino-acid motif in the undefined region of the TLR8 ectodomain is required for species-specific ligand recognition. Mol Immunol. 2010;47(5):1083-90. Epub 2009/12/17. doi: 10.1016/j.molimm.2009.11.003. PubMed PMID: 20004021; PMCID: PMC2815190.
115. Demaria O, Pagni PP, Traub S, de Gassart A, Branzk N, Murphy AJ, Valenzuela DM, Yancopoulos GD, Flavell RA, Alexopoulou L. TLR8 deficiency leads to autoimmunity in mice. J Clin Invest. 2010;120(10):3651-62. Epub 2010/09/03. doi: 10.1172/JCI42081. PubMed PMID: 20811154; PMCID: PMC2947223.

116. Paul AM, Acharya D, Le L, Wang P, Stokic DS, Leis AA, Alexopoulou L, Town T, Flavell RA, Fikrig E, Bai F. TLR8 Couples SOCS-1 and Restrains TLR7-Mediated Antiviral Immunity, Exacerbating West Nile Virus Infection in Mice. J Immunol. 2016;197(11):4425-35. Epub 2016/11/01. doi: 10.4049/jimmunol.1600902. PubMed PMID: 27798161; PMCID: PMC5123688.
117. Kong KF, Delroux K, Wang X, Qian F, Arjona A, Malawista SE, Fikrig E, Montgomery RR. Dysregulation of TLR3 impairs the innate immune response to West Nile virus in the elderly. Journal of virology. 2008;82(15):7613-23. Epub 2008/05/30. doi: 10.1128/JVI.00618-08. PubMed PMID: 18508883; PMCID: 2493309.
118. Daffis S, Samuel MA, Suthar MS, Gale M, Jr., Diamond MS. Toll-like receptor 3 has a protective role against West Nile virus infection. J Virol. 2008;82(21):10349-58. Epub 2008/08/22. doi: 10.1128/JVI.00935-08. PubMed PMID: 18715906; PMCID: PMC2573187.
119. Wang T, Town T, Alexopoulou L, Anderson JF, Fikrig E, Flavell RA. Toll-like receptor 3 mediates West Nile virus entry into the brain causing lethal encephalitis. Nat Med. 2004;10(12):1366-73. Epub 2004/11/24. doi: 10.1038/nm1140. PubMed PMID: 15558055.
120. Samuel MA, Diamond MS. Alpha/beta interferon protects against lethal West Nile virus infection by restricting cellular tropism and enhancing neuronal survival. J Virol. 2005;79(21):13350-61. Epub 2005/10/18. doi: 10.1128/JVI.79.21.13350-13361.2005. PubMed PMID: 16227257; PMCID: PMC1262587.
121. Lazear HM, Pinto AK, Vogt MR, Gale M, Jr., Diamond MS. Beta interferon controls West Nile virus infection and pathogenesis in mice. J Virol. 2011;85(14):7186-94. Epub 2011/05/06. doi: 10.1128/JVI.00396-11. PubMed PMID: 21543483; PMCID: PMC3126609.
122. Pinto AK, Daffis S, Brien JD, Gainey MD, Yokoyama WM, Sheehan KC, Murphy KM, Schreiber RD, Diamond MS. A temporal role of type I interferon signaling in CD8+ T cell maturation during acute West Nile virus infection. PLoS Pathog. 2011;7(12):e1002407. Epub 2011/12/07. doi: 10.1371/journal.ppat.1002407. PubMed PMID: 22144897; PMCID: PMC3228803.
123. Keller BC, Fredericksen BL, Samuel MA, Mock RE, Mason PW, Diamond MS, Gale M, Jr. Resistance to alpha/beta interferon is a determinant of West Nile virus replication fitness and virulence. J Virol. 2006;80(19):9424-34. Epub 2006/09/16. doi: 10.1128/JVI.00768-06. PubMed PMID: 16973548; PMCID: PMC1617238.
124. Rossi SL, Tesh RB, Azar SR, Muruato AE, Hanley KA, Auguste AJ, Langsjoen RM, Paessler S, Vasilakis N, Weaver SC. Characterization of a Novel Murine Model to Study Zika Virus. Am J Trop Med Hyg. 2016;94(6):1362-9. Epub 2016/03/30. doi: 10.4269/ajtmh.16-0111. PubMed PMID: 27022155; PMCID: PMC4889758.
125. Aliota MT, Caine EA, Walker EC, Larkin KE, Camacho E, Osorio JE. Characterization of Lethal Zika Virus Infection in AG129 Mice. PLoS Negl Trop

Dis. 2016;10(4):e0004682. Epub 2016/04/20. doi: 10.1371/journal.pntd.0004682. PubMed PMID: 27093158; PMCID: PMC4836712.
126. Grant A, Ponia SS, Tripathi S, Balasubramaniam V, Miorin L, Sourisseau M, Schwarz MC, Sanchez-Seco MP, Evans MJ, Best SM, Garcia-Sastre A. Zika Virus Targets Human STAT2 to Inhibit Type I Interferon Signaling. Cell Host Microbe. 2016;19(6):882-90. Epub 2016/05/24. doi: 10.1016/j.chom.2016.05.009. PubMed PMID: 27212660; PMCID: PMC4900918.
127. Sommereyns C, Paul S, Staeheli P, Michiels T. IFN-lambda (IFN-lambda) is expressed in a tissue-dependent fashion and primarily acts on epithelial cells in vivo. PLoS Pathog. 2008;4(3):e1000017. Epub 2008/03/29. doi: 10.1371/journal.ppat.1000017. PubMed PMID: 18369468; PMCID: PMC2265414.
128. Sheppard P, Kindsvogel W, Xu W, Henderson K, Schlutsmeyer S, Whitmore TE, Kuestner R, Garrigues U, Birks C, Roraback J, Ostrander C, Dong D, Shin J, Presnell S, Fox B, Haldeman B, Cooper E, Taft D, Gilbert T, Grant FJ, Tackett M, Krivan W, McKnight G, Clegg C, Foster D, Klucher KM. IL-28, IL-29 and their class II cytokine receptor IL-28R. Nat Immunol. 2003;4(1):63-8. Epub 2002/12/07. doi: 10.1038/ni873. PubMed PMID: 12469119.
129. Lazear HM, Daniels BP, Pinto AK, Huang AC, Vick SC, Doyle SE, Gale M, Jr., Klein RS, Diamond MS. Interferon-lambda restricts West Nile virus neuroinvasion by tightening the blood-brain barrier. Sci Transl Med. 2015;7(284):284ra59. Epub 2015/04/24. doi: 10.1126/scitranslmed.aaa4304. PubMed PMID: 25904743; PMCID: PMC4435724.
130. Suthar MS, Pulendran B. Systems analysis of West Nile virus infection. Curr Opin Virol. 2014;6:70-5. Epub 2014/05/24. doi: 10.1016/j.coviro.2014.04.010. PubMed PMID: 24851811; PMCID: PMC4104408.
131. Bigham AW, Buckingham KJ, Husain S, Emond MJ, Bofferding KM, Gildersleeve H, Rutherford A, Astakhova NM, Perelygin AA, Busch MP, Murray KO, Sejvar JJ, Green S, Kriesel J, Brinton MA, Bamshad M. Host genetic risk factors for West Nile virus infection and disease progression. PLoS One. 2011;6(9):e24745. Epub 2011/09/22. doi: 10.1371/journal.pone.0024745. PubMed PMID: 21935451; PMCID: PMC3174177.
132. Glass WG, McDermott DH, Lim JK, Lekhong S, Yu SF, Frank WA, Pape J, Cheshier RC, Murphy PM. CCR5 deficiency increases risk of symptomatic West Nile virus infection. J Exp Med. 2006;203(1):35-40. Epub 2006/01/19. doi: 10.1084/jem.20051970. PubMed PMID: 16418398; PMCID: PMC2118086.
133. Venegas M, Brahm J, Villanueva RA. Genomic determinants of hepatitis C virus antiviral therapy outcomes: toward individualized treatment. Annals of hepatology. 2012;11(6):827-37. PubMed PMID: 23109445.
134. Vannberg FO, Chapman SJ, Hill AV. Human genetic susceptibility to intracellular pathogens. Immunological reviews. 2011;240(1):105-16. doi: 10.1111/j.1600-065X.2010.00996.x. PubMed PMID: 21349089.
135. Juno J, Fowke KR, Keynan Y. Immunogenetic factors associated with severe respiratory illness caused by zoonotic H1N1 and H5N1 influenza viruses. Clinical & developmental immunology. 2012;2012:797180. Epub 2011/11/24. doi: 10.1155/2012/797180. PubMed PMID: 22110538; PMCID: PMC3216312.

136. Gralinski LE, Bankhead A, 3rd, Jeng S, Menachery VD, Proll S, Belisle SE, Matzke M, Webb-Robertson BJ, Luna ML, Shukla AK, Ferris MT, Bolles M, Chang J, Aicher L, Waters KM, Smith RD, Metz TO, Law GL, Katze MG, McWeeney S, Baric RS. Mechanisms of severe acute respiratory syndrome coronavirus-induced acute lung injury. MBio. 2013;4(4). Epub 2013/08/08. doi: 10.1128/mBio.00271-13. PubMed PMID: 23919993; PMCID: PMC3747576.
137. Gelinas R, Chesler EJ, Vasconcelos D, Miller DR, Yuan Y, Wang K, Galas D. A genetic approach to the prediction of drug side effects: bleomycin induces concordant phenotypes in mice of the collaborative cross. Pharmacogenomics and personalized medicine. 2011;4:35-45. doi: 10.2147/PGPM.S22475. PubMed PMID: 23226052; PMCID: 3513218.
138. Aylor DL, Valdar W, Foulds-Mathes W, Buus RJ, Verdugo RA, Baric RS, Ferris MT, Frelinger JA, Heise M, Frieman MB, Gralinski LE, Bell TA, Didion JD, Hua K, Nehrenberg DL, Powell CL, Steigerwalt J, Xie Y, Kelada SN, Collins FS, Yang IV, Schwartz DA, Branstetter LA, Chesler EJ, Miller DR, Spence J, Liu EY, McMillan L, Sarkar A, Wang J, Wang W, Zhang Q, Broman KW, Korstanje R, Durrant C, Mott R, Iraqi FA, Pomp D, Threadgill D, de Villena FP, Churchill GA. Genetic analysis of complex traits in the emerging Collaborative Cross. Genome research. 2011;21(8):1213-22. Epub 2011/03/17. doi: 10.1101/gr.111310.110. PubMed PMID: 21406540; PMCID: PMC3149489.
139. Philip VM, Sokoloff G, Ackert-Bicknell CL, Striz M, Branstetter L, Beckmann MA, Spence JS, Jackson BL, Galloway LD, Barker P, Wymore AM, Hunsicker PR, Durtschi DC, Shaw GS, Shinpock S, Manly KF, Miller DR, Donohue KD, Culiat CT, Churchill GA, Lariviere WR, Palmer AA, O'Hara BF, Voy BH, Chesler EJ. Genetic analysis in the Collaborative Cross breeding population. Genome research. 2011;21(8):1223-38. doi: 10.1101/gr.113886.110. PubMed PMID: 21734011; PMCID: 3149490.
140. Kelada SN, Aylor DL, Peck BC, Ryan JF, Tavarez U, Buus RJ, Miller DR, Chesler EJ, Threadgill DW, Churchill GA, Pardo-Manuel de Villena F, Collins FS. Genetic analysis of hematological parameters in incipient lines of the collaborative cross. G3. 2012;2(2):157-65. doi: 10.1534/g3.111.001776. PubMed PMID: 22384394; PMCID: 3284323.
141. Svenson KL, Gatti DM, Valdar W, Welsh CE, Cheng R, Chesler EJ, Palmer AA, McMillan L, Churchill GA. High-resolution genetic mapping using the Mouse Diversity outbred population. Genetics. 2012;190(2):437-47. doi: 10.1534/genetics.111.132597. PubMed PMID: 22345611; PMCID: 3276626.
142. Mathes WF, Aylor DL, Miller DR, Churchill GA, Chesler EJ, de Villena FP, Threadgill DW, Pomp D. Architecture of energy balance traits in emerging lines of the Collaborative Cross. American journal of physiology Endocrinology and metabolism. 2011;300(6):E1124-34. doi: 10.1152/ajpendo.00707.2010. PubMed PMID: 21427413; PMCID: 3118585.
143. Zombeck JA, Deyoung EK, Brzezinska WJ, Rhodes JS. Selective breeding for increased home cage physical activity in collaborative cross and Hsd:ICR mice. Behavior genetics. 2011;41(4):571-82. doi: 10.1007/s10519-010-9425-2. PubMed PMID: 21184167.

144. Sun W, Lee S, Zhabotynsky V, Zou F, Wright FA, Crowley JJ, Yun Z, Buus RJ, Miller DR, Wang J, McMillan L, Pardo-Manuel de Villena F, Sullivan PF. Transcriptome atlases of mouse brain reveals differential expression across brain regions and genetic backgrounds. G3. 2012;2(2):203-11. doi: 10.1534/g3.111.001602. PubMed PMID: 22384399; PMCID: 3284328.
145. Patel SJ, Molinolo AA, Gutkind S, Crawford NP. Germline genetic variation modulates tumor progression and metastasis in a mouse model of neuroendocrine prostate carcinoma. PloS one. 2013;8(4):e61848. doi: 10.1371/journal.pone.0061848. PubMed PMID: 23620793; PMCID: 3631138.
146. Kovacs A, Ben-Jacob N, Tayem H, Halperin E, Iraqi FA, Gophna U. Genotype is a stronger determinant than sex of the mouse gut microbiota. Microbial ecology. 2011;61(2):423-8. doi: 10.1007/s00248-010-9787-2. PubMed PMID: 21181142.
147. Campbell JH, Foster CM, Vishnivetskaya T, Campbell AG, Yang ZK, Wymore A, Palumbo AV, Chesler EJ, Podar M. Host genetic and environmental effects on mouse intestinal microbiota. The ISME journal. 2012;6(11):2033-44. doi: 10.1038/ismej.2012.54. PubMed PMID: 22695862; PMCID: 3475380.
148. Rogala AR, Morgan AP, Christensen AM, Gooch TJ, Bell TA, Miller DR, Godfrey VL, de Villena FP. The Collaborative Cross as a resource for modeling human disease: CC011/Unc, a new mouse model for spontaneous colitis. Mammalian genome : official journal of the International Mammalian Genome Society. 2014;25(3-4):95-108. Epub 2014/02/04. doi: 10.1007/s00335-013-9499-2. PubMed PMID: 24487921; PMCID: PMC3960486.
149. Durrant C, Tayem H, Yalcin B, Cleak J, Goodstadt L, de Villena FP, Mott R, Iraqi FA. Collaborative Cross mice and their power to map host susceptibility to Aspergillus fumigatus infection. Genome research. 2011;21(8):1239-48. doi: 10.1101/gr.118786.110. PubMed PMID: 21493779; PMCID: 3149491.
150. Shusterman A, Salyma Y, Nashef A, Soller M, Wilensky A, Mott R, Weiss EI, Houri-Haddad Y, Iraqi FA. Genotype is an important determinant factor of host susceptibility to periodontitis in the Collaborative Cross and inbred mouse populations. BMC genetics. 2013;14:68. doi: 10.1186/1471-2156-14-68. PubMed PMID: 23937452; PMCID: 3751202.
151. Ferris MT, Aylor DL, Bottomly D, Whitmore AC, Aicher LD, Bell TA, Bradel-Tretheway B, Bryan JT, Buus RJ, Gralinski LE, Haagmans BL, McMillan L, Miller DR, Rosenzweig E, Valdar W, Wang J, Churchill GA, Threadgill DW, McWeeney SK, Katze MG, Pardo-Manuel de Villena F, Baric RS, Heise MT. Modeling host genetic regulation of influenza pathogenesis in the collaborative cross. PLoS Pathog. 2013;9(2):e1003196. Epub 2013/03/08. doi: 10.1371/journal.ppat.1003196. PubMed PMID: 23468633; PMCID: PMC3585141.
152. Peng X, Gralinski L, Armour CD, Ferris MT, Thomas MJ, Proll S, Bradel-Tretheway BG, Korth MJ, Castle JC, Biery MC, Bouzek HK, Haynor DR, Frieman MB, Heise M, Raymond CK, Baric RS, Katze MG. Unique signatures of long noncoding RNA expression in response to virus infection and altered innate immune signaling. mBio. 2010;1(5). doi: 10.1128/mBio.00206-10. PubMed PMID: 20978541; PMCID: 2962437.

153. Bottomly D, Ferris MT, Aicher LD, Rosenzweig E, Whitmore A, Aylor DL, Haagmans BL, Gralinski LE, Bradel-Tretheway BG, Bryan JT, Threadgill DW, de Villena FP, Baric RS, Katze MG, Heise M, McWeeney SK. Expression quantitative trait Loci for extreme host response to influenza a in pre-collaborative cross mice. G3. 2012;2(2):213-21. doi: 10.1534/g3.111.001800. PubMed PMID: 22384400; PMCID: 3284329.
154. Josset L, Tchitchek N, Gralinski LE, Ferris MT, Eisfeld AJ, Green RR, Thomas MJ, Tisoncik-Go J, Schroth GP, Kawaoka Y, Manuel de Villena FP, Baric RS, Heise MT, Peng X, Katze MG. Annotation of long non-coding RNAs expressed in Collaborative Cross founder mice in response to respiratory virus infection reveals a new class of interferon-stimulated transcripts. RNA biology. 2014;11(7). PubMed PMID: 24922324.
155. Xiong H, Morrison J, Ferris MT, Gralinski LE, Whitmore AC, Green R, Thomas MJ, Tisoncik-Go J, Schroth GP, Pardo-Manuel de Villena FF, Baric RS, Heise MT, Peng X, Katze MG. Genomic Profiling of Collaborative Cross Founder Mice Infected with Respiratory Viruses Reveals Novel Transcripts and Infection-Related Strain-Specific Gene and Isoform Expression. G3. 2014. doi: 10.1534/g3.114.011759. PubMed PMID: 24902603.
156. Peng X, Gralinski L, Ferris MT, Frieman MB, Thomas MJ, Proll S, Korth MJ, Tisoncik JR, Heise M, Luo S, Schroth GP, Tumpey TM, Li C, Kawaoka Y, Baric RS, Katze MG. Integrative deep sequencing of the mouse lung transcriptome reveals differential expression of diverse classes of small RNAs in response to respiratory virus infection. mBio. 2011;2(6). doi: 10.1128/mBio.00198-11. PubMed PMID: 22086488; PMCID: 3221602.
157. Collaborative Cross C. The genome architecture of the Collaborative Cross mouse genetic reference population. Genetics. 2012;190(2):389-401. doi: 10.1534/genetics.111.132639. PubMed PMID: 22345608; PMCID: 3276630.
158. Keane TM, Goodstadt L, Danecek P, White MA, Wong K, Yalcin B, Heger A, Agam A, Slater G, Goodson M, Furlotte NA, Eskin E, Nellaker C, Whitley H, Cleak J, Janowitz D, Hernandez-Pliego P, Edwards A, Belgard TG, Oliver PL, McIntyre RE, Bhomra A, Nicod J, Gan X, Yuan W, van der Weyden L, Steward CA, Bala S, Stalker J, Mott R, Durbin R, Jackson IJ, Czechanski A, Guerra-Assuncao JA, Donahue LR, Reinholdt LG, Payseur BA, Ponting CP, Birney E, Flint J, Adams DJ. Mouse genomic variation and its effect on phenotypes and gene regulation. Nature. 2011;477(7364):289-94. doi: 10.1038/nature10413. PubMed PMID: 21921910; PMCID: 3276836.
159. Flint J, Eskin E. Genome-wide association studies in mice. Nature reviews Genetics. 2012;13(11):807-17. doi: 10.1038/nrg3335. PubMed PMID: 23044826; PMCID: 3625632.
160. Rasmussen AL, Okumura A, Ferris MT, Green R, Feldmann F, Kelly SM, Scott DP, Safronetz D, Haddock E, LaCasse R, Thomas MJ, Sova P, Carter VS, Weiss JM, Miller DR, Shaw GD, Korth MJ, Heise MT, Baric RS, de Villena FP, Feldmann H, Katze MG. Host genetic diversity enables Ebola hemorrhagic fever pathogenesis and resistance. Science. 2014;346(6212):987-91. Epub 2014/11/02. doi: 10.1126/science.1259595. PubMed PMID: 25359852; PMCID: PMC4241145.

161. Ciancanelli MJ, Huang SX, Luthra P, Garner H, Itan Y, Volpi S, Lafaille FG, Trouillet C, Schmolke M, Albrecht RA, Israelsson E, Lim HK, Casadio M, Hermesh T, Lorenzo L, Leung LW, Pedergnana V, Boisson B, Okada S, Picard C, Ringuier B, Troussier F, Chaussabel D, Abel L, Pellier I, Notarangelo LD, Garcia-Sastre A, Basler CF, Geissmann F, Zhang SY, Snoeck HW, Casanova JL. Infectious disease. Life-threatening influenza and impaired interferon amplification in human IRF7 deficiency. Science. 2015;348(6233):448-53. Epub 2015/03/31. doi: 10.1126/science.aaa1578. PubMed PMID: 25814066; PMCID: PMC4431581.
162. Horby P, Nguyen NY, Dunstan SJ, Baillie JK. The role of host genetics in susceptibility to influenza: a systematic review. PLoS One. 2012;7(3):e33180. Epub 2012/03/23. doi: 10.1371/journal.pone.0033180. PubMed PMID: 22438897; PMCID: PMC3305291.
163. Lee MN, Ye C, Villani AC, Raj T, Li W, Eisenhaure TM, Imboywa SH, Chipendo PI, Ran FA, Slowikowski K, Ward LD, Raddassi K, McCabe C, Lee MH, Frohlich IY, Hafler DA, Kellis M, Raychaudhuri S, Zhang F, Stranger BE, Benoist CO, De Jager PL, Regev A, Hacohen N. Common genetic variants modulate pathogen-sensing responses in human dendritic cells. Science. 2014;343(6175):1246980. Epub 2014/03/08. doi: 10.1126/science.1246980. PubMed PMID: 24604203; PMCID: PMC4124741.
164. Cheng Z, Zhou J, To KK, Chu H, Li C, Wang D, Yang D, Zheng S, Hao K, Bosse Y, Obeidat M, Brandsma CA, Song YQ, Chen Y, Zheng BJ, Li L, Yuen KY. Identification of TMPRSS2 as a Susceptibility Gene for Severe 2009 Pandemic A(H1N1) Influenza and A(H7N9) Influenza. J Infect Dis. 2015;212(8):1214-21. Epub 2015/04/24. doi: 10.1093/infdis/jiv246. PubMed PMID: 25904605.
165. Graham JB, Thomas S, Swarts J, McMillan AA, Ferris MT, Suthar MS, Treuting PM, Ireton R, Gale M, Jr., Lund JM. Genetic diversity in the collaborative cross model recapitulates human west nile virus disease outcomes. mBio. 2015;6(3):15. Epub 2015/05/07. doi: 10.1128/mBio.00493-15. PubMed PMID: 25944860; PMCID: 4436067.
166. Marion CL, Katie MOB, Whitney EP, Mark JC, Jennifer ML, Rachel EO, John WH, Brian C, Dale FH, Leslie HT, Nancy K, Harry EP, Lishomwa CN, Douglas FN, Hany TK, David JK, Michael PB, Alexander YR, Michael SD, Philip JN. Tregs control the development of symptomatic West Nile virus infection in humans and mice. The Journal of clinical investigation. 2009;119(11):3266-77. doi: 10.1172/JCI39387.
167. Bah EI, Lamah MC, Fletcher T, Jacob ST, Brett-Major DM, Sall AA, Shindo N, Fischer WA, 2nd, Lamontagne F, Saliou SM, Bausch DG, Moumie B, Jagatic T, Sprecher A, Lawler JV, Mayet T, Jacquerioz FA, Mendez Baggi MF, Vallenas C, Clement C, Mardel S, Faye O, Faye O, Soropogui B, Magassouba N, Koivogui L, Pinto R, Fowler RA. Clinical presentation of patients with Ebola virus disease in Conakry, Guinea. N Engl J Med. 2015;372(1):40-7. Epub 2014/11/06. doi: 10.1056/NEJMoa1411249. PubMed PMID: 25372658.
168. Schieffelin JS, Shaffer JG, Goba A, Gbakie M, Gire SK, Colubri A, Sealfon RS, Kanneh L, Moigboi A, Momoh M, Fullah M, Moses LM, Brown BL, Andersen KG, Winnicki S, Schaffner SF, Park DJ, Yozwiak NL, Jiang PP, Kargbo D, Jalloh

S, Fonnie M, Sinnah V, French I, Kovoma A, Kamara FK, Tucker V, Konuwa E, Sellu J, Mustapha I, Foday M, Yillah M, Kanneh F, Saffa S, Massally JL, Boisen ML, Branco LM, Vandi MA, Grant DS, Happi C, Gevao SM, Fletcher TE, Fowler RA, Bausch DG, Sabeti PC, Khan SH, Garry RF, Program KGHLF, Viral Hemorrhagic Fever C, Team WHOCR. Clinical illness and outcomes in patients with Ebola in Sierra Leone. N Engl J Med. 2014;371(22):2092-100. Epub 2014/10/30. doi: 10.1056/NEJMoa1411680. PubMed PMID: 25353969; PMCID: PMC4318555.

169. Brandes M, Klauschen F, Kuchen S, Germain RN. A systems analysis identifies a feedforward inflammatory circuit leading to lethal influenza infection. Cell. 2013;154(1):197-212. Epub 2013/07/06. doi: 10.1016/j.cell.2013.06.013. PubMed PMID: 23827683; PMCID: PMC3763506.

170. Bouvier NM, Lowen AC. Animal Models for Influenza Virus Pathogenesis and Transmission. Viruses. 2010;2(8):1530-63. Epub 2010/01/01. doi: 10.3390/v20801530. PubMed PMID: 21442033; PMCID: PMC3063653.

171. Muramoto Y, Shoemaker JE, Le MQ, Itoh Y, Tamura D, Sakai-Tagawa Y, Imai H, Uraki R, Takano R, Kawakami E, Ito M, Okamoto K, Ishigaki H, Mimuro H, Sasakawa C, Matsuoka Y, Noda T, Fukuyama S, Ogasawara K, Kitano H, Kawaoka Y. Disease severity is associated with differential gene expression at the early and late phases of infection in nonhuman primates infected with different H5N1 highly pathogenic avian influenza viruses. J Virol. 2014;88(16):8981-97. Epub 2014/06/06. doi: 10.1128/JVI.00907-14. PubMed PMID: 24899188; PMCID: PMC4136255.

172. Cilloniz C, Shinya K, Peng X, Korth MJ, Proll SC, Aicher LD, Carter VS, Chang JH, Kobasa D, Feldmann F, Strong JE, Feldmann H, Kawaoka Y, Katze MG. Lethal influenza virus infection in macaques is associated with early dysregulation of inflammatory related genes. PLoS Pathog. 2009;5(10):e1000604. Epub 2009/10/03. doi: 10.1371/journal.ppat.1000604. PubMed PMID: 19798428; PMCID: PMC2745659.

173. Kash JC, Tumpey TM, Proll SC, Carter V, Perwitasari O, Thomas MJ, Basler CF, Palese P, Taubenberger JK, Garcia-Sastre A, Swayne DE, Katze MG. Genomic analysis of increased host immune and cell death responses induced by 1918 influenza virus. Nature. 2006;443(7111):578-81. Epub 2006/09/29. doi: 10.1038/nature05181. PubMed PMID: 17006449; PMCID: PMC2615558.

174. Hartmann BM, Thakar J, Albrecht RA, Avey S, Zaslavsky E, Marjanovic N, Chikina M, Fribourg M, Hayot F, Schmolke M, Meng H, Wetmur J, Garcia-Sastre A, Kleinstein SH, Sealfon SC. Human Dendritic Cell Response Signatures Distinguish 1918, Pandemic, and Seasonal H1N1 Influenza Viruses. J Virol. 2015;89(20):10190-205. Epub 2015/08/01. doi: 10.1128/JVI.01523-15. PubMed PMID: 26223639; PMCID: PMC4580178.

175. Cerny D, Haniffa M, Shin A, Bigliardi P, Tan BK, Lee B, Poidinger M, Tan EY, Ginhoux F, Fink K. Selective susceptibility of human skin antigen presenting cells to productive dengue virus infection. PLoS Pathog. 2014;10(12):e1004548. Epub 2014/12/05. doi: 10.1371/journal.ppat.1004548. PubMed PMID: 25474532; PMCID: PMC4256468.

176. Balsitis SJ, Coloma J, Castro G, Alava A, Flores D, McKerrow JH, Beatty PR, Harris E. Tropism of dengue virus in mice and humans defined by viral nonstructural protein 3-specific immunostaining. Am J Trop Med Hyg. 2009;80(3):416-24. Epub 2009/03/10. PubMed PMID: 19270292.
177. Kwissa M, Nakaya HI, Onlamoon N, Wrammert J, Villinger F, Perng GC, Yoksan S, Pattanapanyasat K, Chokephaibulkit K, Ahmed R, Pulendran B. Dengue virus infection induces expansion of a CD14(+)CD16(+) monocyte population that stimulates plasmablast differentiation. Cell Host Microbe. 2014;16(1):115-27. Epub 2014/07/02. doi: 10.1016/j.chom.2014.06.001. PubMed PMID: 24981333; PMCID: PMC4116428.
178. Wrammert J, Onlamoon N, Akondy RS, Perng GC, Polsrila K, Chandele A, Kwissa M, Pulendran B, Wilson PC, Wittawatmongkol O, Yoksan S, Angkasekwinai N, Pattanapanyasat K, Chokephaibulkit K, Ahmed R. Rapid and massive virus-specific plasmablast responses during acute dengue virus infection in humans. J Virol. 2012;86(6):2911-8. Epub 2012/01/13. doi: 10.1128/JVI.06075-11. PubMed PMID: 22238318; PMCID: PMC3302324.
179. Konopka JL, Penalva LO, Thompson JM, White LJ, Beard CW, Keene JD, Johnston RE. A two-phase innate host response to alphavirus infection identified by mRNP-tagging in vivo. PLoS Pathog. 2007;3(12):e199. Epub 2008/01/25. doi: 10.1371/journal.ppat.0030199. PubMed PMID: 18215114; PMCID: PMC2151086.
180. Trombetta JJ, Gennert D, Lu D, Satija R, Shalek AK, Regev A. Preparation of Single-Cell RNA-Seq Libraries for Next Generation Sequencing. Current protocols in molecular biology / edited by Frederick M Ausubel [et al]. 2014;107:4 22 1-17. Epub 2014/07/06. doi: 10.1002/0471142727.mb0422s107. PubMed PMID: 24984854; PMCID: PMC4338574.
181. Macosko EZ, Basu A, Satija R, Nemesh J, Shekhar K, Goldman M, Tirosh I, Bialas AR, Kamitaki N, Martersteck EM, Trombetta JJ, Weitz DA, Sanes JR, Shalek AK, Regev A, McCarroll SA. Highly Parallel Genome-wide Expression Profiling of Individual Cells Using Nanoliter Droplets. Cell. 2015;161(5):1202-14. Epub 2015/05/23. doi: 10.1016/j.cell.2015.05.002. PubMed PMID: 26000488; PMCID: PMC4481139.
182. Shin J, Berg DA, Zhu Y, Shin JY, Song J, Bonaguidi MA, Enikolopov G, Nauen DW, Christian KM, Ming GL, Song H. Single-Cell RNA-Seq with Waterfall Reveals Molecular Cascades underlying Adult Neurogenesis. Cell Stem Cell. 2015;17(3):360-72. Epub 2015/08/25. doi: 10.1016/j.stem.2015.07.013. PubMed PMID: 26299571.
183. Miyamoto DT, Zheng Y, Wittner BS, Lee RJ, Zhu H, Broderick KT, Desai R, Fox DB, Brannigan BW, Trautwein J, Arora KS, Desai N, Dahl DM, Sequist LV, Smith MR, Kapur R, Wu CL, Shioda T, Ramaswamy S, Ting DT, Toner M, Maheswaran S, Haber DA. RNA-Seq of single prostate CTCs implicates noncanonical Wnt signaling in antiandrogen resistance. Science. 2015;349(6254):1351-6. Epub 2015/09/19. doi: 10.1126/science.aab0917. PubMed PMID: 26383955; PMCID: PMC4872391.
184. Meredith M, Zemmour D, Mathis D, Benoist C. Aire controls gene expression in the thymic epithelium with ordered stochasticity. Nat Immunol.

2015;16(9):942-9. Epub 2015/08/04. doi: 10.1038/ni.3247. PubMed PMID: 26237550; PMCID: PMC4632529.
185. Shalek AK, Satija R, Shuga J, Trombetta JJ, Gennert D, Lu D, Chen P, Gertner RS, Gaublomme JT, Yosef N, Schwartz S, Fowler B, Weaver S, Wang J, Wang X, Ding R, Raychowdhury R, Friedman N, Hacohen N, Park H, May AP, Regev A. Single-cell RNA-seq reveals dynamic paracrine control of cellular variation. Nature. 2014;510(7505):363-9. Epub 2014/06/12. doi: 10.1038/nature13437. PubMed PMID: 24919153; PMCID: PMC4193940.
186. Shalek AK, Satija R, Adiconis X, Gertner RS, Gaublomme JT, Raychowdhury R, Schwartz S, Yosef N, Malboeuf C, Lu D, Trombetta JJ, Gennert D, Gnirke A, Goren A, Hacohen N, Levin JZ, Park H, Regev A. Single-cell transcriptomics reveals bimodality in expression and splicing in immune cells. Nature. 2013;498(7453):236-40. Epub 2013/05/21. doi: 10.1038/nature12172. PubMed PMID: 23685454; PMCID: PMC3683364.
187. Sen A, Rothenberg ME, Mukherjee G, Feng N, Kalisky T, Nair N, Johnstone IM, Clarke MF, Greenberg HB. Innate immune response to homologous rotavirus infection in the small intestinal villous epithelium at single-cell resolution. Proceedings of the National Academy of Sciences of the United States of America. 2012;109(50):20667-72. Epub 2012/11/29. doi: 10.1073/pnas.1212188109. PubMed PMID: 23188796; PMCID: PMC3528539.
188. Yu J, Zhou J, Sutherland A, Wei W, Shin YS, Xue M, Heath JR. Microfluidics-based single-cell functional proteomics for fundamental and applied biomedical applications. Annu Rev Anal Chem (Palo Alto Calif). 2014;7(1):275-95. Epub 2014/06/05. doi: 10.1146/annurev-anchem-071213-020323. PubMed PMID: 24896308.
189. Rotem A, Ram O, Shoresh N, Sperling RA, Goren A, Weitz DA, Bernstein BE. Single-cell ChIP-seq reveals cell subpopulations defined by chromatin state. Nat Biotechnol. 2015;33(11):1165-72. Epub 2015/10/13. doi: 10.1038/nbt.3383. PubMed PMID: 26458175; PMCID: PMC4636926.
190. Hukelmann JL, Anderson KE, Sinclair LV, Grzes KM, Murillo AB, Hawkins PT, Stephens LR, Lamond AI, Cantrell DA. The cytotoxic T cell proteome and its shaping by the kinase mTOR. Nat Immunol. 2016;17(1):104-12. Epub 2015/11/10. doi: 10.1038/ni.3314. PubMed PMID: 26551880; PMCID: PMC4685757.
191. Hood L, Tian Q. Systems approaches to biology and disease enable translational systems medicine. Genomics Proteomics Bioinformatics. 2012;10(4):181-5. Epub 2012/10/23. doi: 10.1016/j.gpb.2012.08.004. PubMed PMID: 23084773; PMCID: PMC3844613.
192. Lindsey NP, Lehman JA, Staples JE, Fischer M. West Nile Virus and Other Nationally Notifiable Arboviral Diseases - United States, 2014. MMWR Morb Mortal Wkly Rep. 2015;64(34):929-34. doi: 10.15585/mmwr.mm6434a1. PubMed PMID: 26334477.
193. Schmid MA, Harris E. Monocyte recruitment to the dermis and differentiation to dendritic cells increases the targets for dengue virus replication. PLoS Pathog. 2014;10(12):e1004541. doi: 10.1371/journal.ppat.1004541. PubMed PMID: 25474197; PMCID: PMC4256458.

194. Lazear HM, Lancaster A, Wilkins C, Suthar MS, Huang A, Vick SC, Clepper L, Thackray L, Brassil MM, Virgin HW, Nikolich-Zugich J, Moses AV, Gale M, Jr., Fruh K, Diamond MS. IRF-3, IRF-5, and IRF-7 coordinately regulate the type I IFN response in myeloid dendritic cells downstream of MAVS signaling. PLoS Pathog. 2013;9(1):e1003118. Epub 2013/01/10. doi: 10.1371/journal.ppat.1003118. PubMed PMID: 23300459; PMCID: 3536698.
195. Hildner K, Edelson BT, Purtha WE, Diamond M, Matsushita H, Kohyama M, Calderon B, Schraml BU, Unanue ER, Diamond MS, Schreiber RD, Murphy TL, Murphy KM. Batf3 deficiency reveals a critical role for CD8alpha+ dendritic cells in cytotoxic T cell immunity. Science. 2008;322(5904):1097-100. Epub 2008/11/15. doi: 10.1126/science.1164206. PubMed PMID: 19008445; PMCID: 2756611.
196. Suthar MS, Brassil MM, Blahnik G, Gale M, Jr. Infectious clones of novel lineage 1 and lineage 2 West Nile virus strains WNV-TX02 and WNV-Madagascar. J Virol. 2012;86(14):7704-9. Epub 2012/05/11. doi: 10.1128/JVI.00401-12. PubMed PMID: 22573862; PMCID: PMC3416286.
197. Saito T, Owen DM, Jiang F, Marcotrigiano J, Gale M, Jr. Innate immunity induced by composition-dependent RIG-I recognition of hepatitis C virus RNA. Nature. 2008;454(7203):523-7. Epub 2008/06/13. doi: 10.1038/nature07106. PubMed PMID: 18548002; PMCID: 2856441.
198. Bowen JR, Ferris MT, Suthar MS. Systems biology: A tool for charting the antiviral landscape. Virus Res. 2016;218:2-9. doi: 10.1016/j.virusres.2016.01.005. PubMed PMID: 26795869; PMCID: PMC4902762.
199. Langfelder P, Horvath S. WGCNA: an R package for weighted correlation network analysis. BMC Bioinformatics. 2008;9(1):559. doi: 10.1186/1471-2105-9-559. PubMed PMID: 19114008; PMCID: PMC2631488.
200. Janky R, Verfaillie A, Imrichova H, Van de Sande B, Standaert L, Christiaens V, Hulselmans G, Herten K, Naval Sanchez M, Potier D, Svetlichnyy D, Kalender Atak Z, Fiers M, Marine JC, Aerts S. iRegulon: from a gene list to a gene regulatory network using large motif and track collections. PLoS Comput Biol. 2014;10(7):e1003731. doi: 10.1371/journal.pcbi.1003731. PubMed PMID: 25058159; PMCID: PMC4109854.
201. Rubio D, Xu RH, Remakus S, Krouse TE, Truckenmiller ME, Thapa RJ, Balachandran S, Alcami A, Norbury CC, Sigal LJ. Crosstalk between the type 1 interferon and nuclear factor kappa B pathways confers resistance to a lethal virus infection. Cell Host Microbe. 2013;13(6):701-10. doi: 10.1016/j.chom.2013.04.015. PubMed PMID: 23768494; PMCID: PMC3688842.
202. Robertson SJ, Lubick KJ, Freedman BA, Carmody AB, Best SM. Tick-borne flaviviruses antagonize both IRF-1 and type I IFN signaling to inhibit dendritic cell function. Journal of immunology. 2014;192(6):2744-55. doi: 10.4049/jimmunol.1302110.
203. Schindler C, Fu XY, Improta T, Aebersold R, Darnell JE. Proteins of transcription factor ISGF-3: one gene encodes the 91-and 84-kDa ISGF-3 proteins that are activated by interferon alpha. Proceedings of the National Academy of Sciences. 1992;89(16):7836-9. doi: 10.1073/pnas.89.16.7836.

204. Toniolo PA, Liu S, Yeh JE, Moraes-Vieira PM, Walker SR, Vafaizadeh V, Barbuto JA, Frank DA. Inhibiting STAT5 by the BET bromodomain inhibitor JQ1 disrupts human dendritic cell maturation. J Immunol. 2015;194(7):3180-90. doi: 10.4049/jimmunol.1401635. PubMed PMID: 25725100; PMCID: PMC4369449.
205. Bell BD, Kitajima M, Larson RP, Stoklasek TA, Dang K, Sakamoto K, Wagner KU, Kaplan DH, Reizis B, Hennighausen L, Ziegler SF. The transcription factor STAT5 is critical in dendritic cells for the development of TH2 but not TH1 responses. Nat Immunol. 2013;14(4):364-71. doi: 10.1038/ni.2541. PubMed PMID: 23435120; PMCID: PMC4161284.
206. Gouilleux F, Wakao H, Mundt M, Groner B. Prolactin induces phosphorylation of Tyr694 of Stat5 (MGF), a prerequisite for DNA binding and induction of transcription. EMBO J. 1994;13(18):4361-9. PubMed PMID: 7925280; PMCID: PMC395363.
207. Tanabe Y, Nishibori T, Su L, Arduini RM, Baker DP, David M. Role of STAT1, STAT3, and STAT5 in IFN-αβ Responses in T Lymphocytes. The Journal of Immunology. 2005;174(2):609-13. doi: 10.4049/jimmunol.174.2.609.
208. Meinke A, Barahmand-Pour F, Wohrl S, Stoiber D, Decker T. Activation of different Stat5 isoforms contributes to cell-type-restricted signaling in response to interferons. Mol Cell Biol. 1996;16(12):6937-44. doi: 10.1128/MCB.16.12.6937. PubMed PMID: 8943349; PMCID: PMC231697.
209. Fish EN, Uddin S, Korkmaz M, Majchrzak B, Druker BJ, Platanias LC. Activation of a CrkL-stat5 signaling complex by type I interferons. J Biol Chem. 1999;274(2):571-3. doi: 10.1074/jbc.274.2.571. PubMed PMID: 9872990.
210. Seder RA, Paul WE, Davis MM, Fazekas de St Groth B. The presence of interleukin 4 during in vitro priming determines the lymphokine-producing potential of CD4+ T cells from T cell receptor transgenic mice. J Exp Med. 1992;176(4):1091-8. Epub 1992/10/01. PubMed PMID: 1328464; PMCID: PMC2119379.
211. Heufler C, Koch F, Stanzl U, Topar G, Wysocka M, Trinchieri G, Enk A, Steinman RM, Romani N, Schuler G. Interleukin-12 is produced by dendritic cells and mediates T helper 1 development as well as interferon-gamma production by T helper 1 cells. Eur J Immunol. 1996;26(3):659-68. Epub 1996/03/01. doi: 10.1002/eji.1830260323. PubMed PMID: 8605935.
212. Querec T, Bennouna S, Alkan S, Laouar Y, Gorden K, Flavell R, Akira S, Ahmed R, Pulendran B. Yellow fever vaccine YF-17D activates multiple dendritic cell subsets via TLR2, 7, 8, and 9 to stimulate polyvalent immunity. J Exp Med. 2006;203(2):413-24. doi: 10.1084/jem.20051720. PubMed PMID: 16461338; PMCID: PMC2118210.
213. de Saint-Vis B, Vincent J, Vandenabeele S, Vanbervliet B, Pin JJ, Aït-Yahia S, Patel S, Mattei MG, Banchereau J, Zurawski S, Davoust J, Caux C, Lebecque S. A Novel Lysosome-Associated Membrane Glycoprotein, DC-LAMP, Induced upon DC Maturation, Is Transiently Expressed in MHC Class II Compartment. Immunity. 1998;9(3):325-36. doi: 10.1016/s1074-7613(00)80615-9.
214. Kovats S, Turner S, Simmons A, Powe T, Chakravarty E, Alberola-Ila J. West Nile virus-infected human dendritic cells fail to fully activate invariant

natural killer T cells. Clin Exp Immunol. 2016;186(2):214-26. doi: 10.1111/cei.12850. PubMed PMID: 27513522; PMCID: PMC5054575.
215. Lutz MB, Schnare M, Menges M, Rossner S, Rollinghoff M, Schuler G, Gessner A. Differential functions of IL-4 receptor types I and II for dendritic cell maturation and IL-12 production and their dependency on GM-CSF. Journal of Immunology. 2002;169(7):3574-80. PubMed PMID: WOS:000178288800013.
216. Watanabe S, Itoh T, Arai K. JAK2 is essential for activation of c-fos and c-myc promoters and cell proliferation through the human granulocyte-macrophage colony-stimulating factor receptor in BA/F3 cells. Journal of Biological Chemistry. 1996;271(21):12681-6. doi: 10.1074/jbc.271.21.12681. PubMed PMID: WOS:A1996UL66000084.
217. Bowen JR, Quicke KM, Maddur MS, O'Neal JT, McDonald CE, Fedorova NB, Puri V, Shabman RS, Pulendran B, Suthar MS. Zika Virus Antagonizes Type I Interferon Responses during Infection of Human Dendritic Cells. PLOS Pathogens. 2017;13(2):e1006164. doi: 10.1371/journal.ppat.1006164.
218. Al-Shami A, Mahanna W, Naccache PH. Granulocyte-macrophage colony-stimulating factor-activated signaling pathways in human neutrophils. Selective activation of Jak2, Stat3, and Stat5b. J Biol Chem. 1998;273(2):1058-63. PubMed PMID: 9422769.
219. Johnsen IB, Nguyen TT, Bergstroem B, Fitzgerald KA, Anthonsen MW. The tyrosine kinase c-Src enhances RIG-I (retinoic acid-inducible gene I)-elicited antiviral signaling. J Biol Chem. 2009;284(28):19122-31. Epub 2009/05/08. doi: 10.1074/jbc.M808233200. PubMed PMID: 19419966; PMCID: PMC2707193.
220. Lim YJ, Koo JE, Hong EH, Park ZY, Lim KM, Bae ON, Lee JY. A Src-family-tyrosine kinase, Lyn, is required for efficient IFN-beta expression in pattern recognition receptor, RIG-I, signal pathway by interacting with IPS-1. Cytokine. 2015;72(1):63-70. Epub 2015/01/15. doi: 10.1016/j.cyto.2014.12.008. PubMed PMID: 25585356.
221. Chin H, Arai A, Wakao H, Kamiyama R, Miyasaka N, Miura O. Lyn physically associates with the erythropoietin receptor and may play a role in activation of the Stat5 pathway. Blood. 1998;91(10):3734-45.
222. Xiao W, Ando T, Wang HY, Kawakami Y, Kawakami T. Lyn- and PLC-beta3-dependent regulation of SHP-1 phosphorylation controls Stat5 activity and myelomonocytic leukemia-like disease. Blood. 2010;116(26):6003-13. doi: 10.1182/blood-2010-05-283937. PubMed PMID: 20858858; PMCID: PMC3031387.
223. Okutani Y, Kitanaka A, Tanaka T, Kamano H, Ohnishi H, Kubota Y, Ishida T, Takahara J. Src directly tyrosine-phosphorylates STAT5 on its activation site and is involved in erythropoietin-induced signaling pathway. Oncogene. 2001;20(45):6643-50. doi: 10.1038/sj.onc.1204807. PubMed PMID: 11641791.
224. Silva MC, Guerrero-Plata A, Gilfoy FD, Garofalo RP, Mason PW. Differential activation of human monocyte-derived and plasmacytoid dendritic cells by West Nile virus generated in different host cells. J Virol. 2007;81(24):13640-8. doi: 10.1128/JVI.00857-07. PubMed PMID: 17913823; PMCID: PMC2168853.

225. Rodriguez-Madoz JR, Bernal-Rubio D, Kaminski D, Boyd K, Fernandez-Sesma A. Dengue virus inhibits the production of type I interferon in primary human dendritic cells. J Virol. 2010;84(9):4845-50. doi: 10.1128/JVI.02514-09. PubMed PMID: 20164230; PMCID: PMC2863727.
226. Olagnier D, Peri S, Steel C, van Montfoort N, Chiang C, Beljanski V, Slifker M, He Z, Nichols CN, Lin R, Balachandran S, Hiscott J. Cellular oxidative stress response controls the antiviral and apoptotic programs in dengue virus-infected dendritic cells. PLoS Pathog. 2014;10(12):e1004566. Epub 2014/12/19. doi: 10.1371/journal.ppat.1004566. PubMed PMID: 25521078; PMCID: PMC4270780.
227. Lin RJ, Chang BL, Yu HP, Liao CL, Lin YL. Blocking of interferon-induced Jak-Stat signaling by Japanese encephalitis virus NS5 through a protein tyrosine phosphatase-mediated mechanism. J Virol. 2006;80(12):5908-18. doi: 10.1128/JVI.02714-05. PubMed PMID: 16731929; PMCID: PMC1472572.
228. Best SM, Morris KL, Shannon JG, Robertson SJ, Mitzel DN, Park GS, Boer E, Wolfinbarger JB, Bloom ME. Inhibition of interferon-stimulated JAK-STAT signaling by a tick-borne flavivirus and identification of NS5 as an interferon antagonist. J Virol. 2005;79(20):12828-39. Epub 2005/09/29. doi: 10.1128/JVI.79.20.12828-12839.2005. PubMed PMID: 16188985; PMCID: PMC1235813.
229. Sharma N, Kumawat KL, Rastogi M, Basu A, Singh SK. Japanese Encephalitis Virus exploits the microRNA-432 to regulate the expression of Suppressor of Cytokine Signaling (SOCS) 5. Sci Rep. 2016;6:27685. Epub 2016/06/11. doi: 10.1038/srep27685. PubMed PMID: 27282499; PMCID: PMC4901348.
230. Quicke KM, Bowen JR, Johnson EL, McDonald CE, Ma H, O'Neal JT, Rajakumar A, Wrammert J, Rimawi BH, Pulendran B, Schinazi RF, Chakraborty R, Suthar MS. Zika Virus Infects Human Placental Macrophages. Cell Host Microbe. 2016. doi: 10.1016/j.chom.2016.05.015. PubMed PMID: 27247001.
231. Lim SM, Koraka P, Osterhaus AD, Martina BE. Development of a strand-specific real-time qRT-PCR for the accurate detection and quantitation of West Nile virus RNA. J Virol Methods. 2013;194(1-2):146-53. Epub 2013/08/24. doi: 10.1016/j.jviromet.2013.07.050. PubMed PMID: 23965252.
232. McElroy AK, Akondy RS, Davis CW, Ellebedy AH, Mehta AK, Kraft CS, Lyon GM, Ribner BS, Varkey J, Sidney J, Sette A, Campbell S, Stroher U, Damon I, Nichol ST, Spiropoulou CF, Ahmed R. Human Ebola virus infection results in substantial immune activation. Proc Natl Acad Sci U S A. 2015;112(15):4719-24. Epub 2015/03/17. doi: 10.1073/pnas.1502619112. PubMed PMID: 25775592; PMCID: PMC4403189.
233. Oehler E, Watrin L, Larre P, Leparc-Goffart I, Lastere S, Valour F, Baudouin L, Mallet H, Musso D, Ghawche F. Zika virus infection complicated by Guillain-Barre syndrome--case report, French Polynesia, December 2013. Euro surveillance : bulletin Européen sur les maladies transmissibles = European communicable disease bulletin. 2014;19(9).
234. Haddow AJ, Williams MC, Woodall JP, Simpson DI, Goma LK. Twelve Isolations of Zika Virus from Aedes (Stegomyia) Africanus (Theobald) Taken in

and above a Uganda Forest. Bull World Health Organ. 1964;31:57-69. Epub 1964/01/01. PubMed PMID: 14230895; PMCID: PMC2555143.
235. Petersen LR, Jamieson DJ, Powers AM, Honein MA. Zika Virus. N Engl J Med. 2016;374(16):1552-63. Epub 2016/03/31. doi: 10.1056/NEJMra1602113. PubMed PMID: 27028561.
236. Lozier M, Adams L, Febo MF, Torres-Aponte J, Bello-Pagan M, Ryff KR, Munoz-Jordan J, Garcia M, Rivera A, Read JS, Waterman SH, Sharp TM, Rivera-Garcia B. Incidence of Zika Virus Disease by Age and Sex - Puerto Rico, November 1, 2015-October 20, 2016. MMWR Morb Mortal Wkly Rep. 2016;65(44):1219-23. Epub 2016/11/11. doi: 10.15585/mmwr.mm6544a4. PubMed PMID: 27832051.
237. Motta IJ, Spencer BR, Cordeiro da Silva SG, Arruda MB, Dobbin JA, Gonzaga YB, Arcuri IP, Tavares RC, Atta EH, Fernandes RF, Costa DA, Ribeiro LJ, Limonte F, Higa LM, Voloch CM, Brindeiro RM, Tanuri A, Ferreira OC, Jr. Evidence for Transmission of Zika Virus by Platelet Transfusion. N Engl J Med. 2016;375(11):1101-3. Epub 2016/08/18. doi: 10.1056/NEJMc1607262. PubMed PMID: 27532622.
238. Robertson SJ, Lubick KJ, Freedman BA, Carmody AB, Best SM. Tick-borne flaviviruses antagonize both IRF-1 and type I IFN signaling to inhibit dendritic cell function. J Immunol. 2014;192(6):2744-55. Epub 2014/02/18. doi: 10.4049/jimmunol.1302110. PubMed PMID: 24532583; PMCID: PMC4010128.
239. Aleyas AG, Han YW, George JA, Kim B, Kim K, Lee CK, Eo SK. Multifront assault on antigen presentation by Japanese encephalitis virus subverts CD8+ T cell responses. J Immunol. 2010;185(3):1429-41. Epub 2010/06/29. doi: 10.4049/jimmunol.0902536. PubMed PMID: 20581148.
240. Liu S, DeLalio LJ, Isakson BE, Wang TT. AXL-Mediated Productive Infection of Human Endothelial Cells by Zika Virus. Circ Res. 2016;119(11):1183-9. Epub 2016/09/22. doi: 10.1161/CIRCRESAHA.116.309866. PubMed PMID: 27650556; PMCID: PMC5215127.
241. Pulendran B. The varieties of immunological experience: of pathogens, stress, and dendritic cells. Annu Rev Immunol. 2015;33:563-606. Epub 2015/02/11. doi: 10.1146/annurev-immunol-020711-075049. PubMed PMID: 25665078.
242. Schoggins JW, Rice CM. Interferon-stimulated genes and their antiviral effector functions. Curr Opin Virol. 2011;1(6):519-25. Epub 2012/02/14. doi: 10.1016/j.coviro.2011.10.008. PubMed PMID: 22328912; PMCID: PMC3274382.
243. Olagnier D, Scholte FE, Chiang C, Albulescu IC, Nichols C, He Z, Lin R, Snijder EJ, van Hemert MJ, Hiscott J. Inhibition of dengue and chikungunya virus infections by RIG-I-mediated type I interferon-independent stimulation of the innate antiviral response. J Virol. 2014;88(8):4180-94. Epub 2014/01/31. doi: 10.1128/JVI.03114-13. PubMed PMID: 24478443; PMCID: PMC3993760.
244. Prins KC, Cardenas WB, Basler CF. Ebola virus protein VP35 impairs the function of interferon regulatory factor-activating kinases IKKepsilon and TBK-1. J Virol. 2009;83(7):3069-77. Epub 2009/01/21. doi: 10.1128/JVI.01875-08. PubMed PMID: 19153231; PMCID: PMC2655579.

245. Mibayashi M, Martinez-Sobrido L, Loo YM, Cardenas WB, Gale M, Jr., Garcia-Sastre A. Inhibition of retinoic acid-inducible gene I-mediated induction of beta interferon by the NS1 protein of influenza A virus. J Virol. 2007;81(2):514-24. Epub 2006/11/03. doi: 10.1128/JVI.01265-06. PubMed PMID: 17079289; PMCID: PMC1797471.
246. Anglero-Rodriguez YI, Pantoja P, Sariol CA. Dengue virus subverts the interferon induction pathway via NS2B/3 protease-IkappaB kinase epsilon interaction. Clin Vaccine Immunol. 2014;21(1):29-38. Epub 2013/11/01. doi: 10.1128/CVI.00500-13. PubMed PMID: 24173023; PMCID: PMC3910921.
247. Schulz O, Pichlmair A, Rehwinkel J, Rogers NC, Scheuner D, Kato H, Takeuchi O, Akira S, Kaufman RJ, Reis e Sousa C. Protein kinase R contributes to immunity against specific viruses by regulating interferon mRNA integrity. Cell Host Microbe. 2010;7(5):354-61. Epub 2010/05/19. doi: 10.1016/j.chom.2010.04.007. PubMed PMID: 20478537; PMCID: PMC2919169.
248. Schoggins JW, Wilson SJ, Panis M, Murphy MY, Jones CT, Bieniasz P, Rice CM. A diverse range of gene products are effectors of the type I interferon antiviral response. Nature. 2011;472(7344):481-5. Epub 2011/04/12. doi: 10.1038/nature09907. PubMed PMID: 21478870; PMCID: PMC3409588.
249. Schnell G, Loo YM, Marcotrigiano J, Gale M, Jr. Uridine composition of the poly-U/UC tract of HCV RNA defines non-self recognition by RIG-I. PLoS Pathog. 2012;8(8):e1002839. Epub 2012/08/23. doi: 10.1371/journal.ppat.1002839. PubMed PMID: 22912574; PMCID: PMC3410852.
250. Laurent-Rolle M, Boer EF, Lubick KJ, Wolfinbarger JB, Carmody AB, Rockx B, Liu W, Ashour J, Shupert WL, Holbrook MR, Barrett AD, Mason PW, Bloom ME, Garcia-Sastre A, Khromykh AA, Best SM. The NS5 protein of the virulent West Nile virus NY99 strain is a potent antagonist of type I interferon-mediated JAK-STAT signaling. J Virol. 2010;84(7):3503-15. Epub 2010/01/29. doi: 10.1128/JVI.01161-09. PubMed PMID: 20106931; PMCID: PMC2838099.
251. Laurent-Rolle M, Morrison J, Rajsbaum R, Macleod JM, Pisanelli G, Pham A, Ayllon J, Miorin L, Martinez-Romero C, tenOever BR, Garcia-Sastre A. The interferon signaling antagonist function of yellow fever virus NS5 protein is activated by type I interferon. Cell Host Microbe. 2014;16(3):314-27. Epub 2014/09/12. doi: 10.1016/j.chom.2014.07.015. PubMed PMID: 25211074; PMCID: PMC4176702.
252. Goulet ML, Olagnier D, Xu Z, Paz S, Belgnaoui SM, Lafferty EI, Janelle V, Arguello M, Paquet M, Ghneim K, Richards S, Smith A, Wilkinson P, Cameron M, Kalinke U, Qureshi S, Lamarre A, Haddad EK, Sekaly RP, Peri S, Balachandran S, Lin R, Hiscott J. Systems analysis of a RIG-I agonist inducing broad spectrum inhibition of virus infectivity. PLoS Pathog. 2013;9(4):e1003298. Epub 2013/05/02. doi: 10.1371/journal.ppat.1003298. PubMed PMID: 23633948; PMCID: PMC3635991.
253. Chambers TJ, Halevy M, Nestorowicz A, Rice CM, Lustig S. West Nile virus envelope proteins: nucleotide sequence analysis of strains differing in mouse neuroinvasiveness. J Gen Virol. 1998;79 ( Pt 10)(10):2375-80. Epub 1998/10/21. doi: 10.1099/0022-1317-79-10-2375. PubMed PMID: 9780042.

254. Klimstra WB, Ryman KD, Johnston RE. Adaptation of Sindbis virus to BHK cells selects for use of heparan sulfate as an attachment receptor. Journal of virology. 1998;72(9):7357-66.
255. Kaul A, Woerz I, Meuleman P, Leroux-Roels G, Bartenschlager R. Cell culture adaptation of hepatitis C virus and in vivo viability of an adapted variant. J Virol. 2007;81(23):13168-79. Epub 2007/09/21. doi: 10.1128/JVI.01362-07. PubMed PMID: 17881454; PMCID: PMC2169131.
256. Shan C, Xie X, Muruato AE, Rossi SL, Roundy CM, Azar SR, Yang Y, Tesh RB, Bourne N, Barrett AD, Vasilakis N, Weaver SC, Shi PY. An Infectious cDNA Clone of Zika Virus to Study Viral Virulence, Mosquito Transmission, and Antiviral Inhibitors. Cell Host Microbe. 2016;19(6):891-900. Epub 2016/05/21. doi: 10.1016/j.chom.2016.05.004. PubMed PMID: 27198478; PMCID: PMC5206987.
257. Bol SM, van Remmerden Y, Sietzema JG, Kootstra NA, Schuitemaker H, van't Wout AB. Donor variation in in vitro HIV-1 susceptibility of monocyte-derived macrophages. Virology. 2009;390(2):205-11. Epub 2009/06/19. doi: 10.1016/j.virol.2009.05.027. PubMed PMID: 19535121.
258. Travanty E, Zhou B, Zhang H, Di YP, Alcorn JF, Wentworth DE, Mason R, Wang J. Differential Susceptibilities of Human Lung Primary Cells to H1N1 Influenza Viruses. J Virol. 2015;89(23):11935-44. Epub 2015/09/18. doi: 10.1128/JVI.01792-15. PubMed PMID: 26378172; PMCID: PMC4645340.
259. Libraty DH, Pichyangkul S, Ajariyakhajorn C, Endy TP, Ennis FA. Human dendritic cells are activated by dengue virus infection: enhancement by gamma interferon and implications for disease pathogenesis. J Virol. 2001;75(8):3501-8. Epub 2001/03/27. doi: 10.1128/JVI.75.8.3501-3508.2001. PubMed PMID: 11264339; PMCID: PMC114841.
260. Beljanski V, Chiang C, Kirchenbaum GA, Olagnier D, Bloom CE, Wong T, Haddad EK, Trautmann L, Ross TM, Hiscott J. Enhanced Influenza Virus-Like Particle Vaccination with a Structurally Optimized RIG-I Agonist as Adjuvant. J Virol. 2015;89(20):10612-24. Epub 2015/08/14. doi: 10.1128/JVI.01526-15. PubMed PMID: 26269188; PMCID: PMC4580177.
261. Kulkarni RR, Rasheed MA, Bhaumik SK, Ranjan P, Cao W, Davis C, Marisetti K, Thomas S, Gangappa S, Sambhara S, Murali-Krishna K. Activation of the RIG-I pathway during influenza vaccination enhances the germinal center reaction, promotes T follicular helper cell induction, and provides a dose-sparing effect and protective immunity. J Virol. 2014;88(24):13990-4001. Epub 2014/09/26. doi: 10.1128/JVI.02273-14. PubMed PMID: 25253340; PMCID: PMC4249139.
262. Pattabhi S, Wilkins CR, Dong R, Knoll ML, Posakony J, Kaiser S, Mire CE, Wang ML, Ireton RC, Geisbert TW, Bedard KM, Iadonato SP, Loo YM, Gale M, Jr. Targeting Innate Immunity for Antiviral Therapy through Small Molecule Agonists of the RLR Pathway. J Virol. 2015;90(5):2372-87. Epub 2015/12/18. doi: 10.1128/JVI.02202-15. PubMed PMID: 26676770; PMCID: PMC4810700.
263. Moser LA, Ramirez-Carvajal L, Puri V, Pauszek SJ, Matthews K, Dilley KA, Mullan C, McGraw J, Khayat M, Beeri K, Yee A, Dugan V, Heise MT, Frieman MB, Rodriguez LL, Bernard KA, Wentworth DE, Stockwell TB, Shabman

RS. A Universal Next-Generation Sequencing Protocol To Generate Noninfectious Barcoded cDNA Libraries from High-Containment RNA Viruses. mSystems. 2016;1(3):15. Epub 2016/11/09. doi: 10.1128/mSystems.00039-15. PubMed PMID: 27822536; PMCID: PMC5069770.
264. Wang S, Sundaram JP, Stockwell TB. VIGOR extended to annotate genomes for additional 12 different viruses. Nucleic Acids Res. 2012;40(Web Server issue):W186-92. Epub 2012/06/07. doi: 10.1093/nar/gks528. PubMed PMID: 22669909; PMCID: PMC3394299.
265. Lazear HM, Diamond MS. Zika Virus: New Clinical Syndromes and its Emergence in the Western Hemisphere. J Virol. 2016. Epub 2016/03/11. doi: 10.1128/JVI.00252-16. PubMed PMID: 26962217.
266. Rasmussen SA, Jamieson DJ, Honein MA, Petersen LR. Zika Virus and Birth Defects - Reviewing the Evidence for Causality. N Engl J Med. 2016. doi: 10.1056/NEJMsr1604338. PubMed PMID: 27074377.
267. Martines RB, Bhatnagar J, Keating MK, Silva-Flannery L, Muehlenbachs A, Gary J, Goldsmith C, Hale G, Ritter J, Rollin D, Shieh WJ, Luz KG, Ramos AM, Davi HP, Kleber de Oliveria W, Lanciotti R, Lambert A, Zaki S. Notes from the Field: Evidence of Zika Virus Infection in Brain and Placental Tissues from Two Congenitally Infected Newborns and Two Fetal Losses - Brazil, 2015. MMWR Morb Mortal Wkly Rep. 2016;65(6):159-60. Epub 2016/02/20. doi: 10.15585/mmwr.mm6506e1. PubMed PMID: 26890059.
268. Cordeiro MT, Pena LJ, Brito CA, Gil LH, Marques ET. Positive IgM for Zika virus in the cerebrospinal fluid of 30 neonates with microcephaly in Brazil. Lancet. 2016. doi: 10.1016/S0140-6736(16)30253-7. PubMed PMID: 27103126.
269. Jonathan J. Miner BC, Jennifer Govero, Amber M. Smith, Estefania Fernandez, Omar H. Cabrera, Charise Garber, Michelle Noll, Robyn S. Klein, Kevin K. Noguchi, Indira U. Mysorekar, Michael S. Diamond. Zika Virus Infection during Pregnancy in Mice Causes Placental Damage and Fetal Demise. Cell. 2016. doi: http://dx.doi.org/10.1016/j.cell.2016.05.008.
270. Noronha L, Zanluca C, Azevedo ML, Luz KG, Santos CN. Zika virus damages the human placental barrier and presents marked fetal neurotropism. Mem Inst Oswaldo Cruz. 2016. doi: 10.1590/0074-02760160085. PubMed PMID: 27143490.
271. Koi H, Zhang J, Parry S. The mechanisms of placental viral infection. Ann N Y Acad Sci. 2001;943:148-56. PubMed PMID: 11594535.
272. Lewis SH, Fox HE, Reynolds-Kohler C, Nelson JA. HIV-1 in trophoblastic and villous Hofbauer cells, and haematological precursors in eight-week fetuses. The Lancet. 1990;335(8689):565-8. doi: 10.1016/0140-6736(90)90349-a.
273. Johnson EL, Chakraborty R. Placental Hofbauer cells limit HIV-1 replication and potentially offset mother to child transmission (MTCT) by induction of immunoregulatory cytokines. Retrovirology. 2012;9:101. Epub 2012/12/12. doi: 10.1186/1742-4690-9-101. PubMed PMID: 23217137; PMCID: 3524025.
274. Delorme-Axford E, Donker RB, Mouillet JF, Chu T, Bayer A, Ouyang Y, Wang T, Stolz DB, Sarkar SN, Morelli AE, Sadovsky Y, Coyne CB. Human placental trophoblasts confer viral resistance to recipient cells. Proc Natl Acad

Sci U S A. 2013;110(29):12048-53. doi: 10.1073/pnas.1304718110. PubMed PMID: 23818581; PMCID: PMC3718097.
275. Bayer A, Lennemann NJ, Ouyang Y, Bramley JC, Morosky S, Marques ET, Jr., Cherry S, Sadovsky Y, Coyne CB. Type III Interferons Produced by Human Placental Trophoblasts Confer Protection against Zika Virus Infection. Cell Host Microbe. 2016. Epub 2016/04/14. doi: 10.1016/j.chom.2016.03.008. PubMed PMID: 27066743.
276. Garcez PP, Loiola EC, Madeiro da Costa R, Higa LM, Trindade P, Delvecchio R, Nascimento JM, Brindeiro R, Tanuri A, Rehen SK. Zika virus impairs growth in human neurospheres and brain organoids. Science. 2016. Epub 2016/04/12. doi: 10.1126/science.aaf6116. PubMed PMID: 27064148.
277. Tang H, Hammack C, Ogden SC, Wen Z, Qian X, Li Y, Yao B, Shin J, Zhang F, Lee EM, Christian KM, Didier RA, Jin P, Song H, Ming GL. Zika Virus Infects Human Cortical Neural Progenitors and Attenuates Their Growth. Cell Stem Cell. 2016. Epub 2016/03/10. doi: 10.1016/j.stem.2016.02.016. PubMed PMID: 26952870.
278. Loo YM, Fornek J, Crochet N, Bajwa G, Perwitasari O, Martinez-Sobrido L, Akira S, Gill MA, Garcia-Sastre A, Katze MG, Gale M, Jr. Distinct RIG-I and MDA5 signaling by RNA viruses in innate immunity. J Virol. 2008;82(1):335-45. doi: 10.1128/JVI.01080-07. PubMed PMID: 17942531; PMCID: 2224404.
279. Daffis S, Suthar MS, Szretter KJ, Gale M, Jr., Diamond MS. Induction of IFN-beta and the innate antiviral response in myeloid cells occurs through an IPS-1-dependent signal that does not require IRF-3 and IRF-7. PLoS Pathog. 2009;5(10):e1000607. doi: 10.1371/journal.ppat.1000607. PubMed PMID: 19798431; PMCID: 2747008.
280. Querec TD, Akondy RS, Lee EK, Cao W, Nakaya HI, Teuwen D, Pirani A, Gernert K, Deng J, Marzolf B, Kennedy K, Wu H, Bennouna S, Oluoch H, Miller J, Vencio RZ, Mulligan M, Aderem A, Ahmed R, Pulendran B. Systems biology approach predicts immunogenicity of the yellow fever vaccine in humans. Nature immunology. 2009;10(1):116-25. Epub 2008/11/26. doi: 10.1038/ni.1688. PubMed PMID: 19029902; PMCID: 4049462.
281. Thio CL. Host genetic factors and antiviral immune responses to hepatitis C virus. Clinics in liver disease. 2008;12(3):713-26, xi. Epub 2008/07/16. doi: 10.1016/j.cld.2008.03.002. PubMed PMID: 18625436; PMCID: 2597299.
282. Reefhuis J, Gilboa SM, Johansson MA, Valencia D, Simeone RM, Hills SL, Polen K, Jamieson DJ, Petersen LR, Honein MA. Projecting Month of Birth for At-Risk Infants after Zika Virus Disease Outbreaks. Emerging infectious diseases. 2016;22(5):828-32. Epub 2016/04/19. doi: 10.3201/eid2205.160290. PubMed PMID: 27088494; PMCID: 4861542.
283. Chiuppesi F, Wussow F, Johnson E, Bian C, Zhuo M, Rajakumar A, Barry PA, Britt WJ, Chakraborty R, Diamond DJ. Vaccine-Derived Neutralizing Antibodies to the Human Cytomegalovirus gH/gL Pentamer Potently Block Primary Cytotrophoblast Infection. J Virol. 2015;89(23):11884-98. Epub 2015/09/18. doi: 10.1128/JVI.01701-15. PubMed PMID: 26378171; PMCID: 4645301.

284. Scherwitzl I, Mongkolsapaja J, Screaton G. Recent advances in human flavivirus vaccines. Curr Opin Virol. 2017;23:95-101. Epub 2017/05/10. doi: 10.1016/j.coviro.2017.04.002. PubMed PMID: 28486135.
285. Aguirre S, Maestre AM, Pagni S, Patel JR, Savage T, Gutman D, Maringer K, Bernal-Rubio D, Shabman RS, Simon V, Rodriguez-Madoz JR, Mulder LC, Barber GN, Fernandez-Sesma A. DENV inhibits type I IFN production in infected cells by cleaving human STING. PLoS Pathog. 2012;8(10):e1002934. Epub 2012/10/12. doi: 10.1371/journal.ppat.1002934. PubMed PMID: 23055924; PMCID: PMC3464218.
286. Barba-Spaeth G, Longman RS, Albert ML, Rice CM. Live attenuated yellow fever 17D infects human DCs and allows for presentation of endogenous and recombinant T cell epitopes. J Exp Med. 2005;202(9):1179-84. Epub 2005/11/02. doi: 10.1084/jem.20051352. PubMed PMID: 16260489; PMCID: PMC2213233.
287. Tobler LH, Cameron MJ, Lanteri MC, Prince HE, Danesh A, Persad D, Lanciotti RS, Norris PJ, Kelvin DJ, Busch MP. Interferon and interferon-induced chemokine expression is associated with control of acute viremia in West Nile virus-infected blood donors. J Infect Dis. 2008;198(7):979-83. Epub 2008/08/30. doi: 10.1086/591466. PubMed PMID: 18729779.
288. Daffis S, Szretter KJ, Schriewer J, Li J, Youn S, Errett J, Lin TY, Schneller S, Zust R, Dong H, Thiel V, Sen GC, Fensterl V, Klimstra WB, Pierson TC, Buller RM, Gale M, Jr., Shi PY, Diamond MS. 2'-O methylation of the viral mRNA cap evades host restriction by IFIT family members. Nature. 2010;468(7322):452-6. Epub 2010/11/19. doi: 10.1038/nature09489. PubMed PMID: 21085181; PMCID: PMC3058805.
289. Szretter KJ, Daniels BP, Cho H, Gainey MD, Yokoyama WM, Gale M, Jr., Virgin HW, Klein RS, Sen GC, Diamond MS. 2'-O methylation of the viral mRNA cap by West Nile virus evades ifit1-dependent and -independent mechanisms of host restriction in vivo. PLoS Pathog. 2012;8(5):e1002698. Epub 2012/05/17. doi: 10.1371/journal.ppat.1002698. PubMed PMID: 22589727; PMCID: PMC3349756.
290. Widman DG, Young E, Yount BL, Plante KS, Gallichotte EN, Carbaugh DL, Peck KM, Plante J, Swanstrom J, Heise MT, Lazear HM, Baric RS. A Reverse Genetics Platform That Spans the Zika Virus Family Tree. MBio. 2017;8(2):16. Epub 2017/03/09. doi: 10.1128/mBio.02014-16. PubMed PMID: 28270583; PMCID: PMC5340872.
291. Grandvaux N, Servant MJ, tenOever B, Sen GC, Balachandran S, Barber GN, Lin R, Hiscott J. Transcriptional profiling of interferon regulatory factor 3 target genes: direct involvement in the regulation of interferon-stimulated genes. J Virol. 2002;76(11):5532-9. Epub 2002/05/07. doi: 10.1128/JVI.76.11.5532-5539.2002. PubMed PMID: 11991981; PMCID: PMC137057.
292. Lin R, Heylbroeck C, Genin P, Pitha PM, Hiscott J. Essential role of interferon regulatory factor 3 in direct activation of RANTES chemokine transcription. Mol Cell Biol. 1999;19(2):959-66. Epub 1999/01/16. PubMed PMID: 9891032; PMCID: PMC116027.

293. Chew T, Noyce R, Collins SE, Hancock MH, Mossman KL. Characterization of the interferon regulatory factor 3-mediated antiviral response in a cell line deficient for IFN production. Mol Immunol. 2009;46(3):393-9. Epub 2008/11/29. doi: 10.1016/j.molimm.2008.10.010. PubMed PMID: 19038458.
294. Osada N, Kohara A, Yamaji T, Hirayama N, Kasai F, Sekizuka T, Kuroda M, Hanada K. The genome landscape of the african green monkey kidney-derived vero cell line. DNA Res. 2014;21(6):673-83. Epub 2014/10/01. doi: 10.1093/dnares/dsu029. PubMed PMID: 25267831; PMCID: PMC4263300.
295. Emeny JM, Morgan MJ. Regulation of the interferon system: evidence that Vero cells have a genetic defect in interferon production. J Gen Virol. 1979;43(1):247-52. Epub 1979/04/01. doi: 10.1099/0022-1317-43-1-247. PubMed PMID: 113494.
296. Tanabe Y, Nishibori T, Su L, Arduini RM, Baker DP, David M. Cutting Edge: Role of STAT1, STAT3, and STAT5 in IFN- Responses in T Lymphocytes. The Journal of Immunology. 2005;174(2):609-13. doi: 10.4049/jimmunol.174.2.609.
297. Hahn CS, Dalrymple JM, Strauss JH, Rice CM. Comparison of the virulent Asibi strain of yellow fever virus with the 17D vaccine strain derived from it. Proceedings of the National Academy of Sciences of the United States of America. 1987;84(7):2019-23. Epub 1987/04/01. PubMed PMID: 3470774; PMCID: PMC304575.
298. Doceul V, Chauveau E, Lara E, Breard E, Sailleau C, Zientara S, Vitour D. Dual modulation of type I interferon response by bluetongue virus. J Virol. 2014;88(18):10792-802. Epub 2014/07/11. doi: 10.1128/JVI.01235-14. PubMed PMID: 25008919; PMCID: PMC4178850.
299. Fenner JE, Starr R, Cornish AL, Zhang JG, Metcalf D, Schreiber RD, Sheehan K, Hilton DJ, Alexander WS, Hertzog PJ. Suppressor of cytokine signaling 1 regulates the immune response to infection by a unique inhibition of type I interferon activity. Nat Immunol. 2006;7(1):33-9. Epub 2005/11/29. doi: 10.1038/ni1287. PubMed PMID: 16311601.
300. Simoni MK, Jurado KA, Abrahams VM, Fikrig E, Guller S. Zika virus infection of Hofbauer cells. Am J Reprod Immunol. 2017;77(2). Epub 2016/12/15. doi: 10.1111/aji.12613. PubMed PMID: 27966815; PMCID: PMC5299062.